An Analytical Approach to Study the Flow and Heat Transfer of a Newtonian/non-Newtonian Fluids over a Slender Elastic Sheet

A THESIS SUBMITTED

BY

V. RAMANJINI

(Reg. No. PHD16MA08)

FOR THE DEGREE OF

Doctor of Philosophy

IN

MATHEMATICS

UNDER THE SUPERVISION OF

Dr. K. V. PRASAD

DEPARTMENT OF MATHEMATICS
VIJAYANAGARA SRI KRISHNADEVARAYA UNIVERSITY,
BALLARI: 583105, KARNATAKA, INDIA.

2020

Sri Pennobaleshwara Swamy

Dedicated To

My Beloved Parents

and

My Guru K.V. Prasad

DECLARATION

I hereby declare that the thesis entitled **"An analytical approach to study the flow and heat transfer of a Newtonian/ non-Newtonian fluids over a slender elastic sheet"** submitted to the Vijayanagara Sri Krishnadevaraya University for the award of the degree of **"Doctor of Philosophy"** in Mathematics is the result of investigation carried out by me in the Department of Mathematics under the supervision and guidance of **Dr. K.V. Prasad,** Professor, Department of Mathematics, Vijayanagara Sri Krishnadevaraya University, Ballari.

I further declare that the work reported in thesis has not been submitted by me elsewhere for the award of any degree, diploma, fellowship etc., and is not the repetition of the work carried out by others.

Place: Ballari

Date:

Ramanjini. V
Full time, Research scholar
Department of Mathematics
VSK University, Ballari-583105
Karnataka, India.

VIJAYANAGARA SRI KRISHNADEVARAYA UNIVERSITY

Jnana Sagara Campus, Vinayakanagara, Cantonment,

Ballari: 583 105, Karnataka, India.

Dr. K. V. Prasad **Department of Mathematics**

Professor **E-Mail: Prasadkv2007@gmail.com**

CERTIFICATE

This is to certify that, the thesis entitled **"An analytical approach to study the flow and heat transfer of a Newtonian/ non-Newtonian fluids over a slender elastic sheet"** which is being submitted by **Mr. Ramanjini. V** to the Vijayanagara Sri Krishnadevaraya University, Ballari for the award of the degree of **"Doctor of Philosophy"** in Mathematics, is a genuine record of the research work carried out by him under my guidance and Supervision.

I further certify that the matter embodied in this thesis, either partially or fully, has not been submitted by him to any other University or Institution for the award of any degree or diploma. He has carried out his research work at the Department of studies and Research in mathematics, Vijayanagara Sri Krishnadevaraya University, Ballari.

Place: Ballari **Dr. K. V. Prasad**

Date:

ACKNOWLEDGEMENT

First and foremost, I would like to express my deep sense of thanks and gratitude to my mentor, philosopher and supervisor **Dr. K. V. Prasad,** for providing me this opportunity to work in his guidance and gave me the strength I needed to take next steps towards my dream. His dedication, keen interest and above all his overwhelming attitude to help his students has been solely and mainly responsible for completing my research work. His scholarly advice, meticulous scrutiny and scientific approach have helped me to a great extent to accomplish this work.

I would like to acknowledge, **The Ministry of Tribal of Affairs, Govt of India,** who provided me with a **bursary (Award Letter No: 201718-NFST-KAR-00764)** to carry out this research work.

I would like to express my deepest gratitude to **Dr. V. Lokesha, Chairman, Department of Mathematics, VSKU Ballari,** for his inspiration and cooperation throughout the process of my research work.

I am also expressing my deepest and very special thanks to **Dr. Hanumesh Vaidya** and **Dr. Neelufer** for their great help and support throughout my research work.

Also I would like to express my special thanks to Staff members in the Department of Mathematics, VSKUB, **Dr. Jitendra Kumar Singh, Dr. A. Padhmanabha Reddy, Dr. Ashwin Kumar, Dr.Anita and Mrs. Saraswati,** for their valuable suggestions and cooperation throughout the process of my research work.

Also, I would like to thank **my wife** **Lathashri.B,** for cheering me up and standing by me through all the times. Without her loving support, understanding, patience and persistent confidence in me, I would never have completed my research work.

I sincerely acknowledge the help of research colleagues **Dr. M. Prasad, Dr. U.B.Vishwanatha, Dr. B. Srikanth Setty, Mr. Hussain Basha, Mr. D.L. Mahendra, and Miss. J.U. Viharika,** for their fruitful discussion, encouragement and cooperation.

I am also greatfull to all the **research scholars and non teaching staff** of the Department for their kind help and cooperation throughout my research work.

My special expression of gratitude to **Dr. C. Sulochana madam**, Professor, Department of Mathematics, Gulbarga University, Kalaburagi, who were source of motivation and inspiration to carry out this research work.

I also acknowledge grandfather **Eshwarappa,** grandmother **Shanthi** and **Surekha prasad** for their valuable suggestions and motivations.

I thank the **God** for giving me the strength and patience to work through all these years so that today I stand proudly with my head held high.

My dreams would never have been realized without the love and moral support of my beloved family for their continued support in this endeavour. Particularly, my father **Venkatesha.V,** and mother **Bhimalingamma,** father in law **Muddanna.U,** mother in law **Savitramma** and my brothers **Maresh, Narayana, K.Srinivas,** all my reletives and well wishers. I would never have completed my research work without their unconditional support and encouragement.

V. RAMANJINI

LIST OF PUBLICATIONS

- K.V. Prasad, Hanumesh Vaidya, K. Vajravelu, and **V. Ramanjini**, **"Analytical Study of Cattanneo-Christov Heat Flux Model for Williamson -Nanofluid Flow Over a Slender Elastic Sheet with Variable Thicknesss",** Published in the ***Journal of Nanofluids,*** **Vol. 7,** 583-594, 2018.

- K.V. Prasad, Hanumesh Vaidya, K. Vajravelu, **V. Ramanjini**, G. Manjunatha and C. Rajashekhar, **" Influence of variable transport properties on Casson nanofluid over a slender Riga plate: Keller box scheme",** Published in the ***Journal of Advanced Research in Fluid Mechanics and Thermal Science,*** **Vol.64(1),** 19-42, 2019.

- K.V. Prasad, Hanumesh Vaidya, O.D. Makinde, K. Vajravelu, **V. Ramanjini**, **"Mixed convective nanofluid flow over a coagulated Riga plate in the presence of viscous dissipation and chemical reaction,"** communicated after minor revison to the ***Journal of Applied and Computational Mechanics,*** **2020**.

- K.V. Prasad, Hanumesh Vaidya, K. Vajravelu, O.D. Makinde and **V. Ramanjni,** **"Influence of suction/injection and heat transfer on unsteady MHD Flow over a stretchable rotating disk,"** accepted for publication in the ***International Journal of Latin American Applied Research,*** **2019.**

Papers Presentation in National/ International Conferences

- Presented a paper entitled **" Analytical study of Cattanneo – Christov heat flux model for Williamson nanofluid flow over a slender elastic sheet with variable thickness",** in the **national conference on recent advances in Mathematical sciences and applications,** organized by the Department of Mathematics, Tumkur Univrsity, Tumkur, Karnataka, during 1st and 2nd December 2017.

- Presented a paper entitled **"MHD heat transfer of Casson nanofluid over a slender Riga plate", in the international conference on advances in pure and applied Mathematics 2018,** organized by School of Mathematics, Madurai Kamaraj University in association with International Multidisciplinary Research Foundation (IMRF), Madurai, Tamilnadu, 6th - 8th September, 2018.

- Presented a paper entitled **"Influence of variable transport properties on Casson nanofluid over a slender Riga plate: Keller box scheme", in the national conference named as New Vistas in Science and Technology in Common Good,** organized by NMKRV College for women in association with KSTA Bangalore, 1st and 2nd February 2019.

- Presented a paper entitled **"Effect of mixed convective nanofluid flow over a stretchable Riga plate in the presence of viscous dissipation and chemical reaction", in the 2nd international conference on global advancement of Mathematics (GAM-2019),** organized by Acharya institute of graduate studies, Bangalore – 560107, India, held on 25th and 26th June 2019.

ABSTRACT

In recent years the study of boundary layer flow and heat transfer over a stretching sheet has attracted numerous researchers due to their wide range of applications in various fields of technological industry and chemical engineering processes. To mention a few, manufacturing of plastic films and artificial fibers, wire drawing, annealing and tinning of copper wires, cooling and drying of copper wires, metal and polymer extrusion, electronic chips, paper production and so on. Keeping these industrial applications in view, the present thesis explores three types of problems, namely,

- Flow and heat transfer of a non-Newtonian fluid with variable thickness
- Flow and heat transfer of a Newtonian/non-Newtonian fluid over a Riga plate with variable fluid properties
- Unsteady fluid flow and heat transfer over a stretchable rotating disk with variable fluid properties.

The first type of problem concerns with the effect of Cattanneo Christov heat fluid flow model for Williamson-nanofluid flow over a slender elastic sheet with variable thickness. Here, Cattanneo Christov heat flux model is used instead of Fourier law to explore the heat transfer characterstic. Further, the flow is induced by non-linearly stretching of an elastic sheet with variable thickness so that the sheet is sufficiently thin to avoid a measurable pressure gradient along the sheet. The second type of problem concerns with the flow and heat transfer of a Newtonian/non-Newtonian fluid flow over a Riga plate under different physical constraints. This plate is used to generate simultaneous electric and magnetic fileds which can produce Lorentz force parallel to the wall in weakly conducting fluids. This plate consists of a span wise aligned array of alternating electrodes and permanent magnets mounted on a plane surface. This array generates a surface parallel Lorentz force with a neglected pressure gradient, which decreases exponentially in the direction normal to the plate. In addition to this, the author also investigates the fluid properties namely, the transport physical properties are sumed to be the functions of temperature. The third type of problem investigates the unsteady MHD flow and heat transfer of a fluid over stretchable rotating disk in the presence of mass suction/injection with varaible

thickness. Moreover the impact of viscous dissipation and variable fluid properties are also considered for investigation. The effects of the sundry parameters on the velocity, the temperature, the skin friction, the wall temperature gradient, the wall concentration gradient and other associated parameters are also discussed in this thesis. The important aspect of the thesis is to study the effects of non-diemnsional parameters arising in the mathematical modeelling of the physical problem on the flow and heat transfer under different physical situation. This kind of physical situation occurs more frequently in the application of engineering technology. A stretching sheet with variable thickness can be more close to the situation in practical applications. The analytical/semi analytical/numerical results are compared with the results of earlier literature and they are found to be in good agreement. With this inspiration, the thesis is organized into five chatpers and they are described briefly as follows:

Chapter-1 is of introductory in nature and exhibits the brief idea of the slender elastic sheet, nanofluids, basic equations, boundary conditions, dimensionless paramerers, method of numerical/semi-numerical solutions and Nomenclature.

In Chapter-2 we discuss the Williamson nanofluid flow over a slender elastic sheet with variable thickness using Cattaneo – Christov theory. To explore the heat transfer characteristics, Cattaneo-Christov heat flux model is used instead of classical Fourier's law. The nonlinear governing equations with suitable boundary conditions are initially cast into dimensionless form by similarity transformations. The optimal homotopy analysis method is proposed for the development of analytical solutions. For increasing values of the wall thickness parameter the analysis reveals quite interesting flow and heat ransfer patterns. Special prominence is given to the non-dimensional velocity, temperature; concentration and their graphical behavior for various parameters are analyzed and discussed. The impact of Cattanneo-Christov heat flux model is to reduce the temperature and concentration distribution. The obtained numerical results are compared with available results in the literature for some special cases and are found to be in excellent agreement. The skin friction, the wall temperature gradient and the wall concentration gradient are exhibited for various values of the non-dimensional parameters and the salient features are analysed.

In **Chapter-3,** an analysis has been carried out to study the effects of variable viscosity and variable thermal conductivity on the heat transfer characteristics of a Casson nanofluid over a slender Riga plate with zero mass flux and melting heat transfer boundary conditions. The nonlinear governing equations with the suitable boundary conditions are initially cast into dimensionless form by similarity transformations. The resulting coupled highly nonlinear equations are solved numerically by an efficient second-order finite difference scheme known as Keller Box Method. The obtained numerical results are compared with the available results in the literature for some special cases and the results are found to be in very good agreement. The effect of various physical parameters on velocity, temperature, and concentration profiles are illustrated through graphs and the numerical values are presented in tables. One of the critical findings of our study is that the effect of variable viscosity on velocity shows reducing nature, but there is an increasing nature in temperature and concentration.

Chapter-4 concentrates on the heat and mass transfer characteristics of a mixed convective flow of an electrically conducting nanofluid past a slender Riga plate in the presence of viscous dissipation and chemical reaction. The heat and mass transfer characteristics are analyzed by a zero nanoparticle mass flux and convective boundary conditions. The governing nonlinear PDEs are transformed into a system of coupled ODEs by using a suitable similarity transformation. The resulting coupled nonlinear equations with appropriate boundary conditions are solved by an efficient technique known as optimal homotopy analysis method. The impact of emerging parameters on the dimensionless velocity, temperature, and concentration distributions are presented through graphs. It is interesting to note that the contemporary results are in good agreement with the existing literature, which confirms the validity of the present work. It is observed that the temperature distribution improves for the Brownianmotion parameter and the thermopherosis parameter but the concentration distribution shows a dual characteristic.

Impact of suction/injection and heat transfer on unsteady MHD Flow over a stretchable rotating disk on heat and mass transfer is analyzed in **Chapter -5.** The unsteady magnetohydrodynamic two-dimensional boundary layer flow and heat transfer over a stretchable rotating disk with mass suction/injection is investigated. Temperature-dependent physical properties and convective boundary conditions are

taken into account. The governing coupled nonlinear partial differential equations are transformed into a system of ordinary differential equations by adopting the well-known similarity transformations. Further, the solutions are obtained through the semi-analytical method called an Optimal Homotopy Analysis Method (OHAM). The obtained results are discussed graphically to predict the features of the involved key parameters which are monitoring the flow model. The skin friction coefficient and Nusselt number are also examined. The validation of the present work is verified with the earlier published results and is found to be in excellent agreement. It is noticed that an increase in the viscosity parameter leads to decay in momentum boundary layer thickness, and the inverse trend is observed in the case of the temperature profile.

CONTENTS

CHAPTER - 1

INTRODUCTION AND LITERATURE SURVEY

1.1 Literature Survey

1.1.1 Flow over a Stretching Sheet

In recent years the study of boundary layer flow and heat transfer over a stretching sheet has attracted numerous researchers due to their wide range of applications in various fields of technological industry and chemical engineering processes. To mention a few, manufacturing of plastic films and artificial fibers, wire drawing, annealing and tinning of copper wires, cooling and drying of copper wires, metal and polymer extrusion, electronic chips, paper production and so on.

Keeping these industrial applications in view, Blasius (1908) initiated the boundary layer flow on a flat plate with a uniform free stream. Sakiadis (1961) extended the work of Blasius (1908) by considering the boundary layer flow over a continuous solid surface moving with a constant velocity. Crane (1970) extended this work to the concept of stretching sheet by assuming the velocity at the plate is proportional to the distance from the origin. This pioneering work of Crane (1970), i.e., the stretching sheet concept has been further extended to different types of fluids, namely Newtonian and non-Newtonian fluids under different physical constraints. Gupta and Gupta (1977) investigated the heat and mass transfer in the flow over a stretching surface with suction or blowing. Bank (1983) examined a class of similarity solution of the boundary layer equations for the flow due to stretching surface. The ordinary differential equation that arises admits of a one parameter family of a solution, in the same way the parameter values and various results are presented. Analytical solution is also presented for a couple of values of the parameters and these, together with perturbation solutions, support the numerical results. Dutta et al., (1985) analyzed the temperature distribution in a flow over a stretching sheet with uniform heat flux. The governing differential equation transformed to a confluent hyper geometric differential equation and solution was obtained in terms of incomplete gamma function. It was shown that temperature at a point decreased with the increase of Prandtl number. Dutta and Gupta (1987) considered the coupled heat transfer problem for solving the stretching sheet. Variation of the sheet temperature with distance from the slit was found for several values of Prandtl number and stretching speeds. It was shown that for a fixed Prandtl number, the surface temperature decreases with an increase in stretching speed. Dutta (1988) presented an analytical solution of the heat transfer problem for cooling of a thin stretching sheet in a viscous flow in the presence of suction or blowing. The locality of the sheet material was assumed to be proportional to the distance from the slit. The convergence criteria of the solution were also established. Chen and Char (1988) investigated the both power law surface temperature and power law heat flux variations on the heat transfer characteristics of a continuous, linearly stretching sheet subjected to suction or blowing. Soewono et al., (1992) analyzed the existence of solutions of a nonlinear boundary value problem, arising in flow and heat transfer over a stretching sheet with variable thermal conductivity and temperature dependent heat source or sink. Vajravelu (1994) carried out an analysis of convective flow and heat transfer in a viscous heat generating liquid near an infinite vertical stretching surface. Mahapatra and Gupta (2003) examined an exact similarity solution of the Navier – Stokes equation. The solution represents steady asymmetric stagnation point flow towards a stretching surface. It is shown that flow displays a boundary layer structure when the stretching velocity of the surface is less than the free stream velocity. Partha et al., (2005) have studied the mixed convection flow and heat transfer from an exponentially stretching vertical surface in a quiescent liquid using similarity solution. In these studies the fluid was assumed to be Newtonian. However, many industrial fluids are non-Newtonian or rheological in their flow characteristics (such as molten plastics, polymers, suspension, foods, slurries, paints, glues, printing inks, blood). That is, they might exhibit dynamic deviation from Newtonian behaviour depending upon the flow configuration and/or the rate of deformation. These fluids often obey non-linear constitutive equations and the complexity in the equations is the main culprit for the lack of exact analytical solutions. Examples of non-Newtonian fluids are viscoelastic fluids, Maxwell fluids, Rivlin – Erickson fluids, Oldroyd-B fluid, Jeffery fluid, couple stress fluids, micro-polar fluids, power law fluids and etc. Further, visco-elastic and Walters' models considered are simple which are known to be accurate only for weakly elastic fluids subject to slowly varying flows. These two models are known to violate certain rules of thermodynamics. Therefore the significance of the results reported in the above works is limited as far as the polymer industry is concerned. Obviously for the theoretical results to become of any industrial importance, more general visco-elastic fluid models such as upper convected Maxwell model (UCM fluid) or Oldroyd B model should be invoked. Indeed these two fluid models are being used recently to study the visco-elastic fluid flow above stretching and non-stretching sheets with or without heat transfer. Fox et al., (1969) studied the flow of power law fluid past an inextensible flat surface moving with constant velocity in its own plane, this model, however, doesn't exhibits certain non-Newtonian liquid properties like normal stress difference. Rajagopal et al., (1984) analyzed the flow of a second order liquid over a stretching sheet without heat transfer and presented a perturbation solution for the velocity distribution. Siddappa and Abel (1986) examined Walter's liquid B flow past a stretching sheet with suction and obtained the exact solution for the flow and energy equations. Bujurke et al., (1987) discussed the heat transfer in the flow of a second order liquid, obeying Coleman and Noll's constitutive equation, over a stretching sheet. Dandapat and Gupta (1989) studied the flow of second order liquid and heat transfer affected by a stretching sheet. The influence of viscoelasticity on flow behaviour and heat transfer characteristics was examined. Rollins and Vajravelu (1991) discussed the heat transfer in a second order liquid over a continuous stretching surface with power law surface temperature and power law heat flux including the effects of internal heat generation. Usually, the stretching may not be necessarily linear; but it may be quadratic or power law function or exponential function. Keeping such assumptions in mind, Kumaran and Ramanaiah (1996) investigated the viscous boundary layer flow over a quadratically stretching sheet. Magyari and Keller (2000) examined steady boundary layer flow induced by permeable stretching surfaces with variable temperature distribution under Reynolds analogy. This makes use of the advantages of all the exact analytic solutions of the momentum and energy equations. Chen (2003) investigated the thermal behaviour of a power law fluid film over a flat sheet under unsteady stretching. Cortell (2005a) studied the magnetohydrodynamic flow over a stretching of an incompressible fluid obeying the power law fluid using numerical solutions by means of Runge – Kutta algorithm for n^{th} order initial value problems. Anjali Devi and Thiyagarajan (2006) demonstrated the steady nonlinear hydromagnetic flow of an incompressible, viscous and electrically conducting fluid with heat transfer over a surface of variable temperature with power velocity in the presence of variable transverse magnetic field. Cortell (2007) described the numerical solution of the nonlinear problem over a viscous flow of a nonlinear stretching sheet on heat transfer characteristics when the dissipative heat is enclosed in the energy equation. Kandasamy et al., (2008) analyzed the effects of heat and mass transfer on MHD boundary layer flow over a shrinking sheet in the presence of suction. Later, the nonlinear stretching $i.e. u_1 = cx_1^m$ at $x_2 = 0$ for positive odd values of m was described by Akyildiz et al., (2010). Further, Van Gorder and Vajravelu (2010) examined this work for any value of $m \geq 1$.

1.1.2 Flow over a variable thickness of the sheet

All the above mentioned researchers focused their study on linear or nonlinear stretching sheet. Moreover, there is a special form of non-linear stretching, namely, variable thickness or coagulated sheet or slender elastic sheet is defined as $u_{1w}(x_1) = U_0(x_1 + b)^m$ at $x_2 = A(x_1 + b)^{(1-m)/2}$, $m \neq 1$ for different values of m in a thermally stratified environment. In this case the minimum value of x_2 is not starting point of the slot. This implies that all the conditions are not imposed at $x_2 = 0$ hence substituting $x_2 = A(x_1 + b)^{1-m/2}$, $m \neq 1$ is the starting point of the flow at the slot. This special form of stretching sheet is known as variable thickness of the sheet, which seems more realistic than the flat stretching surface. The use of variable thickness helps to reduce the weight of structural elements and improves the utilization of material. The variable thickness has many applications in vibration of orthotropic plates, machine designs, automobile and aeronautical engineering, acoustical components, and nuclear reactor technology etc. In view of these applications, Dawe (1966) considered the effect of variable thickness on rectangular plates and explained the importance of non-uniform thickness of the plates. Lee (1967) introduced theoretically the concept of variable thickness by considering a needle whose thickness is comparable with the boundary layer. Venkateshwara Rao and Raju (1974) studied the comparison of variable and constant thickness of vibrating plates. Keeping in view of the above work, Fang et al., (2012) extended this work by considering the boundary layer flow over a stretching sheet with variable thickness and explained the significant effects of non-flatness of the sheet. Pop et al., (2013) studied the thermal diffusivity flow over a stretching sheet with variable thickness. Khader and Megahed (2015) described the numerical solution for the slip velocity effect on the flow of a Newtonian fluid over a stretching sheet with variable thickness. Farooq et al., (2015) demonstrated the rheological characteristics of Upper Convected Maxwell fluid and Cattanneo – Christov heat flux model in flow over a stretching sheet with variable thickness. Khader (2016) devoted to introduce a numerical simulation with theoretical study for flow of a Newtonian fluid over an impermeable stretching sheet which embedded in a porous medium with a power law velocity surface and variable thickness in the presence of thermal radiation. Salahuddin et al., (2016) examined the

MHD flow of Cattanneo-Christov heat flux model for Williamson fluid over a stretching sheet with variable thickness. Some other important investigations related to variable thickness of the sheet were studied by (Anjali Devi and Prakash (2016), Prasad et al., (2016a), Salahuddin et al., (2017a, 2017b)).

It has been noticed that aforementioned investigators studied the impact of a stretching sheet with variable thickness by neglecting the effect of nanofluid. Practically, convectional heat transfer fluids, including oil, water, grease, ethylene glycol and engine oil contain low thermal conductivity in comparison with solids. To lead this difficult situation by adding small quantity of solid particles to the base fluids as a result thermophysical properties gradually increases and hence these are known as nanofluids. Choi (1995) was the first person who proposed the term as “nanofluid”. These are made up of minute particles namely, metals (Cu, Ag, Au), oxides (Al_2O_3, CuO), carbide ceramics (Sic, Tic/carbon nanotubes/fullerene) having size between 10nm -50nm. In modern days which grabbed more attention of various researchers due to their vast applications in science and engineering problems, such as microelectronic cooling, air conditioning, transpiration and ventilation etc. The Brownian motion and thermophoresis effects on heat and mass transfer analysis were examined by Buongirno (2006). Makinde and Aziz (2011) examined the impact of Brownian motion and thermophoresis on transport equations numerically. Sheikholeslami et al., (2016) studied the effect of viscous dissipation and thermal radiation on MHD nanofluid flow and heat transfer in an enclosure with constant element. Qayyum et al., (2016) analyzed the melting heat transfer in stagnation point flow of nanofluid towards a stretching surface with nonlinear thermal radiation. Vajravelu et al., (2017) studied the mixed convective flow and heat transfer with variable thickness in the presence of magnetic field. Qayyum et al., (2017a) examined the double diffusion heat and mass fluxes in mixed convection flow of Maxwell fluid bounded by variable stretchable sheet. Waqas et al., (2017a, 2017b) reported the characteristics of viscous dissipation and nonlinear radiation in the magneto slip flow of viscous liquid and also explained the characteristics of magneto nanofluid in flow of hyperbolic tangent fluid. Hussain et al., (2017) disclose the analysis for homogeneous heterogeneous reactions for Tiwari- Das nanofluid model. Ellahi et al., (2017) address the effects of melting heat and mixed convection in stagnation point flow of second grade nanofluid towards a nonlinear stretching sheet with variable thickness. Qayyum et al., (2017b) focuses on the modelling and analysis of MHD nonlinear convective flow of Jeffery nanofluid bounded by nonlinear stretching sheet with variable thickness. Ajayi et al., (2017) demonstrated the motion of two dimensional Casson nanofluid flows with temperature dependent plastic dynamic viscosity together with double stratification in the presence of Lorentz force. Zubair et al., (2018) studied nonlinear mixed convection characteristics in stagnation point flow of third grade fluid over a stretching sheet with variable thickness. Aziz et al., (2018) considered the combined effects of thermal stratification, applied electric and magnetic fields, thermal radiation and viscous dissipation on a boundary layer flow of electrically conducting nanofluid over a nonlinear stretching sheet with variable thickness. Ullah et al., (2018) explored the behaviour of double stratification and nanoparticles on MHD flow of second grade liquid bounded by nonlinear stretching of sheet having variable thickness. Lin and Lin (2018) implemented the boundary layer flow over a sheet with variable thickness with the time fractional Maxwell fluid. Hayat et al., (2018a) examined two dimensional stagnation point flow of third grade fluid towards a stretching surface. Daniel et al., (2018) explained the nonlinear stretching sheet with variable thickness for electrical magnetohydrodynamic boundary layer flow of nanofluid with combined influence of thermal radiation, viscous dissipation and joule heating. Recently, Farooq et al., (2019) investigated zero mass flux characteristics in Jeffery nanomaterial flow over a nonlinear stretchable sheet. Sugunamma et al., (2019) described a theoretical analysis on MHD flow of non-Newtonian nanofluid past a nonlinear variable thickness surface in the presence of nonlinear radiation and nonlinear convection. Hayat et al., (2019) predicted stagnation point flow of thixotropic nanofluid towards a variable thicked surface.

At present, the controlling flow of electrically conducting fluids such as liquid metals, plasma, electrolytes etc., is one of the major tasks to the scientists and engineers. These fluids can be significantly controlled by applying an external magnetic field, this mechanism is known as classical electro magneto hydrodynamic (EMHD) fluid flow which plays a vital role in science and industrial applications, few of them mentioned as engineering, geophysics, astrophysics, earth quakes, and sensors. Due to these applications, Gailitis and Lielausis (1961) of the physics institute in Riga, capital city of the Latvia country framed one of the devices known as Riga plate to generate simultaneous electric and magnetic fields which can produce Lorentz force parallel to the wall in weakly conducting fluids. This plate consists of span wise arranged array of alternating electrodes and permanent magnets mounted on the plane surface. Tsinober and Shtern (1961) observed the substantial improvement in the strength of the Blasius flow towards a Riga plate which is due to the greater influence of wall parallel Lorentz force. Further, Pantakratoras and Magyari (2009) extended the work of Gailitis and Lielausis (1961) to the boundary layer flow of low electrical conducting fluids over a Riga plate. Again Pantakratoras (2011) extended this work to the Blasius and Sakiadis flow. Bhatti et al., (2016) examined the boundary layer flow of nanofluid flow over an electrically conducting Riga plate. Anjum et al., (2016) considered the phenomenon of melting heat transfer in the stagnation point flow of viscous fluid towards a variable thicked Riga plate. Rashidi et al., (2017) analyzed the effects of thermal radiation and EMHD on viscous nanofluid over a horizontal Riga plate. Khan et al., (2017) described the convective heat transfer of electro-magnetohydrodynomic squeezed flow past a Riga plate. Ramzan et al., (2018) investigated the effects of a slip boundary condition over a convectively heated Riga plate in the flow of Williamson nanofluid. Recently, Hammouch et al., (2018) considered the two dimensional stagnation point flow of Walter B fluid over a Riga plate. Javed et al., (2018) discussed the variation of physical aspects of Cattanneo – Christov heat flux model on a Riga plate.

Keeping all the above industrial oriented mathematical modelling of the physical problem in mind, in the present thesis the author envisage to analyze the study of Newtonian/non-Newtonian fluid flow, heat, and mass transfer characteristics over a special form stretching sheet called slender elastic sheet with different physical situations, namely,

1. Analytical study of Cattaneo-Christov Heat Flux Model for Williamson-Nanofluid Flow Over a Slender Elastic Sheet with Variable Thickness
2. Influence of Variable Transport Properties on Casson Nanofluid Flow over a Slender Riga Plate: Keller Box Scheme
3. Mixed Convective Nanofluid Flow over a Coagulated Riga Plate in the Presence of Viscous Dissipation and Chemical Reaction.
4. Impact of Suction/Injection and Heat Transfer on Unsteady MHD Flow over a Stretchable Rotating Disk.

1.2 Basic Equations

In the present thesis, the following mathematical modelling of the equations have been used under different physical constraints. The main task in fluid dynamics is to find the velocity field describing the flow in a given domain. The following heat and mass transfer, mathematical modelling equations have been used to derive the governing equations under different physical constraints.

Continuity equation: $\dfrac{\partial u_1}{\partial x_1}+\dfrac{\partial u_2}{\partial x_2}=0$,

Momentum equation: $\dfrac{\partial u_1}{\partial t}+u_1\dfrac{\partial u_1}{\partial x_1}+u_2\dfrac{\partial u_1}{\partial x_2}=\upsilon\dfrac{\partial^2 u_1}{\partial x_2^2}$,

Heat transfer equation: $\dfrac{\partial T}{\partial t}+u_1\dfrac{\partial T}{\partial x_1}+u_2\dfrac{\partial T}{\partial x_2}=K\dfrac{\partial^2 T}{\partial x_2^2}$,

Mass transfer equation: $\dfrac{\partial C}{\partial t}+u_1\dfrac{\partial C}{\partial x_1}+u_2\dfrac{\partial C}{\partial x_2}=D_B\dfrac{\partial^2 C}{\partial x_2^2}$.

Where, u_1 and u_2 are the velocity components in x_1 and x_2 direction respectively, T is the temperature of the fluid and C is the concentration of the fluid. The parameters ν, K and D_B are respectively called the kinematic viscosity, thermal conductivity and Brownian diffusivity coefficient.

1.3 Boundary conditions

Boundary conditions are necessary for the solution of a boundary value problem. A boundary value problem is a differential (partial/ordinary) equation or system of differential equations to be solved in a domain or whose boundary a set of conditions is known. They rise naturally in every problem based on a differential equation. In any flow domain the flow equations must be subjected to a set of conditions that act at the domain of the boundary. The choice of boundary condition is fundamental for the resolution of the computational problem. These boundary conditions are classified as velocity boundary conditions, thermal boundary conditions and concentration boundary conditions.

Velocity boundary conditions

The velocity boundary conditions depend on the nature of the fluid flow and geometry of the boundary surface. Here, in this thesis, we consider a steady, incompressible flow of Newtonian/non-Newtonian fluid past a permeable/ impermeable stretching sheet with/ without convective. In this thesis the variable thickness of the sheet is considered, therefore the resulting velocity boundary conditions are,

$$u_1\left(x_1,x_2\right)= \ U_w=U_0(x_1+b)^m \qquad \text{at } x_2=A(x_1+b)^{1-m/2}$$

$$u_2\left(x_1,x_2\right)=\begin{cases}\pm \mathrm{V_w}, \text{ for permeable}\\ 0, \text{ for impermeable}\end{cases} \qquad \text{at } x_2=A(x_1+b)^{1-m/2}$$

$$u_1\left(x_1,x_2\right)\rightarrow 0 \text{ or } u_1\left(x_1,x_2\right)\rightarrow U_e(x_1)=U_\infty(x_1+b)^m \ \text{ as } x_2\rightarrow\infty$$

here U_w ,U_0 and U_e are velocities at the wall, stretching sheet and free stream, m is the velocity power index, A and b are small constants related to variable thickness of the sheet.

Thermal boundary conditions

Thermal boundary conditions depend on the type of the heating process under consideration. Here, we have considered prescribed power-law surface temperature (PST); melting heat transfer boundary condition and convective boundary condition (CBC), which are defined as fallow.

Prescribed power-law surface temperature (PST)

Here, the temperature boundary surface is prescribed a power law temperature of general degree. Mathematical representation of such a temperature boundary condition is defined below.

$$T=T_w\left(x_1\right)=A_1\left(x_1+b\right)^r \ \text{ at } x_2=A(x_1+b)^{(1-m)/2}$$

$$T\left(x_1,x_2\right)\rightarrow T_\infty \ \text{ as } \ x_2\rightarrow\infty.$$

Here, T is the temperature, T_w is the temperature field of the fluid at the wall, T_∞ is the temperature field of the fluid far away from the sheet, r is the temperature exponent parameter, A, A_1 and b are physical parameters related to variable thickness of the sheet, r is the temperature exponent parameter.

Melting heat transfer boundary condition

Here, heat transfer characteristics are studied by melting point heat transfer boundary condition, this is defined as below,

$K\left(\partial T/\partial x_2\right) = \rho\left[\lambda_1 + c_s(T_M - T_0)\right]\mathrm{u}_2(x_1, x_2),\ T = T_M$ at $x_2 = A(x_1+b)^{(1-m)/2}$ where K is the thermal conductivity, ρ is the temper of density fluid, λ_1 is the latent heat transfer, c_s is the characteristics heat at solid surface, T_M is the temperature at melting surface.

Convective boundary condition (CBC)

In this case the thermal boundary condition is defined in convective heat transfer form; mathematical expression of this condition is given below, $-K\left(\partial T/\partial x_2\right) = h_s\left(T - T_\infty\right)$ at $x_2 = A(x_1+b)^{(1-m)/2}$ where K is the thermal conductivity, c_s is the characteristics heat at solid surface, h_s is the convective heat transfer coefficient.

Concentration boundary conditions

The boundary conditions defined on the surface of the concentration is given by

$$C = C_w\left(x_1\right) = A_2\left(x_1+b\right)^s \text{ at } x_2 = A(x_1+b)^{(1-m)/2}$$
$$C\left(x_1, x_2\right) \to C_\infty \text{ as } x_2 \to \infty.$$

Where C is the concentration, s is the concentration exponent parameter, A, A_2 and b are physical parameters related to variable thickness of the sheet.

Zero mass flux nanoparticle boundary condition

Here, heat and mass transfer characteristics are analyzed by a zero mass flux nanoparticle boundary condition, which is defined by

$D_B\dfrac{\partial C}{\partial x_2} + \dfrac{D_T}{T_\infty}\dfrac{\partial T}{\partial x_2} = 0,$ at $x_2 = A(x_1+b)^{(1-m)/2}$, here D_B is the Brownian diffusion parameter, D_T is the thermophoresis diffusion parameter, C is the concentration, T is the Temperature, A and b are physical parameters related to variable thickness of the sheet.

1.4 Method of Solution

The mathematical problems are used in the present research work are governed by the usual mathematical equations, namely, continuity equation, momentum equation, energy equation and concentration equation. These governing equations are transformed into dimensionless form by using suitable similarity transformations. Obtained dimensionless equations are highly nonlinear coupled higher order differential equations which are very difficult to solve through known analytical methods. Therefore, in the present thesis, the following methods are used to solve the intricate boundary value problems and are described as below with suitable example.

1.4.1 Optimal Homotopy Analysis Method (OHAM)

Optimal Homotopy Analysis Method (OHAM) is a semi-analytical method which has been used to solve the coupled highly nonlinear differential equations. The system of OHAM gives great freedom to choose the auxiliary linear operators, initial guesses and base functions of the problem and which is always valid no matter whether there exist small or large parameters or not. This is achieved by inserting the non-zero auxiliary parameter known as "convergence control parameter". This is the main advantageous over other iterative techniques where convergence is largely tied to a good initial approximation of the solution. The OHAM has been successfully applied to a wide variety of nonlinear problems (for more details see, Liao (2010) and Van Gorder (2019)). Let us consider the non-linear differential equation of the form,

$$N\left[u(\eta)\right]=0 \tag{1.4.1.1}$$

where, N is the non-linear differential operator which acting on an unknown function $u(\eta)$ is the dependent variable and η is the independent variable. Consider auxiliary linear differential operator L. Now, construct a linear homotopy H between linear operator L and nonlinear operator N i.e.

$$(1-q)L\left[\varphi(\eta,q)-u_0(\eta)\right]=qhH(\eta)\,N\left[\varphi(\eta,q)\right], \tag{1.4.1.2}$$

such that $H(N,L;0)=L$ and $H(N,L;1)=N,$ where $q\in[0,1]$ is the embedding parameter and h is convergence control parameter. Here the function defined as $\lim\limits_{q\to 0}\varphi(\eta,q)=u_0(\eta)$ and $\lim\limits_{q\to 1}\varphi(\eta,q)=u(\eta),$ $u_0(\eta)$ is the initial guess which satisfies the given initial and boundary conditions, as q varies from initial guess $u_0(\eta)$ to the solution $u(\eta)$ of the non-linear differential Eq. (1.4.1.1). We have a great freedom to choose initial guess $u_0(\eta)$, auxiliary linear operator L, convergence control parameter h and these are properly chosen so that the solution $\varphi(\eta,q)$ exists for $q\in\left[0,1\right]$. Now, assume the solution of $\varphi(\eta)$ will take the Taylor's series method,

$$\varphi(\eta,q)=u_0(\eta)+\sum_{n=1}^{\infty}u_n(\eta)q^n,\ \text{where}\ u_n(\eta)=(1/n!)\left(\partial^n\varphi(\eta,q)/\partial q^n\right)\Big|_{q=0} \tag{1.4.1.3}$$

Define the vector $u_n=\{u_0(\eta),u_1(\eta),.....,u_n(\eta)\}$. Differentiating equation (1.4.1.2) n times with respect to embedding parameter q and then setting $q=0$ and dividing by $n!$ we get so called n^{th} order deformation equation as

$$L[u_n(\eta)-\chi_n u_{n-1}(\eta)]=h\,H(\eta)R_n(u_{n-1}) \tag{1.4.1.4}$$

where, $R_n(u_{n-1})=\dfrac{1}{(n-1)!}\dfrac{\partial^{n-1}N[\varphi(\eta,q)]}{\partial q^{n-1}}\Bigg|_{q=0}$ and $\chi_n=\begin{cases}0, & n\le 1\\ 1, & n>1\end{cases}$

This is called n^{th} order deformation equation for $n\ge 1$ and $H(\eta)=1$ is linear ordinary differential equation with boundary conditions which are present in original problem and hence which can be solved easily by the computational software such as Mathematica. To get the optimal value of convergence control parameter h, about which the series in equation (1.4.1.3) converges fastest, we evaluate squared residual error which is defined as,

$$E(h)=\int_{\Omega}\left(N\left[\sum_{k=0}^{n}u_k(\eta)\right]\right)^2 d\Omega \tag{1.4.1.5}$$

where $\sum_{k=0}^{n}u_k(\eta)$ is the k^{th} order approximation of OHAM. Hence convergence control parameter h corresponds to the minimum of $\Delta(h)$.

The above OHAM solution is explained through the following example

Consider the nonlinear differential equations,

$$\begin{aligned}&f'''(\eta)+f(\eta)f''(\eta)-f'^2(\eta)-Mnf'(\eta)=0,\\&\theta''(\eta)+\Pr(f(\eta)\theta'(\eta)-f'(\eta)\theta(\eta))=0.\end{aligned} \tag{1.4.1.6}$$

Respective boundary conditions are,

$$\begin{aligned}&f(0)=0,\ f'(0)=1,\ f'(\infty)=0,\\&\theta(0)=1,\theta(\infty)=0.\end{aligned}$$

In order to obtain Optimal Homotopy Analysis Method solutions of above equation, choosing the following initial guesses and linear operators

$$\begin{aligned}&f_0(\eta)=1-e^{-\eta},\quad \theta_0(\eta)=e^{-\eta},\\&L_f=\frac{d^3}{d\eta^3}-\frac{d}{d\eta},\quad L_\theta=\frac{d^2}{d\eta^2}-1,\end{aligned} \tag{1.4.1.7}$$

assuming $f(\eta)$ and $\theta(\eta)$ not only a function of η but also a function of embedding parameter $q \in [0,1]$, and denoting these as $\hat{f}(\eta,q)$ and $\hat{\theta}(\eta,q)$, we have the zeroth order deformation equation for equation (1.4.1.6) as

$$\begin{aligned}
&(1-q)L_f[\hat{f}(\eta,q)-f_0(\eta)] = q\hbar_f N_f[\hat{f}(\eta,q)],\\
&(1-q)L_\theta[\hat{\theta}(\eta,q)-\theta_0(\eta)] = q\hbar_\theta N_\theta[\hat{\theta}(\eta,q)],
\end{aligned} \tag{1.4.1.8}$$

with the respective boundary conditions,

$$\begin{aligned}
&f(0,q)=0,\ f'(0,q)=1,\ f'(\infty,q)=0,\\
&\theta(0,q)=1, \theta(\infty,q)=0.
\end{aligned}$$

Where $\hbar \neq 0$ is the convergence control parameter and $N_f[\hat{f}(\eta,q)]$ and $N_\theta[\hat{\theta}(\eta,q)]$ are non-linear operators defined as,

$$\begin{aligned}
&N_f[\hat{f}(\eta,q)] = \frac{d^3\hat{f}(\eta,q)}{d\eta^3} + \hat{f}(\eta,q)\frac{d^2\hat{f}(\eta,q)}{d\eta^2} - \frac{d\hat{f}(\eta,q)^2}{d\eta} - Mn\frac{d\hat{f}(\eta,q)}{d\eta},\\
&N_\theta[\hat{\theta}(\eta,q)] = \frac{d^2\hat{\theta}(\eta,q)}{d\eta^2} + \Pr\hat{f}(\eta,q)\frac{d\hat{\theta}(\eta,q)}{d\eta} - \Pr\frac{d\hat{f}(\eta,q)}{d\eta}\hat{\theta}(\eta,q).
\end{aligned}$$

From equation (1.4.1.8)

$$\begin{aligned}
q=0 \quad \text{implies} \quad & L_f[\hat{f}(\eta,0)-f_0(\eta)]=0,\\
& L_\theta[\hat{\theta}(\eta,0)-\theta_0(\eta)]=0,\\
\text{implies} \quad & \hat{f}(\eta,0)=f_0(\eta)\\
& \hat{\theta}(\eta,0)=\theta_0(\eta)\\
q=1 \quad \text{implies} \quad & N_f[\hat{f}(\eta,1)]=0,\\
& N_\theta[\hat{\theta}(\eta,1)]=0,\\
\text{implies} \quad & \hat{f}(\eta,1)=f(\eta),\\
& \hat{\theta}(\eta,1)=\theta(\eta),
\end{aligned}$$

so as the embedding parameter $q \in [0,1]$ increases from 0 to 1, the solutions $\hat{f}(\eta,q)$ and $\hat{\theta}(\eta,q)$ varies continuously from $f_0(\eta)$ to $f(\eta)$ and $\theta_0(\eta)$ to $\theta(\eta)$ respectively.

Hence, by definition,

$$\begin{aligned}
&f_m(\eta) = \frac{1}{m!}\frac{d^m f(\eta,q)}{d\eta^m}\bigg|_{q=0},\\
&\theta_m(\eta) = \frac{1}{m!}\frac{d^m\theta(\eta,q)}{d\eta^m}\bigg|_{q=0},
\end{aligned}$$

we expand $\hat{f}(\eta,q)$ and $\hat{\theta}(\eta,q)$ by means of Taylor's series as

$$\begin{aligned}
\hat{f}(\eta,q) &= f_0(\eta)+\sum_{m=1}^{\infty} f_m(\eta)q^m,\\
\hat{\theta}(\eta,q) &= \theta_0(\eta)+\sum_{m=1}^{\infty}\theta_m(\eta)q^m,
\end{aligned} \tag{1.4.1.9}$$

if the series (1.4.1.9) converges at $q=1$ we get the homotopy series solution as

$$\begin{aligned}
f(\eta) &= f_0(\eta)+\sum_{m=1}^{\infty} f_m(\eta),\\
\theta(\eta) &= \theta_0(\eta)+\sum_{m=1}^{\infty}\theta_m(\eta),
\end{aligned} \tag{1.4.1.10}$$

in the above equation (1.4.1.10), $f(\eta)$ and $\theta(\eta)$ contains an unknown convergence control parameter $\hbar \neq 0.$

mth order deformation equations and the conditions is given by

$$\begin{aligned}
L_f\left[f_m(\eta)-\chi_m f_{m-1}(\eta)\right] &= \hbar_f R_m{}^f(\eta),\\
L_\theta\left[\theta_m(\eta)-\chi_m\theta_{m-1}(\eta)\right] &= \hbar_\theta R_m{}^\theta(\eta),
\end{aligned} \tag{1.4.1.11}$$

with boundary conditions,

$$\begin{aligned}
&f_m(0)=0,\ f_m{}'(0)=0,\ f_m{}'(\infty)=0,\\
&\theta_m(0)=1, \theta_m(\infty)=0.
\end{aligned}$$

Where,

$$\begin{aligned}
R_m{}^f &= f'''_{m-1}(\eta)+\sum_{k=0}^{m-1} f''_{m-1-k}\, f_k-\sum_{k=0}^{m-1} f'_{m-1-k}\, f'_k - Mn\, f'_{m-1}(\eta),\\
R_m{}^\theta &= \theta''_{m-1}(\eta)+\Pr\sum_{k=0}^{m-1}\theta'_{m-1-k}\ f_k-\Pr\sum_{k=0}^{m-1} f'_{m-1-k}\theta_k(\eta),
\end{aligned} \tag{1.4.1.12}$$

and $\chi_m=\begin{cases}0, m\le 1\\ 1, m>1\end{cases}.$

The equations (1.4.1.11) is a linear ordinary differential equations that can be easily solved. Now in order to obtain the optimal value of $\hbar$, we evaluate the error and minimize it over $\hbar$.

Error Analysis

For the m^{th} order deformation equation, the exact residual error is given by

$$\hat{E}_m{}^f(\hbar)=\int_0^\infty\left(N_f\left[\sum_{n=0}^{m} f_n(\eta)\right]\right)^2 d\eta,$$

$$\hat{E}_m^{\theta}(\hbar)=\int_0^{\infty}\left(N_{\theta}\left[\sum_{n=0}^{m}f_n(\eta),\sum_{n=0}^{m}\theta_n(\eta)\right]\right)^2 d\eta,$$

Average residual error is defined as:

$$E_m^{f}(\hbar)=\frac{1}{M+1}\sum_{k=0}^{M}\left(N_f\left[\sum_{n=0}^{m}f_n(\eta_k)\right]\right)^2,$$

$$E_m^{\theta}(\hbar)=\frac{1}{M+1}\sum_{k=0}^{M}\left(N_f\left[\sum_{n=0}^{m}f_n(\eta_k)\right],N_{\theta}\left[\sum_{n=0}^{m}\theta_n(\eta_k)\right]\right)^2,$$

where, $\eta_k=k\Delta\eta=\dfrac{k}{M},k=0,1,2,....M$

Now the error function $E_m(\hbar)$ is minimized over $\hbar$ and optimal value of $\hbar$ is obtained, substituting this optimal value in equation (1.4.1.10) we get the approximate solution of (1.4.1.6) with B.C's.

1.4.2 Keller box method

The systems of highly nonlinear coupled differential equations along with respective boundary conditions are solved by finite difference scheme known as Keller box method (see, Vajravelu and Prasad (2014)). This system is not conditionally stable and has a second order accuracy with arbitrary spacing. For solving this system first write the differential equations and respective boundary conditions in terms of first order system, which is then, converted into a set of finite difference equations using central difference scheme. Since the equations are highly nonlinear and cannot be solved analytically, therefore these equations are solved numerically using the symbolic software known as Fedora. Further nonlinear equations are linearized by Newton's method and resulting linear system of equations is solved by block tri-diagonal elimination method. For the sake of brevity, the details of the solution process are not presented here. For numerical calculations, a uniform step size is taken which gives satisfactory results and the solutions are obtained with an error tolerance of 10^{-6} in all the cases. To demonstrate the accuracy of the present method, the results for the dimensionless Skin friction, Nusselt number and Sherwood number are compared with the previous results. The main features of this method are

- Only slightly more arithmetic to solve than the Crank-Nicolson method.
- Second order accuracy with arbitrary (non-uniform) x and y spacing.
- Allow very rapid x variations.

- Allow easy programming of the solution of large numbers of coupled equations.

The solution of an equation by this method can be obtained by the following four steps.

1. Reduce the equation or equations to a first order system.
2. Write difference equations using central difference scheme.
3. Linearize the algebraic equations (if they are nonlinear), and write them in matrix vector form.
4. Solve the linear system by the block- tridiagonal-elimination method.

The above Keller box method can be illustrated through the following example

Consider the equation $\frac{\nu}{\Pr}\frac{\partial^2 T}{\partial y^2} = u\frac{\partial T}{\partial x}$.

To solve the above equation by numerically, first express it in terms of a system of two first-order equations by letting $T' = p$ and $p' = \frac{\Pr}{\nu}u\frac{\partial T}{\partial x}$. (1.4.2.1)

Here the primes denote differentiation with respect to *y*. The finite difference form of the ordinary differential equation (1.4.2.1) is written for the midpoint $\left(x_n, y_{j-1/2}\right)$ of the segment $p_1 p_2$ shown in Fig 1.1, and the finite difference form of the partial differential equation (1.4.2.1) is written for the midpoint $\left(x_{n-1/2}, y_{j-1/2}\right)$ of the rectangle $p_1 p_2 p_3 p_4$. This gives

$$\frac{T_j^n - T_{j-1}^n}{h_j} = \frac{p_j^n + p_{j-1}^n}{2} = p_{j-1/2}^n, \frac{1}{2}\left(\frac{p_j^n - p_{j-1}^n}{h_j} + \frac{p_j^{n-1} - p_{j-1}^{n-1}}{h_j}\right) = \frac{\Pr}{\nu}u_{j-1/2}^{n-1/2}\frac{T_{j-1/2}^n - T_{j-1/2}^{n-1}}{k_n}. \quad (1.4.2.2)$$

Rearranging both expressions in the form

$$T_j^n - T_{j-1}^n - \frac{h_j}{2}\left(p_j^n - p_{j-1}^n\right) = 0, \left(S_1\right)_j p_j^n + \left(S_2\right)_j p_{j-1}^n + \left(S_3\right)_j \left(T_j^n - T_{j-1}^n\right) = R_{j-1/2}^{n-1} \quad (1.4.2.3)$$

Here $\left(S_1\right)_j = 1, \quad \left(S_2\right)_j = -1, \quad \left(S_3\right)_j = -\lambda_j/2, R_{j-1/2}^{n-1} = -\lambda_j + T_{j-1/2}^{n-1} + p_{j-1}^{n-1} - p_j^{n-1}$ (1.4.2.4)

$$\lambda_j = \frac{2\Pr}{\nu}u_{j-1/2}^{n-1/2}\frac{h_j}{k_n}.$$

As before, the superscript on $u_{j-1/2}$ is not necessary but is included for generality. Equations (1.4.2.3) are imposed for $j = 1, 2, ..., J-1$. $A_j = 0$ and for *J*, we have

$$T_0 = T_w \;, T_J = T_e \tag{1.4.2.5}$$

respectively. Since equation(1.4.2.3) is linear as are the corresponding boundary conditions given by equation (1.4.2.5), the system may be written at once in matrix

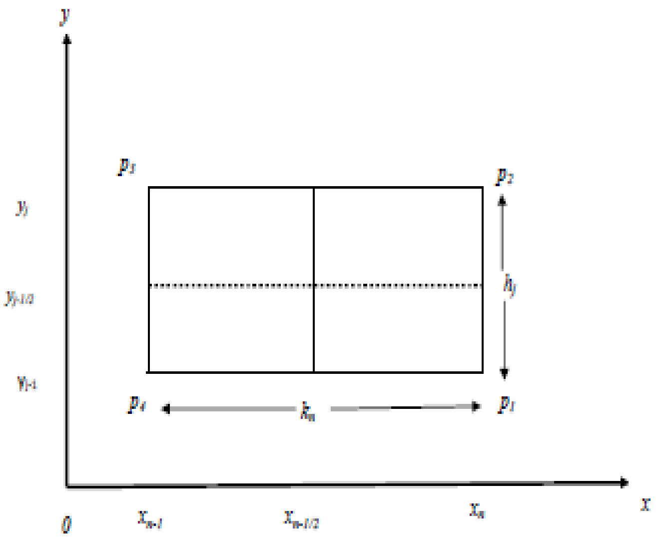

Fig.1.1. Finite difference grid for the Box method.

Note that both h and k can be non-uniform. Here $x_{n-1/2} = 1/2\left(x_n + x_{n-1/2}\right)$ and $y_{j-1/2} = 1/2\left(y_j + y_{j-1}\right)$.

The system of linear equations with the boundary conditions may be written once in matrix vector form as shown below without the linearization needed in the case of the finite difference equations for the velocity field.

$$\begin{bmatrix} 1 & 0 & 0 & 0 & & \\ -1 & \frac{-h_1}{2} & 1 & \frac{-h_1}{2} & & \\ (S_3)_j & (S_2)_j & (S_3)_j & (S_1)_j & 0 & 0 \\ 0 & 0 & -1 & \frac{-h_{j+1}}{2} & 1 & \frac{-h_{j+1}}{2} \\ & & (S_3)_J & (S_2)_J & (S_3)_J & (S_1)_J \\ & & 0 & 0 & 1 & 0 \end{bmatrix} \times \begin{bmatrix} \begin{pmatrix} T_0 \\ p_0 \end{pmatrix} \\ \begin{pmatrix} T_j \\ p_j \end{pmatrix} \\ \begin{pmatrix} T_J \\ p_J \end{pmatrix} \end{bmatrix} = \begin{bmatrix} \begin{pmatrix} (r_1)_0 \\ (r_2)_0 \end{pmatrix} \\ \begin{pmatrix} (r_1)_j \\ (r_2)_j \end{pmatrix} \\ \begin{pmatrix} (r_1)_J \\ (r_2)_J \end{pmatrix} \end{bmatrix}. \tag{1.4.2.6}$$

$$\left(r_1\right)_0 = T_w \;, \left(r_1\right)_j = R_{j-1/2}^{n-1}, \quad 1 \le j \le J \quad \left(r_2\right)_j = 0, \; 1 \le j \le J-1, \quad \left(r_2\right)_J = T_e. \tag{1.4.2.7}$$

The system of equations given by equation (1.4.2.6) can be written as

$$A\delta = r, \tag{1.4.2.8}$$

Where $\begin{bmatrix} A_0 & C_0 & & & & \\ B_1 & A_1 & C_1 & & & \\ & & B_J & A_j & C_j & \\ & & & B_{J-1} & A_{J-1} & C_{J-1} \\ & & & & B_J & A_J \end{bmatrix}$, $\delta = \begin{bmatrix} \delta_0 \\ \delta_1 \\ . \\ \delta_j \\ . \\ \delta_J \end{bmatrix}$, $r = \begin{bmatrix} r_0 \\ r_1 \\ . \\ r_j \\ . \\ r_J \end{bmatrix}$ (1.4.2.9)

$$\delta_j = \begin{bmatrix} T_j \\ p_j \end{bmatrix} , \; r_j = \begin{bmatrix} (r_1)_j \\ (r_2)_j \end{bmatrix} \tag{1.4.2.10}$$

and A_j, B_j, C_j are 2×2 matrices defined as follows

$$A_0 \equiv \begin{bmatrix} 1 & 0 \\ -1 & \frac{-h_1}{2} \end{bmatrix}, \; A_j \equiv \begin{bmatrix} (S_3)_j & (S_1)_j \\ -1 & \frac{-h_{j+1}}{2} \end{bmatrix}, 1 \le j \le J-1$$

$$A_J \equiv \begin{bmatrix} (S_3)_J & (S_1)_J \\ -1 & 0 \end{bmatrix}, B_J \equiv \begin{bmatrix} (S_3)_J & (S_2)_J \\ 0 & 0 \end{bmatrix}, 1 \le j \le J, \;\; C_j \equiv \begin{bmatrix} 0 & 0 \\ 1 & \frac{-h_{j+1}}{2} \end{bmatrix}, 1 \le j \le J-1 \tag{1.4.2.11}$$

Note that, as in the Crank-Nicolson method, the implicit nature of the method has again generated a tridiagonal matrix, but the entries are 2×2 blocks rather than scalars. The solution of equation (1.4.2.8) by the block-elimination method consists of two sweeps. In the forward sweep we compute Γ_j, Δ_j, and w_j from the recursion formulas given by

$$\Delta_0 = A_0, \; \Gamma_j \Delta_{j-1} = B_j, \; \Delta_j = A_j - \Gamma_j C_{j-1} \quad 1 \le j \le J, \tag{1.4.2.12}$$

$$w_0 = r_0 \;, w_j = r_j - \Gamma_j w_{j-1} \quad 1 \le j \le J. \tag{1.4.2.13}$$

Here Γ_j has the same structure as B_j, that is, $\Gamma_j \equiv \begin{bmatrix} (\gamma_{11})_j & (\gamma_{12})_j \\ 0 & 0 \end{bmatrix}$, and although the second row of Δ_j has the same structure as the second row of A_j,

$$\Delta_j \equiv \begin{bmatrix} (\alpha_{11})_j & (\alpha_{12})_j \\ -1 & \frac{-h_{j+1}}{2} \end{bmatrix}.$$

For generality, we write it as $\Delta_j \equiv \begin{bmatrix} (\alpha_{11})_j & (\alpha_{12})_j \\ (\alpha_{21})_j & (\alpha_{22})_j \end{bmatrix}$. In the backward sweep, δ_j is computed from the following recursion formulas: $\Delta_J \delta_J = w_J, \Delta_j \delta_j = w_j - C_j \delta_{j+1}$, $j = J-1, J-2, ..., 0.$

1.5 Dimensionless parameters

To know the relative importance of each term in the equation, we make the equations dimensionless. Dimensional analysis provides information on the qualitative behaviour of the physical problem. The dimensionless parameters help us to understand the physical significance of a particular phenomenon associated with the problem. Generally there are two methods are used for obtaining the dimensionless parameters namely,

- The inspectional analysis
- The dimensionless analysis.

In the inspection analysis, the fundamental equations are reduced to a non-dimensional form and non-dimensional parameters are obtained from the resulting equations. In dimensional analysis, non-dimensional parameters are obtained from the physical quantities occurring in the problem, even when the knowledge of the governing equations is missing. In this research work the second method has been used. The dimensionless parameters used in the thesis are as given below;

Biot number

The Biot number is dimensionless quantity used in heat transfer calculations. It gives a simple index of the ratio of the heat transfer resistance inside and at the surface of body. In mathematical form it can be expressed as $Bi = h_s \left(L_c / K_b \right)$, where h_s is heat transfer coefficient or convective heat transfer coefficient, L_c is the characteristic length, K_b thermal conductivity of the body,

Brownian motion parameter

The random motion of nanoparticles within the base fluid is called Brownian motion and results from continuous collisions between the nanoparticles and the molecules of the base fluid. The nanoparticles themselves can be viewed effectively as large molecules with an average kinetic energy equal to that of the fluid molecules

$(k_B T/2)$ and thus with a considerable lower velocity. Brownian motion is described by the Brownian diffusion coefficient D_B, which is given by the Einstein-Stokes's equation as $D_B = K_B T / 3\pi\mu d_p$. Here K_B is the Boltzmann's constant, d_p is the nanoparticle diameter and T is the nanofluid temperature. Brownian motion parameter is defined as $Nb = \tau D_B \left(C_w - C_\infty\right)/\nu$.

Chemical reaction parameter

It is a dimensional parameter which is defined as the ratio of reaction rate to the reference velocity and mathematically expressed as $K_c = K_1/U_0$. Where is K_1 the reaction rate and U_0 reference velocity. Physically, $K_c > 0$ gives a destructive chemical reaction and for $K_c < 0$ yields constructive chemical reaction, whereas $K_c = 0$ shows the absence of chemical reaction.

Concentration buoyancy parameter

The dimensionless quantity $\lambda_C = \beta_C (C_w - C_\infty)/\beta_T (T_w - T_\infty)$, which characteristics the mass diffusion species, is known as concentration buoyancy parameter, where g is the acceleration due to gravity, β_C is the coefficient of species expansion, C_w and C_∞ are two species concentration at the wall and free stream.

Eckert number

Eckert number $Ec = U^2 / c_p (T_w - T_\infty)$, is a dimensionless number used to study the energy dissipation of the fluid flow. Here U, c_p T_w and T_∞ are called velocity of the fluid, specific heat at constant pressure, temperature at the wall and free stream respectively; it is introduced by German scientist, E.R.G. Eckert.

Fluid viscosity parameter

It is a dimensionless number which describes the internal friction of a moving fluid. A fluid with large viscosity resists motion because its molecular makeup gives it a lot of internal friction. It is defined as $\theta_r = 1/\left[\delta\left(T_w - T_\infty\right)\right]$, where T_w is the sheet temperature and T_∞ is the temperature far away from the sheet.

Hartman number/ Magnetic parameter

It is defined as the ratio of electromagnetic force to the viscous force and it was introduced by Hartman to describe his experiments with viscous MHD flow. The magnitude of Hartman number indicates the relative effects of magnetic and viscous drag force. For the lower value of Mn the Lorentz force is very small and it implies the low or moderate conductivities of the fluid. Mathematically, it can be expressed as $Mn = \sigma B_0^2 / \rho c_0$, where σ is the electrical conductivity and B_0 is the electric field strength, ρ is the density of the fluid, c_0 is a constant.

Heat Source/Sink Parameter

It is defined as the ratio of volumetric heat to the density of the fluid at specific gravity and constant pressure. It is a system of units designed to supply heat consistently and safely over a wide range of extreme conditions. A heat sink is an object that transfers thermal energy from a higher temperature to a lower temperature fluid medium. It is defined as the ratio of volumetric heat to the density of the fluid at specific gravity and constant pressure. $\lambda = Q_0 / \rho c_p U_0$, where Q_0 represents the temperature – dependent volumetric rate of heat source when $Q_0 > 0$ and heat sink when $Q_0 < 0$. These deal with the situation of exothermic and endothermic chemical reactions respectively.

Lewis number

Lewis number is a dimensionless number which the ratio of thermal diffusivity and mass diffusivity. This is used to characterize the flows in which there is simultaneous heat and mass transfer (convection). Which is mathemtically expressed as $Le = \nu / D_B$ where ν is the kinematic viscosity and D_B is the species diffusivity respectively. If $Le > 1$ gives predominance of constructive boundary layer. If $Le = 1$ gives the presence of velocity boundary layer which hinders the transport of heat and mass.

Modified Hartman number

The modified Hartman number is a dimensionless parameter which is defined as fallow $Q = \pi j_0 M_0 x_1 / 8 \rho U_w^2$, where j_0 is the applied current density in the electrodes,

M_0 is the magnetization of the permanent magnets mounted on the surface of the Riga plate, b is constant related to variable thickness, ρ is the density of the fluid, U_w is the velocity of the sheet.

Nusselt number

The Nusselt number is a dimensionless parameter associated with heat transfer problems and it is defined as the ratio of actual heat transfer rate to the rate which heat would be transported by the conduction alone for given temperature difference between the plates. It is used to study the heat transfer characteristics of the fluid; it is named after German engineer Ernst Wilhelm Nusselt. It can be mathematically expressed as $Nu = q_w(x_1+b)/(T_w - T_\infty)$, where $q_w = \partial T/\partial x_2$ at $x_2 = A(x_1+b)^{(1-m)/2}$ is the convective heat transfer coefficient.

Prandtl number

The ratio of the kinematic viscosity to the thermal diffusivity of the fluid i.e. $\Pr = \nu/\alpha_1 = \mu c_p / K$ is called as the Prandtl number named after the German scientist Ludwig Prandtl. Here ν is the kinematic viscosity, α_1 is the thermal diffusivity, μ is the dynamic viscosity, c_p is the specific heat at constant pressure and K is the thermal conductivity. It is a measure of the relative importance of heat conduction and viscosity of the fluid. The Prandtl number varies from fluid to fluid. For air $\Pr = 0.7$ (approx) and for water at $60F^\circ$, $\Pr = 7.0$ (approx), for liquid metals Prandtl number is very small and it may be very large for viscous fluids.

Reynolds Number

The dimensionless quantity Re is defined as the ratio of inertial forces to viscous forces i.e. $\mathrm{Re} = UL_\rho/\mu = UL/\nu$, where $U, L, \rho, \mu,$ and ν are velocity, length, density and dynamic viscosity/ kinematic viscosity respectively, is known as the Reynolds number in honour of the British scientist Osborne Reynolds, who in 1883 demonstrated the importance of Re in the dynamic of the viscous fluid. If Re is very small, then the viscous forces will predominant and the effect of viscosity will be felt in the whole flow field. On the other hand, if Re is large, the inertial forces will be predominant and in such a case, the effect of viscosity can be considered to be confined in a thin layer known as boundary layer adjacent to a solid boundary. However, if Re is very large the flow ceases to be laminar and becomes turbulent. The Reynolds number at which the transition, from laminar to turbulent, occurs is known as critical Reynolds number.

Schmidt number

Schmidt number is a dimensionless number defined as the ratio of momentum diffusivity to the mass diffusivity, and is used to characterized fluid flows in which there are simultaneous momentum and mass diffusion convection processes. It was named after the German engineer Ernst Heinrich Wilhelm Schmidt (1892-1975). Mathematically Schmidt number is given as $Sc = \gamma / D_B$, where γ is the kinematic viscosity and D_B is the species diffusivity respectively.

Sherwood number

The Sherwood number (or the mass transfer Nusselt number) is a dimensionless number used in mass transfer mechanism. It is defined as the ratio of convective mass transfer to the conductive mass transfer, and is named in honour of Thomas Kilgore Sherwood. It is defined as $Sh = j_w (x_2 + b) / (C_w - C_\infty)$, where $j_w = \partial C / \partial x_2$ at $x_2 = A(x_1 + b)^{(1-m)/2}$ is the mass transfer coefficient, D_C is the mass diffusion.

Skin friction

The dimensionless shearing stress on the surface of the body, due to a fluid motion is known as skin friction coefficient and defined as $C_f = \tau_w / U_w^2$, where $\tau_w = v \partial u / \partial x_2$ at $\eta = 0$ is surface shearing stress.

Suction or injection parameter

Suction or injection parameter f_w is defined as $f_w = -(\mathrm{v}_s / U)(2m/m+1)\mathrm{Re}^{1/1+m}$, where v_s is the suction/ blowing velocity across the stretching sheet. (Here, $f_w > 0$ corresponds to suction whereas $f_w < 0$ corresponds to injection).

Thermal buoyancy parameter

The dimensionless quantity $\lambda_T = \pm g\beta_T(T_w - T_\infty)/U_0^2(x_1 + b)^{2m-1}$, which characteristics the free convection, is known as Thermal buoyancy parameter, where g in the acceleration due to gravity, β_T the co-efficient of thermal expansion, b is the constant related to variable thickness, T_w and T_∞ are temperatures at the wall and free stream.

Thermophoresis parameter

Thermophoresis is a mechanism in which the hot particle move from hot region to a cold region and consequently temperature rises, it is mathematically expressed as $Nt = \tau D_T\left(T_w - T_\infty\right)/T_\infty \nu$.

1.6 Nomenclature

a_1	Width of magnets between electrodes
a_2	Constant
A^*	Stretching rate ratio parameter
A, b	Physical parameters related to stretching sheet
B, B_0	Magnetic field and magnetic field strength $(tesla)$
Bi	Biot number
C	Concentration of the stretching sheet
C_f	Skin friction coefficient
C_M	Concentration at melting surface
C_w	Concentration at the wall
c_p	Specific heat at constant pressure $(J\,kg^{-1}K^{-1})$
c_s	Surface heat capacity parameter
C_∞	Ambient concentration/ concentration far away from the sheet
D_B	Brownian diffusion coefficient $(kgm^{-1}s)$
D_T	Thermophoresis diffusion coefficient $(kgm^{-1}s\,K)$
e_{ij}	The rate of deformation at $(i,\ j)^{th}$ components
E	Electrical field (NC^{-1})
Ec	Eckert number
F, f	Dimensionless velocities (ms^{-1})
f_w	Mass suction/injection parameter
F_1	Force (N)
g	Dimensionless velocities (ms^{-1})
h_s	Heat transfer coefficient/ wall heat transfer
j_0	Applied current density in the electrodes (Am^{-2})
K	The thermal conductivity of the fluid $(Wm^{-1}K^{-1})$
K_1	Chemical reaction rate
K_c	Chemical reaction parameter
Le	Lewis number
m	Velocity power index parameter
M	Dimensionless melting point parameter
M_0	Magnetization parameter $(tesla)$
Mn	Hartman number/Magnetic parameter $(tesla)$
Nb	Brownian motion parameter
Nt	Thermophoresis parameter
$\Pr$	Prandtl number
q	Heat flux per unit area (Wm^{-2})
Q	Modified Hartmann number
Q_0	Heat generation/absorption parameter $(Wm^{-3}K^{-1})$

T	Temperature (K)
S	Unsteady parameter
Sc	Schmidt number
T_0	Solid temperature (K)
T_M	Temperature at melting surface (K)
T_w	Temperature at the wall (K)
T_∞	Ambient temperature/temperature far away from the sheet (K)
u_1, u_2	Velocity components in x_1 and x_2 directions (ms^{-1})
u_r, u_∞, u_z	Velocity components in direction of cylindrical coordinate system r, θ*,z (ms^{-1})
U_0	Reference velocity (ms^{-1})
U_e	Free stream velocity (ms^{-1})
U_w	Stretching velocity (ms^{-1})
V	Velocity vector
x_1, x_2	Cartesian coordinates
We	Weissenberg number

Greek Symbols

α	Wall thickness parameter/stretching parameter (m)
α_1	Thermal diffusivity
β	Casson parameter
β_1	Dimensionless parameter
β_C	Concentration expansion coefficient
β_T	Thermal expansion coefficient
γ	Thermal relaxation parameter $(m^2 s^{-1})$
Γ	Williamson parameter
δ	Dimensional constant
ε_1	Variable thermal conductivity parameter
ε_2	Variable species diffusivity parameter
η, ξ	Similarity variables
λ	Heat source/sink parameter
λ_2	Thermal relaxation time
λ_C	Concentration buoyancy parameter
λ_T	Thermal buoyancy parameter
μ	Dynamic viscosity $(Ns\,m^{-2})$
μ_B	Plastic dynamic viscosity
μ_∞	Ambient viscosity parameter
ν	Kinematic viscosity $(m^2 s^{-1})$
Ω	Angular velocity $(m^2 s^{-1})$
π	Product of deformation rate

π_c	Critical value of product of deformation rate
ϕ	Dimensionless concentration
ρ_∞	Fluid density (kgm^{-3})
ψ	Stream function $(m^2 s^{-1})$
σ	Electrical conductivity (Sm^{-1})
θ	Dimensionless temperature (K)
θ_r	Fluid viscosity parameter $(Pa\,s)$
τ_∞	Effective heat capacity of nanoparticle $(J\,K^{-1})$
τ_{zr}	Radial shear stress
$\tau_{r\theta}$	Tangential shear stress

Subscripts

∞	Condition at infinity
w	Condition at the wall
'	Differentiation with respect to η

CHAPTER - 2

ANALYTICAL STUDY OF CATTANNEO CHRISTOV HEAT FLUX MODEL FOR WILLIAMSON – NANOFLUID FLOW OVER A SLENDER ELASTIC SHEET WITH VARIABLE THICKNESS

Part of this work was published in the "*Journal of Nanofluids"*, *American Scientific Publication (ASP)*, Vol.7 (3), 583-594, 2018.

2.1. Introduction

The technological industry has embraced several methodologies to improve the efficiency of the heat transfer, namely, utilization of extended surfaces, application of vibration to the heat transfer surfaces, and usage of microchannels. The thermal conductivity of a fluid plays a vital role in the process of improving the efficiency of the heat transfer. Most commonly used heat transfer fluids are water, ethylene glycol, and engine oil which are with relatively low thermal conductivities in comparison with solids. The addition of small quantity of solid particles with high thermal conductivity to the base fluid (ethylene glycol + water, water + propylene glycol etc.,) results in an increase in the thermal conductivity of a fluid. The Argonne National Laboratory revisited the concept of enhancement of thermal conductivity of a fluid by considering suspensions like nano scale metallic particle and carbon nanotube suspensions and several things remain intangible about this nanostructured material suspension, which has been coined as "nanofluids" by Choi (1995). However, Masuda et al., (1993) have observed the similar kind of results earlier to Choi (1995). The term nanofluid attracted numerous researchers, which is a new kind of heat transfer medium with nanoparticles (1–100 nm) which are uniformly disseminated in the base fluid. Choi and Eastman (1995) documented that nanofluids exhibit high thermal conductivities compared to other heat transfer fluids and concluded by establishing a dramatic reduction in the heat exchanger pumping power. Moreover, the temperature is one more impartment aspect in the enhancement of thermal conductivity of nanofluids. Das et al., (2003), Chon and Kihm (2005), Li and Peterson (2006) have conducted experimental studies on the determination of the thermal conductivity of nanofluids at room temperature and Murshed et al., (2008) has reported an experimental and theoretical study on the thermal conductivity and viscosity of nanofluids and concluded that the thermal conductivity of nanofluids depends strongly on temperature. Literature survey reveals that the behavioral study of nanofluids was mainly done by numerous researcher using two models, that is, the Tiwari and Das model (2007) and Buongiorno model. Buongiorno (2006) model explains the effects of thermophysical properties of the nanofluid and also focus on the heat transfer enhancement observed in convective situations. Further, Zahmatkesh (2008) invoked hybrid Eulerian – Lagrangian procedure to evaluate the air flow and temperature distribution and analyzed the importance of thermophoresis as well as Brownian diffusion in the process of particle deposition. The model used by Rana and

Bhargava (2012) for the nanofluid incorporates the effects of Brownian motion and thermophoresis. Rashidi et al., (2014a) examined the model used by Rana and Bhargava (2012) by considering the effects of suction or injection. Many researchers have focused on the behaviour of nanofluid using Buongiorno model with different geometry (Khan and Aziz (2011), Makinde and Aziz (2011), Bachok et al., (2012), Prasad et al., (2015, 2016a)).

Heat transfer mechanism in several significant situations was classically explained by Fourier's law of heat conduction by Fourier in (1822). In spite of being the most successful model for the description of heat transfer mechanism, it has a major limitation such as this law leads to parabolic energy equation for the temperature field which contradicts with the principle of causality. The pioneering work of Cattaneo (1948) has managed to provide a successful alternative to the Fourier's law of heat conduction with the vital characteristic of thermal relaxation time to present "thermal inertia", which is popularly known as Maxwell-Cattaneo law. Moreover, Cattaneo-Christov heat flux model is the improved version of Maxwell Cattaneo's model in which Christov (2009) replaced the time derivative with the Oldroyd's Upper-Convected derivative to preserve the material-invariant formulation. Several researchers used Cattaneo-Christov heat flux model on Newtonian/non-Newtonian fluids with different physical constraints (Liu et al., (2016), Hayat et al., (2016a), Tanveer et al., (2016), Nadeem and Muhammad (2016) and Hayat et al., (2017a)).

All the above-mentioned researchers restricted their analyses to study the boundary layer flow over a linear or nonlinear stretching sheet in a thermally stratified environment which has several engineering applications. However, not much work has been carried out for a special type of nonlinear stretching (that is, stretching sheets with variable thickness; for details, see Fang et al., (2012)). The stretching sheet variable thickness has applications to the vibration of orthotropic plates and is observed in many engineering applications more frequently than a flat surface such as machine design, architecture, nuclear reactor technology, naval structures, and acoustical components. Ishak et al., (2007) examined the boundary layer flow over a horizontal thin needle and Ahmed et al., (2008) analyzed mixed convection flow over a vertically moving thin needle. Recently, Khader and Megahed (2015), Salahuddin et al., (2016), Prasad et al., (2017a, 2017b) analyzed the effects of various physical parameters on the flow and heat transfer by considering this special form of nonlinear stretching sheet. In the present analysis, Optimal Homotopy Analysis Method

(OHAM) (Liao (2003, 2007), Fan and You (2013)) is applied for obtaining the solutions of nonlinear BVPs. We carry out an analytical study to observe the impact of Cattaneo – Christov heat flux model on the flow of Williamson fluid over a slender elastic sheet with variable thickness. The obtained results are analyzed graphically for different sundry variables and analysis reveals that the fluid flow is appreciably influenced by the physical parameters. It is expected that the results presented here will not only complement the existing literature but also provide useful information for industrial applications.

2. 2. Mathematical Formulation of the Williamson -Nanofluid Model

Consider a steady two-dimensional boundary layer flow, heat and mass transfer of a viscous incompressible and electrically conducting non-Newtonian Williamson fluid with nanoparticles, in the presence of a transverse magnetic field $B(x_1)$, past an impermeable stretching sheet ($u_{2w} = 0$, see Liao (2007)) with variable thickness. The origin is located at the slit, through which the sheet is drawn in the fluid (see Fig. 2.2.1 for details). The x_1-axis is chosen in the direction of the motion and the x_2-axis is perpendicular to it. The stretching velocity of the surface is $U_w(x_1) = U_0\left(x_1 + b\right)^m$ where U_0 is constant, *b* is the physical parameter related to stretching sheet, and *m* is the velocity exponent parameter. Here $\mathrm{T_w}$ and $\mathrm{C_w}$ are respectively the constant surface temperature and the constant nanoparticle species diffusion. Cattaneo – Christov heat flux model is used instead of Fourier's law to explore the heat transfer characteristic. We assume that the sheet is not flat but rather is defined as $x_2 = \mathrm{A}\left(x_1 + b\right)^{(1-m)/2}$. The coefficient A is chosen as a small constant so that the sheet is sufficiently thin to avoid a measurable pressure gradient along the sheet $(\partial \mathrm{p}/\partial \mathrm{x}_1 = 0)$. For different applications, due to the acceleration or deceleration of the sheet, the thickness of the stretched sheet may decrease or increase with distance from the slot, which is dependent on the value of the velocity power index *m*. The problem is valid for $m \neq 1$, since $m = 1$ refers to the flat sheet case. Viscous and Joule dissipation were neglected. The physical model of the Williamson nanofluid is shown in Fig2.2.1.

Under such assumptions, and by using the usual boundary layer approximation, the governing equations for basic steady conservation of mass, momentum, thermal energy and nanoparticles equations for the non-Newtonian Williamson fluid with nanoparticles can be written in Cartesian coordinates x_1 and x_2 as (see, Salahuddin et al., (2016), Prasad et al., (2017b))

$$\frac{\partial u_1}{\partial x_1}+\frac{\partial u_2}{\partial x_2}=0 \tag{2.2.1}$$

$$u_1\frac{\partial u_1}{\partial x_1}+u_2\frac{\partial u_2}{\partial x_2}=\nu\left(\frac{\partial^2 u_1}{\partial x_2^2}+\sqrt{2}\,\Gamma\left(x_1\right)\frac{\partial u_1}{\partial x_2}\frac{\partial^2 u_1}{\partial x_2^2}\right)-\frac{\sigma B_0^2}{\rho}u_1 \tag{2.2.2}$$

$$\rho c_p \mathbf{v}.\nabla T=-\nabla.\mathbf{q} \tag{2.2.3}$$

$$u_1\frac{\partial C}{\partial x_1}+u_2\frac{\partial C}{\partial x_2}=D_B\frac{\partial^2 C}{\partial x_2^2}+\frac{D_T}{T_\infty}\frac{\partial^2 T}{\partial x_2^2} \tag{2.2.4}$$

Where, $\mathbf{v}=\left(u_1,u_2,u_3\right)$ is the velocity vector, u_1 and u_2 are the fluid velocity components measured along the x_1 and x_2 directions, respectively, ρ is the constant fluid density, c_p is the specific heat at constant pressure, ν is kinematic viscosity, D_B is the Brownian diffusion coefficient, D_T is the thermophoresis coefficient, q is normal heat flux vector, T is the temperature, T_∞ is the constant values of the temperature. Also, σ is the electrical conductivity, $\Gamma\left(x_1\right)=\Gamma\left(x_1+b\right)^{(3m-1)/2}$ is the Williamson parameter, and $B_0^2\left(x_1\right)=B_0^2\left(x_1+b\right)^{1-m}$ is the variable magnetic field, This forms of $B_0^2\left(x_1\right)$ and $\Gamma\left(x_1\right)$ has also been considered by several researchers to study MHD non-Newtonian flow problems and to obtain similarity solution (see Prasad et al., (2016), Salahuddin et al., (2016) for details) over a moving or fixed flat plate. $\tau=(\rho c_p)_p/(\rho c_p)_f$ is the ratio between the effective heat capacity of the nanoparticle material and heat capacity of the fluid, ρ_p is the density of the nanoparticle, c_{p_f} is the specific heat of the fluid, and c_{p_p} the specific heat of the nanoparticle.

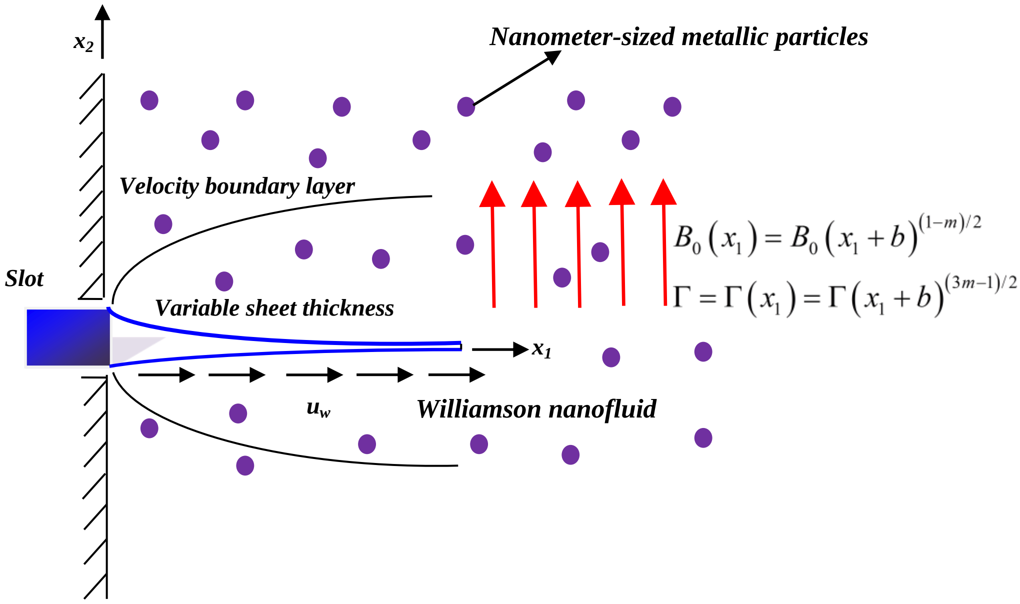

Fig.2.2.1: Schematic diagram of the Williamson nanofluid model with a variable stretching sheet.

The boundary conditions for the physical problem under consideration are given by

$$
\begin{aligned}
&u_1=U_w=U_0\left(x_1+b\right)^m, \quad u_2=0, \quad T=T_w, \quad C=C_w, \quad \text{at} \quad x_2=A\left(x_1+b\right)^{1-m/2},\\
&u_1\to 0, \quad T\to T_\infty, \quad C\to C_\infty \quad \text{as} \quad x_2\to\infty.
\end{aligned} \tag{2.2.5}
$$

The positive and negative values of m represent two different cases, namely, stretching and shrinking sheets, respectively. The new flux model is known as Cattaneo - Christov heat flux model (see Cattaneo (1948), Christov (2009)) which is the generalized form of Fourier's law and is given by

$$
q+\lambda_2\left(\frac{\partial q}{\partial t}+\mathbf{V}.\nabla.\mathbf{q}-\mathbf{q}.\nabla\mathbf{V}+(\nabla.\mathbf{V})\mathbf{q}\right)=-K\nabla T+\tau\left[D_B\frac{\partial C}{\partial x_2}\frac{\partial T}{\partial x_2}+\frac{D_T}{T_\infty}\left(\frac{\partial T}{\partial x_2}\right)^2\right] \tag{2.2.6}
$$

where $\mathbf{V}$ is the velocity vector, λ_2 is the thermal relaxation time, K is the thermal conductivity of the fluid. It is noted that for $\lambda_2=\tau=0$, Eq. (2.2.6) reduces to classical Fourier's law. As it is assumed that fluid is incompressible therefore Eq. (2.2.6) takes the form

$$
q+\lambda_2\left(\frac{\partial q}{\partial t}+\mathbf{V}.\nabla\mathbf{q}-\mathbf{q}.\nabla\mathbf{V}\right)=-K\nabla T+\tau\left[D_B\frac{\partial C}{\partial x_2}\frac{\partial T}{\partial x_2}+\frac{D_T}{T_\infty}\left(\frac{\partial T}{\partial x_2}\right)^2\right] \tag{2.2.7}
$$

eliminating q from Eqns. (2.2.3) and (2.2.7) we get

$$
\begin{aligned}
&u_1\frac{\partial T}{\partial x_1}+u_2\frac{\partial T}{\partial x_2}+\lambda_2\begin{pmatrix} u_1\dfrac{\partial u_1}{\partial x_1}\dfrac{\partial T}{\partial x_1}+u_2\dfrac{\partial u_2}{\partial x_2}\dfrac{\partial T}{\partial x_2}+u_1\dfrac{\partial u_2}{\partial x_1}\dfrac{\partial T}{\partial x_2}+u_2\dfrac{\partial u_1}{\partial x_2}\dfrac{\partial T}{\partial x_1}+\\ 2u_1u_2\dfrac{\partial^2 T}{\partial x_1\partial x_2}+u_1^2\dfrac{\partial^2 T}{\partial x^2}+u_2^2\dfrac{\partial^2 T}{\partial x_2^2} \end{pmatrix}\\
&=\frac{k}{\rho c_p}\frac{\partial^2 T}{\partial x_2^2}+\tau\left[D_B\frac{\partial C}{\partial x_2}\frac{\partial T}{\partial x_2}+\frac{D_T}{T_\infty}\left(\frac{\partial T}{\partial x_2}\right)^2\right]
\end{aligned} \tag{2.2.8}
$$

The dimensionless stream function $\psi(x_1,x_2)$ is given by $\left(u_1,u_2\right)=\left(\partial\psi/\partial x_2,-\partial\psi/\partial x_1\right)$, which satisfies (2.2.1) automatically. We transform the system of Eqns. (2.2.2), (2.2.4) and (2.2.8) into a dimensionless form. The suitable similarity transformations for the problem are

$$
\begin{aligned}
&\psi=F(\eta)\sqrt{\frac{2}{m+1}U_0\nu}\,\left(x_1+b\right)^{\frac{m+1}{2}}, \quad \Theta(\eta)=\frac{T-T_\infty}{T_w-T_\infty}, \quad \Phi(\eta)=\frac{C-C_\infty}{C_w-C_\infty},\\
&\eta=x_2\sqrt{\frac{m+1}{2}\frac{U_0}{\nu}}\,\left(x_1+b\right)^{\frac{m-1}{2}}.
\end{aligned} \tag{2.2.9}
$$

with Eq. (2.2.9), the velocity components can be written as

$$u_1 = U_w F'(\eta) \text{ and } u_2 = -\sqrt{\nu \frac{m+1}{2} U_0} \; (x_1 + b)^{\frac{m-1}{2}} \left[F(\eta) + \eta F'(\eta) \left(\frac{m-1}{m+1} \right) \right]. \quad (2.2.10)$$

Here prime denotes differentiation with respect to η. In the present work, it is assumed $m > -1$ for the validity of the similarity variable. With the use of (2.2.9) and (2.2.10), Eqns. (2.2.2), (2.2.4), (2.2.8) and (2.2.5) reduces to

$$\left(1 + We\ F''\right) F''' + FF'' - \frac{2m}{m+1} F'^2 - Mn\ F' = 0 \quad (2.2.11)$$

$$\left(1 - \Pr \frac{\gamma(m+1)}{2} F^2\right) \Theta'' + \Pr\left(Nb \Theta' \Phi' + Nt\, \Theta'^2\right) + \Pr F\, \Theta' \left(1 + \frac{\gamma(m-3)}{2} F'\right) = 0 \quad (2.2.12)$$

$$\Phi'' + \left(\frac{Nt}{Nb}\right) \Theta'' + Le\, F\, \Phi' = 0 \quad (2.2.13)$$

$$\begin{aligned} &F(\alpha) = \alpha \left(\frac{1-m}{1+m}\right), \quad F'(\alpha) = 1, \quad \Theta(\alpha) = 1, \quad \Phi(\alpha) = 1, \\ &F'(\infty) \to 0, \quad \Theta(\infty) \to 0, \quad \Phi(\infty) \to 0. \end{aligned} \quad (2.2.14)$$

The nondimensional parameters Mn, We, γ, Pr, Le, Nb, Nt, and α, denoting magnetic parameter, Weissenberg number, thermal relaxation parameter, Prandtl number, Lewis number, Brownian motion parameter, thermophoresis parameter, and wall thickness parameter, respectively, are given by

$$\begin{aligned} &Mn = \frac{2\sigma B_0^{\,2}}{\rho U^2{}_0 (1+m)}, \; \mathrm{We} = \Gamma U_0^3 \sqrt{\frac{U_0}{\nu}(m+1)}, \quad \gamma = \frac{\beta U_0 U_w}{\nu \,\mathrm{Re}}, \Pr = \frac{\rho c_p}{k}, Le = \frac{\nu}{D_B}, \\ &Nb = \frac{\tau D_B (C_w - C_\infty)}{\nu}, Nt = \frac{\tau D_T (T_w - T_\infty)}{T_\infty \nu}, \; \alpha = A\sqrt{\frac{m+1}{2} \frac{U_0}{\nu}}, \quad \mathrm{Re} = \frac{U_0 (x_1 + b)}{\nu}. \end{aligned} \quad (2.2.15)$$

Here $\eta = \alpha$ indicates the plate surface. For the purpose of computation, we define $f(\xi) = F(\eta)$, $\theta(\xi) = \Theta(\eta)$, and $\phi(\xi) = \Phi(\eta)$ where $\xi = \eta - \alpha$. Now the Eqns. (2.2.11) to (2.2.13) becomes,

$$\left(1 + we\ f''\right) f''' + f\ f'' - \frac{2m}{m+1} f'^2 - Mn\ f' = 0 \quad (2.2.16)$$

$$\left(1 - \Pr\ \gamma \frac{(m+1)}{2} f^2\right) \theta'' + \Pr\left(Nb\ \theta' \phi' + Nt\ \theta'^2\right) + \Pr\left(1 + \gamma \frac{(m-3)}{2} f'\right) f \theta' = 0 \quad (2.2.17)$$

$$\phi'' + \left(\frac{Nt}{Nb}\right) \theta'' + Le\ f \phi' = 0 \quad (2.2.18)$$

and the corresponding boundary conditions (2.2.14) for $m \neq -1$ are

$$f(0)=\alpha\frac{1-m}{1+m}, \qquad f'(0)=1, \qquad \phi(0)=1, \qquad \theta(0)=1,$$
$$\lim_{\xi\to\infty} f'(\xi)=\lim_{\xi\to\infty}\theta(\xi)=\lim_{\xi\to\infty}\phi(\xi)\to 0, \tag{2.2.19}$$

where the prime denotes the differentiation with respect to ξ. With reference to variable transformation, the integration domain will be fixed from 0 to ∞. When we observe the boundary condition $f(0)=\alpha(1-m)/(1+m)$ and for $\alpha=0$ or $m = 1$, the boundary condition reduces to $f(0)=0$ which indicates an impermeable surface. The important physical quantities of interest, the skin friction coefficient C_f the local Nusselt number Nu, and the local Sherwood number Sh are defined as,

$$C_f = \frac{2\nu\left(\partial u/\partial x_2\right)_{x_2=A(x_1+b)^{\frac{1-m}{2}}}}{U_w^2} = \left(\mathrm{Re}/2(m+1)\right)^{-1/2} f''(0),$$
$$Nu=\frac{(x_1+b)\left(\partial T/\partial x_2\right)_{x_2=A(x_1+b)^{\frac{1-m}{2}}}}{T_w-T_\infty} = -\left((m+1)/2\ \mathrm{Re}\right)^{1/2}\theta'(0), \tag{2.2.20}$$
$$Sh=\frac{(x_1+b)\left(\partial C/\partial x_2\right)_{x_2=A(x_1+b)^{\frac{1-m}{2}}}}{C_w-C_\infty} = -\left((m+1)/2\ \mathrm{Re}\right)^{1/2}\phi'(0),$$

where $\mathrm{Re}=U_0(x_1+b)/\nu$ is the local Reynolds number.

2.3. Exact solutions for some special cases

Here we present exact solutions for certain special cases and these solutions serve as a baseline for computing general solutions through numerical schemes. We notice that in the absence of Weissenberg number, thermal relaxation parameter, magnetic field, nanoparticle volume fraction parameter and heat transfer reduces to those of Fang et al., (2012).In the limiting case of $\theta_r\to\infty$ and $m=1$ the boundary layer flow and heat transfer equations degenerate. The solution for the velocity in the presence of magnetic field out to be $f'(\xi)=e^{-\chi\xi}$ where $\chi=\pm\sqrt{1+Mn}$.

In the absence of variable Weissenberg number, thermal relaxation parameter, magnetic field, nanoparticle volume fraction parameter, heat and mass transfer; but in the presence of variable thickness, i.e., $\left(\mathbf{We=Mn=\gamma=Nt=Le=Pr=0,\ m\neq 1}\right)$

Case (i): When $m=-1/3$, Eq. (2.2.16) becomes

$$f'''+ff''+f'^2=0 \tag{2.3.1}$$

with the boundary conditions $f(0)=2\alpha,\ f'(0)=1\ ,\ f'(\infty)=0$ (2.3.2)

On integrating (2.3.1) twice yields to $f' + f^2/2 = (\vartheta + 2\alpha)\eta + (2\alpha^2 + 1),$ (2.3.3)

where $\vartheta = f''(0).$ To obtain finite solution it is essential to consider $\vartheta = -2\alpha.$

Thus (2.3.1) reduces to $f' + f^2/2 = (2\alpha^2 + 1).$ (2.3.4)

The solution is $f(\xi) = \sqrt{2+4\alpha^2}\tanh\left[\sqrt{2+4\alpha^2}/2\,\xi + \tanh^{-1}\left(2\alpha/\sqrt{2+4\alpha^2}\right)\right].$ (2.3.5)

and $f'(\xi) = 1 + 2\alpha^2 \mathrm{Sech}^2\left[\sqrt{2+4\alpha^2}/2\,\xi + \tanh^{-1}\left(2\alpha/\sqrt{2+4\alpha^2}\right)\right].$ (2.3.6)

Case (ii): When $m = -1/2,$ Eq. (2.2.16) becomes

$$f''' + ff'' + 2f'^2 = 0 \tag{2.3.7}$$

with the boundary conditions $f(0) = 3\alpha,\ f'(0) = 1,\ f'(\infty) = 0.$ (2.3.8)

Eq. (2.3.7) is equivalent to $1/f\, d/d\xi\left[f^{3/2}\, d/d\xi\left(f^{-1/2} f' + 2/3\, f^{3/2}\right)\right] = 0.$ (2.3.9)

Integrating (2.3.9) once reduces to the following form

$$\left(-1/2\right) f'^2 + ff'' + f^2 f' = \left(-1/2\right) + 3\alpha\vartheta + 9\alpha^2 \tag{2.3.10}$$

Appling for free boundary condition we obtain

$$\vartheta = -3\alpha + 1/6\,\alpha. \tag{2.3.11}$$

An integration of (2.3.10) leads to $f^{-1/2} f' + 2/3\, f^{3/2} = 2/3(3\alpha)^{3/2} + 1/\sqrt{3\alpha}.$ (2.3.12)

The final solution is

$$\xi + D = 1/2d^2 \ln\left[f + d\sqrt{f} + d^2/\left(d - \sqrt{f}\right)^2\right] + \sqrt{3}/d^2 \tan^{-1}\left(2\sqrt{f} + d/d\sqrt{3}\right) \tag{2.3.13}$$

$$\text{where } d = \left[(3\alpha)^{3/2} + 3/2\sqrt{3\alpha}\right]^{1/3} \text{ and } D = 1/2d^2 \ln\left(\left(3\alpha + d\sqrt{3\alpha} + d^2\right)/\left(d - \sqrt{3\alpha}\right)^2\right) + \sqrt{3}/d^2 \tan^{-1}\left(\left(2\sqrt{3\alpha} + d\right)/d\sqrt{3}\right). \tag{2.3.14}$$

Since the system of equations (2.2.16) to (2.2.18) with conditions (2.2.19) has no exact analytical solutions, the equations are solved analytically via Optimal Homotopy Analysis Method.

2.4. Semi-analytical solution: Optimal Homotopy Analysis Method (OHAM)

Optimal homotopy analysis method has been employed to solve the nonlinear, coupled system of equations (2.2.16) - (2.2.18) with boundary conditions (2.2.19). The OHAM scheme breaks down a nonlinear differential equation into infinitely many linear ordinary differential equations whose solutions are found analytically. In the framework of the OHAM, the nonlinear equations are decomposed into their linear and nonlinear parts as follows:

In accordance with the boundary conditions (2.2.19), consider the base functions as $\{e^{-n\xi}\ for\ n \geq 0\}$ then, the dimensionless velocity $f'(\xi)$,temperature $\theta(\xi)$, and concentration $\phi(\xi)$ and can be expressed in the series form as follows

$$f(\xi) = \sum_{n=0}^{\infty} a_n\, e^{-n\xi}, \quad \theta(\xi) = \sum_{n=0}^{\infty} b_n\, e^{-n\xi}, \text{ and } \quad \phi(\xi) = \sum_{n=1}^{\infty} c_n\, e^{-n\xi}$$

where a_n, b_n and c_n are the coefficients. According to the solution expression and boundary conditions (2.2.19), we assume the following auxiliary linear operators as

$$\mathrm{L}_f = \frac{d^3}{d\xi^3} - \frac{d}{d\xi}, \quad \mathrm{L}_\theta = \frac{d^2}{d\xi^2} - f, \text{ and } \quad \mathrm{L}_\theta = \frac{d^2}{d\xi^2} - f, \tag{2.4.1}$$

Initial approximations satisfying the boundary conditions (2.2.14) are found to be

$$f_0(\xi) = 1 + \alpha\left(\frac{1-m}{1+m}\right) - e^{-\xi}, \quad \theta_0(\xi) = e^{-\xi}, \quad \phi_0(\xi) = e^{-\xi}.$$

Let us consider the so-called zero-th order deformation equations

$$(1-q)L_f\left[\hat{f}(\xi;q) - f_0(\xi)\right] = qH_f(\xi)\hbar_f N_f\left[\hat{f}(\xi;q)\right], \tag{2.4.2}$$

$$(1-q)L_\theta\left[\hat{\theta}(\xi;q) - \theta_0(\xi)\right] = qH_\theta(\xi)\hbar_\theta N_\theta\left[\hat{\theta}(\xi;q), \hat{f}(\xi;q), \hat{\phi}(\xi;q)\right], \tag{2.4.3}$$

$$(1-q)L_\phi\left[\hat{\phi}(\xi;q) - \phi_0(\xi)\right] = qH_\phi(\xi)\hbar_\phi N_\phi\left[\hat{\phi}(\xi;q), \hat{\theta}(\xi;q), \hat{f}(\xi;q)\right]. \tag{2.4.4}$$

Here $q \in [0,1]$ is an embedding parameter, while $\left(\hbar_f, \hbar_\phi, \hbar_\theta\right) \neq 0$ are the convergence control parameters, and the nonlinear differential operators are defined from Eqns. (2.2.16) - (2.2.18) as

$$\mathrm{N}_f[\hat{f}] = \frac{\partial^3 \hat{f}}{\partial \xi^3} + \hat{f}\frac{\partial^2 \hat{f}}{\partial \xi^2} - \left(\frac{2m}{m+1}\right)\left(\frac{\partial \hat{f}}{\partial \xi}\right)^2 + \mathrm{We}\frac{\partial^2 \hat{f}}{\partial \xi^2}\frac{\partial^3 \hat{f}}{\partial \xi^3} - Mn\frac{\partial \hat{f}}{\partial \xi} \tag{2.4.5}$$

$$\begin{aligned}\mathrm{N}_\theta[\hat{f}, \hat{\theta}, \hat{\phi}] = \frac{\partial^2 \hat{\theta}}{\partial \xi^2} + \Pr\left(Nb\frac{\partial \hat{\theta}}{\partial \xi}\frac{\partial \hat{\phi}}{\partial \xi} + Nt\left(\frac{\partial \hat{\theta}}{\partial \xi}\right)^2 + \hat{f}\frac{\partial \hat{\theta}}{\partial \xi}\right) \\ + \Pr\gamma\left(\left(\frac{m-3}{2}\right)\hat{f}\frac{\partial \hat{f}}{\partial \xi}\frac{\partial \hat{\theta}}{\partial \xi} - \left(\frac{m+1}{2}\right)\hat{f}^2\frac{\partial \hat{\theta}''}{\partial \xi}\right)\end{aligned} \tag{2.4.6}$$

$$\mathrm{N}_\phi[\hat{f}, \hat{\theta}, \hat{\phi}] = \frac{\partial^2 \hat{\phi}}{\partial \xi^2} + \left(\frac{Nt}{Nb}\right)\frac{\partial^2 \hat{\theta}}{\partial \xi^2} + Le\hat{f}\frac{\partial \hat{\phi}}{\partial \xi}. \tag{2.4.7}$$

We choose the auxiliary functions as $H_f(\xi)=H_\theta(\xi)=H_\phi(\xi)=e^{-\xi}$. It can be seen from Eqns. (2.4.2) to (2.4.4) that, when $q=0$, we have $\hat{f}(\xi;0)=f_0(\xi)$, etc., while when $q=1$, we have $\hat{f}(\xi;1)=f(\xi)$, etc., so we recover the exact solutions when q = 1. Expanding in q, we write

$$\hat{f}(\xi;q)=f_0(\xi)+\sum_{n=1}^{\infty}f_n(\xi)q^n,$$

$$\hat{\theta}(\xi;q)=\theta_0(\xi)+\sum_{n=1}^{\infty}\theta_n(\xi)q^n \text{ and}$$

$$\hat{\phi}(\xi;q)=\phi_0(\xi)+\sum_{n=1}^{\infty}\phi_n(\xi)q^n$$

As q varies from 0 to 1, the homotopy solutions vary from the initial approximations to the solutions of interest. It should be noted that the homotopy solutions contain the unknown convergence control parameters $\left(\hbar_f,\hbar_\phi,\hbar_\theta\right)\neq 0$, which can be used to adjust and control the convergence region and the rate of convergence of the series solution. To obtain the approximate solutions, we recursively solve the so-called nth-order deformation equations

$$\mathrm{L}_f[f_n(\xi)-\chi_n f_{n-1}(\xi)]=\hbar_f\mathrm{R}_n^f,$$

$$\mathrm{L}_\theta[\theta_n(\xi)-\chi_n\theta_{n-1}(\xi)]=\hbar_\theta\mathrm{R}_n^\theta,$$

$$\mathrm{L}_\phi[\phi_n(\xi)-\chi_n\phi_{n-1}(\xi)]=\hbar_\phi\mathrm{R}_n^\phi,$$

$$\mathrm{R}_n^f=\frac{1}{(n-1)!}\frac{\partial^{n-1}\mathrm{N}_f[\hat{f}(\xi;q)]}{\partial q^{n-1}}\Big|_{q=0},$$

$$\mathrm{R}_n^\theta=\frac{1}{(n-1)!}\frac{\partial^{n-1}\mathrm{N}_\theta[\hat{f}(\xi;q),\hat{\theta}(\xi;q),\hat{\phi}(\xi;q)]}{\partial q^{n-1}}\Big|_{q=0},$$

$$\mathrm{R}_n^\phi=\frac{1}{(n-1)!}\frac{\partial^{n-1}\mathrm{N}_\phi[\hat{f}(\xi;q),\hat{\phi}(\xi;q),\hat{\theta}(\xi;q)]}{\partial q^{n-1}}\Big|_{q=0},$$

$$\chi_n=\begin{cases}0, & n\leq 1,\\ 1, & n>1.\end{cases}$$

In practice, we can only calculate finitely many terms in the homotopy series solution. We therefore define the kth order approximate solution can by the partial sums

$$f_{[k]}(\xi) = f_0(\xi) + \sum_{n=1}^{k} f_n(\xi)\ ,$$

$$\theta_{[k]}(\xi) = \theta_0(\xi) + \sum_{n=1}^{k} \theta_n(\xi),\ \text{and} \tag{2.4.8}$$

$$\phi_{[k]}(\xi) = \phi_0(\xi) + \sum_{n=1}^{k} \phi_n(\xi).$$

With these approximations, we may evaluate the residual error and minimize it over the parameters $\hbar_f$, $\hbar_\theta$ and $\hbar_\phi$ in order to obtain the optimal value of $\hbar_f$, $\hbar_\theta$ and $\hbar_\phi$ giving the least possible residual error. To do so, one may use the integral of squared residual errors, however, this is very computationally demanding. To get around this, we use the averaged squared residual errors, defined by

$$\overline{\mathrm{E}_n^f}(\hbar_f) = \frac{1}{M+1}\sum_{k=0}^{M}\left(\mathrm{N}_f\left[f_{[\mathrm{M}]}(\xi_k)\right]\right)^2 ,$$

$$\overline{\mathrm{E}_n^\theta}(\hbar_\theta) = \frac{1}{M+1}\sum_{k=0}^{M}\left(\mathrm{N}_\theta\left[f_{[\mathrm{M}]}(\xi_k), \theta_{[\mathrm{M}]}(\xi_k), \phi_{[\mathrm{M}]}(\xi_k)\right]\right)^2 ,$$

$$\overline{\mathrm{E}_n^\phi}(\hbar_\phi) = \frac{1}{M+1}\sum_{k=0}^{M}\left(\mathrm{N}_\phi\left[f_{[\mathrm{M}]}(\xi_k), \theta_{[\mathrm{M}]}(\xi_k), \phi_{[\mathrm{M}]}(\xi_k)\right]\right)^2 ,$$

Where $\xi_k = k/M$, $k = 0,1,2,....M.$ Now we minimize the error function $\overline{\mathrm{E}_n^f}(\hbar_f), \overline{\mathrm{E}_n^\theta}(\hbar_\theta)$ and $\overline{\mathrm{E}_n^\phi}(\hbar_\phi)$ in $\hbar_f, \hbar_\theta$ and $\hbar_\phi$ and obtain the optimal value of $\hbar_f, \hbar_\theta$ and $\hbar_\phi$. For n^{th} order approximation, the optimal value of $\hbar_f, \hbar_\theta$ and $\hbar_\phi$ for f , θ and ϕ is given by

$\dfrac{d\overline{\mathrm{E}_n^f}(\hbar_f)}{dh} = 0$, $\dfrac{d\overline{\mathrm{E}_n^\theta}(\hbar_\theta)}{dh} = 0$ and $\dfrac{d\overline{\mathrm{E}_n^\phi}(\hbar_\phi)}{dh} = 0$ respectively. Evidently, $\lim\limits_{m\to\infty}\overline{\mathrm{E}_n^f}(\hbar_f) = 0$, $\lim\limits_{m\to\infty}\overline{\mathrm{E}_n^\theta}(\hbar_\theta) = 0$ and $\lim\limits_{m\to\infty}\overline{\mathrm{E}_n^\phi}(\hbar_\phi) = 0$ corresponds to a convergent series solution. Substituting these optimal values of $\hbar_f, \hbar_\theta$ and $\hbar_\phi$ in equation (2.4.8) we get the approximate solutions of equations (2.2.16) to (2.2.18) which satisfies the conditions (2.2.19). For the assurance of the validity of this method, $-f''(0)$ obtained via OHAM has been compared with Fang, et al., (2012), Khader and Megahed (2015) and Prasad et al., (2017b) for various special cases and the results are found to be in excellent agreement (see Table 2.1). In Tables 2.2, the optimal values of h_f, h_θ and h_ϕ for the functions $-f''(0), -\theta'(0)$ and $-\phi'(0)$ corresponding to various values of the parameters are given and the corresponding averaged residuals are represented as $\overline{E_{10}^{f}}$, $\overline{E_{10}^{\theta}}$ and $\overline{E_{10}^{\phi}}$.

2.5. Results and Discussion

The system of equations (2.2.16) to (2.2.18) subject to the boundary conditions (2.2.19) is solved analytically via efficient OHAM. The computations are being carried out using Mathematica 8and obtained the flow, heat,and mass transfer characteristics of Williamson fluid with nanoparticles by considering Cattaneo – Christov heat flux model for several values of the governing parameters such as Weissenberg number We, thermal relaxation parameter γ, velocity power index parameter m, the variable thickness parameter α ,the Prandtl number Pr, Magnetic parameter Mn, the thermophoresis parameter Nt and the Brownian motion parameter Nb, and the Lewis number Le. Fig.2.5.1 - 2.5.5 describes the influence of various physical parameters on the horizontal velocity profile $f'(\xi)$, the temperature profile $\theta(\xi)$, and the concentration profile $\phi(\xi)$ graphically. These profiles $f'(\xi)$, $\theta(\xi)$, and $\phi(\xi)$ are unity at the wall, decreases monotonically and tend to zero asymptotically as the distance increases from the boundary. The computed numerical values for the skin friction $f''(0)$, the Nusselt number $\theta'(0)$ and the wall Sherwood number $\phi'(0)$ are presented in Table 2.2.

Figs.2.5.1 (a) to 2.5.1(c) illustrates the effect of Mn and We on $f'(\xi)$, $\theta(\xi)$, and $\phi(\xi)$. It is noticed that $f'(\xi)$ decreases for increasing values of Mn. This is due to the fact that the retarding/ drag forces called the Lorentz forces generated by the applied magnetic field act as resistive drag forces opposite to the flow direction which results in a decrease in velocity. Consequently, the thickness of the momentum boundary layer reduces with an increase in Mn.A similar trend is observed in the case of We, this is because the relaxation time of the fluid enhances for higher values of We causing a decrease in velocity of the fluid. The exact opposite trend is observed in the case of $\theta(\xi)$ and $\phi(\xi)$ (see Fig.2.5.1(c)). Fig.2.5.2 (a) through 2.5.2(e) depicts the impact of α and m on $f'(\xi)$, $\theta(\xi)$, and $\phi(\xi)$. An interesting pattern may be observed in the case of positive and negatives of α and m. The behavior of the boundary condition $f(0)=\alpha(1-m/1+m)$ depends on the values of α and m. For a given range $\alpha>0$ and $m<1$ or $\alpha<0$ and $m>1$, it is observed that $f(0)>0$ which is the case of injection and for the other opposite set of range α and m, we have $f(0)<0$ which is a suction case. From the Fig.2.5.2 (a), it is clear that as $\alpha>0$ and $m=-0.3$ the velocity profiles are increasing for the decreasing values of α and the reverse trend is observed in the case of $\alpha>0$ and $m=5$. The opposite pattern is noticed in the case of temperature and concentration profiles with $\alpha>0$ and $m=-0.3, 2, 10$ (see Fig.2.5.2 (b) to 2.5.2(e)). Injection enhances both temperature and nanoparticle concentration. Thermal and concentration boundary layer thickness for the injection case is significantly greater than for the suction case. Effectively suction achieves a strong suppression of nano-particle species diffusion and also regulates the diffusion of thermal energy (heat) in the boundary layer. This response to suction has significant effects on the constitution of engineered nanofluids and shows that suction is an excellent mechanism for achieving flow control, cooling, and nano-particle distribution in nanofluid fabrication. Fig.2.5.3 exhibits the impact of increasing values of γ and $\Pr$ on $\theta(\xi)$. Temperature decreases considerably when γ increases and hence thermal boundary layer decreases. In fact, for larger values of γ, the particles of measurable material require more opportunity to hand over heat to its adjacent particles. Thus, larger γ is responsible for the decrease of temperature. Physically, γ appears because of the heat flux relaxation time. The greater values of γ, the liquid particles require more time to exchange heat to their neighboring particles which make a reduction in the temperature. The Cattaneo – Christov heat flux model can be reduced to fundamental Fourier's law of heat conduction in the absence of γ. This observation gives us an insight that, the temperature in Cattaneo – Christov heat flux model is lower than the Fourier's model (In the absence of γ heat transfer instantly throughout the material). Furthermore, the behavior of Pr on the thermal boundary layer with the consideration of γ found to be decreasing the temperature and thereby reduce the thickness of the thermal boundary layer. Fig.2.5.4 elucidates the influence of Nt and Nb on $\phi(\xi)$. It is noted that the nanoparticle volume fraction increases with the increase in Nt (increase in thermophoresis force) and thus augments the concentration boundary layer thickness. In this case, the nanoparticles move away from the hot stretching sheet towards the cold ambient fluid under the influence of temperature gradient. But in the case of Nb (smaller nano-particles), the result is there verse. Moreover, larger values of Nb will stifle the diffusion of nanoparticles away from the surface, which results in a decrease in nano-particle concentration values in the boundary layer. Finally, Fig. 2.5.5(a) to Fig.2.5.5(c) exhibits the residual error for $f'(\xi), \theta(\xi)$ and $\phi(\xi)$ which is early shows the accuracy and convergence of OHAM. These figures show thata tenth-order approximation yields the best accuracy for the present model.

The impact of the physical parameters on $f''(0), \theta'(0)$ and $\phi'(0)$, is presented in Table 2.2. We notice a decrease in the skin friction as Mn increases, while the opposite pattern is observed for the Nusselt number and the Sherwood number. Increasing Weissenberg number We enhances the Nusselt number and the Sherwood number where as thermal relaxation parameter γ decreases the Nusselt number. Sherwood number decreases for increasing values of *Le*.

2.6.Conclusions

In this article, MHD flow, heat and mass transfer of Williamson-Nano fluid over a stretching sheet with variable thickness has been examined. Cattaneo – Christov heat flux model was used to investigate the heat transfer mechanism. Some of the interesting conclusions are as follows:

- The strong variation in the velocity, temperature, and concentration fields is noticed as wall thickness parameter increases accordingly with $m > 1$ or $1 > m > -1$.
- In comparison with Fourier's law, the behavior of temperature profile is of decreasing nature for Cattaneo - Christov heat flux model
- An increase in the nanoparticle concentration profiles is due to the increase in the thermophoresis parameter and the Brownian motion parameter.
- Due to the effect of Lorentz force, fluid finds a drag force and hence velocity profile decreases while temperature and concentration profiles increases for increasing values of magnetic parameter,
- Weissenberg number is decreasing function of velocity whereas Lewis number reduces the Sherwood number.

Table 2.1: Comparison of results for $-f''(0)$ when $Mn = \lambda = \gamma = Nt = Le = 0$ and $Nb \to 0$.

α	m	Fang et al.,(2012) By shooting method	Khader and Megahed (2015) when $\lambda = 0$ By Chebyshev spectral method	Prasad et al., (2017b) When $\varepsilon_1 = \varepsilon_2 = 0, \theta_r \to \infty$	Present Result			
					OHAM			
					$-f''(0)$	h_f	E_{10}^{f}	CPU Time
0.5	10	1.0603	1.0603	1.0605	1.0604	1.3249	$2.234 x 10^{-8}$	273.14
	9	1.0589	1.0588	1.0511	1.0512	1.3248	$1.927 x 10^{-8}$	269.41
	7	1.0550	1.0551	1.0552	1.0551	1.3241	$1.187 x 10^{-8}$	257.01
	5	1.0486	1.0486	1.0487	1.0487	1.0095	$0.975 x 10^{-8}$	245.99
	3	1.0359	1.0358	1.0358	1.0358	1.0099	$3.189 x 10^{-9}$	245.52
	2	1.0234	1.0234	1.0230	1.0231	1.0184	$2.586 x 10^{-9}$	267.50
	1	1.0	1.0	1.0	1.0	0	0	98.016
	0.5	0.9799	0.9798	0.9791	0.9790	1.0013	$6.932 x 10^{-8}$	264.260
	0	0.9576	0.9577	0.9571	0.9572	1.5586	0.981×10^{-7}	230.339
	-1/3	1.0000	1.0000	0.9998	1.0000	1.5691	0.989×10^{-7}	313.672
	-1/2	1.1667	1.1666	1.6689	1.1668	1.1992	1.089×10^{-7}	273.826
0.25	10	1.1433	1.1433	1.1439	1.1439	1.2583	$1.9986 x 10^{-9}$	280.32
	9	1.1404	1.1404	1.1402	1.1401	1.2586	$1.975 x 10^{-9}$	258.82
	7	1.1323	1.1323	1.1329	1.1328	1.2635	$1.456 x 10^{-9}$	253.80
	5	1.1186	1.1186	1.1189	1.1182	1.2724	$0.986 x 10^{-9}$	308.51
	3	1.0905	1.0904	1.0908	1.0907	0.8474	$0.965 x 10^{-8}$	278.76
	1	1.0	1.0	1.0	1.0	0	0	214.23
	0.5	0.9338	0.9337	0.9330	0.9331	1.4012	$1.999 x 10^{-8}$	252.13
	0	0.7843	0.7843	0.7840	0.7841	1.13919	$0.927 x 10^{-7}$	238.16
	-1/3	0.5000	0.5000	0.4999	0.49999	0.7633	$0.946 x 10^{-6}$	241.33
	-1/2	0.0833	0.08322	0.08330	0.08331	1.2948	$4.446 x 10^{-6}$	265.18

Table 2.2: Values of Skin friction, Nusselt number and Sherwood number for different physical parameters.

Le	***Nt***	***Nb***	***γ***	**Pr**	***M***	***α***	***Mn***	***We***	$-f''(0)$	h_f	E_{10}^{f}	$-\theta'(0)$	h_θ	E_{10}^{θ}	$-\phi'(0)$	h_ϕ	E_{10}^{ϕ}	CPU time
								0	1.37855	-0.873272	8.63x10^{-10}	0.625582	-0.66598	4.08x10^{-6}	0.694768	-1.02251	1.53x10^{-4}	104.641
0.2	0.5	0.5	0.2	1	0.5	0.25	1	**0.5**	1.76270	-0.462871	2.12 x10^{-3}	0.585092	-0.83649	4.23 x10^{-5}	0.656452	-1.03779	4.10 x10^{-4}	102.29
								0.75	1.86308	-0.236984	9.61 x10^{-3}	0.525560	-0.83791	2.60 x10^{-4}	0.629833	-0.98909	1.26 x10^{-4}	106.89
							0		1.19176	-1.979380	7.13 x10^{-6}	0.664449	-0.56982	5.38 x10^{-5}	0.740098	-0.99473	3.22 x10^{-5}	103.62
0.2	0.5	0.5	0.2	1	0.5	0.25	**1**	0.5	1.76270	-0.462871	2.12 x10^{-3}	0.585092	-0.83649	4.21 x10^{-5}	0.656452	-1.07438	4.10 x10^{-4}	106.89
							2		1.86308	-0.236932	9.61 x10^{-3}	0.525562	-0.83791	2.69 x10^{-4}	0.629833	-0.98909	1.26 x10^{-3}	102.93
						0.2			1.40883	-1.406572	1.28 x10^{-6}	0.578156	-1.22059	3.18 x10^{-4}	0.674939	-1.15809	2.62 x10^{-3}	108.56
0.2	0.5	0.5	0.2	1	0.6	**0.4**	0.5	0.5	1.36813	-1.385160	1.02 x10^{-6}	0.548096	-1.15795	4.28 x10^{-4}	0.641979	-1.22383	3.32 x10^{-3}	111.07
						0.6			1.32904	-1.365751	7.79 x10^{-7}	0.515830	-1.22647	5.46 x10^{-4}	0.610702	-1.58361	4.04 x10^{-3}	112.20
					-0.3				1.28285	-2.270433	4.69 x10^{-4}	1.022861	-1.35472	5.75 x10^{-3}	1.123012	-1.28715	2.09 x10^{-3}	112.09
					0				1.28606	-2.055212	8.25 x10^{-6}	0.837784	-0.43759	1.08 x10^{-4}	0.904501	-1.25581	6.17 x10^{-5}	109.14
0.2	0.5	0.5	0.2	1	**2**	0.25	0.5	0.5	1.36813	-1.385130	1.02 x10^{-4}	0.548096	-1.15795	4.28 x10^{-4}	0.661497	-1.22383	3.32 x10^{-3}	111.59
					5				1.39324	-1.301973	5.64 x10^{-7}	0.483733	-1.20376	1.31 x10^{-3}	0.577634	-1.22383	4.62 x10^{-3}	110.62
					10				1.40469	-1.271321	4.29 x10^{-7}	0.244992	-1.18419	4.19 x10^{-3}	0.535254	-1.17625	4.95 x10^{-3}	111.30
				1					0.98183	-1.607461	1.77x10^{-6}	0.552611	-0.65837	1.36x10^{-3}	0.296702	-1.14837	9.86x10^{-4}	102.32
0.22	0.2	0.2	0.5	**2**	0.3	0.1	0.2	0.1	0.98183	-1.607461	1.77x10^{-6}	0.652891	-0.35027	1.53x10^{-3}	0.283287	-1.09906	6.31 x10^{-3}	111.21
				3					0.98183	-1.607461	1.77x10^{-6}	0.690607	-0.27337	1.99 x10^{-3}	0.285916	-1.05317	2.14 x10^{-3}	106.23
			0.1						1.20094	-1.159821	3.62x10^{-3}	0.417221	-1.03785	5..96 x10^{6}	.0.07092	-1.03785	2.09 x10^{-4}	104.79
0.22	0.3	0.3	**0.5**	1	0.3	0.1	0.5	0.2	1.20094	-1.159821	3.62x10^{-3}	0.450824	-0.54876	1.01 x10^{-4}	0.127017	-0.73465	2.35 x10^{-4}	102.14
			0.9						1.20094	-1.159821	3.62x10^{-3}	0.471138	-0.42114	2.31 x10^{-3}	0.152528	-0.69573	1.74 x10^{-4}	104.06
		1.0							1.22231	-1.538241	3.73 x10^{-6}	0.370061	-0.95174	1.01 x10^{-4}	0.534933	-0.90221	4.03x10^{-3}	48.796
0.2	0.5	**1.5**	0.2	1	-0.3	0.1	0.5	0.1	1.22231	-1.538241	3.73 x10^{-6}	0.323654	-0.89234	1.61 x10^{-4}	0.584933	-0.83298	2.30 x10^{-3}	48.125
		2.0							1.22231	-1.538241	3.73 x10^{-6}	0.198278	-1.01025	2.23 x10^{-3}	0.676833	-0.93904	2.41 x10^{-3}	50.109
	0.5								1.22231	-1.538241	3.73 x10^{-6}	0.334784	-1.06167	1.01 x10^{-3}	0.638336	-0.97481	1.59 x10^{-3}	48.796
0.2	**1.0**	1	0.2	1	-0.3	0.1	0.5	0.1	1.22231	-1.538241	3.73 x10^{-6}	0.291184	-0.95155	1.63 x10^{-3}	0.662644	-0.87605	1.80 x10^{-3}	48.125
	1.5								1.22231	-1.538241	3.73 x10^{-6}	0.200652	-0.87058	3.83 x10^{-3}	1.24781	-0.85781	3.41 x10^{-3}	52.281
1									1.22231	-1.538241	3.73 x10^{-6}	0.334784	-1.06167	1.01 x10^{-3}	0.638362	-0.97481	1.59 x10^{-4}	101.02
2	0.5	0.5	0.2	1	-0.3	0.1	0.5		1.22231	-1.538241	3.73 x10^{-6}	0.295675	-1.06154	1.51 x10^{-4}	0.884259	-0.26653	2.87 x10^{-5}	104.62
3									1.22231	-1.538241	3.73 x10^{-6}	0.257765	-1.05890	2.60 x10^{-3}	1.226140	-1.88671	6.07 x10^{-3}	112.06

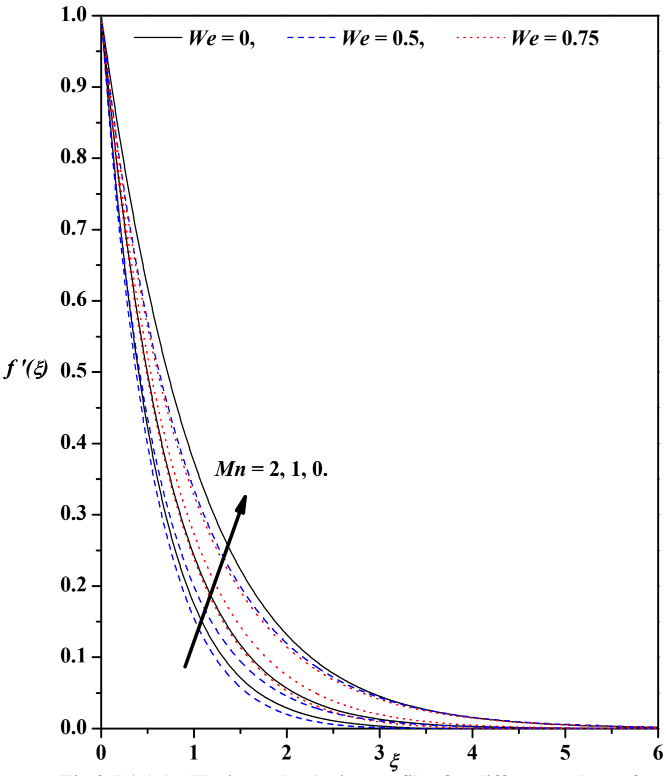

Fig.2.5.1 (a) : Horizontal velocity profiles for different values of *We* and *Mn* with*Pr* = 1, *Nb* = 0.5, *Nt* = 0.5, *Le* = 0.2, *m* = 0.5, $\alpha = 0.2$, $\gamma = 0.2$.

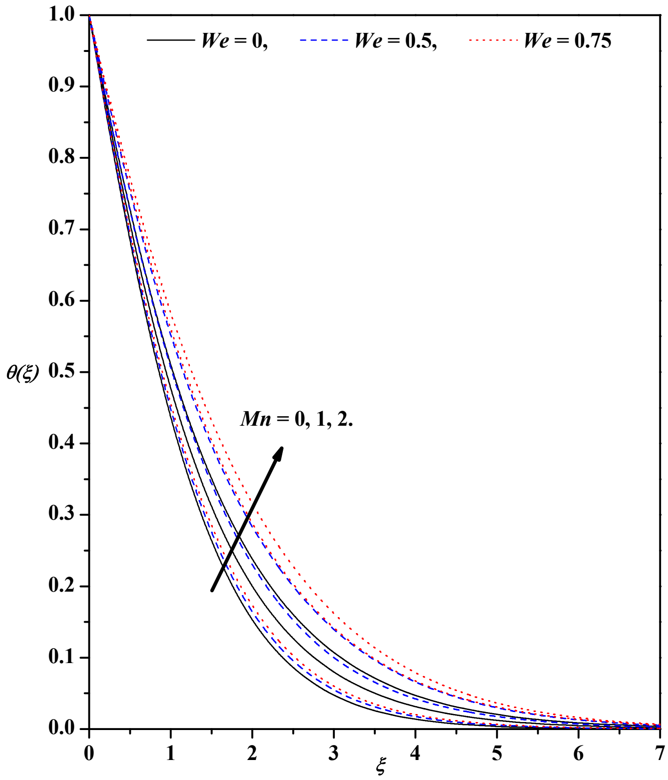

Fig.2.5.1 (b) :Temperature profiles for different values of *We* and *Mn* with Pr=1, *Nb* = 0.5, *Nt* = 0.5, *Le* = 0.2, *m* = 0.5, $\alpha = 0.2$, $\gamma = 0.2$.

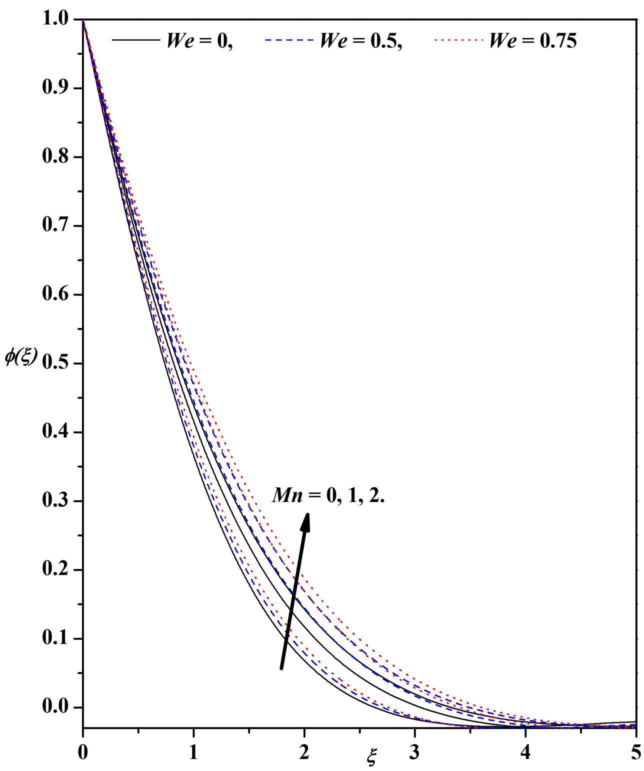

Fig.2..5.1 (c) :Concentration profiles for different values of *We* and *Mn* with *Pr* = 1, *Nb* = 0.5, *Nt* = 0.5, *Le* = 0.2, *m* = 0.5, $\alpha = 0.2$, $\gamma = 0.2$.

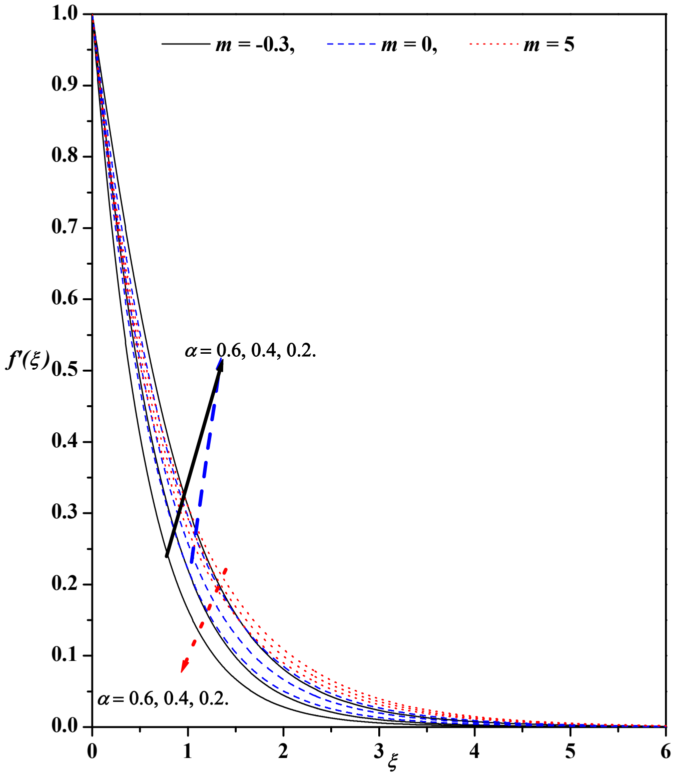

Fig.2.5.2 (*a*) : Horizontal velocity profiles for different values of α and m with $Pr = 1, Nb = 0.5, Nt = 0.5, Le = 0.2, Mn = 0.5, We = 0.2, \gamma = 0.2$.

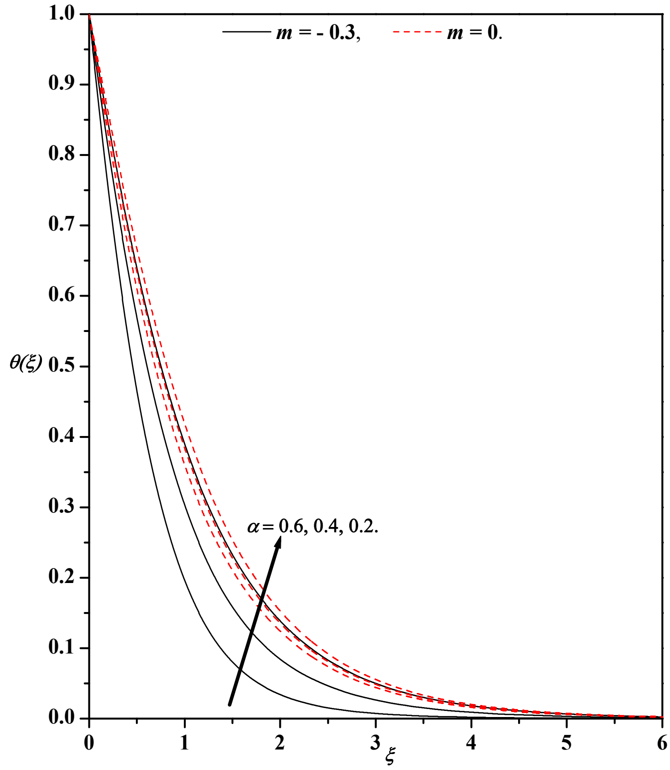

Fig.2.5.2 (*b*) : Temperature profiles for different values of α and m with $Pr = 1, Nb = 0.5, Nt = 0.5, Le = 0.2, Mn = 0.5, We = 0.2, \gamma = 0.2$.

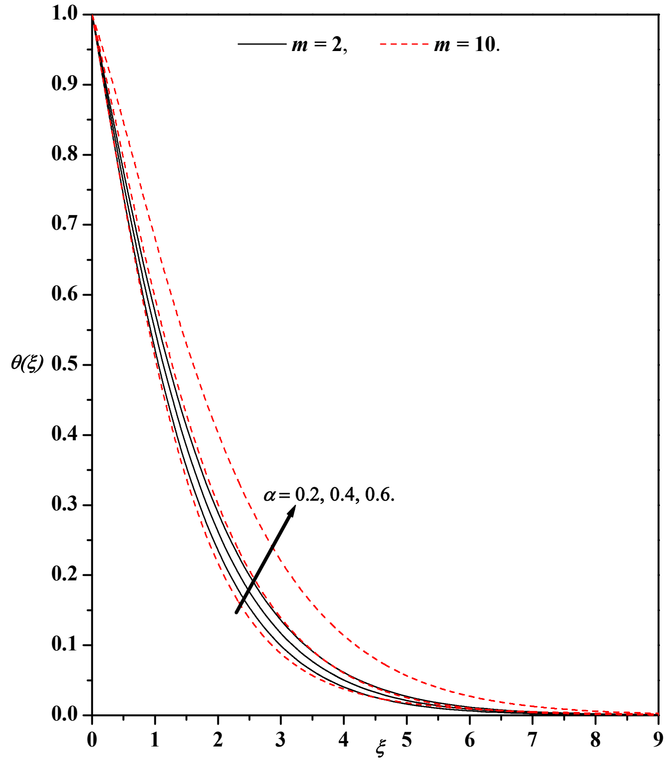

Fig.2.5.2 (*c*) : Temperature profiles for different values of α and m with $Pr = 1, Nb = Nt = 0.5, Le = 0.2, Mn = 0.5, We = 0.2, \gamma = 0.2$.

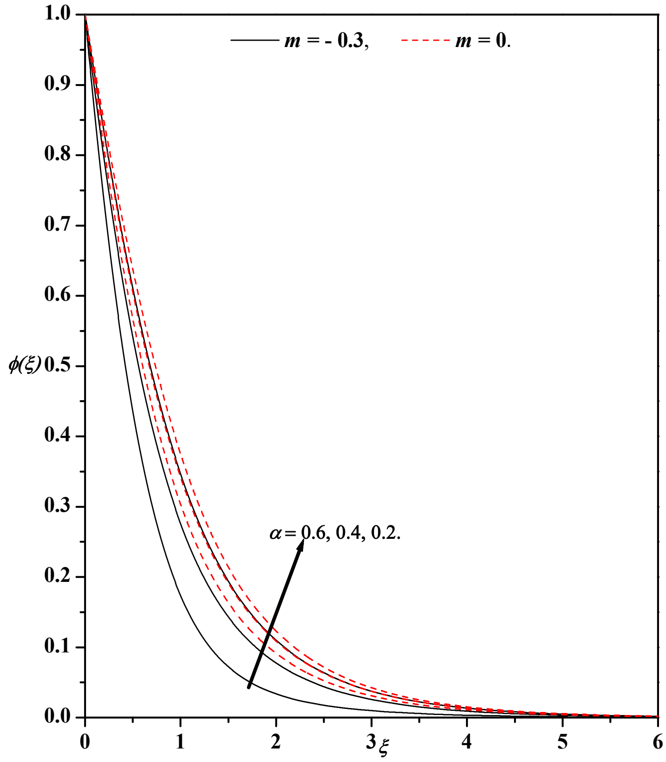

Fig.2.5.2 (d) : Concentration profiles for different values of α and m with $Pr = 1, Nb = Nt = 0.5, Le = 0.2, Mn = 0.5, We = 0.2, \gamma = 0.2$.

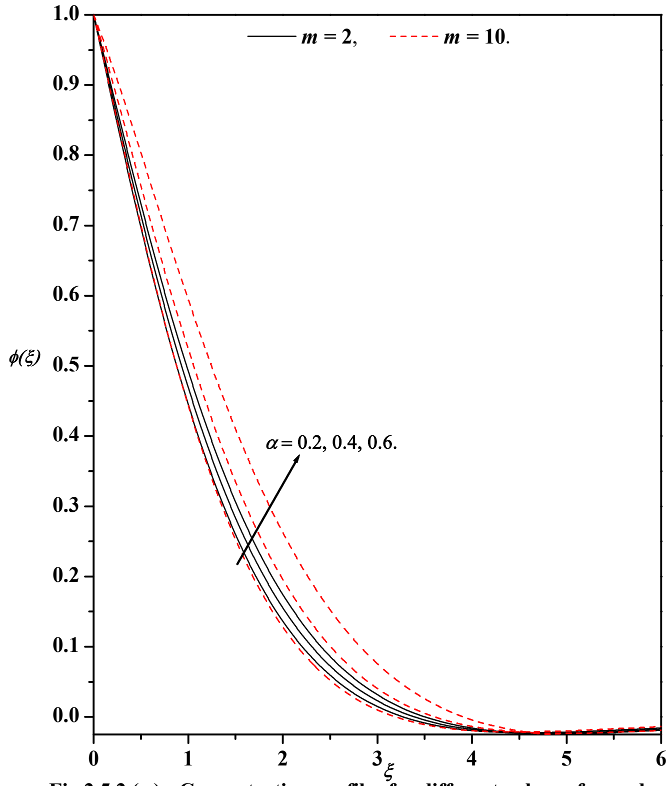

Fig.2.5.2 (*e*) : Concentration profiles for different values of α and m with $Pr = 1$, $Nb = 0.5$, $Nt = 0.5$, $Le = 0.2$, $Mn = 0.5$, $We = 0.2$, $\gamma = 0.2$.

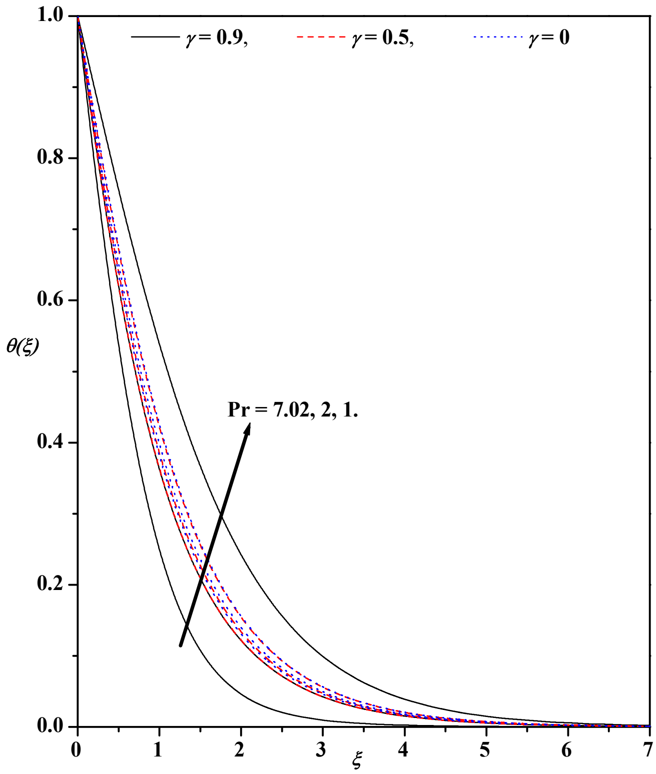

Fig.2.5.3 : Temperature profiles for different values of γ and Pr with $Mn = 0.5$, $m = 0.3$, $Nb = 0.5$, $Nt = 0.5$, $Le = 0.22$, $\alpha = 0.1$, $We = 0.2$

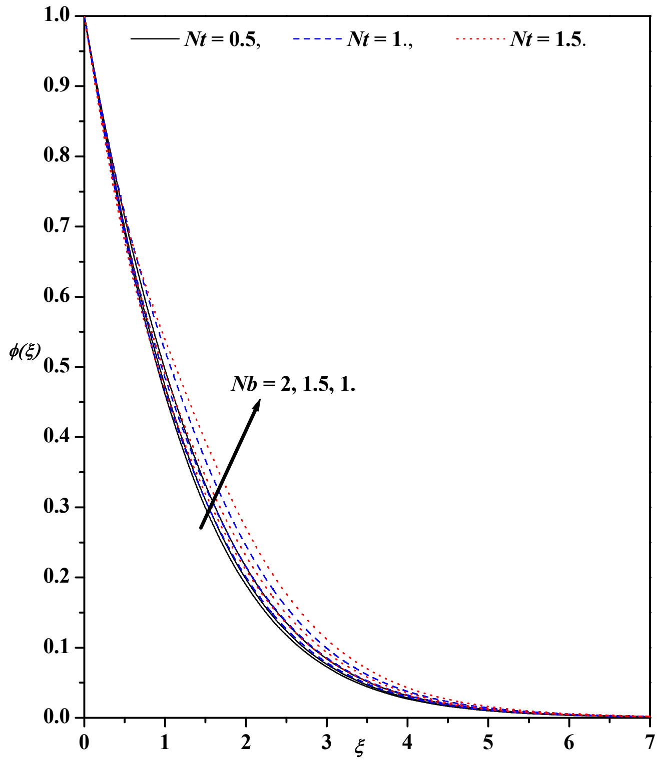

Fig.2.5.4 : Concentration profiles for different values of Nt and Nb with $Pr = 1$, $m = 0.5$ $Le = 1$, $Mn = 0.5$, $We = 0.1$, $\gamma = 0.2$, $\alpha = 0.25$.

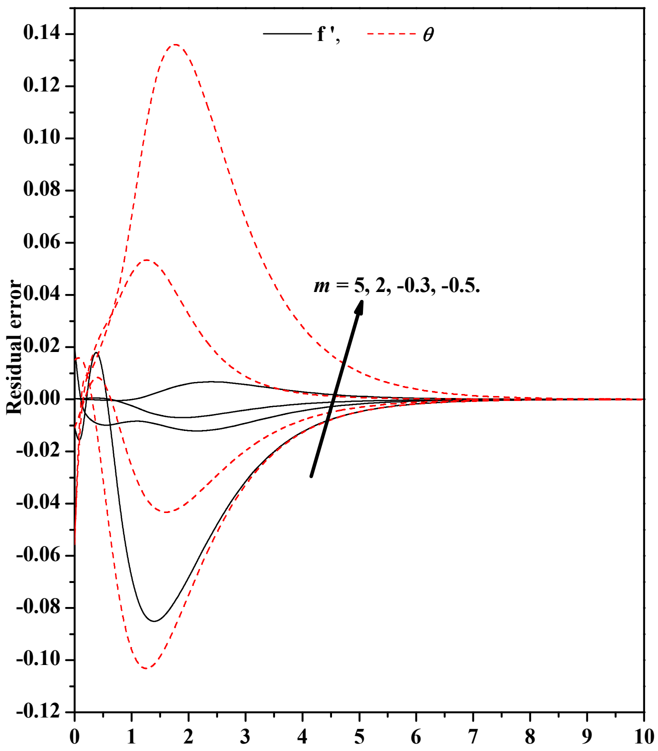

Fig.2.5.5 (a): Residual error profile for velocity and temperature for mwith different values m = 0.5, α = 0.2, We = 0.2, γ = 0.2, Nt = 0.5, Nb = 0.5, Le = 0.2, Pr = 1.0, Mn = 0.5.

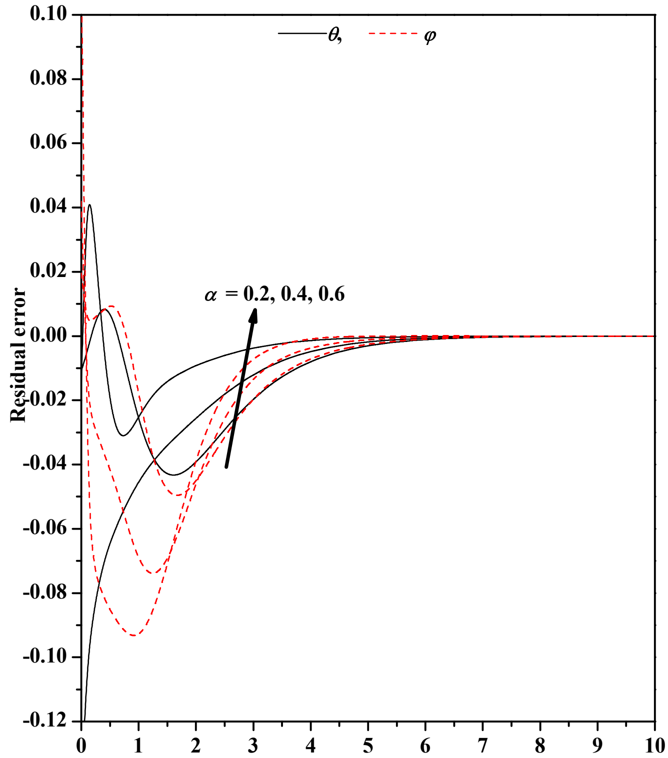

Fig.2.5.5 (b): Residual error profile for temperature and concentration for α with different values m = 0.5, We = 0.2, γ = 0.2, Nt = 0.5, Nb = 0.5, Le = 0.2, Pr = 1.0, Mn = 0.5.

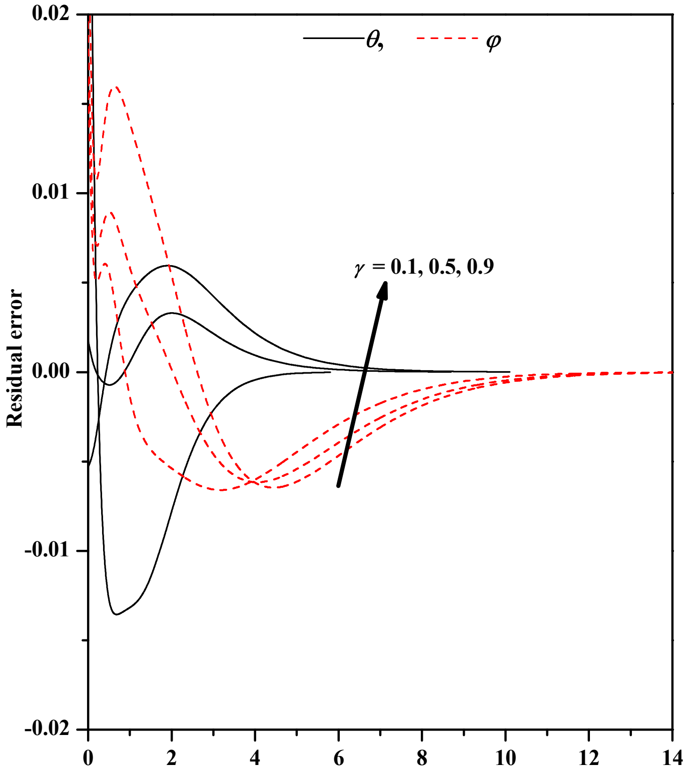

Fig.2.5.5 (c): Residual error profile for temperature and concentration for γ with different values m = 0.5, We = 0.2, α = 0.2, Nt = 0.5, Nb = 0.5, Le = 0.2, Pr = 1.0, Mn = 0.5.

CHAPTER - 3

INFLUENCE OF VARIABLE TRANSPORT PROPERTIES ON CASSON NANOFLUID FLOW OVER A SLENDER RIGA PLATE: KELLER BOX SCHEME

Part of this work has published in the *"Journal of Advanced Research in Fluid Mechanics and Thermal Science ",* Vol.64 (1), 19-42, 2019.

3.1. Introduction

In recent years, controlling the flow of electrically conducting fluids is one of the primary tasks to the scientists and engineers. The controlled flow of these fluids has enormous applications in industrial and technological processes involving heat and mass transfer phenomenon. However, the polymer industry has adopted a few conventional methods to control the fluid flow such as of suction/blowing and wall motion methods with the assistance of electromagnetic body forces. The flow of the fluids having high electrical conductivity such as liquid metals, plasma, and electrolytes, etc. can be significantly controlled by applying an external magnetic field. This concept can be used for controlling the classical electro magnetohydrodynamic (EMHD) fluid flows. In view of the industrial applications, Gailitis and Lielausis (1961) of the physics institute in Riga, the capital city of the Latvia country designed one of the devices known as Riga plate to generate simultaneous electric and magnetic fields which can produce Lorentz force parallel to the wall in weakly conducting fluids. This plate consists of a span wise aligned array of alternating electrodes and permanent magnets mounted on a plane surface. This array generates a surface-parallel Lorentz force with a neglected pressure gradient, which decreases exponentially in the direction normal to the (horizontal) plate. However, in vector product form the volume density of a Lorentz force is written as $\mathbf{F}_1 = \mathbf{J}\times\mathbf{B}$ and in terms of Ohm's law it can be expressed as $\mathbf{J} = \boldsymbol{\sigma}\left(\mathbf{E}+\mathbf{V}\times\mathbf{B}\right)$ where $\boldsymbol{\sigma}$ is an electrical conductivity of the fluid, V is the fluid velocity, and E is the electric field. In the absence of any extrinsic magnetic field, a complete contactless flow can be attained when $\boldsymbol{\sigma}\approx 10^{-6}$ S/m. Where as in the presence of extrinsic magnetic field, an induced high current density $\boldsymbol{\sigma}\left(\mathbf{V}\times\mathbf{B}\right)$ can be obtained and we have $\mathbf{F}_1 = \mathbf{J}\times\mathbf{B} = \boldsymbol{\sigma}\left(\mathbf{V}\times\mathbf{B}\right)\times\mathbf{B} = \boldsymbol{\sigma}\left[\left(\mathbf{V}\times\mathbf{B}\right)\mathbf{B}\text{-}\mathbf{B}^2\mathbf{V}\right]$. On the contrary, when $\boldsymbol{\sigma}\approx 10^{6}$ S/m, a low current density $\boldsymbol{\sigma}\left(\mathbf{V}\times\mathbf{B}\right)$ can be seen. To tackle with such cases, an extrinsic magnetic field is used to obtain the EMHD flow. The expression $\mathbf{F}_1 = \mathbf{J}\times\mathbf{B}\approx\boldsymbol{\sigma}\left(\mathbf{E}\times\mathbf{B}\right)$ reveals that the electrical conductivity of a fluid is very small, and it does not rely upon the flow field. According to Grinberg (1961), the density force can be written as $\mathbf{F}_1 = \left(\pi_1 M_0 j_0/8\right)e^{(-\pi_1/a)x_2}$. Tsinober and Shtern (1961) observed the substantial improvement in the strength of the Blasius flow towards a Riga plate, which is due to the more significant influence of wall parallel Lorentz forces. Further, the boundary layer flow of low electrical conductivity of fluids over a Riga plate was scrutinized by Pantokratoras and Magyari (2009). Pantokratoras (2011) extended the work of Pantokratoras and Magyari (2009) to Blasius and Sakiadis flow.

In addition to controlling the flow of electrically conducting fluids, the technological industry demands the control of heat transfer in a process. This can be achieved with the help of nanofluids technology. Nanofluid is the blend of the nanometer-scale (1nm to100 nm) solid particles and low thermal conductivity base liquids such as water, ethylene glycol (EG), oils, etc. Two different phases are used to simulate nanofluid. In both the methods researchers assumed as the common pure fluid and more precisely in the second method, the mixer or blend is with the variable concentration of nanoparticles. Choi (1995) proposed the term nanofluid and verified that the thermal conductivity of fluids could be improved by the inclusion of nanometer-sized metals,oxides (Al_2O_3, CuO), carbide ceramics (Sic, Tic/carbon nanotubes/fullerene) into the base fluids. Buongiorno (2006) established that Brownian diffusion and thermophoresis are important slip mechanisms in nanofluids. Makinde and Aziz (2011) examined the impact of Brownian motion and thermophoresis on transport equations numerically. Ahmad et al., (2016) and Ayub et al., (2016) examined the boundary layer flow of nanofluid due to Riga plate. Further, Hayat et al., (2017b, 2017c) analysed squeezing flow of a nanofluid between two parallel Riga plates by considering different external effects. Recently, Naveed et al., (2019) continued the work of Hayat et al., (2017c) and studied salient features of $(Ag\text{-}Fe_3O_4/H_2O)$ hybrid nanofluid between two parallel Riga plates. Furthermore, several research articles can be found in the literature that covers the different physical and geometrical aspects of the classical liquids. Few of them can be seen in the references.,(Sheikholeslami and Rokni (2017), Wakif et al., (2018a, 2018b, 2018c), Jawad et al., (2018), Prasad et al., (2019a), Oudina (2019), Hayat et al., (2017d), Daniel et al., (2018), Hayat et al., (2018b), Abd El-Aziz et al., (2019), Manjunatha et al., (2018)).

All the researchers, as mentioned earlier, have concentrated on conventional nonlinear stretching but not on the stretching. Fang et al., (2012) have coined the word variable thickness for the specific type of nonlinear stretching and examined the performance of boundary layer flow over a stretching sheet with variable thickness. Khader and Megahed (2015) reviewed the work of Fang et al., (2012) via Numerical method to explain velocity slip effects. Farooq et al., (2016) considered variable thickness geometry with Riga plate to analyze stagnation point flow and Prasad et al., (2016b, 2017a, 2018a, 2018b, 2019b) examined the impact of variable fluid properties on the Newtonian/non-Newtonian fluid flow field.

The main objective of the present work is to reduce the skin friction or drag force of the fluids by applying an external electric field in the presence of variable fluid properties over a slender elastic Riga plate under the influence of zero mass flux and heat transfer boundary conditions. Suitable similarity variables are introduced to transform the coupled nonlinear partial differential equations into a set of coupled nonlinear ordinary differential equations. These equations are solved numerically via Keller Box method (See Vajravelu and Prasad (2014)). The effects of various governing physical parameters for velocity, temperature, and nanoparticle concentration are discussed through the graphs and tables. The obtained results are compared with the actual results in previous literature and are found to be in excellent agreement. From this, it can be concluded that the present research work provides useful information for Science and industrial sector.

3.2. Mathematical Analysis of the problem

Consider an electromagnetic flow of a steady, incompressible non-Newtonian nanofluid over a slender Riga plate with variable fluid properties. Here the non-Newtonian fluid model is the Casson model and the rheological equation of state for an isotropic and incompressible fluid is given by (for details see, Prasad et al., (2018a)).

$$\tau_{ij} = \begin{cases} 2(\mu_B + P_{x_2} / \sqrt{2\pi}) e_{ij}, \pi > \pi_c \\ 2(\mu_B + p_{x_2} / \sqrt{2\pi_c}) e_{ij}, \pi < \pi_c \end{cases} \tag{3.2.1}$$

Where $\pi = e_{ij} e_{ij}$ and e_{ij} is the $(i, j)^{th}$ component of deformation rate, π is the product of the component of deformation rate with itself, π_B is the plastic dynamic viscosity of Casson fluid, P_{x_2} is yield stress of the fluid and π_c is a critical value of this product depending on the non-Newtonian model. Further, the Riga plate is considered as an alternating array consisting of electrodes and permanent magnets mounted on a plane surface situated at $x_2 = 0$ having x_1-axis vertically upwards. The fluid is characterized by a nanoparticle and is analyzed by considering Brownian motion and thermophoresis phenomena. The following assumptions are made,

- Joule heating and viscous dissipation are neglected.
- The fluid is isotropic, homogeneous, and has constant electric conductivity.
- The velocity of the stretching Riga plate and the free stream velocity are respectively, assumed to be $U_w(x_1) = U_0(x_1+b)^m$ and $U_e(x_1) = U_\infty(x_1+b)^m$, where U_∞ and U_0 are positive constants, m is the velocity power index and b is the physical parameter related to slender elastic sheet.
- The Riga plate is not flat and is defined as $\mathrm{x}_2 = \mathrm{A}\left(x_1+b\right)^{(1-m)/2}$, $\mathrm{m} \neq 1$, where the coefficient A is chosen as small so that the sheet is sufficiently thin, to avoid pressure gradient along the Riga plate $(\partial p / \partial x_1 = 0)$
- The temperature and nanoparticle concentration at the melting variable thickness of the Riga plate are T_M and C_M respectively and further T_∞ and C_∞ denote the ambient temperature and nanoparticle concentration of the fluid respectively.
- For different applications, the thickness of the stretching Riga plate is assumed to vary with the distance from the slot due to acceleration/deceleration of an extruded plate.

For m =1 thickness of the plate become flat. The physical model of the problem is shown in Fig.3.2.1 (a) and Fig.3.2.1 (b). Based on the above assumptions and the usual boundary layer approximations, the governing equations for continuity, momentum, thermal energy, and concentration for the nanofluid model are expressed as follows:

$$\frac{\partial u_1}{\partial x_1} + \frac{\partial u_2}{\partial x_2} = 0 \tag{3.2.2}$$

$$u_1 \frac{\partial u_1}{\partial x_1} + u_2 \frac{\partial u_1}{\partial x_2} = \left(1 + \frac{1}{\beta}\right) \frac{1}{\rho_\infty} \frac{\partial}{\partial x_2}\left(\mu(T) \frac{\partial u_1}{\partial x_2}\right) + U_e \frac{dU_e}{dx_1} + \frac{\pi_1 j_0 M_0\left(x_1\right)}{8\rho_\infty} \exp\left(\frac{-\pi_1}{a_1\left(x_1\right)} x_2\right) \tag{3.2.3}$$

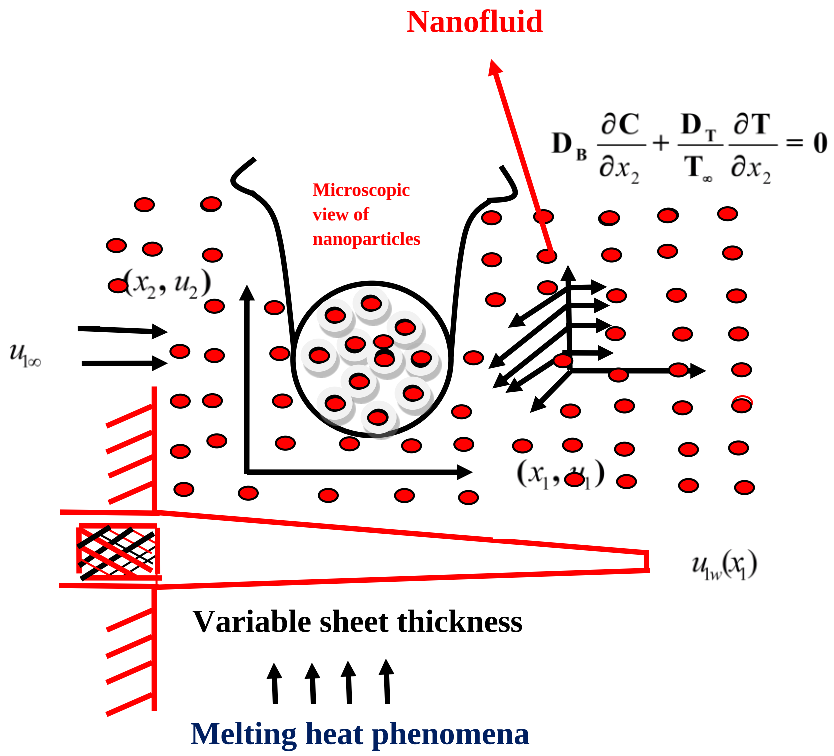

Fig.3.2.1 (a): Physical model of Variable thickness

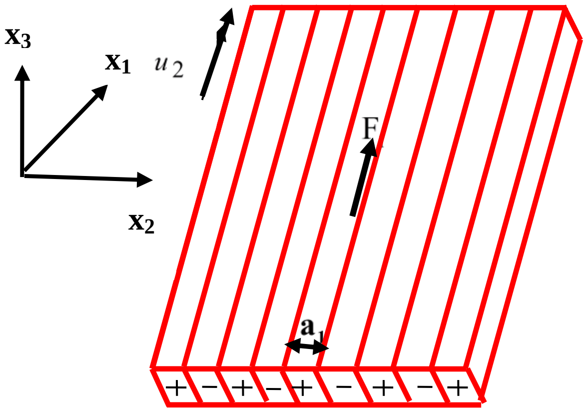

Fig.3.2.1 (b): Physical model of Riga plate

$$u_1\frac{\partial T}{\partial x_1}+u_2\frac{\partial T}{\partial x_2}=\frac{1}{\rho_\infty c_p}\frac{\partial}{\partial x_2}\left(K(T)\frac{\partial T}{\partial x_2}\right)+\frac{Q_0(x_1)}{\rho_\infty c_p}(T-T_\infty)+\tau\left[D_B(C)\frac{\partial C}{\partial x_2}\frac{\partial T}{\partial x_2}+\frac{D_T}{T_\infty}\left(\frac{\partial T}{\partial x_2}\right)^2\right] \quad (3.2.4)$$

$$u_1\frac{\partial C}{\partial x_1}+u_2\frac{\partial C}{\partial x_2}=\frac{\partial}{\partial x_2}\left(D_B(C)\frac{\partial C}{\partial x_2}\right)+\frac{D_T}{T_\infty}\frac{\partial^2 T}{\partial x_2^2} \quad (3.2.5)$$

where u_1 and u_2 are velocity components along x_1 and x_2 directions respectively. β is the Casson parameter, c_p is the specific heat at constant pressure, and ρ_∞ is the fluid density. The transport properties of the fluid are assumed to be constant, except for the fluid viscosity $\mu(T)$, the fluid thermal conductivity $K(T)$ and Brownian diffusion of the fluid D_B, are assumed to be functions of temperature and nanoparticle concentration, and are expressed as follows

$$\mu(T)=\frac{\mu_\infty}{1+\delta(T-T_M)},\ \text{i.e}\quad \mu(T)=\frac{1}{a_2(T-T_r)}, \quad (3.2.6)$$

$$K(T)=K_\infty\left[1+\varepsilon_1\left(\frac{T-T_M}{T_\infty-T_M}\right)\right] \quad (3.2.7)$$

$$D_B(C)=D_{B_\infty}\left[1+\varepsilon_2\left(\frac{C-C_M}{C_\infty-C_M}\right)\right] \quad (3.2.8)$$

here $a_2=\delta/\mu_\infty$ and $T_r=T_\infty-1/\delta$ are constants and their values depend on the reference state and the small parameter δ is known as thermal property of the fluid. Generally, the positive and negative values of a_2 describes two different states, namely, liquids and gases respectively, i.e. for $a_2>0$ represents the liquid state and $a_2<0$ represents gas state. Here μ_∞, K_∞ and D_{B_∞} are ambient fluid viscosity, thermal conductivity and Brownian diffusion coefficient respectively. ε_1 and ε_2 are small parameters known as the variable thermal conductivity parameter and variable species diffusivity parameter respectively. The term $Q_0(x_1)$ represents the heat generation when $Q_0>0$ and heat absorption when $Q_0<0$, and are used to describe exothermic and endothermic chemical reactions respectively. Further, j_0 is the applied current density in the electrodes, $M_0(x_1)$ is the magnetization of the permanent magnets mounted on the surface of the Riga plate and $a_1(x_1)$ is width between the magnets and electrodes. The special forms $Q_0(x_1)=Q_0(x_1+b)^{(1-m)/2}$,

$M_0(x_1) = M_0(x_1+b)^{(1-m)/2}$ and $a_1(x_1) = a_1(x_1+b)^{(1-m)/2}$ are chosen to obtain the similarity solutions. τ is defined as the ratio between the effective heat capacity of the nanoparticle material and heat capacity of the fluid, i.e. $\tau = (\rho_\infty c_p)_p / (\rho_\infty c_p)_f$, D_T is the thermophoresis diffusion coefficient and T_0 is solid temperature. The appropriate boundary conditions are

$$\left.\begin{aligned} &u_1 = U_w(x_1) = U_0(x_1+b)^m, \quad D_B \frac{\partial C}{\partial x_2} + \frac{D_T}{T_\infty}\frac{\partial T}{\partial x_2} = 0, \quad T = T_M \\ &K\left(\partial T/\partial x_2\right) = \rho\left[\lambda_1 + c_s(T_M - T_0)\right]u_2(x_1,x_2), \end{aligned}\right\} \text{at } x_2 = A\left(x_1+b\right)^{1-m/2} \tag{3.2.9}$$

$$u_1 \to U_e(x_1) = U_\infty(x_1+b)^m, \; T \to T_\infty, \; C \to C_\infty \quad \text{as } x_2 \to \infty$$

The third condition defined in equation (3.2.9) $K\left(\partial T/\partial x_2\right) = \rho\left[\lambda_1 + c_s(T_M - T_0)\right]\mathrm{v}(x_1,x_2)$ represents the melting temperature in which λ_1 is the latent heat of fluid, T_M is the melting temperature, T_0 and C_s are the temperature and heat capacity of the concrete surface respectively. On substituting equations (3.2.6) - (3.2.8) in the basic equations (3.2.3) - (3.2.5), it reduces to

$$\begin{aligned} u_1\frac{\partial u_1}{\partial x_1} + u_2\frac{\partial u_1}{\partial x_2} = &\left(1+\frac{1}{\beta}\right)\frac{1}{\rho_\infty}\frac{\partial}{\partial x_2}\left(\frac{\mu_\infty}{1+\delta(T-T_\infty)}\frac{\partial u_1}{\partial x_2}\right) \\ &+ U_e\frac{dU_e}{dx_1} + \frac{\pi j_0 M_0(x_1)}{8\rho_\infty}\exp\left(\frac{-\pi}{a_1(x_1)}x_2\right) \end{aligned} \tag{3.2.10}$$

$$\begin{aligned} u_1\frac{\partial T}{\partial x_1} + u_2\frac{\partial T}{\partial x_2} = &\frac{\partial}{\partial x_2}\left(\frac{K_\infty}{\rho_\infty c_p}\left(1+\varepsilon_1\left(\frac{T-T_M}{T_\infty - T_M}\right)\right)\frac{\partial T}{\partial x_2}\right) + \frac{Q_0(x_1)}{\rho_\infty c_p}(T-T_\infty) \\ &+ \tau\left[D_{B_\infty}\left(1+\varepsilon_2\left(\frac{C-C_M}{C_\infty - C_M}\right)\right)\frac{\partial C}{\partial x_2}\frac{\partial T}{\partial x_2} + \frac{D_T}{T_\infty}\left(\frac{\partial T}{\partial x_2}\right)^2\right] \end{aligned} \tag{3.2.11}$$

$$u_1\frac{\partial C}{\partial x_1} + u_2\frac{\partial C}{\partial x_2} = \frac{\partial}{\partial x_2}\left(D_{B_\infty}\left(1+\varepsilon_2\left(\frac{C-C_M}{C_\infty - C_M}\right)\right)\frac{\partial C}{\partial x_2}\right) + \frac{D_T}{T_\infty}\frac{\partial^2 T}{\partial x_2^2} \tag{3.2.12}$$

Now, we transform the system of equations (3.2.10) - (3.2.12) into dimensionless form. To this end, the dimensionless similarity variable be,

$$\eta = x_2\sqrt{\left(m+1/2\right)\frac{U_0(x_1+b)^{(m-1)}}{\nu_\infty}} \tag{3.2.13}$$

and the dimensionless stream function, the dimensionless temperature and the dimensionless nanoparticle concentration are,

$$\psi = \sqrt{\left(2/m+1\right)\nu_\infty U_0 (x_1+b)^{(m+1)}}\,\mathrm{F}(\eta),\quad \Theta(\eta)=\frac{T-T_M}{T_\infty - T_M},\quad \Phi(\eta)=\frac{C-C_M}{C_\infty - C_M},\qquad (3.2.14)$$

with the use of Eq. (3.2.13) and (3.2.14), the velocity components are,

$$\begin{aligned} u_1 &= \partial\psi/\partial x_2 = U_0 (x_1+b)^m F'(\eta), \\ u_2 &= -\partial\psi/\partial x_1 = -\sqrt{\frac{2}{(m+1)}\nu_\infty U_0 (x_1+b)^{(m-1)}}\left[\frac{(m+1)}{2}F(\eta)+\eta\frac{(m-1)}{2}F'(\eta)\right], \end{aligned}\qquad (3.2.15)$$

here prime denotes differentiation with respect to η . In the present work, it is assumed $m > -1$ for the validity of the similarity variable. With the use of Eqns. (3.2.13) - (3.2.15), then Eqns. (3.2.10) - (3.2.12) and the corresponding boundary conditions reduce to:

$$\left(1+\frac{1}{\beta}\right)\left(\left(1-\frac{\Theta}{\theta_r}\right)^{-1}F''\right)' + F\,F'' - \frac{2m}{m+1}\left[F'^2 - A^* - Qe^{-\beta_1\eta}\right]=0 \qquad (3.2.16)$$

$$\left(\left(1+\varepsilon_1\Theta\right)\Theta'\right)' + \Pr\Theta'\left[Nb(1+\varepsilon_2\Phi)\Phi' + Nt\Theta' + F\right] + \frac{2\Pr}{(m+1)}\lambda\Theta = 0$$

(3.2.17) $$\left(\left(1+\varepsilon_2\Phi\right)\Phi' + \left(\frac{Nt}{Nb}\right)\Theta'\right)' + Le\ F\ \ \Phi' = 0 \qquad (3.2.18)$$

$$\begin{aligned} &M\Theta'(\alpha) + \Pr\left(F(\alpha) - \alpha\frac{1-m}{1+m}\right) = 0,\ F'(\alpha)=1,\quad \Theta(\alpha)=0, \\ &Nb\Phi'(\alpha) + Nt\Theta'(\alpha) = 0, \\ &F'(\infty)\to A^*,\ \ \Theta(\infty)\to 1,\ \ \Phi(\infty)\to 1 \end{aligned}\qquad (3.2.19)$$

The non-dimensional parameters $\theta_r,\ A^*,\ Q,\ \beta_1, \Pr,\ \alpha, Nb, Nt,\ \lambda, Le$ and M represent the variable viscosity parameter, stretching rate ratio parameter, modified Hartman number, dimensionless parameter, Prandtl number, wall thickness parameter, Brownian motion parameter, thermophoresis parameter, heat source/sink parameter, Lewis number and the dimensionless melting heat parameter respectively and which are defined as follows.

$$\theta_r = \frac{-1}{\delta(T_\infty - T_M)},\ A^* = \frac{U_\infty}{U_0},\ Q=\frac{\pi j_0 M_0}{8\rho_\infty U_0^2},\ \beta_1 = \frac{\pi}{a_1}\sqrt{\frac{2}{(m+1)}\frac{\nu_\infty}{U_0(x_1+b)^{(m-1)}}},\ \Pr=\frac{\nu_\infty}{\alpha_\infty},$$

$$\alpha = A\sqrt{\frac{U_0(m+1)}{2\nu_\infty}}, Nb = \frac{\tau_\infty D_{B_\infty}(C_\infty - C_M)}{\nu_\infty}, Nt = \frac{\tau_\infty D_{T_\infty}(T_\infty - T_M)}{T_\infty \nu_\infty}, \quad \lambda = \frac{Q_0}{\rho_\infty c_p U_0},$$
$$Le = \frac{\nu_\infty}{D_{B_\infty}} \text{ and } \mathrm{M} = \frac{c_p(T_\infty - T_M)}{\lambda_1 + c_s(T_M - T_0)}. \tag{3.2.20}$$

The value of the θ_r is determined by the viscosity of the fluid under consideration, it is worth mentioning here that for $\delta \to 0$ *i.e* $\mu = \mu_\infty$ (constant) then $\theta_r \to \infty$. It is also important to note that θ_r is negative for liquids and positive for gases when $(T_\infty - T_M)$ is positive, this is due to fact that the viscosity of a liquid usually decreases with increasing in temperature. Further, $M = 0$ shows that there is no melting phenomenon, also it should be noted that M comprises of the Stefan constants $c_p(T_\infty - T_0)/\lambda_1$ and $c_s(T_M - T_0)$ of liquid and solid phase respectively. Now, we define the following $F(\eta) = f(\xi), \Theta(\eta) = \theta(\xi), \Phi(\eta) = \phi(\xi),$ *where* $\xi = \eta - \alpha$ here $\eta = \alpha$ indicates the flat surface. Then Esq. (3.2.16) to (3.2.19) reduces to:

$$\left(1+\frac{1}{\beta}\right)\left(\left(1-\frac{\theta}{\theta_r}\right)^{-1} f''\right)' + f\ f'' - \frac{2m}{(m+1)}\left[f'^2 - A^* - Qe^{-\beta_1(\xi+\alpha)}\right] = 0 \tag{3.2.21}$$

$$\left((1+\varepsilon_1\theta)\theta'\right)' + \Pr\theta'\left[Nb(1+\varepsilon_2\phi)\phi' + Nt\theta' + f\right] + \frac{2}{m+1}\Pr\lambda\theta = 0 \tag{3.2.22}$$

$$\left((1+\varepsilon_2\phi)\phi' + \left(\frac{Nt}{Nb}\right)\theta'\right)' + Le\ \ f\phi' = 0 \tag{3.2.23}$$

$$M\theta'(0) + \Pr\left[f(0) - \alpha\left(\frac{1-m}{1+m}\right)\right] = 0, \quad f'(0) = 1, \quad \theta(0) = 0$$
$$Nb\ \phi'(0) + Nt\theta'(0) = 0, \tag{3.2.24}$$
$$f'(\infty) \to A^*, \quad \theta(\infty) \to 1, \quad \phi(\infty) \to 1$$

Physical quantities of interest

The important physical quantities of interest for the governing flow problem, such as skin friction C_f, the local Nusselt number Nu, and Sherwood number Sh are defined as follow.

$$C_f = \frac{\tau_w}{U_w^2},$$
$$Nu = (x_1 + b)\frac{q_w}{T_\infty - T_M}, \tag{3.2.25}$$
$$Sh = (x_1 + b)\frac{j_w}{C_\infty - C_M}$$

where $\tau_w = \dfrac{\mu(T)}{\rho_\infty}\dfrac{\partial u_1}{\partial x_2}$, $q_w = \dfrac{\partial T}{\partial x_2}$ and $j_w = \dfrac{\partial C}{\partial x_2}$ at $x_2 = A(x_1 + b)^{1-m/2}$

are respectively called the skin friction, the heat flux and the mass flux at the wall. These parameters in dimensionless form can be written as

$$\mathrm{Re}^{1/2} C_f = \sqrt{\frac{m+1}{2}} \quad f''(0),$$

$$\mathrm{Re}^{-1/2} Nu = -\sqrt{\frac{m+1}{2}} \quad \theta'(0) \text{ and}$$

$$\mathrm{Re}^{-1/2} Sh = -\sqrt{\frac{m+1}{2}} \quad \phi'(0),$$

where $\mathrm{Re} = U_w(x_1 + b)/\nu_\infty$ is called local Reynolds number.

3.3. Exact analytical solutions for some special cases

In this section, we study the exact solutions for some special cases. It is important to analyze some theoretical analysis of the certain solutions for some given physical parameters and these solutions serve as the base function for computing general solutions through numerical schemes. In the case of absence of Casson parameter β, variable fluid viscosity parameter θ_r, stretching rate ratio parameter A^*, and modified Hartman number Q the present problem reduces to Fang et al., (2012). The discussions here will be emphasized on other parameters except $m \neq 1$.

Case (i): when $m=-1/3$ then Eq. (3.2.21) reduces to the following form,

$$f''' + ff'' + (f')^2 = 0 \tag{3.3.1}$$

with the associated boundary conditions (3.2.24) becomes,

$$f(0) = 2\alpha, \quad f'(0) = 1, \quad f'(\infty) = 0 \tag{3.3.2}$$

On integration Eq. (3.3.1) twice yields to

$$f' + f^2/2 = (\gamma + 2\alpha)\eta + (2\alpha^2 + 1) \tag{3.3.3}$$

where $\gamma = f''(0),$ in order to have a finite solution it is essential to consider $\gamma = -2\alpha$

$f' + f^2/2 = (2\alpha^2 + 1)$ when $\xi \to \infty,$ we have

$$f(\infty) = \sqrt{2 + 4\alpha^2}. \tag{3.3.4}$$

The solution is $f(\xi) = \sqrt{2+4\alpha^2}\tanh\left[\left(\sqrt{2+4\alpha^2}/2\right)\xi + \tanh^{-1}\left(2\alpha/\sqrt{2+4\alpha^2}\right)\right]$ and (3.3.5)

$$f'(\xi) = 1 + 2\alpha^2 \operatorname{Sech}^2\left[\left(\sqrt{2+4\alpha^2}/2\right)\xi + \tanh^{-1}\left(2\alpha/\sqrt{2+4\alpha^2}\right)\right]. \tag{3.3.6}$$

It should be noted that, for $m = -1/3,$ the above solutions reduce to the solutions for a flat stretching surface. This confirms that the present numerical solutions are in good agreement with those of Fang et al., (2012) and these can be used for numerical code validation in this work.

Case (ii): For $m = -1/2,$ we can obtain another analytical solution, for this case, Eq. (3.2.21) reduces to,

$$f''' + ff'' + 2(f')^2 = 0 \tag{3.3.7}$$

with the respective boundary conditions (3.2.24) becomes as,

$$f(0) = 3\alpha, \quad f'(0) = 1, \quad f'(\infty) = 0. \tag{3.3.8}$$

Equation (3.3.7) can be written in the form of

$$(1/f)\, d/d\xi\left[f^{3/2}\, d/d\xi\left(f^{-1/2} f' + 2/3\, f^{3/2}\right)\right] = 0 \tag{3.3.9}$$

Integrating Eq. (3.3.9) once reduces to the following form

$$(-1/2)(f')^2 + ff'' + f^2 f' = (-1/2) + 3\alpha\gamma + 9\alpha^2 \tag{3.3.10}$$

Applying free boundary condition,

$$\gamma = -3\alpha + (1/6\alpha) \tag{3.3.11}$$

On integration Eq. (3.3.10) leads to

$$f^{-1/2} f' + (2/3) f^{3/2} = (2/3)(3\alpha)^{3/2} + \left(\sqrt{3\alpha}\right) \tag{3.3.12}$$

The final solution is

$$\xi + D = 1/2d^2 \ln\left[\left(\left(f + d\sqrt{f} + d^2\right)\Big/\left(d - \sqrt{f}\right)^2\right)\right] + \left(\sqrt{3}/d^2\right)\tan^{-1}\left(\left(2\sqrt{f} + d\right)\Big/ d\sqrt{3}\right) = 0 \qquad (3.3.13)$$

where $d = [(3\alpha)^{3/2} + 3/(2\sqrt{3\alpha})^{1/3}$ and

$$D = 1/2d^2 \ln\left[\left(3\alpha + d\sqrt{3\alpha} + d^2\right)\Big/\left(d - \sqrt{3\alpha}\right)^2\right] + \sqrt{3}/d^2 \tan^{-1}\left(\left(2\sqrt{3\alpha} + d\right)\Big/ d\sqrt{3}\right) = 0 \qquad (3.3.14)$$

Since the system of Eqns. (3.2.21) - (3.2.23) with boundary conditions (3.2.24) has no exact analytical solutions, they are solved numerically via a Keller-Box method.

3.4. Method of solution

The systems of highly nonlinear coupled differential equations (3.2.21) to (3.2.23) along with appropriate boundary conditions (3.2.24) are solved by finite difference scheme known as Keller Box Method. This system is not conditionally stable and has a second order accuracy with arbitrary spacing. For solving this system first write the differential equations and respective boundary conditions in terms of first order system, which is then, converted into a set of finite difference equations using central difference scheme. Since the equations are highly nonlinear and cannot be solved analytically, therefore these equations are solved numerically using the symbolic software known as Fedora. Further nonlinear equations are linearized by Newton's method and resulting linear system of equations is solved by block tri-diagonal elimination method. For the sake of brevity, the details of the solution process are not presented here. For numerical calculations, a uniform step size is taken which gives satisfactory results and the solutions are obtained with an error tolerance of 10^{-6} in all the cases. To demonstrate the accuracy of the present method, the results for the dimensionless Skin friction, Nusselt number and Sherwood number are compared with the previous results.

Validation of Methodology

The main objective of this section is to check the validation of the present work. The present numerical results are compared with the existing work of Farooq et al., (2016) and Prasad et al.,(2018b) in the absence and presence of Riga plate with $\Pr = A^* = \varepsilon_1 = \varepsilon_2 = Nt = \lambda = Le = M = 0, Nb \to 0, \beta \to \infty, \theta_r \to \infty$ and the results are in good agreement with the previous literature and the same has been depicted in Table 3.1

3.5. Results and discussion of the problem

The systems of nonlinear ordinary differential equations (3.2.21) to (3.2.23) together with the appropriate boundary conditions (3.2.24) are numerically solved by using Keller Box method. The influence of various physical parameters such as Casson parameter β, variable fluid viscosity parameter θ_r, velocity power index m, stretching rate ratio parameter $A*$, modified Hartman number Q, dimensionless parameter β_1, variable thermal conductivity parameter ε_1, Brownian motion parameter Nb, thermophoresis parameter Nt, Prandtl number $\Pr$, heat source/sink parameter λ, variable species diffusivity parameter ε_2, Lewis number Le, and wall thickness parameter α on the horizontal velocity profile $f'(\xi)$, the temperature profile $\theta(\xi)$, and the concentration profile $\phi(\xi)$ are exhibited through Figs.(3.5.1-.3.5.8). The computed numerical values for the skin friction $f''(0)$, the Nusselt number $\theta'(0)$ and the wall Sherwood number $\phi'(0)$ are presented in Table 3.2.

The effect of velocity power index m and wall thickness parameter α on velocity, temperature and concentration boundary layers are depicted in Figs. 3.5.1(a-c). Fig. 3.5.1(a) elucidates that, for increasing values of m, $f'(\xi)$ reduce and this is due to the fact that the stretching velocity enhances for larger values of m which causes more deformation in the fluid, consequently velocity profiles decrease. A similar trend may be observed in the case of $\theta(\xi)$ (Fig.3.5.1(b)), where as concentration distribution (Fig.3.5.1(c)) shows a dual characteristic, that is for larger values of m concentration profiles reduces near the sheet and opposite behaviour is observed away from the sheet. When $m=1,$ the sheet become flat. Similarly, for higher values of wall thickness parameter $\alpha,$ velocity profiles fall, but the temperature distribution upgrade near the sheet and downwards away from the sheet. Whereas, the impact of α is quite opposite in the case of concentration distribution. Fig.3.5.2 (a) through 3.5.2(c) indicates the influence of β and β_1 on $f'(\xi), \theta(\xi)$ and $\phi(\xi)$. For greater values of β velocity profiles are compressed, this is because as β increases the corresponding value of yield stress fall as a result velocity boundary layer thickness decreases. The temperature distribution rises for different estimations of β and concentration distribution exhibits exactly reverse trend. Effect of β_1 on these three profiles is same as that of β . It is noticed from in Figs.3.5.3 (a-c) that both θ_r and A^* exhibits opposite trend, increasing variable fluid viscosity reduces the velocity and concentration profiles while the enhancement is observed in the case of temperature profiles. This may be due to the fact that, lesser θ_r implies higher temperature difference between the wall and the ambient nanofluid and the profiles explicitly manifest that θ_r is the indicator of the variation of fluid viscosity with temperature which has a substantial effect on $f'(\xi)$ and hence on $f''(\xi)$, where as in the case of temperature the effect is reversed. Fig.3.5.4 illustrates the impact of A^* and Q on $f'(\xi)$. An improvement in A^* corresponds to the enhancement of velocity boundary layer thickness. The enhancement in the velocity profile is observed for amplifying Q. Conventionally the velocity profiles are the decreasing function of Hartman number where as in this case the Lorentz force which is produced due to the magnetic arrays parallel to the surface is responsible for the enhancement of the momentum boundary layer thickness. The influence of Nb and Nt on temperature and concentration distribution are sketched in Figs.3.5.5 (a-b). It is seen that the higher values of Nb enhances temperature profiles and its boundary layer thickness, whereas concentration distribution suppressed near the sheet and swells away from the sheet. The larger Nt creates a thermophoresis force which compels the nanoparticles to flow from the hotter region to the colder region which results in raising temperature profiles. In the case of concentration distribution, the duel behavior is noticed which reduces near the sheet and increases away from it (See Fig. 3.5.5(b)). The characteristic of Prandtl number $\Pr$ and variable thermal conductivity parameter ε_1 on temperature distribution is demonstrated in Fig.3.5.6. Usually temperature distribution reduces for higher values of $\Pr$ and enhances for larger values of ε_1, but in this work quite opposite behaviour can be seen, this is due to the presence of melting heat transfer parameter M and stretching rate ratio parameter A^*. Fig.3.5.7 records the effect of heat source/sink parameter λ on $\theta(\xi)$, an increase in λ means rise in the temperature difference $(T_\infty - T_M)$, which leads to an increment in temperature distribution. Fig.3.5.8 is plotted for different values of Le and ε_2 on $\phi(\xi)$. Lower the Brownian diffusion coefficient $D_{B\infty}$ the higher Lewis number: This leads to a decrease in the thickness of the nanoparticle concentration boundary layer. It is interesting to note that a distinct rock bottom in the nanoparticle volume fraction profiles occur in the fluid adjacent to the boundary for higher values of Le and lower values of ε_2. This means that the nanoparticle volume fraction near the boundary is lesser than the nanoparticle volume fraction at the boundary; accordingly, nanoparticles are likely to transfer to the boundary.

In Table 3.2 we present the results for $f''(0)$, $\theta'(0)$ and $\phi'(0)$ corresponding to different values of the physical parameters. The skin friction coefficient is a decreasing function of the parameters m, α, β, β_1, θ_r and increasing function of A^*, Q. Nusselt number reduces for m, α, A^*, ε_1 and increases for $\beta, \beta_1\, \theta_r\, Nb, Nt, \mathrm{Pr}, \text{and}\, \lambda.$ Further, the Sherwood number decreases for $\beta\,\&\,\beta_1$ and increases for A^*.

3.6. Some important key points of the problem (Conclusions)

The present article examines the effects of variable fluid properties on the heat transfer characteristics of a Casson nanofluid over a slender Riga plate with zero mass flux and melting heat transfer boundary conditions. Here, the thickness of the sheet is erratic. The critical points of the present study are summarized as follows:

- The effect of velocity power index *m* on velocity and temperature field is similar, that is, in both the cases the profiles increases as *m* reduces, whereas in the case of concentration distribution dual nature is observed.
- Velocity and concentration distributions reduces for increasing values of Casson parameter, but the temperature distributions shows exactly opposite behavior for larger values of Casson parameter.
- Enhanced variable fluid viscosity parameter influences the velocity and temperature field in opposite manner.
- The modified Hartmann number enhances the velocity distribution and reduces the temperature distribution.
- The squeezed thermal boundary layer is observed for the increasing values of variable thermal conductivity parameter.
- The concentration distribution improves for higher values of variable species diffusivity parameter. The duel nature of the concentration profiles is recorded for the Brownian motion parameter and thermophoresis parameter.

Table 3.1: Comparison of skin friction coefficient $-f''(0)$ for different values of wall thickness parameter α and velocity power index m when the presence and absence of a Riga plate at fixed values of $\mathrm{Pr} = A^* = \varepsilon_1 = \varepsilon_2 = \mathrm{Nt} = \lambda = \mathrm{Le} = \mathrm{M} = 0,\ \mathrm{Nb} \to 0, \beta \to \infty, \theta_r \to \infty.$

α	m	**Presence of Riga plate Farooq et al., (2016) by OHAM when** $Q = 0.1, \beta_1 = 0.2$	**Absence of Riga plate Prasad et al., (2018b) by OHAM, when** $\lambda = 0, Mn = Q = \beta_1 = 0$	**Present results, Keller Box Method**	
				Presence of Riga plate	**Absence of Riga plate**
0.25	02	0.9990	1.0614	0.9990	1.06140
	03	1.0465	1.0907	1.0456	1.09050
	05	1.0908	1.1182	1.0902	1.11860
	07	1.1120	1.1328	1.1121	1.13230
	09	1.1244	1.1401	1.1247	1.14041
	10	1.1289	1.1439	1.1288	1.14334
0.5	02	0.9673	1.0231	0.9672	1.02341
	03	0.9976	1.0358	0.9975	1.03588
	05	1.0252	1.0487	1.0253	1.04862
	07	1.0382	1.0551	1.0383	1.05506
	09	1.0458	1.0512	1.0458	1.05893
	10	1.0485	1.0604	1.0485	1.06034

Table 3.2: Values of Skin friction, Nussult number and Sherwood number for different physical parameters.

Pr	Le	Nb	Nt	ε_1	ε_2	λ	A^*	M	β_1	β	Q	θ_r	m	$\alpha=0.25$			$\alpha=0.5$		
														$f''(0)$	$\theta'(0)$	$\phi'(0)$	$f''(0)$	$\theta'(0)$	$\phi'(0)$
1	0.96	0.5	0.5	0.1	0.1	0.1	0.01	0.2	2	1	0.1	-5	**-0.3**	-0.0573	1.883	-1.8833	-0.1095	2.4189	-2.4189
													-0.1	-0.1990	1.520	-.15201	-0.2243	1.8289	-1.8289
													0.0	-0.2369	1.390	-1.3905	-0.2561	1.6311	-1.6311
													0.5	-0.3297	1.025	-1.0256	-0.3356	1.0937	-1.0937
													1.0	-0.3697	08643	-0.8643	-0.3685	0.8643	-0.8643

Pr	Le	Nb	Nt	ε_1	ε_2	λ	A^*	M	m	θ_r	Q	β	α	$\beta_1=1.0$			$\beta_1=2.0$		
1	0.96	0.5	0.5	0.1	0.1	0.1	0.01	0.2	0.5	-5	0.1	**0.5**	0.25	-0.4136	0.987	-0.9876	-0.4489	0.9879	-0.9879
												1.0		-0.4925	0.996	-0.9962	-0.5414	0.9969	-0.9969
												2.0		-0.5851	1.003	-1.0036	-0.6519	1.0044	-1.0044
												5.0		-0.6114	1.004	-1.0045	-0.6839	1.0056	-1.0056

Pr	Le	Nb	Nt	ε_1	ε_2	λ	A^*	M	β_1	Q	θ_r	β	α	$m=0.5$			$m=1.0$		
1	0.96	0.5	0.5	0.1	0.1	0.1	0.1	0.2	2	1	**-10**	1	0.25	-0.5288	0.968	-0.9682	-0.5628	0.8093	-0.8093
											-5.0			-0.5165	0.971	-0.9710	-0.5516	0.8105	-0.8105
											-2.0			-0.4863	0.977	-0.9776	-0.5234	0.8128	-0.8128
											-1.0			-0.4494	0.984	-0.9842	-0.4878	0.8143	-0.8143
											-0.5			-0.4009	0.989	-0.9890	-0.4395	0.8152	-0.8152

θ_r	Le	Nb	Nt	A^*	ε_2	λ	m	M	β_1	Pr	Q	β	α	$\varepsilon_1=0.2$			$\varepsilon_1=0.4$		
-5	0.96	0.5	0.5	0.01	0.1	0.1	0.5	0.2	2	**0.72**	0.1	1	0.25	-0.5275	0.873	-0.8735	-0.5283	0.8758	-0.8758
										1.0				-0.5113	1.042	-1.0429	-0.5118	1.0531	-1.0531
										2.0				-0.4932	1.394	-1.3949	-0.4934	1.4314	-1.4314
										5.0				-0.4844	1.681	-1.6814	-0.4850	1.7462	-1.7462

Pr	Le	m	λ	A^*	ε_2	β_1	ε_1	M	Nb	θ_r	Q	β	α	$Nt=0.5$			$Nt=1$		
1.0	0.96	0.5	0.1	0.01	0.1	0.3	0.1	0.2	**0.5**	-5	0.1	1	0.25	-0.5111	1.036	-1.0366	-0.5149	0.9594	-1.9188
									1.0					-0.5101	1.054	-1.5272	-0.5113	1.0229	-1.0229
									2.0					-0.3415	4.900	-3.6755	-0.5096	1.0544	-0.5272

β_1	M	Nb	Nt	A^*	ε_1	m	λ	Le	Pr	θ_r	Q	β	α	$\varepsilon_2=0.2$			$\varepsilon_2=0.2$		
0.3	0.2	0.5	0.5	0.01	0.1	0.5	0.1	**1.5**	1	-5	0.1	1	0.25	-0.3365	1.0526	-1.0526	-0.3394	0.9289	-0.9289
								2.0						-0.3358	1.0755	-1.0755	-0.3385	0.9599	-0.9599
								5.0						-0.3339	1.1495	-1.1495	-0.3359	1.0579	-1.0579

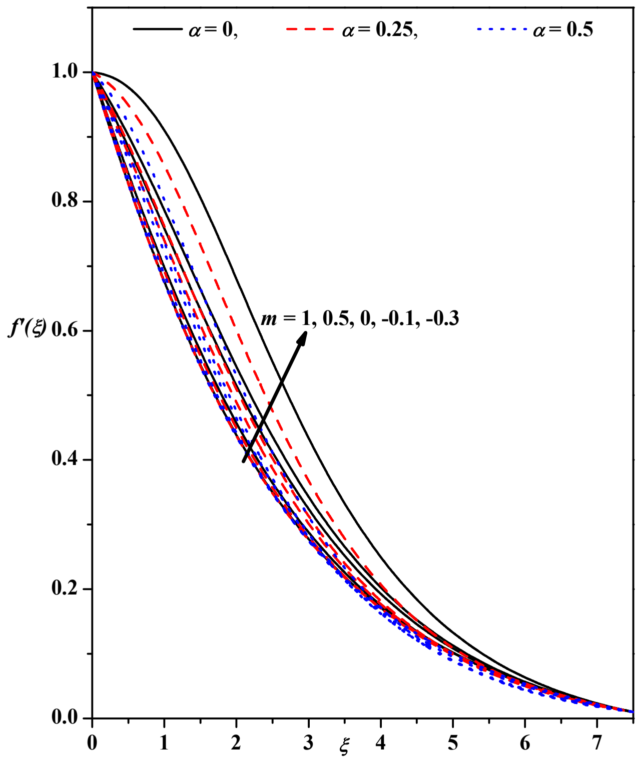

Fig.3.5.1(a) : Horizontal velocity profiles for different values of α and m with $Pr = 1$, $Nb = Nt = 0.5$, $\lambda = 0.1$, $Le = 0.96$, $Q = 0.2$, $\varepsilon_1 = 0.1$, $\varepsilon_2 = 0.1$, $\theta_r = -5$, $\beta_1 = 0.3$, $\beta = 0.2$, $M = 0.2$, $A^* = 0.01$.

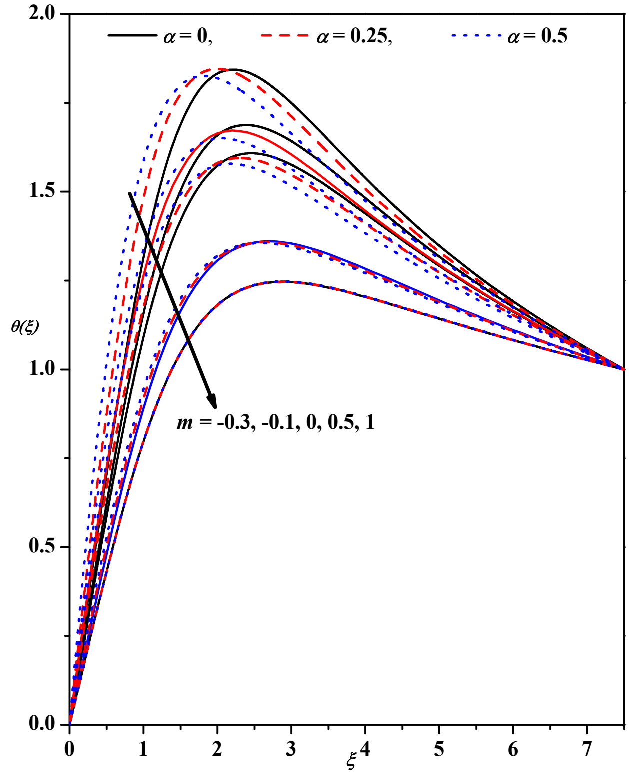

Fig.3.5.1(b) : Temperature profiles for different values of α and m with $Pr = 1$, $Nb = Nt = 0.5$, $Le = 0.96$, $M = 0.2$, $\lambda = 0.1$, $\varepsilon_1 = 0.1$, $\varepsilon_2 = 0.1$, $\theta_r = -5$, $Q = 0.2$, $\beta_1 = 0.3$, $\beta = 0.2$, $A^* = 0.01$.

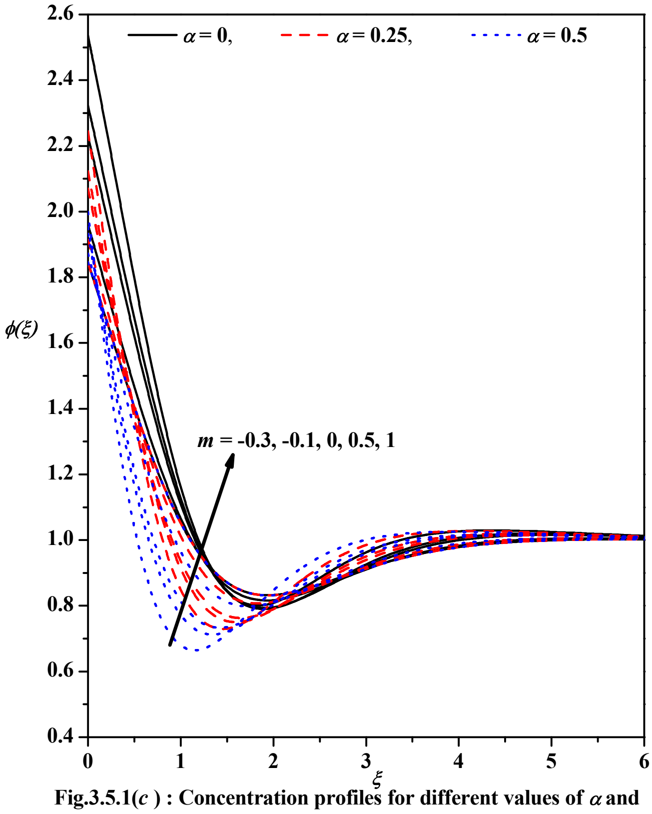

Fig.3.5.1(c) : Concentration profiles for different values of α and m with $Pr = 1$, $Nb = Nt = 0.5$, $Le = 0.96$, $M = 0.2$, $\lambda = 0.1$, $\varepsilon_1 = 0.1$, $\varepsilon_2 = 0.1$, $\theta_r = -5$, $Q = 0.2$, $\beta_1 = 0.3$, $\beta = 0.2$, $A^* = 0.01$.

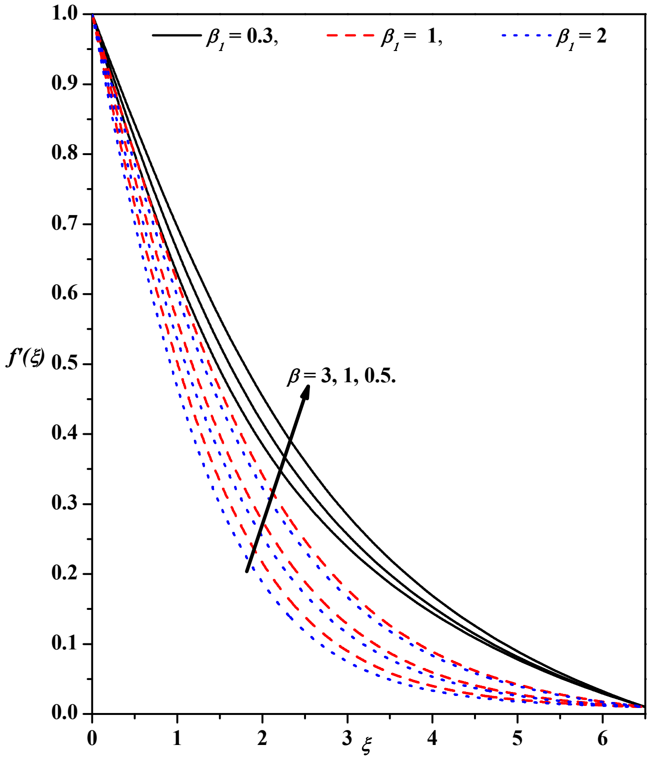

Fig.3.5.2(a) : Horizontal velocity profiles for different values of β and β_1 with $Pr = 1$, $Nb = 0.5$, $Nt = 0.5$, $Le = 0.96$, $M = 0.2$, Q = 0.1, $\varepsilon_1 = 0.1$, $\varepsilon_2 = 0.1$, $\theta_r = -5$, $m = 0.5$, $\alpha = 0.25$, $\lambda = 0.1$, $A^* = 0.01$.

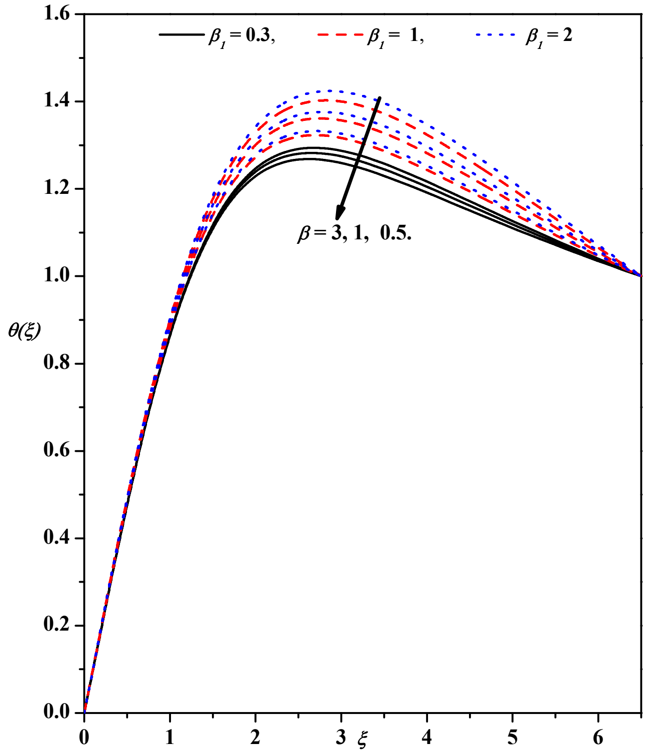

Fig.3.5.2(b) : Temperature profiles for different values of β and β_1 with $Pr = 1$, $Nb = 0.5$, $Nt = 0.5$, $Le = 0.96$, $M = 0.2$, $\varepsilon_1 = 0.1$, $\varepsilon_2 = 0.1$, $\theta_r = -5$, $m = 0.5$, Q = 0.1, $\alpha = 0.25$, $\lambda = 0.1$, $A^* = 0.01$.

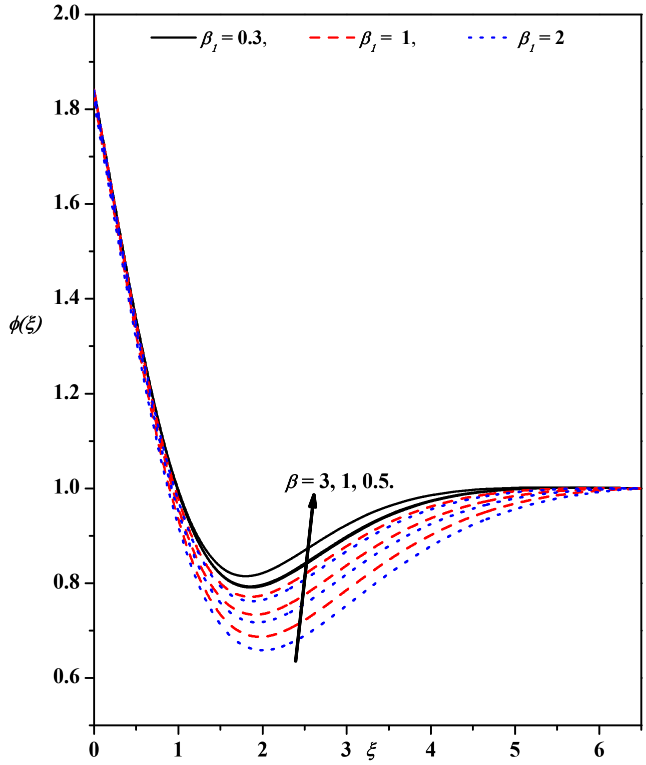

Fig.3.5.2(c) : Concentration profiles for different values of β and β_1 with $Pr = 1$, $Nb = Nt = 0.5$, $Le = 0.96$, $M = 0.2$, Q = 0.1, $\varepsilon_1 = 0.1$, $\varepsilon_2 = 0.1$, $\theta_r = -5$, $m = 0.5$, $\alpha = 0.25$, $\lambda = 0.1$, $A^* = 0.01$.

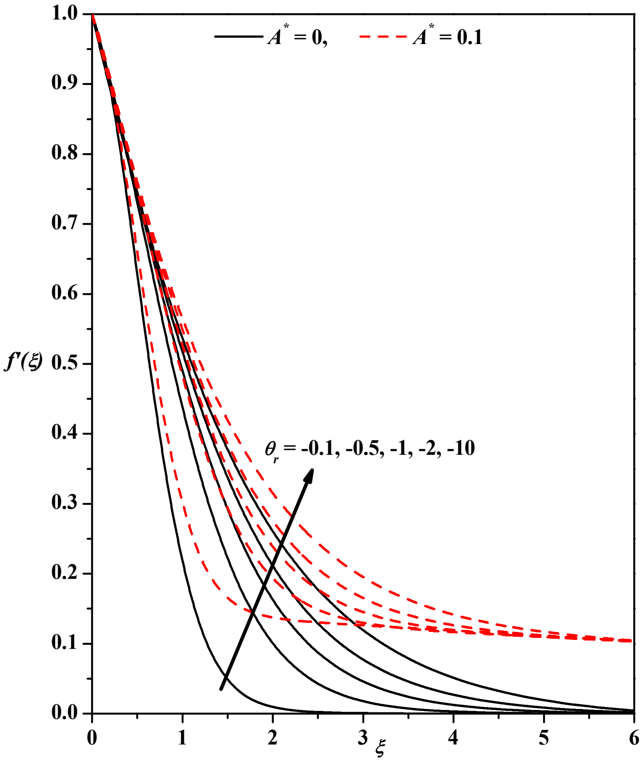

Fig.3.5.3(*a*) : Horizontal velocity profiles for different values of θ_r and A^* with $Pr = 1$, $Nb = Nt = 0.5$, $Le = 0.96$, $M = 0.2$, $\lambda = 0.1$, $\varepsilon_1 = 0.1$, $\varepsilon_2 = 0.1$, $\alpha = 0.25$, $Q = 1$, $\beta_1 = 2$, $\beta = 1$, $m = 0.5$.

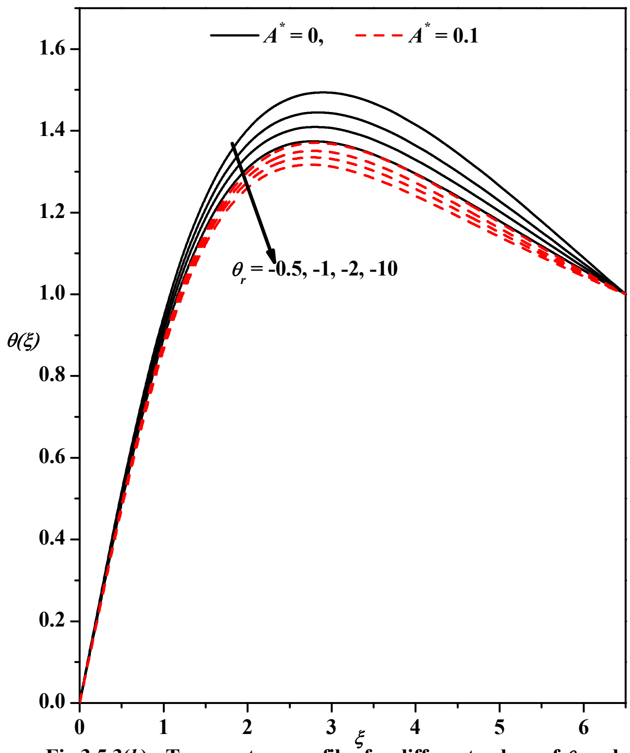

Fig.3.5.3(*b*) : Temperature profiles for different values of θ_r and A^* with $Pr = 1$, $Nb = Nt = 0.5$, $Le = 0.96$, $M = 0.2$, $\lambda = 0.1$, $\varepsilon_1 = 0.1$, $\varepsilon_2 = 0.1$, $\alpha = 0.25$, $Q = 1$, $\beta_1 = 2$, $\beta = 1$, $m = 0.5$.

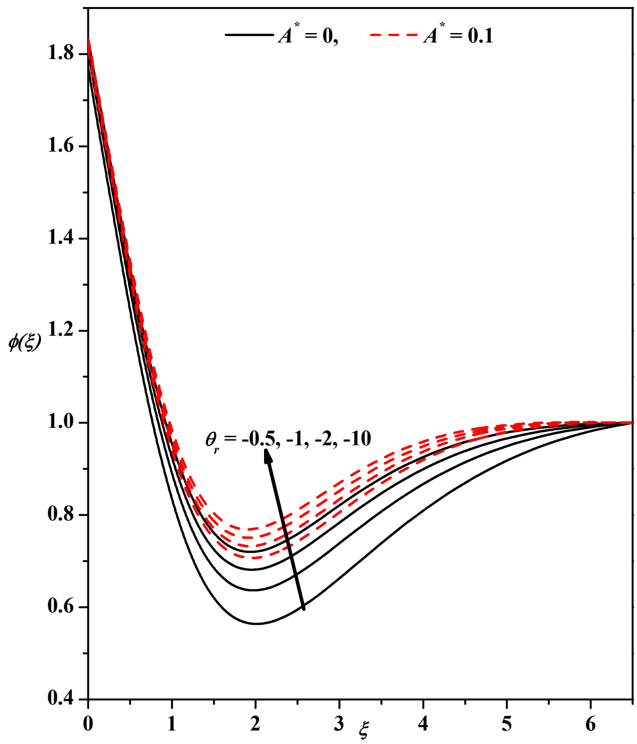

Fig.3.5.3(*c*) : Concentration profiles for different values of θ_r and A^* with $Pr = 1$, $Nb = 0.5$, $Nt = 0.5$, $Le = 0.96$, $M = 0.2$, $\lambda = 0.1$, $\varepsilon_1 = 0.1$, $\varepsilon_2 = 0.1$ $\alpha = 0.25$, $Q = 1$, $\beta_1 = 2$, $\beta = 1$, $m = 0.5$.

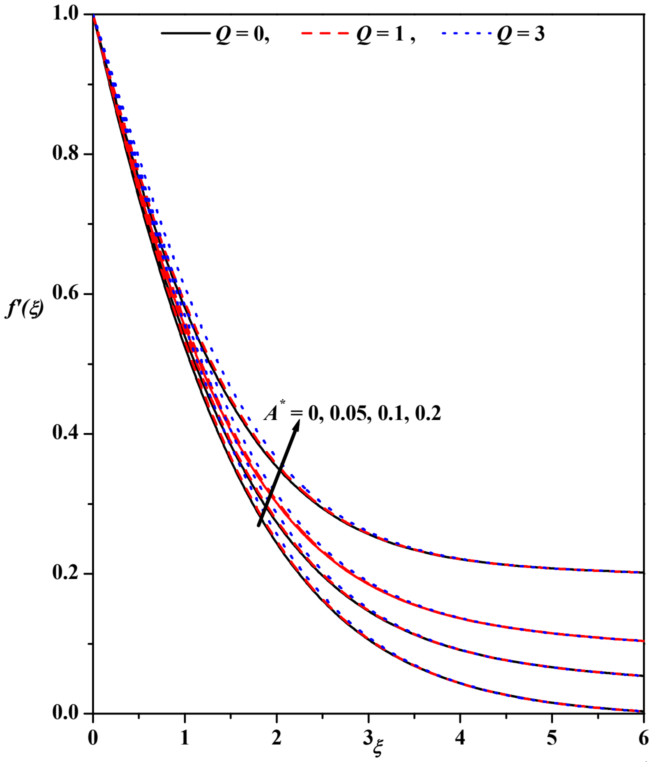

Fig.3.5.4: Horizontal velocity profiles for different values of A^* and Q with $Pr = 1$, $Nb = Nt = 0.5$, $Le = 0.96$, $M = 0.2$, $\lambda = 0.1$, $\alpha = 0.25$, $\varepsilon_1 = 0.1$, $\varepsilon_2 = 0.1$, $\theta_r = -5$, $m = 0.5$, $\beta_1 = 0.3$, $\beta = 1$.

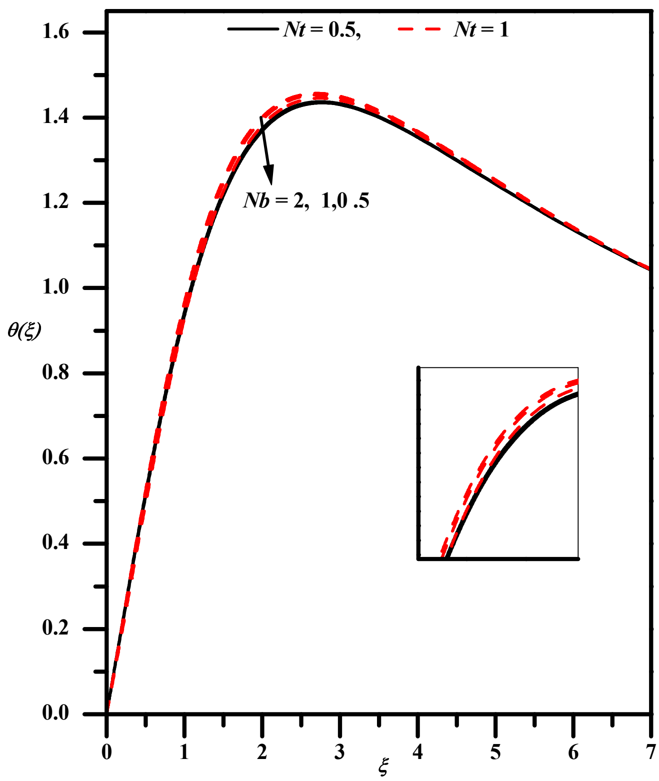

Fig.3.5.5(a) : Temperature profiles for different values of Nb and Nt with $Pr = 1$, $Le = 0.96$, $M = 0.2$, $\lambda = 0.1$, $\varepsilon_1 = 0.1$, $\varepsilon_2 = 0.1$, $\alpha = 0.25$, $Q = 1$, $\beta_1 = 2$, $\beta = 1$, $\theta_r = -0.5$, $A^* = 0.01$.

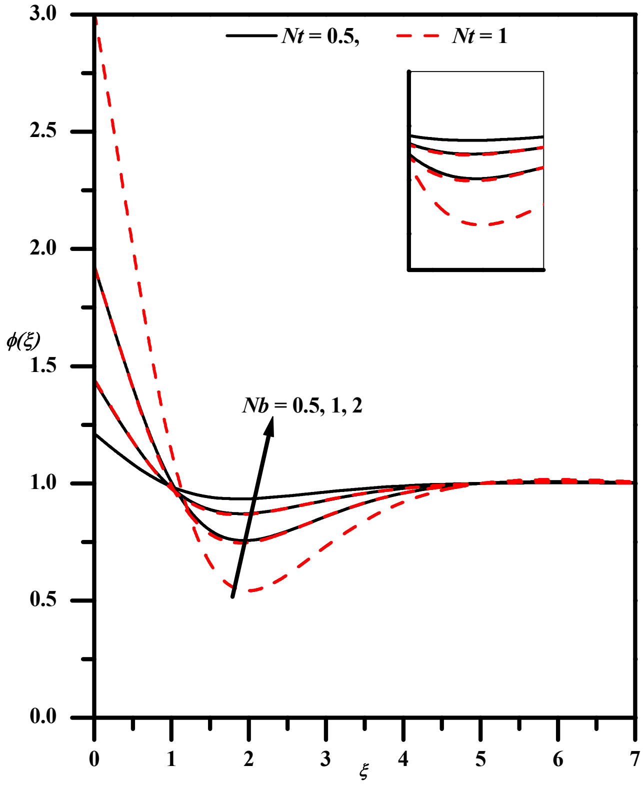

Fig.3.5.5(b) : Concentration profiles for different values of Nb and Nt with $Pr = 1$, $Le = 0.96$, $M = 0.2$, $\lambda = 0.1$, $\varepsilon_1 = 0.1$, $\varepsilon_2 = 0.1$, $\alpha = 0.25$, $Q = 1$, $\beta_1 = 2$, $\beta = 1$, $\theta_r = -0.5$, $A^* = 0.01$.

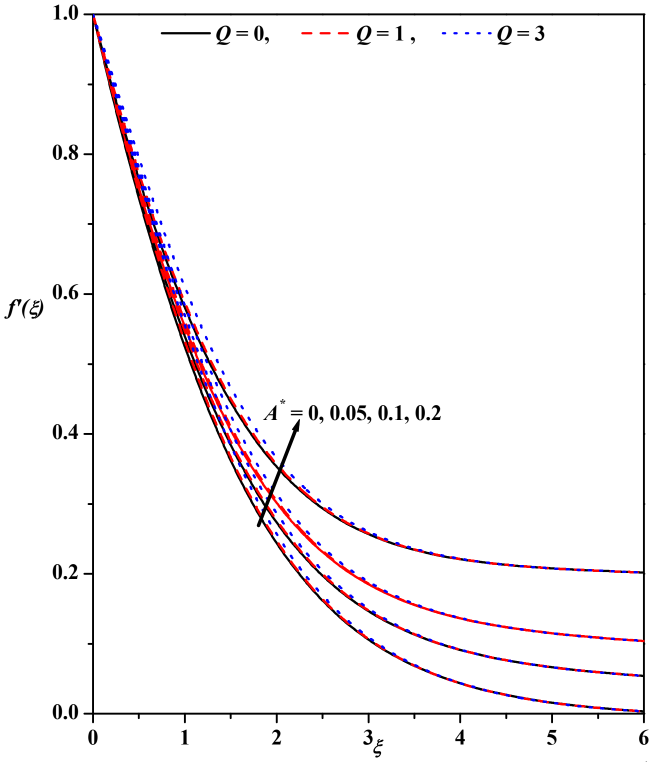

Fig.3.5.4: Horizontal velocity profiles for different values of A^* and Q with $Pr = 1$, $Nb = Nt = 0.5$, $Le = 0.96$, $M = 0.2$, $\lambda = 0.1$, $\alpha = 0.25$, $\varepsilon_1 = 0.1$, $\varepsilon_2 = 0.1$, $\theta_r = -5$, $m = 0.5$, $\beta_1 = 0.3$, $\beta = 1$.

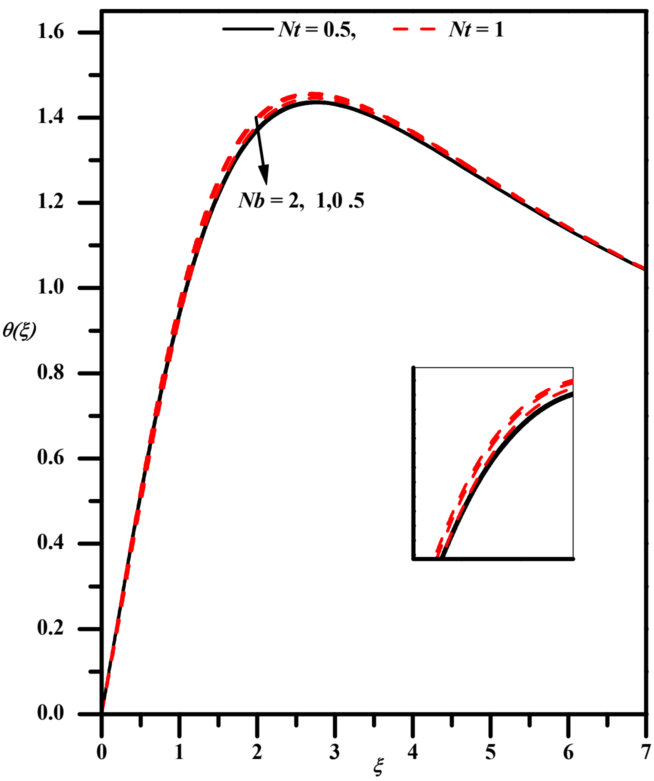

Fig.3.5.5(a) : Temperature profiles for different values of Nb and Nt with $Pr = 1$, $Le = 0.96$, $M = 0.2$, $\lambda = 0.1$, $\varepsilon_1 = 0.1$, $\varepsilon_2 = 0.1$, $\alpha = 0.25$, $Q = 1$, $\beta_1 = 2$, $\beta = 1$, $\theta_r = -0.5$, $A^* = 0.01$.

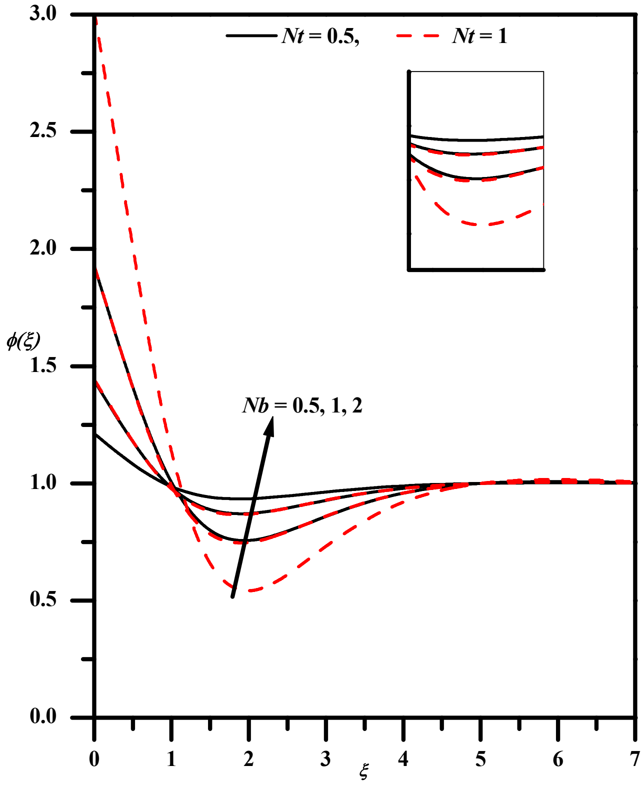

Fig.3.5.5(b) : Concentration profiles for different values of Nb and Nt with $Pr = 1$, $Le = 0.96$, $M = 0.2$, $\lambda = 0.1$, $\varepsilon_1 = 0.1$, $\varepsilon_2 = 0.1$, $\alpha = 0.25$, $Q = 1$, $\beta_1 = 2$, $\beta = 1$, $\theta_r = -0.5$, $A^* = 0.01$.

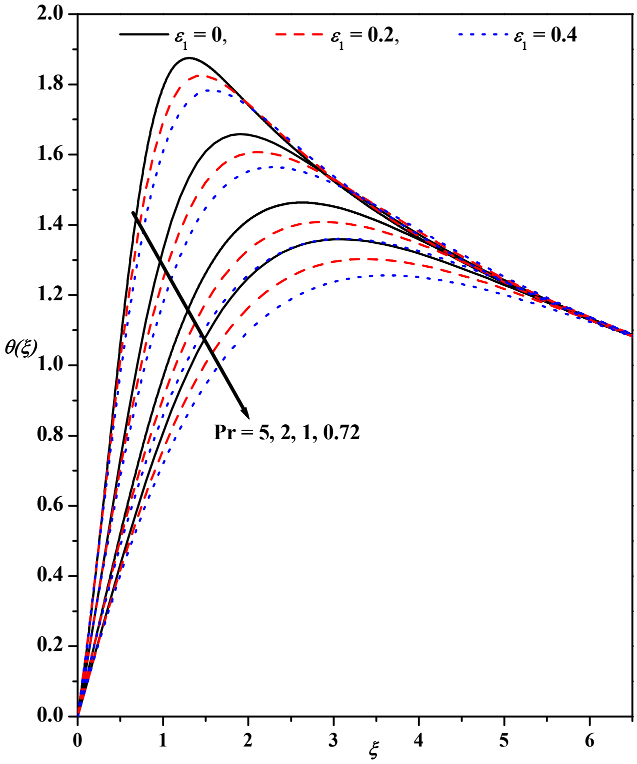

Fig.3.5.6 : Temperature profiles for different values of ε_1 and Pr with $m = 0.5$, $Nb = 0.5$, $Nt = 0.5$, $Le = 0.96$, $M = 0.2$, $\lambda = 0.1$, $\alpha = 0.25$, $\varepsilon_2 = 0.1$, $\theta_r = -5$, $Q = 1$, $\beta_1 = 0.3$, $\beta = 1$, $A^* = 0.01$.

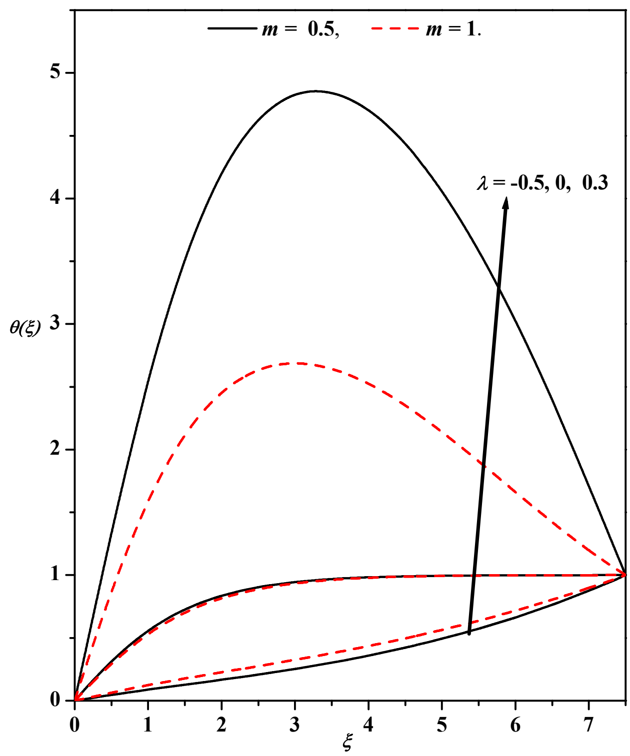

Fig.3.5.7: Temperature profiles for different values of λ and m with $Le = 0.96$, $Nb = Nt = 0.5$, $M = 0.2$, $\lambda = 0.1$, $Q = 1$, $\alpha = 0.25$, $\varepsilon_2 = 0.1$, $A^* = 0.01$, $\theta_r = -5$, $\beta_1 = 0.3$, $\beta = 1$.

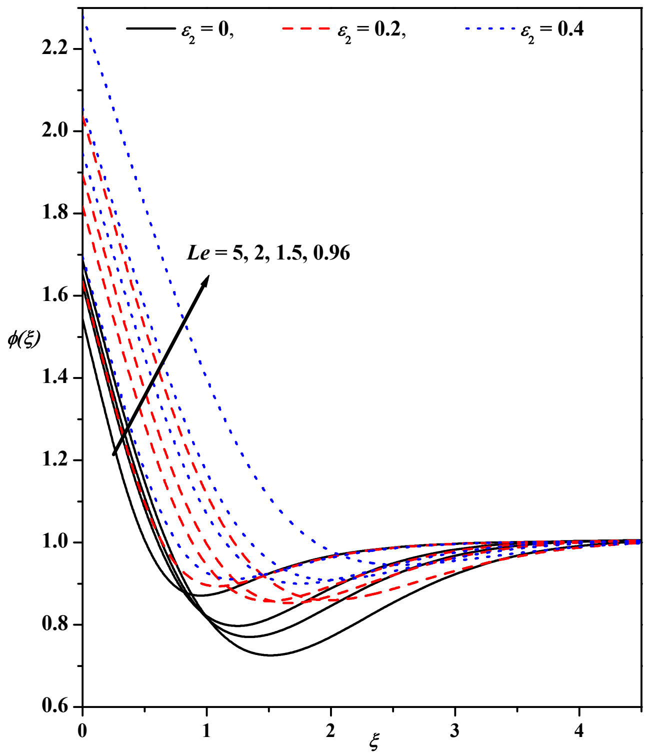

Fig.3.5.8 : Concentration profiles for different values of ε_2 and Le with $m = 0.5$, $Nb = Nt = 0.5$, $M = 0.2$, $\lambda = 0.1$, $\alpha = 0.25$, $\varepsilon_2 = 0.1$, $A^* = 0.01$, $\theta_r = -5$, $Q = 1$, $\beta_1 = 0.3$, $\beta = 1$.

CHAPTER - 4

MIXED CONVECTIVE NANOFLUID FLOW OVER A COAGULATED RIGA PLATE IN THE PRESESNCE OF VISCOUS DISSIPATION AND CHEMICAL REACTION

Part of this work has communicated to the ***"Journal of Applied and Computational Mechanics"*** **2020**

4.1.Introduction

The stretching sheet is a blend of metal and polymer sheets that are used in the polymer extrusion processes. The flow induced by a special form of a stretching sheet has received the attention of numerous researchers. The special form of a stretching sheet is called a variable thickened sheet; it helps to reduce the weight of structural elements in the mechanical, civil, automobile, and aeronautical engineering. Because of these facts, Lee (1967) has introduced the concept of a needle whose thickness is comparable with the boundary layer. Fang et al., (2012) extended the work of Lee (1967) by considering slip velocity and obtained a dual solution. Khader and Megahed (2015) investigate the numerical solution for the slip velocity on the flow of a Newtonian fluid over stretching with variable thickness and Anjali Devi and Prakash (2016) considered similar geometry for MHD flow and heat transfer. The combined effect of variable viscosity and thermal conductivity on the flow field over a slender elastic sheet was examined by Vajravelu et al., (2017). Recently, Prasad et al., (2017a) and Muhammad et al., (2018) described the mixed convection boundary layer flow and heat transfer of a variably thickened vertically stretched heated sheet. The aspect of mixed convective boundary layer flow has a wide range of applications. Few such applications may include, solar receivers exposed to wind currents, electronic devices cooled by fans, nuclear reactors cooled during an emergency shutdown, heat exchangers placed in a low-velocity environment, drying technologies, etc. In studies (Vajravelu (1994), Ishak et al., (2008), Prasad et al., (2010), Das et al., (2015)) characteristics of the mixed convective boundary layer flows are analyzed.

In modern days, nanotechnology becomes one of the most powerful research areas due to its importance in various fields of science and the industrial sector. Practically, convectional heat transfer fluids, including oil, water, grease, ethylene glycol, and engine oil, contain low thermal conductivity in comparison with solids. To lead this situation, adding a small number of solid particles to the fluids; as a result, thermophysical properties gradually improve, and hence these are known as nanofluids (see details, Choi (1995)). These are made up of tiny minute particle suspensions (metals, oxides, carbide ceramics, and carbon nanotubes, etc.) having size 10-50 nm. An instant research work grabbed more attention from various researchers due to their applications in science and engineering fields, such as microelectronic cooling, air conditioning, transpiration, ventilation, etc. The Brownian motion and thermophoresis effects on heat and mass transfer analysis were examined by Buongiorno (2006). To get more details of these fluids, some relevant investigations have mentioned in Refs. (Makinde and Aziz (2011), Shiekholeslami and Rokni (2017), Prasad et al., (2017a), Wakif et al.,(2018a, 2018b, 2018c)).

For highly conducting fluids such as liquid metals, plasma and electrolytes, etc, can be significantly controlled by applying an external magnetic fields, this type of mechanism is known as classical electro magnetohydrodynamic fluid flow control, which plays a vital role in science and industrial applications, such as in engineering, geophysics, astrophysics earthquakes, and sensors, etc. However, some of the fluids have low electrical conductivity and very small induced current when the magnetic field is present; therefore, to lead this difficult situation, it is necessary to apply an external electric field to control EMHD flow. To overcome these problems, two scientists named Gailitis and Lielausis (1961) framed the control device called the Riga plate to produce electric and magnetic fields simultaneous and, therefore, which can create wall parallel Lorentz force in weakly conducting fluids. Tsinober and Shtern (1961) extended this work to Blasius flow. Further, Pantokratoras and Magyari (2009) improved the work of Gailitis and Lielausis (1961) by considering a very basic aspect of the boundary layer flow of low electrically conducting fluids over the Riga plate. Hayat et al., (2016b, 2016c) described the convective heat transfer in the boundary layer flow of an electrically conducting nanofluid over a stretchable Riga plate with variable thickness. Recently, Bhatti et al., (2016) and Iqbal et al., (2017) examined the effects of thermal radiation and melting heat transport of electromagnetic hydrodynamics on viscous nanofluid through a Riga plate. Furthermore, Nayak et al., (2018a, 2018b, 2019) considered NaCl-CNP nanofluid, third grade nanofluid and tangent hyperbolic nanofluid to examine the flow nature through vertical Riga plate.

The preceding works of literature give inspiration for the authors to study the flow, heat, and mass transfer characteristics of a mixed convective nanofluid over a coagulated Riga plate in the presence of viscous dissipation and chemical reaction. The physical impacts of the governing partial differential equations are converted into a set of ordinary differential equations with the help of appropriate similarity transformations. In the present work, an optimal homotopy analysis method (OHAM) (see Liao (2010), Van Gorder (2019)) is used to solve the coupled nonlinear ordinary differential equations. The outcomes of the numerical computation via MATHEMATICA 12 software are graphically manifested and tabulated for the nanofluid velocity, temperature, and concentration within the appropriate scope of the relevant parameters. The obtained results are compared with the earlier published results and are found to be in excellent agreement. Here it is to be expected that the present literature provides useful information for science and industrial applications.

4.2. Mathematical Formulation

A steady two – dimensional convective boundary layer flow of a viscous incompressible nanofluid past an impermeable vertical heated coagulated Riga plate with zero mass flux at the surface is imposed for the investigation. Riga plate comprises permanent magnets and alternating electrodes in which x_1- axis is considered vertically above, as shown in Fig. 4.2.1(a). These arrays produce a Lorentz force which is parallel to the surface and exponentially decreases in the direction horizontal to the plate. The origin is situated at the ¸slot of the coagulated Riga plate with positive x_1-axis measured along the upward course of the plate and negative being measured opposite to it as exhibited in Fig.4.2.1(b). The flow is confined in the positive direction of the x_2-axis , which is caused due to continuous stretching of the plate with the simultaneous application of two equal opposite forces along the x_1-axis , such that the origin (variable thickness of the plate) is fixed. The velocity of the coagulated Riga plate is assumed to be $U_w(x_1) = U_0(x_1 + b)^m$, where U_0 is a positive constant, b is a small physical parameter which is related to the slender of an elastic sheet and m is the velocity exponent parameter. The sheet is not uniform, and its thickness is taken as $x_2 = A(x_1 + b)^{(1-m)/2}, m \neq 1,$ where A is very small constant related to the stretching sheet. At $m = 1,$ the present physical problem reduces to plane stretching sheet. Heat transfer characteristics are analyzed by considering the effects of viscous dissipation, Brownian motion and thermophoresis phenomena, the temperature and nanoparticle concentration at the non-uniform (variable thickness) surface of the coagulated Riga plate is assumed as $T_w(x_1) = A_1(x_1 + b)^r$ and $C_w(x_1) = A_2(x_1 + b)^s$ respectively, r and s are positive constants, and the ambient temperature and nanoparticle concentration are respectively denoted as T_∞ and C_∞. The physical diagram of the present problem is given as,

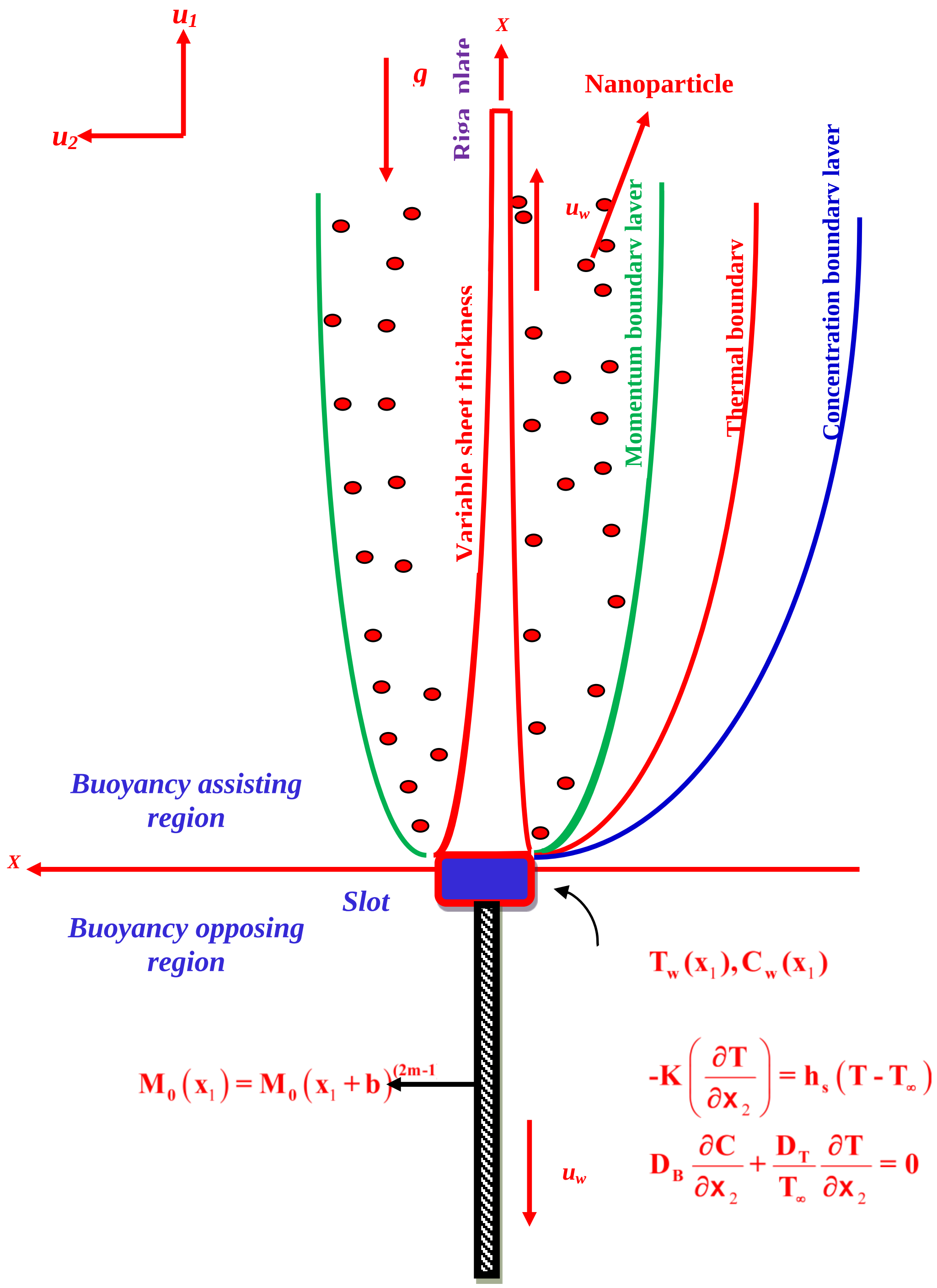

Fig.4.2.1 (a) : Physical model of variable thickness of the sheet.

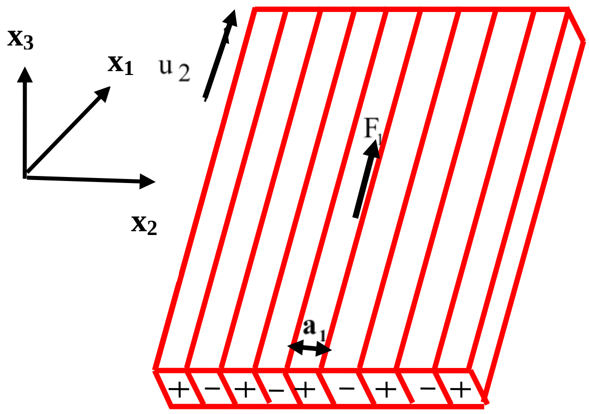

Fig.4.2.1(b): Riga plate.

Under the above assumptions and the usual boundary layer approximations, the governing equations for the mixed convective flow heat and mass transfer in usual notations can be written as,

$$\frac{\partial u_1}{\partial x_1}+\frac{\partial u_2}{\partial x_2}=0 \tag{4.2.1}$$

$$u_1\frac{\partial u_1}{\partial x_1}+u_2\frac{\partial u_1}{\partial x_2}=\nu\frac{\partial^2 u_1}{\partial x_2^2}+\frac{\pi j_0 M_0\left(x_1\right)}{8\rho}\exp\left(\frac{-\pi}{a_1\left(x_1\right)}x_2\right)+g\beta_T\left(T-T_\infty\right)+g\beta_C\left(C-C_\infty\right) \tag{4.2.2}$$

$$u_1\frac{\partial T}{\partial x_2}+u_2\frac{\partial T}{\partial x_2}=\alpha_1\frac{\partial^2 T}{\partial x_2^2}+\tau\left[D_B(C)\frac{\partial C}{\partial x_2}\frac{\partial T}{\partial x_2}+\frac{D_T}{T}\left(\frac{\partial T}{\partial x_2}\right)^2\right]+\frac{Q_0\left(x_1\right)}{\rho c_p}(T-T_\infty)+\frac{\mu}{\rho c_p}\left(\frac{\partial u_1}{\partial x_2}\right)^2 \tag{4.2.3}$$

$$u_1\frac{\partial C}{\partial x_1}+u_2\frac{\partial C}{\partial x_2}=D_B\frac{\partial^2 C}{\partial x_2^2}+\frac{D_T}{T_\infty}\frac{\partial^2 T}{\partial x_2^2}-K_1\left(x_1\right)\left(C-C_\infty\right) \tag{4.2.4}$$

and the corresponding boundary conditions can be written as,

$$\left.\begin{aligned}&u_1=U_w(x_1)=U_0(x_1+b)^m, && u_2=0\\ &-K\left(T\right)\frac{\partial T}{\partial x_2}=h_s(x_1)(T_w-T), && D_B\frac{\partial C}{\partial x_2}+\frac{D_T}{T_\infty}\frac{\partial T}{\partial x_2}=0,\end{aligned}\right\}\text{at } x_2=A(x_1+b)^{1-m/2}$$
$$u_1\to U_e(x_1)=U_\infty(x_1+b)^m,\ T\to T_\infty,\ C\to C_\infty \quad \text{as} \quad x_2\to\infty \tag{4.2.5}$$

in the above equations u_1 and u_2 are the velocity components along the Cartesian coordinates x_1 and x_2 respectively, ν is the kinematic viscosity, j_0 is the applied current density in the electrodes, ρ is the fluid density, g is the acceleration due to gravity, β_T is thermal expansion coefficient, β_C is the concentration expansion coefficient, α_1 is the thermal diffusivity, τ is the ratio between the effective heat capacity of the nanoparticle material and heat capacity of the fluid, D_B is the Brownian diffusion coefficient, D_T is the thermophoresis diffusion coefficient, c_p is the specific heat at constant pressure, μ is dynamic viscosity, and $K_1(x_1)$ is the local chemical reaction rate parameter and exhibits destructive chemical reaction and generative chemical reaction for greater than zero and less than zero respectively. thermal conductivity, T and C are temperature and nanoparticle concentration of the fluid respectively. The special forms of $M_0\left(x_1\right)=M_0\left(x_1+b\right)^{2m-1}, a_1\left(x_1\right)=a_1\left(x_1+b\right)^{1-m/2}, K_1\left(x_1\right)=K_1\left(x_1+b\right)^{m-1},, Q_0\left(x_1\right)=Q_0\left(x_1+b\right)^{m-1}$ and $h_s\left(x_1\right)=h_s\left(x_1+b\right)^{1-m/2}$ are respectively the variable magnetization of the permanent magnets mounted on the surface of the Riga plate, the variable width between the magnets and electrodes, the variable chemical reaction rate, the variable heat generation/absorption coefficient, and is the surface variable heat transfer coefficient. These special forms are chosen to obtain the similarity solution. The third term on the right-hand side of the equation (4.2.2) represents the buoyancy force term, with "+" and "-" signs refer to the buoyancy assisting and buoyancy opposing flows, respectively. Fig.4.2.1(a) provides the necessary information of such a flow field for a stretching vertical heated sheet with the upper half of the flow field being assisted and the lower half of the flow field being opposed by the buoyancy force. For the assisting flow, the x_1-axis points upward in the direction of the stretching hot surface such that the stretching induced flow and the buoyant thermal flow assist each other. For the opposing flow, the x_1- axis points vertically downward in the direction of the stretching hot surface, but in this case, the stretching induced flow and the buoyant thermal flow oppose each other. The reverse trend occurs if the sheet is cooled below the ambient temperature.

The mathematical analysis of the present problems is simplified by introducing the following dimensionless similarity variables,

$$\eta = x_2 \sqrt{\frac{(m+1)}{2} \frac{U_0 (x_1 + b)^{(m-1)}}{\nu}}. \tag{4.2.6}$$

and the dimensionless stream function, temperature, and the nanoparticle concentration are given by;

$$\psi = \sqrt{\frac{2}{m+1} \nu U_0 (x_1 + b)^{(m+1)}} \mathrm{F}(\eta), \qquad \Theta(\eta) = \frac{T - T_\infty}{T_w - T_\infty}, \qquad \Phi(\eta) = \frac{C - C_\infty}{C_w - C_\infty} \tag{4.2.7}$$

The stream function satisfies automatically the equation of continuity and the velocity components are

$$u_1 = U_0 (x_1 + b)^m F'(\eta), \quad u_2 = -\sqrt{\frac{2}{m+1} \nu_\infty U_0 (x_1 + b)^{(m-1)}} \left[\frac{m+1}{2} F(\eta) + \eta \frac{m-1}{2} F'(\eta) \right], \tag{4.2.8}$$

where primes denote the differentiation concerning η, with the use of Eqs. (4.2.6) - (4.2.8), the Eqs. (4.2.2) to (4.2.5) reduces to,

$$F''' + FF'' - \frac{2m}{(m+1)} \left[F'^2 - Qe^{-\beta_1 \eta} - \lambda_T \left(\Theta + \lambda_C \Phi \right) \right] = 0 \tag{4.2.9}$$

$$\Theta'' + \Pr\Theta'[Nb\Phi' + Nt\Theta' + F] - \frac{\mathbf{2}\Pr}{m+\mathbf{1}}\left[\left(\mathbf{2}m-\mathbf{1}\right)F'\Theta - \lambda\Theta\right] + \Pr Ec\ \ F''^{2} = \mathbf{0} \tag{4.2.10}$$

$$\Phi'' + \left(\frac{Nt}{Nb}\right)\Theta'' - \frac{2}{m+1}\left[\left(2m-1\right)ScF'\Phi + K_c\Phi\right] + Sc\,F\Phi' = 0 \tag{4.2.11}$$

$$\begin{gathered} F(\alpha) = \alpha\left(\frac{1-m}{1+m}\right),\ F'(\alpha) = 1,\ \Theta'(\alpha) = -Bi\left(1-\Theta(\alpha)\right),\ \ Nb\Phi'(\alpha) + Nt\Theta'(\alpha) = 0, \\ F'(\infty) \to 0, \qquad \Theta(\infty) \to 0, \qquad \Phi(\infty) \to 0. \end{gathered} \tag{4.2.12}$$

It is worth mentioning that for $\lambda > 0$ assist the flow and for $\lambda < 0$ opposes the flow, whereas for $\lambda = 0$ represents the case when the buoyancy forces are absent. On the other hand, if λ is of a significantly greater order of magnitude than one, the buoyancy forces will predominant, and the flow will essentially be free convective. Hence, combined convective flow exists when $\lambda = O(1)$. The non-dimensional parameters $Q,\ \beta_1, \lambda_T, \lambda_C$ Pr, $Nb, Nt,\ \lambda, Ec, Sc,\ K_c,\ \alpha$ and Bi represents the modified Hartman number, dimensionless parameter, thermal buoyancy parameter, concentration buoyancy parameter, Prandtl number, Brownian motion parameter, thermophoresis parameter, heat source/sink parameter, Eckert number, Schmidt number, Chemical reaction parameter, wall thickness parameter, and the dimensionless Biot number respectively and which are defined by,

$$\begin{gathered} Q = \frac{\pi j_0 M_0}{8\rho_\infty U_0^2},\ \ \beta_1 = \frac{\pi}{a_1}\sqrt{\frac{2}{(m+1)}\frac{\nu}{U_0}},\quad \lambda_T = \pm\frac{g\beta A_1}{U_0^2},\quad \lambda_C = \frac{g\beta_C A_2}{U_0^2},\quad \Pr = \frac{\nu}{\alpha_1}, \\ Nb = \frac{\tau D_B(C_w - C_\infty)}{\nu},\quad Nt = \frac{\tau D_T(T_w - T_\infty)}{T_\infty \nu},\quad \lambda = \frac{Q_0}{\rho c_p U_0},\quad Ec = \frac{U_w^2}{c_p\left(T_w - T_\infty\right)}, \\ Sc = \frac{\nu}{D_B}, K_c = \frac{K_1}{U_0},\ \alpha = A\sqrt{\frac{U_0(m+1)}{2\nu}},\ Bi = \frac{h_s}{k}\sqrt{\frac{2}{(m+1)}\frac{\nu}{U_0}}. \end{gathered} \tag{4.2.13}$$

Now, we define the following $F(\eta) = f(\xi),\ \Theta(\eta) = \theta(\xi)\ \ \Phi(\eta) = \phi(\xi)\ \ where\ \xi = \eta - \alpha$: here $\eta = \alpha$ indicates the flat surface. Then Eqs. (4.2.9) to (4.2.12) reduces to,

$$f''' + ff'' - \frac{2m}{m+1}\left[f'^2 - Qe^{-\beta_1(\xi+\alpha)} - \lambda_T\left(\theta + \lambda_C\phi\right)\right] = 0 \tag{4.2.14}$$

$$\theta'' + \Pr\theta'[Nb\phi' + Nt\theta' + f] - \frac{2\Pr}{m+1}\left[\left(2m-1\right)f'\theta - \lambda\theta\right] + \Pr Ec\ \ f''^2 = 0 \tag{4.2.15}$$

$$\phi'' + \left(\frac{Nt}{Nb}\right)\theta'' - \frac{2}{m+1}\left[\left(2m-1\right)Scf'\phi + K_c\phi\right] + Scf\phi' = 0 \tag{4.2.16}$$

$$f(0)=\alpha\left(\frac{1-m}{1+m}\right), \quad f'(0)=1,\ \theta(0)=-Bi\left(1-\theta(0)\right),\ Nb\,\phi'(0)+Nt\,\theta'(0)=0,$$
$$f'(\infty)\to 0, \qquad \theta(\infty)\to 0, \qquad \phi(\infty)\to 0. \tag{4.2.17}$$

The important physical quantities of interest for the governing flow problem, such as skin friction C_f, local Nusselt number $Nu,$ and Sherwood number Sh are defined as follow, $C_f=\frac{\tau_w}{U_w^2}, Nu=\frac{(x_1+b)q_w}{T_w-T_\infty}, Sh=\frac{(x_1+b)\,j_w}{C_w-C_\infty},$

where $\tau_w=\nu\left(\partial u_1/\partial x_2\right),\ q_w=\left(\partial T/\partial x_2\right)$ and $j_w=\left(\partial C/\partial x_2\right)$ at $x_2=A\left(x_1+b\right)^{1-m/2}$, respectively called wall skin friction, wall heat flux, and mass flux. Using the above-mentioned similarity transformations, the Skin friction, Nusselt number, and Sherwood number in dimensionless form can be written as,

$$\mathrm{Re}^{1/2}C_f=\sqrt{\frac{m+1}{2}}f''(0),\ \mathrm{Re}^{-1/2}Nu=-\sqrt{\frac{m+1}{2}}\theta'(0)\text{ and }\mathrm{Re}^{-1/2}Sh=-\sqrt{\frac{m+1}{2}}\phi'(0),$$

where $\mathrm{Re}=U_w(x_1+b)/\nu_\infty$ is called local Reynolds number.

4.3. Semi-analytical solution: Optimal Homotopy Analysis Method (OHAM)

The system of highly nonlinear coupled differential equations (4.2.14) – (4.2.16) along with appropriate boundary conditions (4.2.17) is solved by a semi-analytical method known as Optimal Homotopy Analysis Method (OHAM). The detailed information of OHAM procedure can be seen in Liao (2010), Fan and You (2013) and Van Gorder (2019). Depending on the respective boundary conditions (4.2.17), the appropriate initial guesses for the functions f, θ and ϕ are defined as.

$$f_0(\xi)=\alpha\left(\frac{1-m}{1+m}\right)+1-e^{-\xi},\quad \theta_0(\xi)=\frac{Bi}{1+Bi}e^{-\xi}\quad \text{and } \phi_0(\xi)=\frac{-Bi}{1+Bi}\left(\frac{Nt}{Nb}\right)e^{-\xi}, \tag{4.3.1}$$

and the auxiliary linear operators which can satisfy above initial guesses are.

$$\mathrm{L}_f=\frac{d^3}{d\xi^3}-\frac{d}{d\xi},\ \mathrm{L}_\theta=\frac{d^2}{d\xi^2}-1\text{ and }\mathrm{L}_\phi=\frac{d^2}{d\xi^2}-1. \tag{4.3.2}$$

The generalized homotopic equations for Eqns. (4.2.14)-(4.2.16) are,

$$\begin{aligned}
(1-q)L_f\left[\hat{f}(\xi;q)-f_0(\xi)\right]&=qH_f(\xi)\hbar_f N_f\left[\hat{f}(\xi;q),\hat{\theta}(\xi;q),\hat{\phi}(\xi;q)\right],\\
(1-q)L_\theta\left[\hat{\theta}(\xi;q)-\theta_0(\xi)\right]&=qH_\theta(\xi)\hbar_\theta N_\theta\left[\hat{\theta}(\xi;q),\hat{f}(\xi;q),\hat{\phi}(\xi;q)\right],\\
(1-q)L_\phi\left[\hat{\phi}(\xi;q)-\phi_0(\xi)\right]&=qH_\phi(\xi)\hbar_\phi N_\phi\left[\hat{\phi}(\xi;q),\hat{\theta}(\xi;q),\hat{f}(\xi;q)\right].
\end{aligned} \tag{4.3.3}$$

Here q is defined as an embedding parameter which takes values as $0 \le q \le 1$, while $\left(\hbar_f, \hbar_\theta, \hbar_\phi\right) \neq 0$ are the convergence control parameters, and the nonlinear differential operators are defined as fallow,

$$\begin{aligned} \mathrm{N}_f[\hat{f},\hat{\theta},\hat{\phi}] &= \frac{\partial}{\partial\xi}\left(\frac{\partial^2 \hat{f}}{\partial\xi^2}\right) + \hat{f}\frac{\partial^2 \hat{f}}{\partial\xi^2} - \left(\frac{2m}{m+1}\right)\left(\frac{\partial\hat{f}}{\partial\xi}\right)^2 + \left(\frac{2}{m+1}\right)\left(Qe^{-\beta_1(\xi+\alpha)} + \lambda_T\left(\hat{\theta} + \lambda_C\hat{\phi}\right)\right) \\ \mathrm{N}_\theta[\hat{f},\hat{\theta},\hat{\phi}] &= \frac{\partial}{\partial\xi}\left(\frac{\partial\hat{\theta}}{\partial\xi}\right) + \Pr\frac{\partial\hat{\theta}}{\partial\xi}\left(Nb\frac{\partial\hat{\phi}}{\partial\xi} + Nt\frac{\partial\hat{\theta}}{\partial\xi} + \hat{f}\right) + \left(\frac{2}{m+1}\right)\Pr\lambda\hat{\theta} + Ec\left(\frac{\partial^2\hat{f}}{\partial\xi^2}\right)^2 \\ &\quad - 2\Pr\left(\frac{2m-1}{m+1}\right)\frac{\partial\hat{f}}{\partial\xi}\hat{\theta} \\ \mathrm{N}_\phi[\hat{f},\hat{\theta},\hat{\phi}] &= \frac{\partial}{\partial\xi}\left(\frac{\partial\hat{\phi}}{\partial\xi} + \frac{Nt}{Nb}\frac{\partial\hat{\theta}}{\partial\xi}\right) + Sc\hat{f}\frac{\partial\hat{\phi}}{\partial\xi} - \left(\frac{2K_c}{(1+m)}\right)\hat{\phi} - 2Sc\left(\frac{2m-1}{m+1}\right)\frac{\partial\hat{f}}{\partial\xi}\hat{\phi}. \end{aligned} \tag{4.3.4}$$

Choosing the auxiliary functions as $H_f(\xi) = H_\theta(\xi) = H_\phi(\xi) = e^{-\xi}$. It is easily verified that Eqns. (4.3.3) becomes linear when the embedding parameter $q=0$ and which reduces to nonlinear when $q=1$. Expanding the governing problems by Taylor series solution in the form of q, it can reduced as,

$$\begin{aligned} \hat{f}(\xi;q) &= f_0(\xi) + \sum_{n=1}^{\infty} f_n(\xi)q^n, \\ \hat{\theta}(\xi;q) &= \theta_0(\xi) + \sum_{n=1}^{\infty} \theta_n(\xi)q^n \text{ and} \\ \hat{\phi}(\xi;q) &= \phi_0(\xi) + \sum_{n=1}^{\infty} \phi_n(\xi)q^n. \end{aligned} \tag{4.3.5}$$

The homotopy solutions vary from the initial approximations to the solutions of interest as q varies from 0 to 1. It should be noted that the homotopy solutions contain the unknown convergence control parameters $\left(\hbar_f, \hbar_\theta, \hbar_\phi\right) \neq 0$ which can be used to adjust and control the convergence region and the rate of convergence of the series solution. To obtain the approximate solutions, here recursively solved the so-called nth-order deformation equations.

$$\begin{aligned} \mathrm{L}_f[f_n(\xi) - \chi_n f_{n-1}(\xi)] &= \hbar_f \mathrm{R}_n^f, \\ \mathrm{L}_\theta[\theta_n(\xi) - \chi_n \theta_{n-1}(\xi)] &= \hbar_\theta \mathrm{R}_n^\theta, \\ \mathrm{L}_\phi[\phi_n(\xi) - \chi_n \phi_{n-1}(\xi)] &= \hbar_\phi \mathrm{R}_n^\phi, \end{aligned} \tag{4.3.6}$$

where

$$\mathrm{R}_n^f = \frac{1}{(n-1)!}\frac{\partial^{n-1}\mathrm{N}_f[\hat{f}(\xi;q),\hat{\theta}(\xi;q),\hat{\phi}(\xi;q)]}{\partial q^{n-1}}\Big|_{q=0},$$

$$\mathrm{R}_n^\theta = \frac{1}{(n-1)!}\frac{\partial^{n-1}\mathrm{N}_\theta[\hat{f}(\xi;q),\hat{\theta}(\xi;q),\hat{\phi}(\xi;q)]}{\partial q^{n-1}}\Big|_{q=0}, \quad \chi_n = \begin{cases} 0 & n \le 1 \\ 1 & n > 1 \end{cases} \tag{4.3.7}$$

$$\mathrm{R}_n^\phi = \frac{1}{(n-1)!}\frac{\partial^{n-1}\mathrm{N}_\phi[\hat{f}(\xi;q),\hat{\phi}(\xi;q),\hat{\theta}(\xi;q)]}{\partial q^{n-1}}\Big|_{q=0},$$

In practice, this can only calculate finitely many terms in the homotopy series solution. Therefore k^{th} order approximate solution by the partial sums defined by.

$$f_{[k]}(\xi) = f_0(\xi) + \sum_{n=1}^{k} f_n(\xi)\ ,$$

$$\theta_{[k]}(\xi) = \theta_0(\xi) + \sum_{n=1}^{k}\theta_n(\xi) \text{ and} \tag{4.3.8}$$

$$\phi_{[k]}(\xi) = \phi_0(\xi) + \sum_{n=1}^{k}\phi_n(\xi).$$

With these approximations, we may evaluate the residual error and minimize it over the parameters $\left(\hbar_f, \hbar_\theta, \hbar_\phi\right) \neq 0$ in order to obtain the optimal value of $\left(\hbar_f, \hbar_\theta, \hbar_\phi\right) \neq 0$ giving the least possible residual error. To do so, one may use the integral of squared residual errors, however, this is very computationally demanding. To get around this, we use the averaged squared residual errors and which can be given as,

$$E_n^f = \frac{1}{M+1}\sum_{k=0}^{M}\left(\mathrm{N}_f\left[f_{[\mathrm{M}]}(\xi_k), \theta_{[\mathrm{M}]}(\xi_k), \phi_{[\mathrm{M}]}(\xi_k)\right]\right)^2$$

$$E_n^\theta = \frac{1}{M+1}\sum_{k=0}^{M}\left(\mathrm{N}_\theta\left[f_{[\mathrm{M}]}(\xi_k), \theta_{[\mathrm{M}]}(\xi_k), \phi_{[\mathrm{M}]}(\xi_k)\right]\right)^2 \tag{4.3.9}$$

$$E_n^\phi = \frac{1}{M+1}\sum_{k=0}^{M}\left(\mathrm{N}_\phi\left[f_{[\mathrm{M}]}(\xi_k), \theta_{[\mathrm{M}]}(\xi_k), \phi_{[\mathrm{M}]}(\xi_k)\right]\right)^2$$

where $\xi_k = k/M$, $k = 0,1,2,....M,$ is the function E_n^f, E_n^θ and E_n^ϕ in $\hbar_f, \hbar_\theta$ and $\hbar_\phi$ are defined as minimized error functions and which obtained by the optimal values of $\hbar_f, \hbar_\theta$ and $\hbar_\phi$ respectively. For n^{th} order approximation, the optimal value of $\hbar_f, \hbar_\theta$ and $\hbar_\phi$ for f , θ and ϕ is given by $dE_n^f(\hbar_f)/dh = 0, dE_n^\theta(\hbar_\theta)/dh = 0,$ and $dE_n^\phi(\hbar_\phi)/dh = 0$ respectively.Evidently, $\lim_{n\to\infty} E_n^f(\hbar_f) = 0, \lim_{n\to\infty} E_n^\theta(\hbar_\theta) = 0$ and $\lim_{n\to\infty} E_n^\phi(\hbar_\phi) = 0$ corresponds to a convergent series solution. Substituting these optimal values of $\hbar_f, \hbar_\theta$ and $\hbar_\phi$ in equation (4.3.8), thus the nonlinear system of equations (4.2.14) to (4.2.16) with required boundary conditions (4.2.17) is now reduced to several linear differential equations given in (4.3.7) and (4.3.8). Which can be solved exactly with the help of the computational software such as Mathematica $n = 1, 2, 3, ...$.For the assurance of the validity of this method the optimal values of $\hbar_f, \hbar_\theta$ and $\hbar_\phi$ for the functions $-f''(0), -\theta'(0)$ and $-\phi'(0)$ corresponding to various values of the pertinent parameters are given and the corresponding averaged residuals are represented as E_{10}^f, E_{10}^θ and E_{10}^ϕ.

According to Liao (2010), the total residual error is defined as, $E_n^t = E_n^f + E_n^\theta + E_n^\phi$, $\delta y = 0.5,\ k = 20,$ which can be solved exactly with the help of the computational software such as Mthematica8, for $n = 1, 2, 3, ...$ In this case the numerical code is evaluated at $\Pr = 1,\ Bi = 1, Sc = 0.22, \lambda = 0.1, \alpha = 0.6, m = 2, Nb = Nt = 0.5, \lambda_T = 0.2,$ $\lambda_C = 0.1, Q = 0.1, \beta_1 = 0.3, Ec = 0.3$ and $K_c = 0.2.$ To verify the reliability of the OHAM method the optimal values of the individual residual errors and total residual errors are computed up to 15th order of approximation which is shown in Tables (4.1 - 4.2) and Figs. 4.3.1 (a-b). From the graph, it is clearly elucidated that the individual residual errors decrease for larger values of approximation p. The corresponding optimal convergence control parameters are found to be, $\hbar_f = -1.2258,\ \hbar_\theta = -1.1596$ and $\hbar_\phi = -1.2561$ respectively.

4.4. Results and discussion

The system of coupled nonlinear partial differential equations is converted into a set of ordinary differential equations (4.2.14) to (4.2.16) together with appropriate boundary conditions (4.2.17) are solved by a semi-analytical method known as optimal homotopy analysis method (OHAM) (see for clear details, Liao (2010), Van Gorder (2019)). A symbolic computational software such as MATHEMATICA8 is used to examine the relevant physical parameters. To approve the technique and to pass judgment on the precision of the examination, different values of wall thickness parameter α and velocity power index m in the case of absence and presence of the Riga plate are compared with the previously published results for special cases (see Table 4.3). To get a clear insight into the governing physical problems, the numerical results are presented graphically in Figs. (4.4.1- 4.4.9) and Table 4.4. These figures show the variation of the horizontal velocity profile $f'(\xi)$, the temperature profile $\theta(\xi)$ and the concentration profile $\phi(\xi)$ for different values of the relevant physical parameters, namely, velocity power index m, wall thickness parameter α, dimensionless parameter β_1, modified Hartman number Q, thermal buoyancy parameter λ_T, concentration buoyancy parameter λ_C, Eckert number Ec, Prandtl number $\Pr$, Brownian motion parameter Nb, thermophoresis parameter Nt, Schmidt number Sc and chemical reaction parameter K_c.

Figs.4.4.1 (a-c) illustrates the impact of velocity power index and wall thickness parameter on the velocity profile, temperature profile, and the concentration profile. When $m>1$, $f'(\xi)$ and $\theta(\xi)$ reduces, whereas exactly opposite pattern is found in the case of $\phi(\xi)$ (see Fig. 4.4.1(c)), while when $m<1$ the profile pattern is reversed. This interesting behavior of α and m results in suction and blowing cases which may be attributed to the boundary condition $f(0)=\alpha((1-m)/(1+m))$. For different values of *m*, we observe the transpiration. More precisely, when $m>1$, that is, $f(0)<0$, this has a similar impact as that of mass injection at the sheet. Furthermore, when $-1<m<1$, that is, $f(0)>0$ is a case of suction that can significantly change the flow field. The suction has a greater impact on the constitution of engineered nanofluids and is an excellent mechanism for achieving flow control, cooling, and nano-particle distribution in nanofluid fabrication. The impact of m and β_1 on $f'(\xi)$, $\theta(\xi)$ and $\phi(\xi)$ is elucidated in the Figs.4.4.2 (a-c). The velocity profile diminishes for extending values of β_1 because β_1 is inversely related U_0. In the case of temperature distribution, the impact of β_1 is significant and the enhancement in the profile is recorded, whereas the concentration distribution shows dual nature. Figs.4.4.3 (a-c) sketched to exhibit the impact of Q and β_1 on $f'(\xi)$, $\theta(\xi)$ and $\phi(\xi)$. The velocity profile increases as Q enhances, consequently a thicker momentum boundary layer is observed. Usually, the velocity profiles are the decreasing function of Hartman number, but in this case, the velocity profiles enhance because of Lorentz force, which is produced due to the alternating array of magnets and electrodes parallel to the surface of the Riga plate (see Fig.4.4.3a). The temperature distribution declines as Q grows and the concentration distribution exhibits dual characteristics.

The significance of λ_T and m on profiles $f'(\xi)$, $\theta(\xi)$ and $\phi(\xi)$ is portrayed in Figs.4.4.4 (a-c). For increasing values of λ_T there is a rise in $f'(\xi)$. Physically, the positive values of λ_T corresponds to assisting flow and negative values of λ_T results opposing flow, whereas $\lambda_T = 0$ shows the absence of buoyancy forces. However, quite the opposite pattern may be observed in the case of $\theta(\xi)$, and the concentration distribution shows dual nature. Fig.4.4.5 and Fig.4.4.6 is drawn to see the behavior of velocity and temperature profiles respectively for different values of λ_C, Ec and m. For higher values of λ_C the velocity profiles reduces and the temperature of the fluid enhances as Eckert number increases and the phenomenon is due to the relation between Ec and temperature difference, that is, $Ec \propto 1/(T_w - T_\infty)$. Fig.4.4.7 is drawn to explain the effects of distinct values of $\Pr$ and Bi on $\theta(\xi)$. It is evident from the figure that the temperature profile reduces for extending values of $\Pr$ (Reduction in K_∞) and increases for Bi. Higher values of Pr indicate a large heat capacity, which intensifies the heat transfer. Therefore, the cooling of the heated sheet can be improved by choosing a coolant with a large Pr. Analysis of the effect of Nb and Nt on $\theta(\xi)$ and $\phi(\xi)$ is demonstrated through the Figs. 4.4.8(a-b). The temperature profiles enhance for the larger values of both Nb and Nt (see Fig. (4.4.8a)), by the definition, thermophoresis is a mechanism in which nanoparticles move from hotter region to colder region; as a result temperature distribution rises. In the case of concentration distribution gives dual characteristics for Nt and Nb exhibit different results, which is opposite to Nt (see Fig.4.4.8b). Fig.4.4.9 represents the influence of K_c and Sc on concentration, since Sc is an inverse function of the Brownian diffusion coefficient D_B (i.e., ratio of kinematic viscosity to that of mass diffusivity), therefore, a gradual increase in Sc reduces the nanoparticle concentration and the corresponding concentration boundary layer thickness. Larger K_c results in the squeezed concentration profile. Physically, $K_c > 0$ gives a destructive chemical reaction and for $K_c < 0$ yields constructive chemical reaction, whereas $K_c = 0$ shows the absence of chemical reaction.

Table 4.4.4 gives the impact of various governing parameters on the Skin friction coefficient $f''(0)$ Nusselt number $\theta'(0)$ and Sherwood number $\phi'(0)$. It is evident that the Skin friction coefficient decrease for higher values of $\alpha, m, \beta_{1,}\ \lambda_C$ and enhances for larger values of $Q, \lambda_T, Ec.$ The Nusselt number raises for extending values of m, β_1, Ec, Nb, Nt and Bi and decreases for different values of α, Q, λ_T and $\Pr$. Further, the Sherwood number exhibits dual characteristics for several physical parameters.

4.5. Closed remarks of the present work

- For different values wall thickness parameter and velocity power index ($\alpha > 0$ and $m > 1$), velocity and temperature profiles decrease, whereas exactly opposite pattern is found in the case of concentration, while when $\alpha > 0$ and $m < 1$ the profile pattern is reversed.
- For larger values dimensionless parameter, the velocity profiles reduce and the temperature profiles increases, whereas the concentration profiles exhibit dual characteristics.
- Higher values of thermal buoyancy parameter, the velocity profiles enhance and temperature profiles decreases, while the concentration profiles initially lessen and then improves.
- Velocity distribution rises and temperature distribution falls in the case of a higher modified Hartman number.
- Enhancement of concentration buoyancy parameter results in the reduced velocity profiles and temperature profiles enhance for higher values viscous dissipation parameter.
- Temperature distribution improves for the Brownian motion parameter and thermophoresis parameter but the concentration distribution shows a dual characteristic.

Table 4.1: Individual residual error at a different approximation p, when the parameters are fixed at $\mathbf{Q = 0.1,\ Bi = 1, Nb = Nt = 0.5, Pr = 1,}$ $\boldsymbol{\lambda = 0.1, \alpha = 0.6, m = 2, \beta_1 = 0.3, \lambda_T = 0.2,\ \lambda_C = 0.1,\ Ec = 0.3,}$ $\mathbf{Sc = 0.22,\ K_c = 0.2.}$

p	$E_p^{\,f}(\hbar_f)$	$E_p^{\,\theta}(\hbar_\theta)$	$E_p^{\,\theta}(\hbar_\phi)$	CPU times **(S)**
1	5.165×10^{-5}	5.206×10^{-4}	5.192×10^{-4}	0.3692
3	3.183×10^{-8}	4.839×10^{-7}	1.377×10^{-4}	3.6593
5	5.992×10^{-10}	3.058×10^{-7}	1.156×10^{-4}	17.689
7	2.149×10^{-10}	1.138×10^{-8}	1.379×10^{-6}	69.350
9	1.554×10^{-11}	1.605×10^{-10}	1.320×10^{-7}	192.12
13	9.849×10^{-12}	3.475×10^{-11}	1.678×10^{-9}	1361.5
15	9.422×10^{-15}	5.322×10^{-12}	2.059×10^{-10}	4526.4

Table 4.2: Total residual error at a different approximation p

p	$-\hbar_f$	$-\hbar_\theta$	$-\hbar_\phi$	$E_p^{\,t}$	CPU times **(S)**
1	0.9008	0.4153	1.1176	1.377×10^{-3}	0.3692
3	0.9452	1.0053	1.1220	2.684×10^{-4}	3.6593
5	1.1395	1.0473	1.1192	1.672×10^{-6}	17.689
7	1.0609	1.0612	1.1582	1.356×10^{-7}	69.350
9	1.2150	1.0782	1.2062	2.391×10^{-8}	192.12
14	1.2255	1.1961	1.2749	1.403×10^{-9}	1361.5
15	1.2258	1.1596	1.2583	4.574×10^{-10}	4526.4

Table 4.3: Comparison results of Skin friction coefficient $-f''(0)$ for different values wall thickness parameter α and velocity power index parameter m, when the absence and presence of Riga Plate at $\mathrm{Pr} = \mathrm{Bi} = \mathrm{Q} = \beta_1 = \mathrm{Ec} = \mathrm{K_c} = 0$ $\lambda_T = \lambda_C = \mathrm{Nt} = \lambda = \mathrm{Sc} = 0$ and Nb $\uparrow$0.

		Absence of Riga plate $(Q = 0, \beta_1 = 0)$			Presence of Riga plate $(Q = 0.1, \beta_1 = 0.3)$		
α	m	Fang et al., (2012)	Prasad et al., (2018b) when $(\lambda = 0, Mn = 0)$	Present results	Hayat et al.,(2016 c)	Iqbal et al., (2017) when $M = 0$	Present results
0.25	-0.5	0.0833	0.0832	0.0799	0.0949	0.0945	0.0931
	-0.3	0.5000	0.5000	0.5021	0.7214	0.7123	0.7222
	02	1.0614	1.0614	1.0621	0.9990	1.0614	1.0021
	03	1.0905	1.0905	1.1023	1.0456	1.0905	1.0572
	05	1.1186	1.1186	1.1186	1.0902	1.1186	1.0899
	07	1.1323	1.1323	1.1323	1.1121	1.1323	1.1265
	09	1.1404	1.1404	1.1404	1.1247	1.1404	1.1358
	10	1.1433	1.1433	1.1433	1.1288	1.1433	1.1352
0.5	-0.5	1.1667	1.1665	1.1665	1.1665	1.1665	1.1521
	-0.3	1.0000	1.0000	1.0000	1.0131	1.0093	1.0027
	02	1.0234	1.0234	1.0234	0.9672	1.0234	1.0195
	03	1.0359	1.0358	1.0358	0.9975	1.0358	1.0287
	05	1.0486	1.0486	1.0486	1.0253	1.0486	1.0387
	07	1.0550	1.0550	1.0550	1.0383	1.0550	1.0487
	09	1.0589	1.0589	1.0589	1.0458	1.0589	1.0578
	10	1.0606	1.0603	1.5999	1.0485	1.0603	1.0485

Table 4.4: Values of Skin friction, Nusselt number and Sherwood number with the computed CPU time (in seconds) for different physical parameters and fixed values of Sc = 0.22, Bi = 1, λ = 0.1, at 10th approximation.

Pr	Kc	Nt	Nb	Ec	λ_C	λ_T	Q	m	α	$-f''(0)$	$-h_f$	E_{10}^{f}	$-\theta'(0)$	$-h_\theta$	E_{10}^{θ}	$\phi'(0)$	$-h_\phi$	E_{10}^{ϕ}	CPU time (S)
									0.2	0.9887	0.9433	$1.29\text{x}10^{-10}$	0.5213	0.9555	$2.29\text{x}10^{-10}$	0.5212	1.2987	$2.16\ \text{x}10^{-8}$	388.41
1	0.22	0.5	0.5	0.3	0.1	0.2	0.1	2	**0.4**	0.9628	0.9089	$5.87\text{x}10^{-10}$	0.5166	0.9999	$1.33\text{x}10^{-10}$	0.5165	1.2945	$2.71\text{x}10^{-8}$	346.48
									0.6	0.9375	0.9163	$1.8\ \text{x}10^{-11}$	0.5118	1.1498	$7.07\ \text{x}10^{-11}$	0.5118	1.2226	$7.61\ \text{x}10^{-8}$	374.61
								-0.1		0.2288	0.8162	$1.88\text{x}10^{-11}$	0.6259	1.0395	$4.01\text{x}10^{-7}$	0.6227	1.0272	$5.87\text{x}10^{-7}$	339.08
1	0.22	0.5	0.5	0.3	0.1	0.2	0.1	**2**	0.2	0.9887	0.9433	$1.29\text{x}10^{-10}$	0.5613	0.9555	$2.29\text{x}10^{-10}$	0.5622	1.0277	$2.16\ \text{x}10^{-8}$	388.41
								5		1.0981	0.9703	$8.79\text{x}10^{-11}$	0.5248	0.9750	$1.17\ \text{x}10^{-9}$	0.5231	1.3662	$5.87\text{x}10^{-7}$	347.05
							0.1			0.5115	0.9651	$3.74\text{x}10^{-7}$	0.3417	0.9496	$2.68\ \text{x}10^{-6}$	0.3366	1.2377	$1.05\ \text{x}10^{-5}$	571.90
1	0.22	0.5	0.5	0.3	0.1	0.2	**0.2**	2	2	0.3641	0.8704	$1.53\ \text{x}10^{-6}$	0.3739	0.8085	$1.36\ \text{x}10^{-5}$	0.3607	1.1036	$6.34\ \text{x}10^{-5}$	351.57
							0.3			0.2256	0.8119	$4.39\ \text{x}10^{-6}$	0.3963	0.7153	$3.73\ \text{x}10^{-5}$	0.3851	0.4709	$2.76\ \text{x}10^{-4}$	360.26
						-0.1				1.0295	0.9405	$5.37\text{x}10^{-11}$	0.5166	0.9828	$1.51\text{x}10^{-10}$	0.5166	1.2486	$4.97\text{x}10^{-8}$	413.25
1	0.22	0.5	0.5	0.3	0.1	**0.5**	0.1	2	0.2	0.9495	1.2244	$5.0\ \text{x}10^{-11}$	0.5255	1.1842	$5.75\text{x}10^{-9}$	0.5240	1.1508	$1.69\ \text{x}10^{-7}$	338.72
						1				0.8877	1.0031	$1.79\text{x}10^{-10}$	0.5316	1.0318	$4.94\ \text{x}10^{-8}$	0.5316	1.1614	$1.16\text{x}10^{-8}$	348.83
					1					0.9929	1.2567	$5.16\text{x}10^{-11}$	0.5221	0.9470	$1.75\text{x}10^{-9}$	0.5221	1.2287	$5.91\text{x}10^{-8}$	343.92
1	0.22	0.5	0.5	0.3	**3**	0.2	0.1	2	0.2	1.0023	1.1786	$1.66\text{x}10^{-8}$	0.5237	0.8401	$5.75\ \text{x}10^{-9}$	0.5240	1.1508	$1.69\ \text{x}10^{-7}$	338.89
					7					1.0201	1.0831	$1.12\ \text{x}10^{-6}$	0.5268	0.7495	$3.79\text{x}10^{-8}$	0.5299	1.0386	$4.71\ \text{x}10^{-7}$	332.53
				0.5						0.8212	1.4113	$4.34\ \text{x}10^{-9}$	0.2416	1.2322	$1.131\ \text{x}10^{-9}$	0.2379	0.8697	$3.65\ \text{x}10^{-6}$	316.29
1	0.22	0.5	0.5	**1.0**	0.1	0.2	0.1	2	0.2	0.8047	1.0990	$7.87\ \text{x}10^{-9}$	0.1439	1.2213	$4.852\ \text{x}10^{-7}$	0.1420	0.9606	$6.77\ \text{x}10^{-6}$	329.06
				1.5						0.7890	1.0519	$8.32\ \text{x}10^{-9}$	0.0510	1.4180	$3.816\ \text{x}10^{-6}$	0.0499	1.0331	$8.35\ \text{x}10^{-6}$	335.55
			0.5							1.0023	1.1786	$1.66\ \text{x}10^{-8}$	0.5237	0.8407	$5.57\text{x}10^{-9}$	0.5240	1.1508	$1.69\text{x}10^{-7}$	338.36
1	0.22	0.5	**1.0**	0.3	0.1	0.2	0.1	2	0.2	0.9952	1.2309	$4.12\ \text{x}10^{-8}$	0.5242	0.9152	$2.80\text{x}10^{-9}$	0.2612	1.1202	$2.02\ \text{x}10^{-8}$	331.44
			2.0							0.9905	1.2885	$4.4\ \text{x}10^{-12}$	0.5261	1.3131	$3.49\ \text{x}10^{-9}$	0.0869	1.2661	$2.01\ \text{x}10^{-9}$	343.59
		0.5								0.9952	1.2309	$4.12\ \text{x}10^{-8}$	0.5242	0.9152	$2.80\text{x}10^{-9}$	0.2612	1.1202	$2.02\ \text{x}10^{-8}$	331.44
1	0.22	**1.0**	0.5	0.3	0.1	0.2	0.1	2	0.2	1.0091	1.2422	$1.26\text{x}10^{-7}$	0.5210	0.7949	$5.91\text{x}10^{-9}$	0.7833	1.0910	$5.55\text{x}10^{-7}$	328.23
		2.0								1.0170	1.3138	$4.66\text{x}10^{-7}$	0.5218	0.7598	$2.31\ \text{x}10^{-8}$	1.0451	1.2129	$8.68\ \text{x}10^{-7}$	347.72
	-0.2									0.9855	1.4185	$1.03\text{x}10^{-9}$	0.5221	1.1308	$1.20\ \text{x}10^{-8}$	0.5222	1.4358	$4.58\text{x}10^{-5}$	426.12
1	**0.5**	0.5	0.5	0.3	0.1	0.2	0.1	2	0.2	0.9886	0.9329	$8.31\text{x}10^{-12}$	0.5208	0.8914	$6.11\text{x}10^{-11}$	0.5208	1.0413	$1.34\ \text{x}10^{-9}$	389.11
	1.0									0.8850	0.9446	$6.22\text{x}10^{-12}$	0.5201	0.8866	$6.20\ \text{x}10^{-11}$	0.5210	0.9918	$6.13\text{x}10^{-10}$	394.15
0.72	0.22	0.5	0.5	0.3	0.1	0.2	0.1	0.2	0.2	0.9839	0.8244	$1.24\text{x}10^{-10}$	0.4824	1.8454	$533\text{x}10^{-5}$	0.4888	1.3466	$2.68\ \text{x}10^{-8}$	346.25
1.0										0.9887	0.9433	$1.29\text{x}10^{-10}$	0.5213	0.9552	$2.29\text{x}10^{-10}$	0.5212	1.2989	$2.16\ \text{x}10^{-8}$	388.36

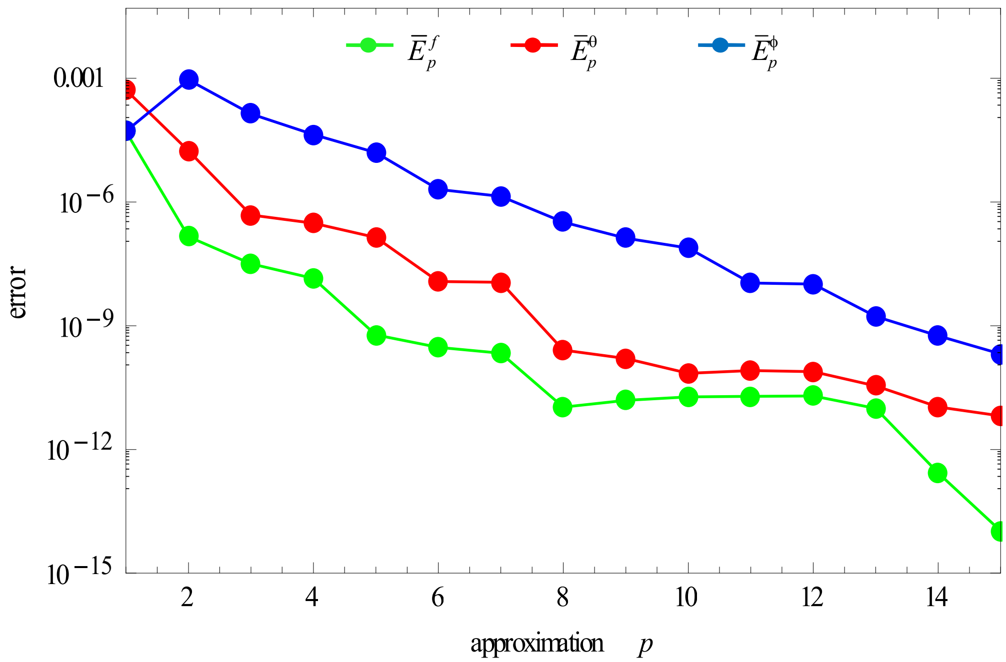

Fig.4.3.1 (a): Individual residual error at a different approximation p

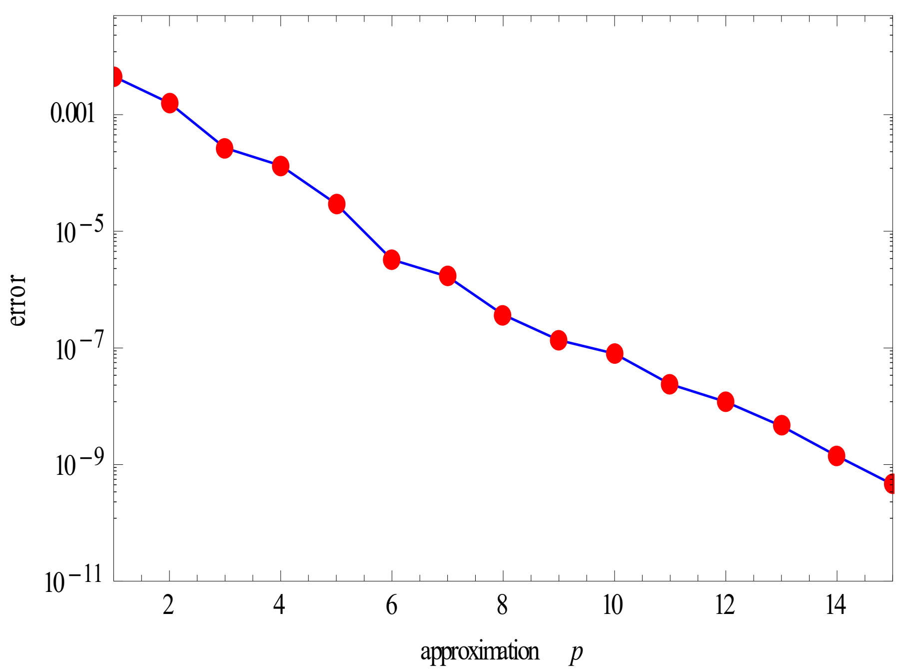

Fig.4.3.1 (b): Total residual error at a different approximation p

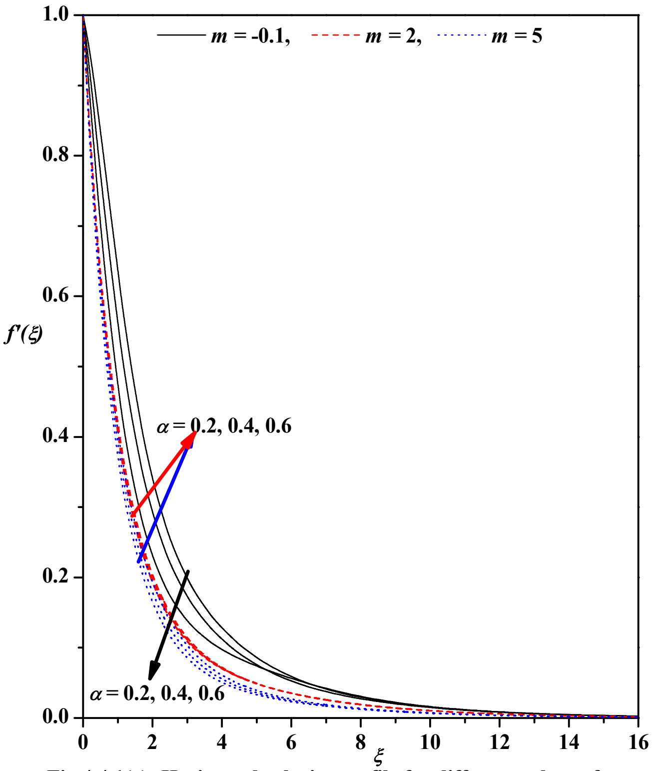

Fig.4.4.1(a): Horizontal velocity profile for different values of α and m with $Pr = 1$, $\lambda = 0.1$, $\lambda_T = 0.2$, $\lambda_C = 0.2$, $\beta_1 = 0.3$, $Q = 0.1$, Bi = 1, $Nb = Nt = 0.5$, $Sc = 0.22$, $Ec = 0.3$, $K_c = 0.2$.

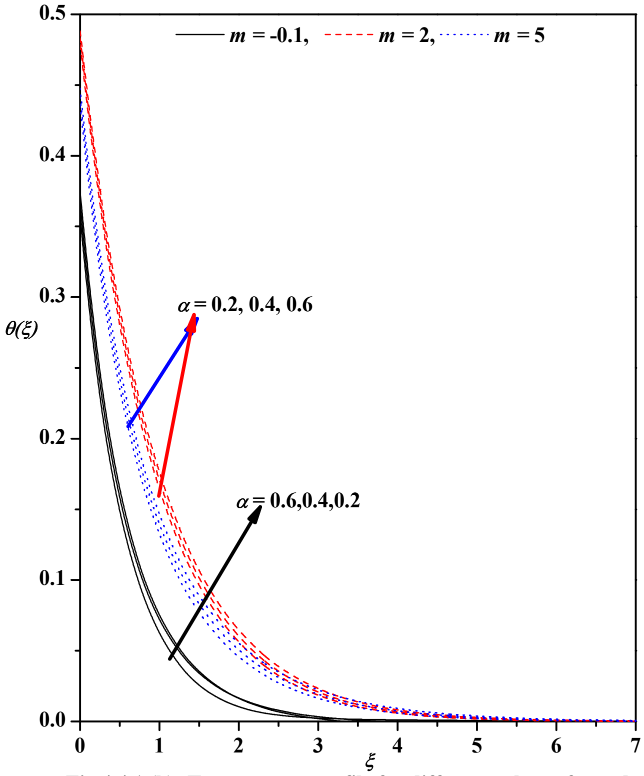

Fig.4.4.1 (b): Temperature profile for different values of α and m with $Pr = 1$,Bi = 1, $\lambda = 0.1$, $\lambda_T = 0.2$, $\lambda_C = 0.2$, $\beta_1 = 0.3$, $Q = 0.1$, $Sc = 0.22$, $Nb = Nt = 0.5$, $Ec = 0.3$, $K_c = 0.2$.

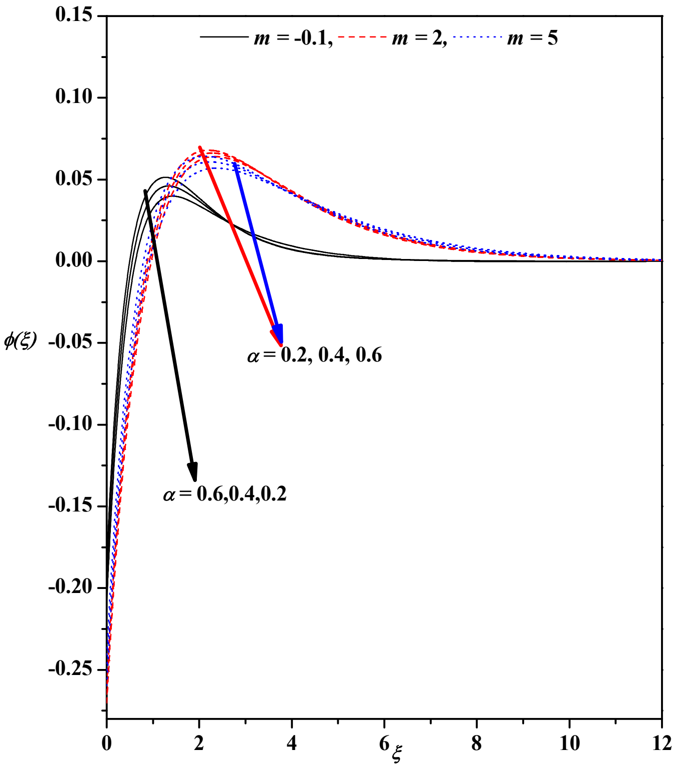

Fig.4.4.1(c): Concentration profile for different values of α and m with $Pr = 1$,Bi = 1, $\lambda = 0.1$, $\lambda_T = 0.2$, $\lambda_C = 0.2$, $\beta_1 = 0.3$, $Q = 0.1$, $Nb = Nt = 0.5$, $Sc = 0.22$, $Ec = 0.3$, $K_c = 0.2$.

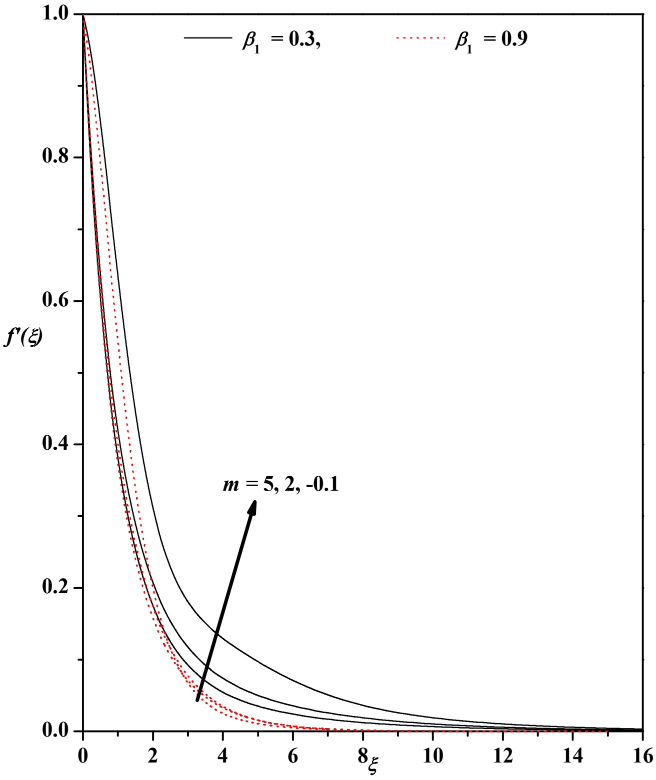

Fig.4.4.2(a): Horizontal velocity profile for different values of β_1 and m with Pr = 1, Bi = 1, $\lambda = 0.1$, $\lambda_T = 0.2$, $\lambda_C = 0.1$, $Q = 0.1$, $Nb = Nt = 0.5$, $Sc = 0.22$, $\alpha = 0.2$, $Ec = 0.3$, $K_c = 0.2$.

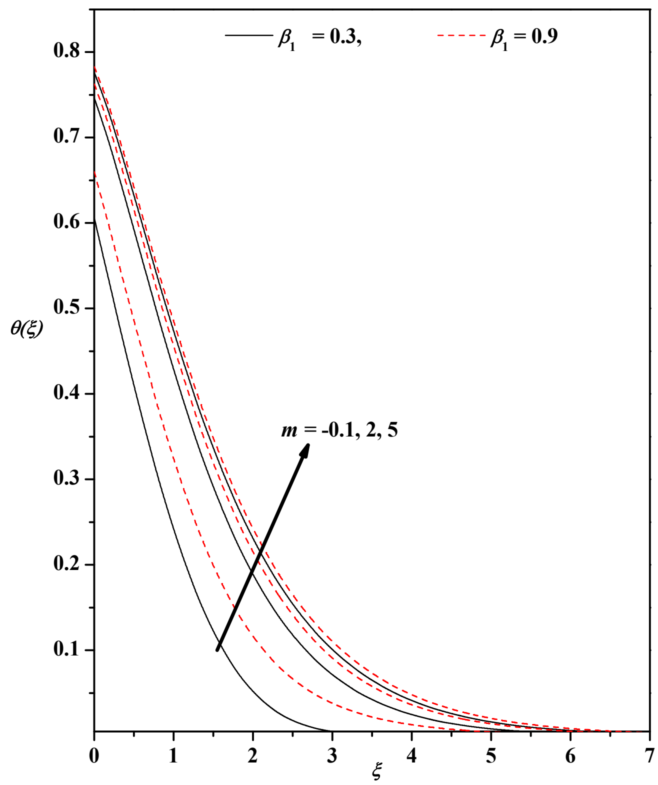

Fig.4.4.2(b): Temperature profile for different values of β_1 and m with Pr = 1, Bi = 1, $\lambda = 0.1$, $\lambda_T = 0.2$, $\lambda_C = 0.1$, $Q = 0.1$, $Nb = Nt = 0.5$, $Sc = 0.22$, $\alpha = 0.2$, $Ec = 0.3$, $K_c = 0.2$.

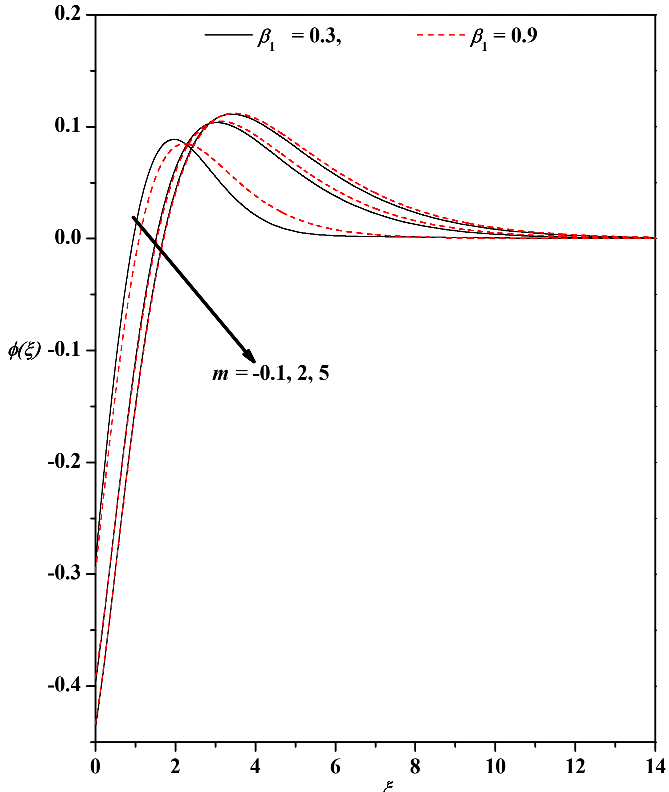

Fig.4.4.2(c): Concentration profile for different values of β_1 and m with Pr = 1, Bi = 1, $\lambda = 0.1$, $\lambda_T = 0.2$, $\lambda_C = 0.1$, $Q = 0.1$, $Nb = Nt = 0.5$, $Sc = 0.22$, $\alpha = 0.2$, $Ec = 0.3$, $K_c = 0.2$.

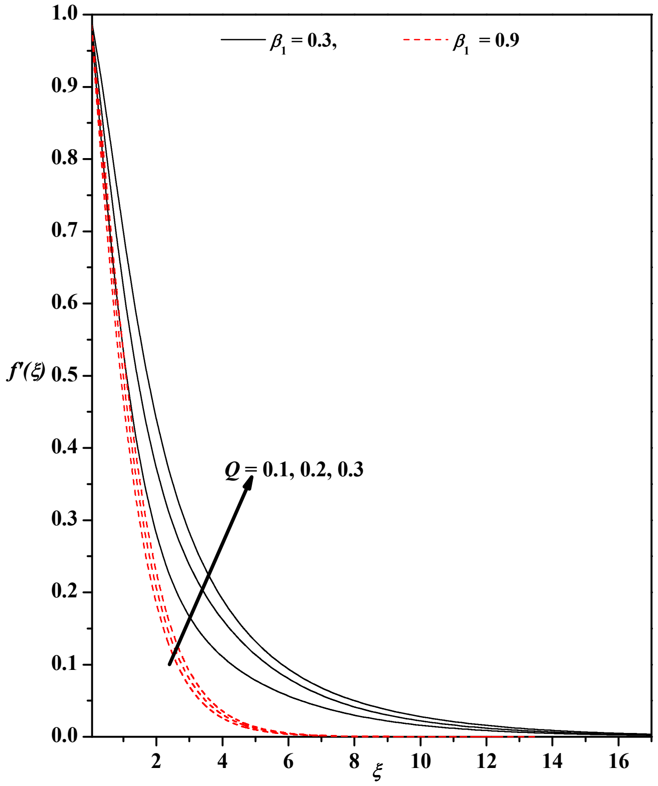

Fig.4.4.3 (a): Horizontal velocity profile for different values of Q and β_1 with $Pr = 1$, $\alpha = 0.2$, $\lambda_T = 0.2$, $Nb = Nt = 0.5$, $\lambda_C = 0.2$, $\lambda = 0.1$, Bi = 1, $Sc = 0.22$, $m = 2$, $Ec = 0.3$, $K_c = 0.2$.

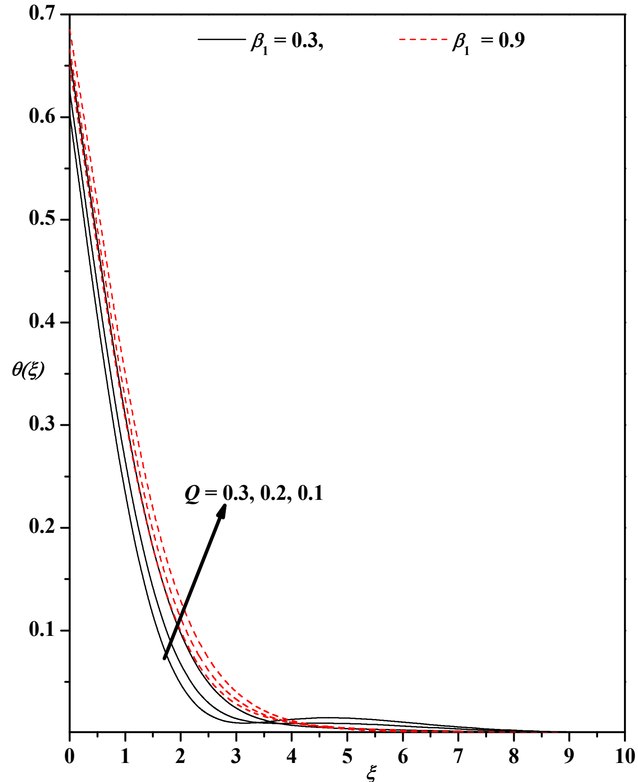

Fig.4.4.3 (b): Temperature profile for different values of Q and β_1 with $Pr = 1$, $\alpha = 0.2$, $\lambda = 0.1$, $\lambda_T = 0.2$, $\lambda_C = 0.2$, $Nb = Nt = 0.5$, Bi = 1, $Sc = 0.22$, $m = 2$, $Ec = 0.3$, $K_c = 0.2$.

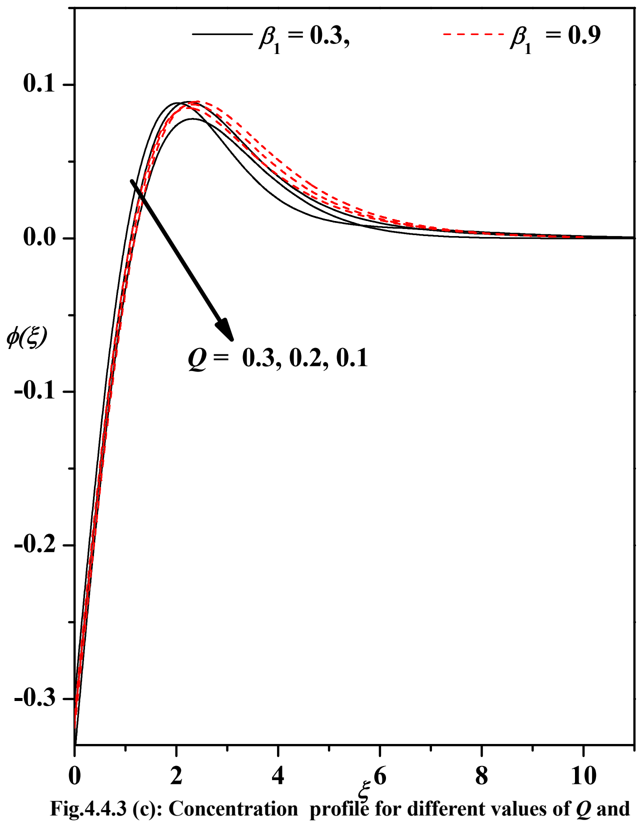

Fig.4.4.3 (c): Concentration profile for different values of Q and β_1 with $Pr = 1$, $\alpha = 0.2$, $\lambda = 0.1$, $\lambda_T = 0.2$, $\lambda_C = 0.2$, $Nb = Nt = 0.5$, Bi = 1, $Sc = 0.22$, $m = 2$, $Ec = 0.3$, $K_c = 0.2$.

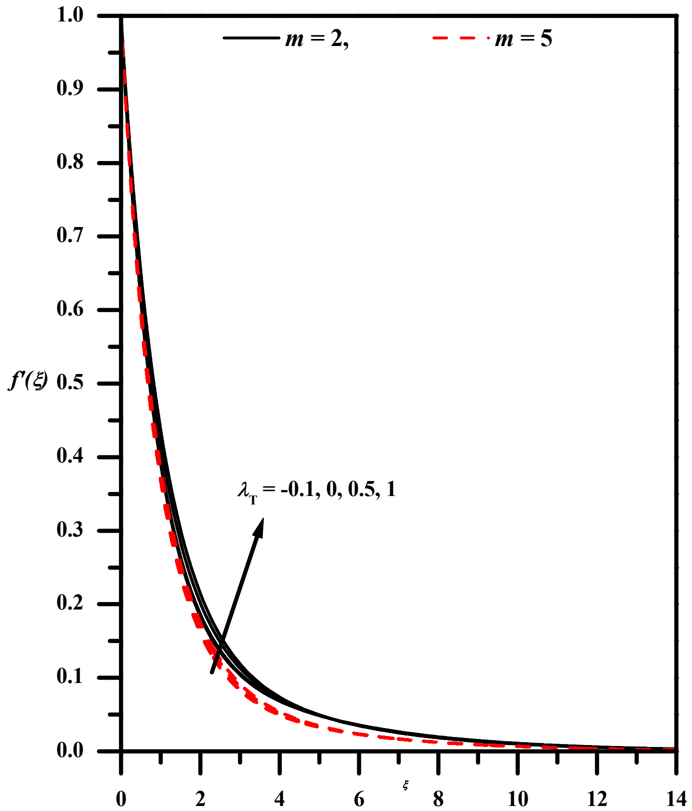

Fig.4.4.4(a): Horizontal velocity profiles for different values of λ_T and m with $Pr = 1$, $\lambda = 0.1$, $\lambda_C = 0.2$, $\beta_1 = 0.3$, $Q = 0.1$, $Nb = Nt = 0.5$, $\alpha = 0.2$, $Sc = 0.22$, Bi = 1, $Ec = 0.3$, $K_c = 0.2$.

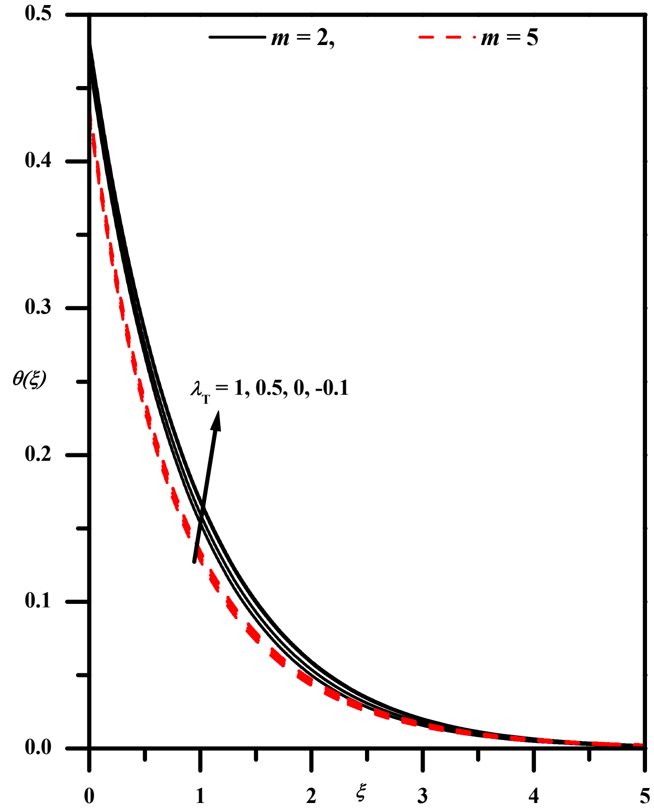

Fig.4.4.4(b): Temperature profiles for different values of λ_T and m with $Pr = 1$, $\lambda = 0.1$, $\lambda_C = 0.2$, $\beta_1 = 0.3$, $Q = 0.1$, $Nb = Nt = 0.5$, $\alpha = 0.2$, $Sc = 0.22$, Bi = 1, $Ec = 0.3$, $K_c = 0.2$.

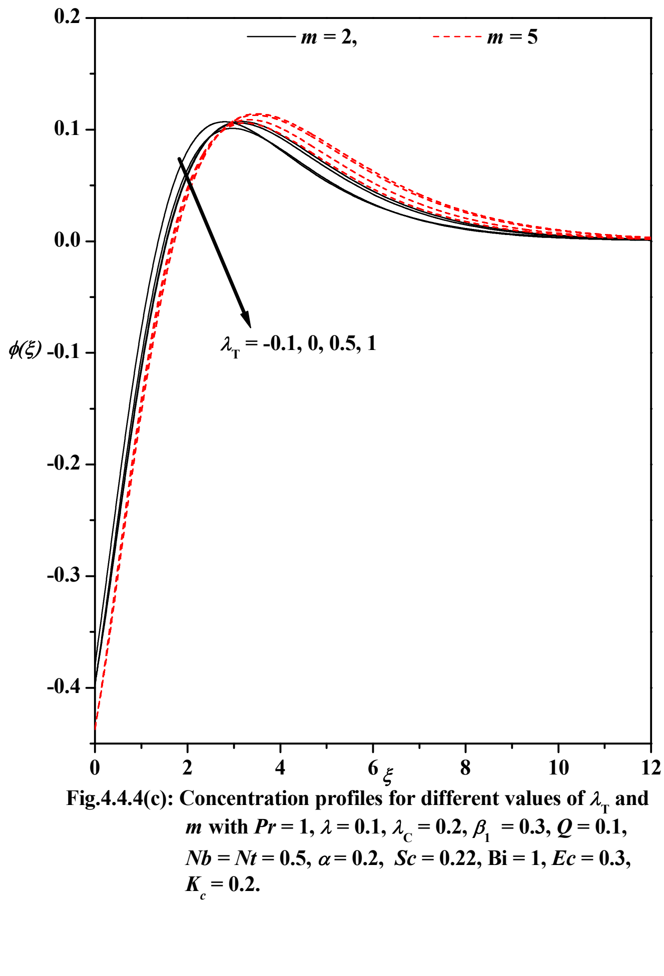

Fig.4.4.4(c): Concentration profiles for different values of λ_T and m with $Pr = 1$, $\lambda = 0.1$, $\lambda_C = 0.2$, $\beta_1 = 0.3$, $Q = 0.1$, $Nb = Nt = 0.5$, $\alpha = 0.2$, $Sc = 0.22$, Bi = 1, $Ec = 0.3$, $K_c = 0.2$.

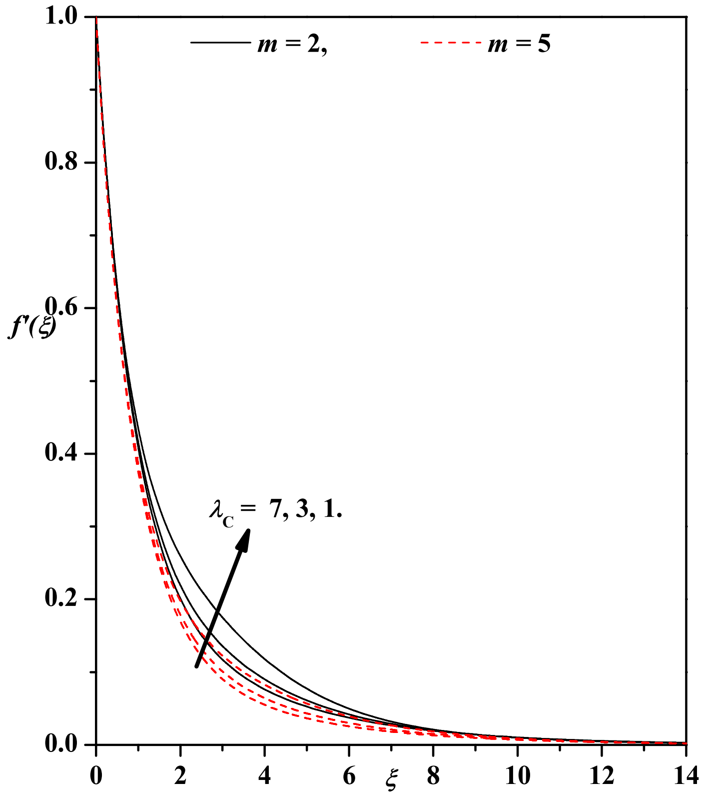

Fig.4.4.5: Horizontal velocity profile for different values of λ_C and m with $Pr = 1$, $\lambda = 0.1$, $\alpha = 0.2$, $\lambda_T = 0.2$, Bi = 1, $\beta_1 = 0.3$, $Q = 0.1$, $Nb = Nt = 0.5$, $Sc = 0.22$, $Ec = 0.3$, $K_c = 0.2$.

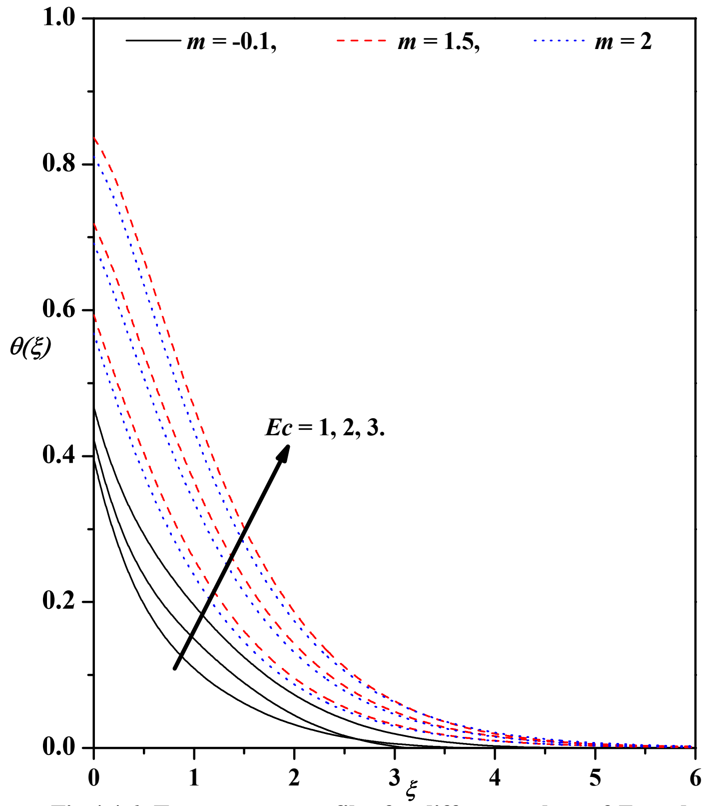

Fig.4.4.6: Temperature profiles for different values of Ec and m with $Pr = 1$, $\alpha = 0.2$, Bi = 1, $\lambda = 0.1$, $\lambda_T = 0.2$, $\lambda_C = 0.2$, $Q = 0.1$, $Sc = 0.22$, $Kc = 0.1$, $\beta_1 = 0.2$, $Nb = Nb = 0.5$.

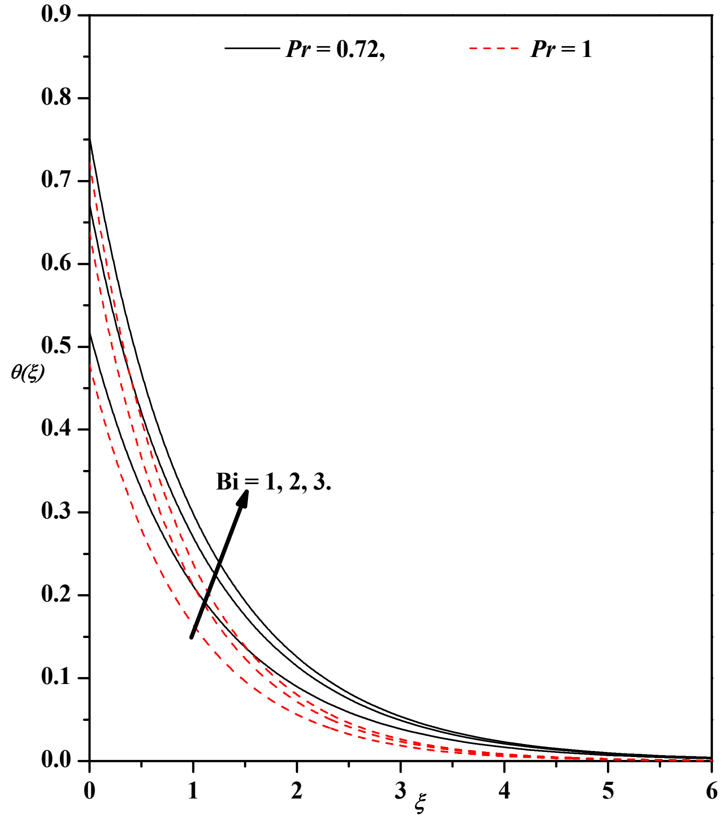

Fig.4.4.7: Temperature profile for different values of Bi and Pr with $m = 2$, $\alpha = 0.2$, $\lambda = 0.1$, $\lambda_T = 0.2$, $\lambda_C = 0.2$, $Q = 0.1$, $\beta_1 = 0.3$, $Nb = Nt = 0.5$, $Sc = 0.22$, $Ec = 0.3$, $K_c = 0.2$.

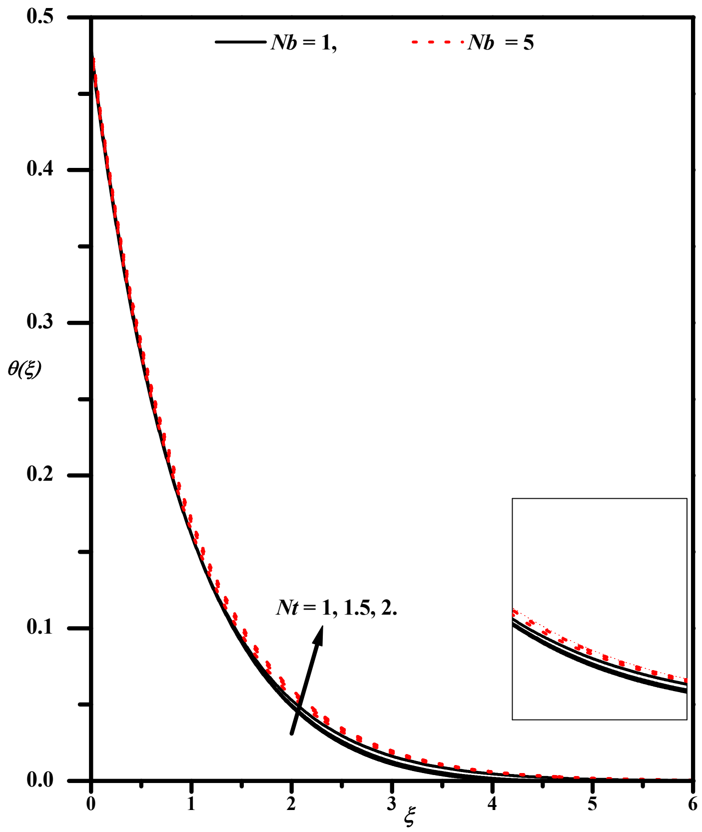

Fig.4.4.8(a): Temperature profiles for different values of *Nb* and *Nt* with $Pr = 1$, $\alpha = 0.2$, Bi = 1, $\lambda = 0.1$, $\lambda_T = 0.2$, $\lambda_C = 0.2$, $Sc = 0.22$, $Kc = 0.1$, $Q = 0.1$, $Ec = 0.3$, $\beta_1 = 0.2$, $m = 2$.

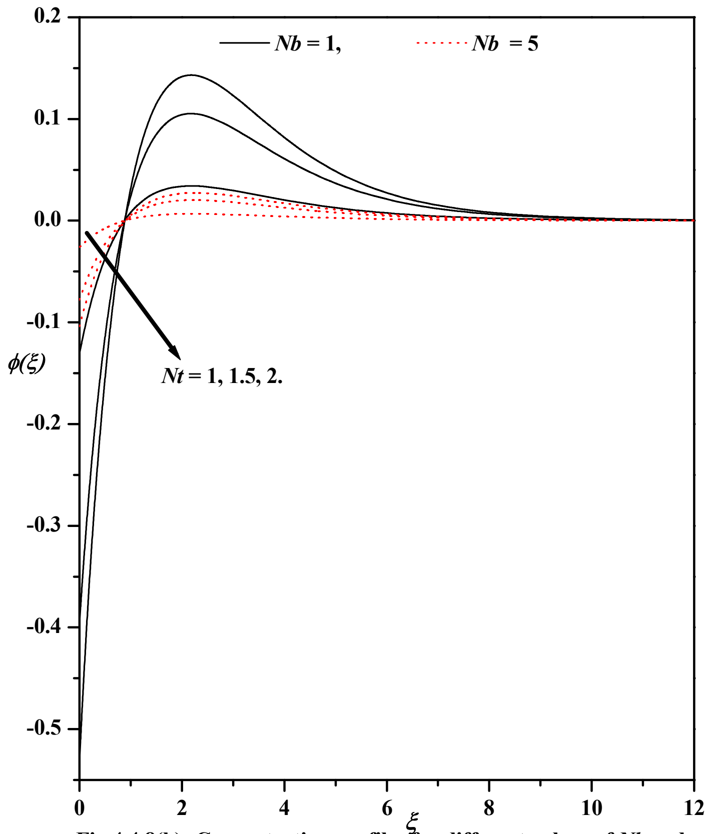

Fig.4.4.8(b): Concentration profiles for different values of *Nb* and *Nt* with $Pr = 1$, $\alpha = 0.2$, Bi = 1, $\lambda = 0.1$, $\lambda_T = 0.2$, $\lambda_C = 0.2$, $Sc = 0.22$, $Kc = 0.1$, $Q = 0.1$, $Ec = 0.3$, $\beta_1 = 0.2$, $m = 2$.

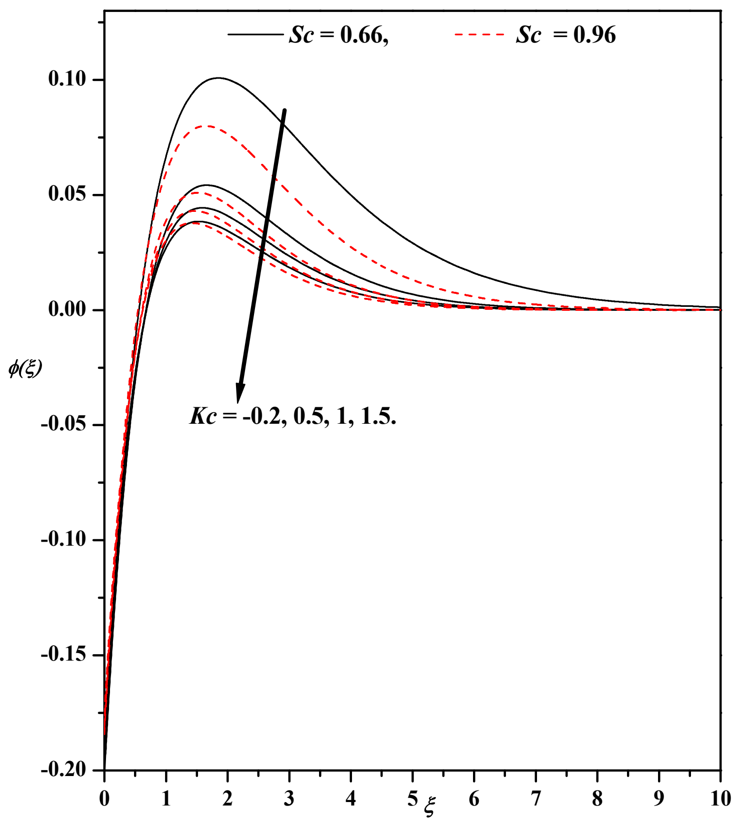

Fig.4.4.9: Concentration profile for different values of *Kc* and *Sc* with $Pr = 1$, $\alpha = 0.2$, Bi = 1, $\lambda_T = 0.2$, $\lambda_C = 0.2$, $\lambda = 0.1$, $Q = 0.1$, $Nb = Nt = 0.5$, $Ec = 0.3$, $m = 2$, $\beta_1 = 0.2$.

CHAPTER - 5

IMPACT OF SUCTION/ IJECTION AND HEAT TRANSFER ON UNSTEADY MHD FLOW OVER A STRETCHABLE ROTATING DISK

Part of this work has accepted for publication "*International Journal of Latin American Applied Research*" 2020.

5.1. Introduction

In recent years, numerous researchers analyzed the suction and injection process over different geometries because of its vast applications in engineering and technological domain such as thrust bearing design, radial diffusers, thermal oil recovery and many others. Erickson et al., (1966), considered the stretchable surface to examine the impact of Suction/ injection on the flow field. Fox et al., (1968) contributed similar work for uniform surface velocity and temperature. Gupta and Gupta (1977) continued the work of Erickson et al., (1966) by making the changes in the speed of the surface. Chen and Char (1988) explored the impacts of suction and injection on the heat transfer attributes of a continuous, linearly elastic sheet for both the variations of power law surface temperature and heat flux. The examination of the behavior of suction /injection on the flow and heat transfer with power law stretching sheet was reported by Ali et al., (1995). Cortel (2005b) added the permeability to the linear stretching sheet and analyzed the internal heat generation/ absorption nature on the flow pattern. Prasad and Vajravelu (2009) investigated the behavior of power law fluids over a flat surface in the presence of magnetic field and suction/injection parameter. Recently, Khan et al., (2018) utilized OHAM to obtain the numerical results of an unsteady Casson fluid past a stretching sheet in the presence of mass suction/injection. Further, Maleki et al., (2019a, 2019b) considered pseudo plastic non-Newtonian fluid over a permeable elastic surface and studied effects of suction or injection. Recently, Shakiba and Rahimi (2019) used the vertical cylindrical surface geometry and reported the impact of suction/ injection on the flow of nanofluid.

In addition to flow over a stretching sheet, the flow induced by rotating disk has also got several applications in the science and technological industry such as jet motors, electronic devices, and rotational air cleaners, computer storage devices, rotating machinery, medical equipment, spin coating and many others. Von Karman (1921) introduced the method to solve the problem of the Navier-Stokes equations for a rotating disk of infinite radius. Cochran (1931) extended the work of Von Karman (1921) using numerical integration method and obtained more accurate results. The impact of the blowing through a porous rotating disk was reported by Kuiken (1971) Watson and Wang (1979), Watson et al., (1985) examined the unsteady flow over a porous rotating disk and discussed deceleration case. Takhar et al., (1995) investigated the unsteady flow of a micropolar fluid due to a decelerating porous rotating disk with suction/ injection. Fang and Tao, (2012) visited the work of Watson et al., (1985) examined the unsteady flow induced by a stretchable rotating disk and obtained physically feasible solution branch. Rashidi et al., (2013) discussed the unsteady MHD flow over a rotating surface in presence of artificial neural network. Numerical solution via shooting method for unsteady viscous flow due to a nonlinear stretchable rotating disk was reported by Hobiny et al., (2015). Further, Turkyilmazoglu (2018) scrutinized the unsteady flow and heat characteristics over a vertically moving rotating disk and Prasad et al., (2019a) investigated the MHD Casson nanofluid flow over a rotating disk with heat source/sink and slip effects.

All the above researchers analyzed the flow and heat transfer characteristics over disk/sheet by considering the constant thermo physical properties. However, several researchers (Vajravelu et al., (2013), Prasad et al., (2017a, 2017c)) considered variable thermo physical properties. Here, the ambient fluid may change with temperature namely viscosity and thermal conductivity of the fluid. Effects of Hall current and variable fluid properties on MHD flow due to a rotating porous disk was reported by Abdul Maleque and Abdus Sattar (2005). Fresteri and Osalusi (2007) discussed the MHD slip flow over a porous rotating disk in the presence of variable fluid properties. Rashidi et al., (2014b) investigated the MHD slip flow over a porous rotating disk with variable fluid properties. Vajravelu et al., (2016a) studied the effects of variable transport properties and velocity-temperature slips of MHD squeeze flow between parallel disks with transpiration using OHAM. Recently, Prasad et al., (2018c) scrutinized the effects of variable viscosity and variable thermal conductivity on the Casson fluid flow past a vertical stretching sheet with transpiration.

To the author’s best knowledge, no combined work has been made earlier to study the unsteady MHD convective boundary layer flow and heat transfer over a stretchable rotating disk in the presence of mass suction/ injection. Moreover, the impact of viscous dissipation and variable fluid properties are considered. The solutions are obtained via Optimal Homotopy Analysis Method (Liao (2010) and Von Garder (2019)). An important finding for instance the unsteady parameter; viscosity parameter and Hartmann number squeezes the momentum boundary layer thickness which complements the existing results in the literature.

5.2. Mathematical formulation

Consider an unsteady two dimensional viscous incompressible axially symmetric convective flow and heat transfer of an electrically conducting fluid over a stretchable rotating disk, which has an angular velocity varying with time $\left(\Omega/1-\beta_2 t\right)$ in the presence of external magnetic field along the z-axis. The physical model of the rotating disk is presented in Fig. 5.2.1. Under these assumptions, governing equations for continuity, momentum and energy in cylindrical coordinates as follows,

$$\frac{1}{r}\frac{\partial}{\partial r}\left(ru_r\right)+\frac{\partial u_z}{\partial r}=0 \tag{5.2.1}$$

$$\frac{\partial u_r}{\partial t}+u_r\frac{\partial u_r}{\partial r}+u_z\frac{\partial u_r}{\partial z}-\frac{u_\theta^2}{r}=\frac{1}{\rho_\infty}\frac{\partial}{\partial z}\left(\mu\left(T\right)\frac{\partial u_r}{\partial z}\right)-\frac{\sigma B^2}{\rho_\infty}u_r \tag{5.2.2}$$

$$\frac{\partial u_\theta}{\partial t}+u_r\frac{\partial u_\theta}{\partial r}+u_z\frac{\partial u_\theta}{\partial z}+\frac{u_r u_\theta}{r}=\frac{1}{\rho_\infty}\frac{\partial}{\partial z}\left(\mu\left(T\right)\frac{\partial u_\theta}{\partial z}\right)-\frac{\sigma B^2}{\rho_\infty}u_\theta \tag{5.2.3}$$

$$\frac{\partial T}{\partial t}+u_r\frac{\partial T}{\partial r}+u_z\frac{\partial T}{\partial z}=\frac{1}{\rho_\infty C_P}\frac{\partial}{\partial z}\left(K\left(T\right)\frac{\partial T}{\partial z}\right)+\frac{1}{\rho_\infty c_P}\mu\left(T\right)\left(\left(\frac{\partial u_r}{\partial z}\right)^2+\left(\frac{\partial u_\theta}{\partial z}\right)^2\right), \tag{5.2.4}$$

where, $\left(u_r,u_\theta,u_z\right)$ are the velocity components in the direction of cylindrical coordinate system $\left(r,\theta^*,z\right)$, t is the time, ρ_∞ is the density of the fluid, σ is the electrical conductivity, $B(t)=\mathrm{B}_0\left(1-\beta_2 t\right)^{-1/2}$ is the special form of magnetic field imposed along z-axis, c_p is the specific heat at constant pressure. Further, it is assumed that the thermo-physical transport properties of the fluid are constant except for the fluid viscosity $\mu(T)$ and thermal conductivity $\mathrm{K}(T)$ which varies as a function of temperature in the following forms:

$$\mu\left(T\right)=\frac{\mu_\infty}{1+\delta\left(T-T_\infty\right)}\quad i.e.\ \frac{1}{\mu}=a_2\left(T-T_r\right), \tag{5.2.5}$$

where, $a_2=\delta/\mu_\infty$ and $T_r=T_\infty-1/\delta$ are constants and their values depend on the reference state and thermal property of the fluid. In general $a_2>0$ indicates the liquid, $a_2<0$ indicates the gases.

$$K(T)=K_\infty\left(1+\varepsilon_1\Delta T^{-1}\left(T-T_\infty\right)\right), \tag{5.2.6}$$

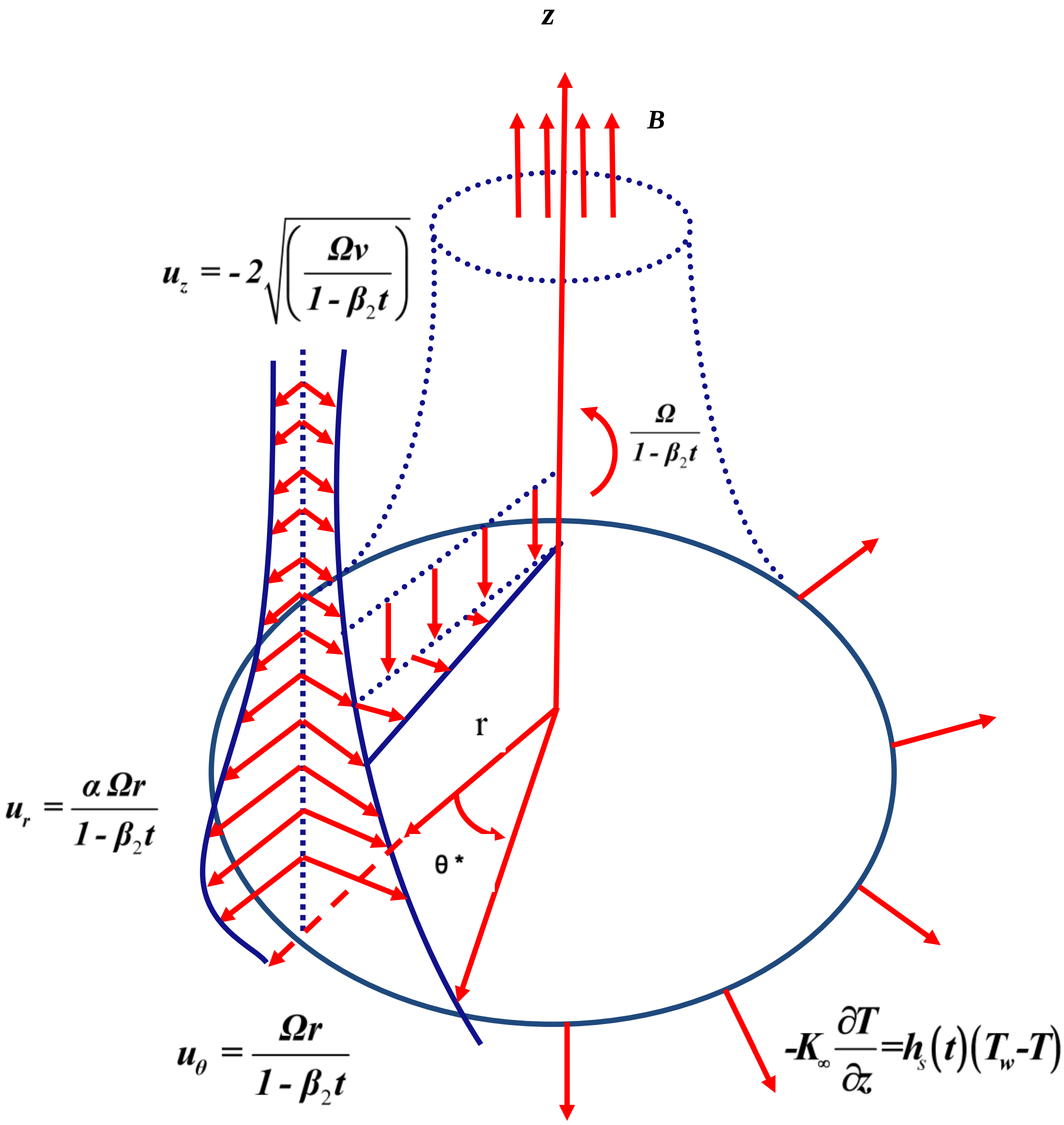

Fig.5.2.1: Geometry of the physical model

where $\mu(T), K(T), \mu_\infty$ and K_∞ are respectively called variable fluid viscosity, variable thermal conductivity, coefficient of viscosity of the fluid and thermal conductivity of the fluid far away from the disk, δ is the thermal property of the fluid, $\varepsilon_1 = (K - K_\infty)/K_\infty$ is a variable thermal conductivity parameter, $\Delta T = T_w - T_\infty$ is the temperature difference, K is the thermal conductivity, $\theta_r = (T_r - T_\infty)/\Delta T = -1/(\delta \Delta T)$ is the fluid viscosity parameter, which is negative for liquids and positive for gases (for more details see Prasad et al., (2017c)). Using Eqns. (5.2.5) and (5.2.6) in (5.2.2) to (5.2.4) reduces to,

$$\frac{\partial u_r}{\partial t} + u_r \frac{\partial u_r}{\partial r} + u_z \frac{\partial u_r}{\partial z} - \frac{u_\theta^2}{r} + \frac{\sigma B^2}{\rho_\infty} u_r = \frac{1}{\rho_\infty} \frac{\partial}{\partial z}\left(\frac{\mu_\infty}{\left[1+\delta\left(T - T_\infty\right)\right]} \frac{\partial u_r}{\partial z} \right) \tag{5.2.7}$$

$$\frac{\partial u_\theta}{\partial t} + u_r \frac{\partial u_\theta}{\partial r} + u_z \frac{\partial u_\theta}{\partial z} + \frac{u_r u_\theta}{r} + \frac{\sigma B^2}{\rho_\infty} u_\theta = \frac{1}{\rho_\infty} \frac{\partial}{\partial z}\left(\frac{\mu_\infty}{\left[1+\delta\left(T - T_\infty\right)\right]} \frac{\partial u_\theta}{\partial z} \right) \tag{5.2.8}$$

$$\begin{aligned} \frac{\partial T}{\partial t} + u_r \frac{\partial T}{\partial r} + u_z \frac{\partial T}{\partial z} &= \frac{1}{\rho_\infty c_P} \frac{\partial}{\partial z}\left(K_\infty \left(1 + \frac{\varepsilon_1}{\Delta T}\left(T - T_\infty\right)\right) \frac{\partial T}{\partial z} \right) \\ &+ \frac{1}{\rho_\infty c_P} \frac{\mu_\infty}{\left[1+\delta\left(T - T_\infty\right)\right]} \left(\left(\frac{\partial u_r}{\partial z}\right)^2 + \left(\frac{\partial u_\theta}{\partial z}\right)^2 \right) \end{aligned} \tag{5.2.9}$$

Appropriate boundary conditions are,

$$\begin{aligned} & u_r = \frac{\alpha \Omega r}{1-\beta_2 t}, u_\theta = \frac{\Omega r}{1-\beta_2 t}, u_z = -2\sqrt{\frac{\Omega \nu}{1-\beta_2 t}} f_w, \; -K_\infty \frac{\partial T}{\partial z} = h_s\left(t\right)\left(T_w - T\right) \text{ at } z = 0, \\ & u_r \to 0, \qquad u_\theta \to 0, \qquad T \to T_\infty \qquad \text{as} \qquad z \to \infty. \end{aligned} \tag{5.2.10}$$

where, $\alpha = b/\Omega$ is the disk stretching parameter, $h_s\left(t\right) = h_s\left(1-\beta_1 t\right)^{-1/2}$ is the special form of heat transfer coefficient. Now the following similarity transformations are introduced to reduce the governing equations into dimensionless form (for more details see Fang and Tao (2012).

$$\begin{aligned} & u_r = u_w = \frac{\Omega r}{1-\beta_2 t} f'\left(\xi\right), \; u_\theta = \frac{\Omega r}{1-\beta_2 t} g\left(\xi\right), \quad u_z = -2\sqrt{\frac{\Omega \nu_\infty}{1-\beta_2 t}} f\left(\xi\right), \\ & \theta\left(\xi\right) = \frac{T - T_\infty}{T_w - T_\infty} \left(= \frac{\Omega r}{1-\beta_2 t}\right), \quad \xi = \sqrt{\frac{\Omega}{\nu_\infty\left(1-\beta_2 t\right)}}\, z, \; \mathrm{B}^2 = \frac{B_0^2}{1-\beta_2 t}. \end{aligned} \tag{5.2.11}$$

Using Eq. (5.2.11), Eq. (5.2.1) is automatically satisfied and Eqns. (5.2.7) to (5.2.10) takes the self similar form,

$$\left(f''\left(1-\theta/\theta_r\right)^{-1}\right)' + g^2 + 2ff'' - f'^2 - S\left(f' + (1/2)\xi f''\right) - Mnf' = 0 \tag{5.2.12}$$

$$\left(g'\left(1-\theta/\theta_r\right)^{-1}\right)' + 2fg' - 2f'g - S\left(g + (1/2)\xi g'\right) - Mng = 0 \tag{5.2.13}$$

$$\begin{aligned}&\left(\left(1+\varepsilon_1\theta\right)\theta'\right)' + 2\Pr\left(f\theta' - f'\theta\right) - \Pr S\left(\theta + (1/2)\xi\theta'\right)\\ &\qquad + \Pr Ec\left(1-\theta/\theta_r\right)^{-1}\left(f''^2 + g'^2\right) = 0\end{aligned} \tag{5.2.14}$$

$$\begin{aligned}&f\left(0\right) = f_w, \quad f'\left(0\right) = \alpha, \quad g\left(0\right) = 1, \quad \theta'\left(0\right) = -Bi\left(1-\theta\left(0\right)\right),\\ &f'\left(\infty\right) \to 0, \quad g\left(\infty\right) \to 0, \quad \theta\left(\infty\right) \to 0.\end{aligned} \tag{5.2.15}$$

here prime denotes derivative with respect to η, $\left(f\left(\xi\right), f'\left(\xi\right), g\left(\xi\right), \theta\left(\xi\right)\right)$ are respectively called the axial, radial, tangential velocity profiles and temperature profile, $Mn = \sigma B^2/\rho_\infty\Omega, \Pr = \mu_\infty c_p/K_\infty, Ec = u_w\Omega/cc_p$ and $Bi = h_s/K_\infty\sqrt{\nu_\infty/\Omega}$ are respectively called Hartmann number, Prandtl number, Eckert number and Biot number, $S = \beta_2/\Omega$ is called unsteady parameter where $S > 0$ corresponds disk acceleration and $S < 0$ corresponds disk deceleration, f_w is called mass transfer parameter where $f_w > 0$ indicate mass suction and $f_w < 0$ indicate mass injection. Important physical parameters for engineering interest are local skin friction and Nusselt number given by,

$$C_f = \left(1-\beta_2 t\right)^2/\rho_\infty\left(r\Omega\right)^2\sqrt{\left(\left(\tau_{zr}\right)^2 + \left(\tau_{z\theta}\right)^2\right)}, \; Nu = rq_w/K_\infty\left(T_w - T_\infty\right), \tag{5.2.16}$$

where τ_{zr} and $\tau_{z\theta}$ are called radial and tangential shear stress at the surface of the disk and q_w is the heat flux which are defined as follow,

$$\tau_{zr} = \mu\left(T\right)\left(\frac{\partial u_r}{\partial z}\right)_{\text{at } z=0}, \; \tau_{z\theta} = \mu\left(T\right)\left(\frac{\partial u_\theta}{\partial z}\right)_{\text{at } z=0}, q_w = -K\left(T\right)\left(\frac{\partial T}{\partial z}\right)_{\text{at } z=0}.$$

Substituting Eqn. (5.2.11) in (5.2.16) we get,

$$C_f\left(\mathrm{Re}\right)^{1/2} = \frac{1}{\left(1-\theta/\theta_r\right)}\left[\left(f''\left(0\right)\right)^2 + \left(g'\left(0\right)\right)^2\right]^{1/2}, Nu\left(\mathrm{Re}\right)^{-1/2} = -\left(1+\varepsilon_1\theta\right)\theta'\left(0\right). \tag{5.2.17}$$

Here $\mathrm{Re} = \Omega r^2/\nu_\infty\left(1-\beta_2 t\right)$ is the Reynolds number.

5.3. Method of solution

In order to obtain the appropriate solutions for the system of highly coupled nonlinear ordinary differential equations (5.2.12) - (5.2.14) with boundary condition (5.2.15), we adopt the following semi-analytical technique such as Optimal Homotopy Analysis Method (OHAM). Now we can pick the initial guesses for velocity and temperature profiles keeping in view of boundary conditions,

$$f_0(\xi) = f_w + \alpha e^{-\xi}, \qquad g_0(\xi) = e^{-\xi}, \text{ and } \qquad \theta_0(\xi) = \frac{Bi}{1+Bi} e^{-\xi}. \tag{5.3.1}$$

Now select the linear operators in the form,

$$L_f = \frac{d^3}{d\xi^3} + \frac{d^2}{d\xi^2}, \qquad L_g = \frac{d^2}{d\xi^2} - 1, \text{ and } \qquad L_\theta = \frac{d^2}{d\xi^2} - 1. \tag{5.3.2}$$

Let us consider the zeroth order deformation equations are,

$$\begin{aligned}
&(1-q) L_f \left[\hat{f}(\xi,q) - f_0(\xi) \right] = q H_f(\xi) \hbar_f N_f \left[\hat{f}(\xi,q), \hat{g}(\xi,q), \hat{\theta}(\xi,q) \right], \\
&(1-q) L_g \left[\hat{g}(\xi,q) - g_0(\xi) \right] = q H_g(\xi) \hbar_g N_g \left[\hat{g}(\xi,q), \hat{h}(\xi,q), \hat{f}(\xi,q) \right], \\
&(1-q) L_\theta \left[\hat{\theta}(\xi,q) - \theta_0(\xi) \right] = q H_\theta(\xi) \hbar_\theta N_\theta \left[\hat{\theta}(\xi,q), \hat{f}(\xi,q), \hat{g}(\xi,q) \right],
\end{aligned} \tag{5.3.3}$$

with respective boundary conditions are,

$$\begin{aligned}
&\hat{f}(0,q) = f_w, \ \ \hat{f}'(0,q) = \alpha, \ \ \hat{g}(0,q) = 1, \ \ \hat{\theta}'(0,q) = -Bi\left(1 - \hat{\theta}(0,q)\right), \\
&\hat{f}'(\infty,q) = 0, \ \ \hat{g}(\infty,q) = 0, \ \ \hat{\theta}(\infty,q) = 0,
\end{aligned}$$

here q is an embedding parameter its values lies between 0 and 1, $\left(\hbar_f, \hbar_g, \hbar_\theta\right) \neq 0$ are the convergence control parameters and N_f, N_g, N_θ are nonlinear operators which are defined as,

$$\begin{aligned}
N_f = &\left(\frac{\partial^2 \hat{f}(\xi,q)}{\partial \xi^2} \left(1 - \frac{\hat{\theta}(\xi,q)}{\theta_r} \right)^{-1} \right)' + \hat{g}^2(\xi,q) - \left(\frac{\partial \hat{f}(\xi,q)}{\partial \xi} \right)^2 \\
&- S\left(\frac{\partial \hat{f}(\xi,q)}{\partial \xi} + \frac{1}{2}\xi \frac{\partial^2 \hat{f}(\xi,q)}{\partial \xi^2} \right) - Mn \frac{\partial \hat{f}(\xi,q)}{\partial \xi},
\end{aligned}$$

$$\begin{aligned}
N_g = &\left(\frac{\partial \hat{g}(\xi,q)}{\partial \xi} \left(1 - \frac{\hat{\theta}(\xi,q)}{\theta_r} \right)^{-1} \right)' - 2\frac{\partial \hat{f}(\xi,q)}{\partial \xi} \hat{g}(\xi,q) + 2\frac{\partial \hat{g}(\xi,q)}{\partial \xi} \hat{f}(\xi,q) \\
&- S\left(\hat{g}(\xi,q) + \frac{1}{2}\xi \frac{\partial \hat{g}(\xi,q)}{\partial \xi} \right) - Mn\hat{g}(\xi,q),
\end{aligned} \tag{5.3.4}$$

$$N_\theta = \left(\left(1+\varepsilon_1\theta\right)\frac{\partial\hat{\theta}(\xi,q)}{\partial\xi} \right)' + \Pr Ec\left(1-\frac{\hat{\theta}(\xi,q)}{\theta_r}\right)^{-1}\left(\left(\frac{\partial^2\hat{f}(\xi,q)}{\partial\xi^2}\right)^2 + \left(\frac{\partial\hat{g}(\xi,q)}{\partial\xi}\right)^2 \right)$$
$$+2\Pr\hat{f}(\xi,q)\frac{\partial\hat{\theta}(\xi,q)}{\partial\xi} - \Pr\hat{\theta}(\xi,q)\frac{\partial\hat{f}(\xi,q)}{\partial\xi} - \Pr S\left(\hat{\theta}(\xi,q)+\frac{1}{2}\xi\frac{\partial\hat{\theta}(\xi,q)}{\partial\xi}\right).$$

Now choose the auxiliary functions as $H_f(\xi)=H_g(\xi)=H_\theta(\xi)=e^{-\xi}$. It can be seen from Eqn.(5.3.3) that when $q=0$ and $q=1$, we have

$$\hat{f}(\xi,0)=f_0(\xi),\quad \hat{g}(\xi,0)=g_0(\xi),\quad \hat{\theta}(\xi,0)=\theta_0(\xi),$$
$$\hat{f}(\xi,1)=f(\xi),\quad \hat{g}(\xi,1)=g(\xi),\quad \hat{\theta}(\xi,1)=\theta(\xi).$$

Now expand $\hat{f}(\xi,q),\hat{g}(\xi,q)$ and $\hat{\theta}(\xi,q)$ by Taylors series,

$$\begin{aligned} \hat{f}(\xi,q) &= f_0(\xi)+\sum_{p=1}^{\infty} f_p(\xi)q^p, \\ \hat{g}(\xi,q) &= g_0(\xi)+\sum_{p=1}^{\infty} g_p(\xi)q^p, \text{ and} \\ \hat{\theta}(\xi,q) &= \theta_0(\xi)+\sum_{p=1}^{\infty} \theta_p(\xi)q^p, \end{aligned} \tag{5.3.5}$$

where,

$$f_p(\xi)=\frac{1}{p!}\frac{d^p f(\xi,q)}{d\xi^p}\bigg|_{q=0},\quad g_p(\xi)=\frac{1}{p!}\frac{d^p g(\xi,q)}{d\xi^p}\bigg|_{q=0}, \text{and}\quad \theta_p(\xi)=\frac{1}{p!}\frac{d^p\theta(\xi,q)}{d\xi^p}\bigg|_{q=0}.$$

If equation (5.3.5) converges at q=1, now obtain the Homotopy series solutions,

$$\begin{aligned} \hat{f}(\xi) &= f_0(\xi)+\sum_{p=1}^{\infty} f_p(\xi), \\ \hat{g}(\xi) &= g_0(\xi)+\sum_{p=1}^{\infty} g_p(\xi), \text{and} \\ \hat{\theta}(\xi) &= \theta_0(\xi)+\sum_{p=1}^{\infty} \theta_p(\xi). \end{aligned} \tag{5.3.6}$$

It is be noticed that OHAM solution contains the unknown convergence control parameters $(\hbar_f,\hbar_g,\hbar_\theta)\neq 0$, which can be adjusted and control the convergence region and the rate of convergence of the series solution. The p$^{\text{th}}$ order deformation equations are as follows,

$$\begin{aligned} L_f\left[f_p(\xi)-\chi_p f_{p-1}(\xi)\right] &= \hbar_f R_m^f(\xi) \\ L_g\left[g_p(\xi)-\chi_p g_{p-1}(\xi)\right] &= \hbar_g R_m^g(\xi) \text{ and} \\ L_\theta\left[\theta_p(\xi)-\chi_p \theta_{p-1}(\xi)\right] &= \hbar_\theta R_m^\theta(\xi) \end{aligned} \tag{5.3.7}$$

and the boundary conditions are,

$$f_p(0)=f_w,\quad f_p'(0)=\alpha,\quad g_p(0)=1,\quad \theta_p'(0)=-Bi\big(1-\theta_p(0)\big),$$
$$f_p(\infty)=0,\quad g_p(\infty)=0,\quad \theta_p(\infty)=0,$$

where

$$R_p^f=\left(f''_{p-1}\left(1-\frac{\theta_p}{\theta_{r_p}}\right)^{-1}\right)'-\sum_{k=0}^{p-1}f'_{p-1-k}f'_k+\sum_{k=0}^{p-1}g_{p-1-k}g_k-S\left(f'_{p-1}+\frac{1}{2}\xi f''_{p-1}\right)-Mn\,f'_{p-1},$$

$$R_p^g=\left(g'_{p-1}\left(1-\frac{\theta_p}{\theta_{r_p}}\right)^{-1}\right)'-2\sum_{k=0}^{p-1}f'_{p-1-k}g_k+\sum_{k=0}^{p-1}g'_{p-1-k}f_k-S\left(g_{p-1}+\frac{1}{2}\xi g'_{p-1}\right)-Mn\,g_{p-1},$$

$$R_p^\theta=\left[\left(\left(1+\varepsilon_1\theta_p\right)\theta'_{p-1}\right)'+Ec\Pr\left(1-\frac{\theta_p}{\theta_{r_p}}\right)^{-1}\left(\sum_{k=0}^{p-1}f''_{p-1-k}f''_k+\sum_{k=0}^{p-1}g'_{p-1-k}g'_k\right)\right]$$
$$+2\Pr\sum_{k=0}^{p-1}\theta'_{p-1-k}f_k-\Pr\sum_{k=0}^{p-1}f'_{p-1-k}\theta_k-S\left(\theta_{p-1}+\frac{1}{2}\xi\theta'_{p-1}\right),$$

where,

$$\chi_p=\begin{cases}0, & p\le 1\\ 1, & p>1.\end{cases}$$

Now calculate the error and minimize over $\hbar_f,\hbar_g,\hbar_\theta$ in order to get the optimal values for $\hbar_f,\hbar_g,\hbar_\theta$ and the least possible error. In the process of error analyses, we have two methods namely, exact residual error and average residual error. For different order approximation, CPU time required for evaluation of $f''(0), g'(0)$ and $\theta'(0)$ is observed. As for as CPU time is concerned, the average residual error needs less time compared to that of the exact residual error for increasing values of p. At p^{th} order deformation equation, the exact residual errors can be written as,

$$\bar{E}_p^f(\hbar_f)=\int_0^1\left(N_f\left[\sum_{y=0}^{p}\hat{f}_y(\xi)\right]\right)^2 d\xi$$
$$\bar{E}_p^g(\hbar_g)=\int_0^1\left(N_g\left[\sum_{y=0}^{p}\hat{g}_y(\xi)\right]\right)^2 d\xi \quad \text{and} \qquad (5.3.8)$$
$$\bar{E}_p^\theta(\hbar_\theta)=\int_0^1\left(N_\theta\left[\sum_{y=0}^{p}\hat{\theta}_y(\xi)\right]\right)^2 d\xi.$$

We used the average squared residual error instead of exact residual error $\bar{E}_p^f\left(\hbar_f\right)$, $\bar{E}_p^g\left(\hbar_g\right)$ and $\bar{E}_p^\theta\left(\hbar_\theta\right)$ because of the less time factor.

$$\bar{E}_p^f\left(\hbar_f\right)=\frac{1}{P+1}\sum_{y=0}^{P}\left(N_f\left[\hat{f}_{[P]}\left(\xi_y\right),\hat{g}_{[P]}\left(\xi_y\right),\hat{\theta}_{[P]}\left(\xi_y\right)\right]\right)^2$$

$$\bar{E}_p^g\left(\hbar_g\right)=\frac{1}{P+1}\sum_{y=1}^{P}\left(N_g\left[\hat{g}_{[P]}\left(\xi_y\right),\hat{f}_{[P]}\left(\xi_y\right)\right]\right)^2 \qquad and \tag{5.3.9}$$

$$\bar{E}_p^\theta\left(\hbar_\theta\right)=\frac{1}{P+1}\sum_{y=0}^{P}\left(N_\theta\left[\hat{\theta}_{[P]}\left(\xi_y\right),\hat{f}_{[P]}\left(\xi_y\right),\hat{g}_{[P]}\left(\xi_y\right)\right]\right)^2.$$

and

$$\bar{E}_p^t\left(\hbar\right)=\bar{E}_p^f\left(\hbar_f\right)+\bar{E}_p^g\left(\hbar_g\right)+\bar{E}_p^\theta\left(\hbar_\theta\right), \tag{5.3.10}$$

where $\bar{E}_p^t\left(\hbar\right)$ is the total residual error and $\xi_y = y/\mathrm{p}, y=0,1,..\mathrm{p}$. Now minimize the error function $\bar{E}_p^f\left(\hbar_f\right)$, $\bar{E}_p^g\left(\hbar_g\right)$ and $\bar{E}_p^\theta\left(\hbar_\theta\right)$ in $\hbar_f,\hbar_g,\hbar_\theta$ and obtain the optimal values of $\hbar_f,\hbar_g,\hbar_\theta$. For p$^{\text{th}}$ order approximation, the optimal value of $\hbar_f,\hbar_g,\hbar_\theta$ for f,g,θ is given by, $\dfrac{\partial\bar{E}_p^f\left(\hbar_f\right)}{\partial h}=0, \dfrac{\partial\bar{E}_p^g\left(\hbar_g\right)}{\partial h}=0, \dfrac{\partial\bar{E}_p^\theta\left(\hbar_\theta\right)}{\partial h}=0$ respectively. Evidently, $\lim_{p\to\infty}\bar{E}_p^f\left(\hbar_f\right)$, $\lim_{p\to\infty}\bar{E}_p^g\left(\hbar_g\right)$, $\lim_{p\to\infty}\bar{E}_p^\theta\left(\hbar_\theta\right)$, corresponding to a convergent series solution. Table 5.1 and Table 5.2 represent the values of the individual average residual error and total residual error for the different order of approximations. It can be noted that average residual error and total residual error converges consistently with the higher order approximation. As such, by taking the order of approximation sufficiently large and by choosing the convergence control parameters to minimize the average residual error, we can get an appropriate solution.

5.4. Validation of the methodology

The main purpose of this section is to provide the liability of the current method utilized in the present article. Consider the case $\alpha=Mn=S=1, Bi=\mathrm{Ec}=0.5,$ $\mathrm{Pr}=0.72,\ \varepsilon_1=0.1, \mathrm{f}_w=0.1, \theta_r=-10.$ The 14$^{\text{th}}$ order of approximation is obtained and the corresponding convergence control parameters are $\hbar_f=-0.984215,\ \hbar_g=-0.987565,$ and $\hbar_\theta=-1.04934$ and it is clearly observed that residual error of each governing equation reduces as we increase the order of approximation (see in Figs. 5.3.1(a-b)). Further,

Table 5.3 discussed for the assurance of the OHAM technique, the results are compared with Fang and Tao (2012) and Rashidi et al., (2014b) and found to be in excellent manner.

5.5. Results and discussions

System of coupled nonlinear ODEs (5.2.12) to (5.2.14) together with appropriate boundary conditions (5.2.15) are solved by a semi-analytical method known as Optimal Homotopy Analysis Method (OHAM) (see detail, Liao (2010) and Von Gorder (2019)). The semi-analytical computations are being carried out using Mathematica 8 software to obtain numerical values for the flow and heat transfer characteristics. The influence of various physical parameters, such as, unsteady parameter S, variable fluid viscosity parameter θ_r, disk stretching parameter α, mass suction/injection parameter f_w, Hartmann number Mn, variable thermal conductivity parameter ε_1, Prandtl number $\Pr$, Eckert number Ec and Biot number Bi on the axial velocity profile $f(\xi)$, radial velocity profile $f'(\xi)$, tangential velocity profile $g(\xi)$ and temperature profile $\theta(\xi)$ are exhibited through Figs.(5.5.1 - 5.5.4). The local skin friction coefficients $f''(0)\&g'(0)$ and Nusselt number $\theta'(0)$ are also discussed and presented in Table 5.4.

Fig. 5.5.1 (a-c) illustrates the effect of variable fluid viscosity parameter θ_r and unsteady parameter S on axial, radial and tangential velocity profiles. It is observed that all velocity profiles decreases with increasing values of θ_r and tends to zero as the distance increase from the boundary. Fig. 5.5.1 (d) explains the effect of θ_r on temperature distribution. From the figure, it is seen that the increasing values of θ_r is to enhance the temperature distribution. This may be due to the fact that $\theta_r \propto 1/\Delta T$, as lesser θ_r implies higher temperature difference. The influence of the unsteady parameter is to decrease the velocity profiles $f(\xi)$ $f'(\xi)$ and $g(\xi)$ (see Fig. 5.5.1(a-c)); this is due to the fact that the velocity gradient at the surface is larger for larger values S which produces the larger skin friction coefficient and hence boundary layer thickness decreases. The effect of increasing values of the unsteady parameter is to decrease the temperature field and hence reduces the thermal boundary layer thickness (see Fig.5.5.1 (d)). The impact of mass suction/ injection parameter f_w and disk stretching parameter α on axial velocity $f(\xi)$ is presented in Fig. 5.5.2 (a). The mass suction/injection parameter f_w gives three different cases, namely, $f_w > 0$ is a case of mass suction, $f_w < 0$ is a mass injection case and $f_w = 0$ shows the absence of suction/injection. For increasing values of f_w the axial velocity profile increases. But in the case of radial velocity $f'(\xi)$ the mass suction/ injection parameter gives exactly opposite results (see Fig. 5.5.2 (b)). This is due to the fact that the suction reduces the velocity boundary layer thickness whereas the injection has the opposite effect. These results are consistent with the physical situation (see Table 5.4). An increasing values of disk stretching parameter α the axial and radial velocity profiles enhances, this is because an increase in stretching parameter creates more pressure on fluid flow which leads to be augment in $f(\xi)$ and $f'(\xi)$. Fig. 5.5.3 (a) is drawn to see the behavior of Prandtl number $\Pr$ and Biot number Bi on temperature profile. The figure demonstrates that an increase in $\Pr$ results reduction in thermal boundary layer thickness. Clearly, higher values of $\Pr$ indicates a large heat capacity, which intensifies the heat transfer. Therefore the cooling of heated sheet can be improved by choosing a coolant with increasing $\Pr$. The temperature of the fluid increases as Biot number Bi extends, since Bi is directly proportional to the heat transfer coefficient h_s, due to this Bi cause's stronger convection which leads to increment in the temperature profile. Fig. 5.5.3 (b) exhibits the impact of Eckert number Ec and variable thermal conductivity parameter ε_1 on temperature distribution $\theta(\xi)$. For increasing values of Ec the temperature profiles extends, this is due to the assumption of the relation between Ec and temperature difference, i.e., $Ec \propto 1/(T_w - T_\infty)$. A similar behavior may be observed in the case of ε_1, this is due the fact that the temperature dependent thermal conductivity $K(T) = K_\infty\left(1 + (\varepsilon_1/\Delta T)(T - T_\infty)\right)$ which boosts the temperature distribution. The significance of Hartman number Mn and unsteady parameter S on axial, radial and tangential velocity profiles are depicted in Fig.5.5.4 (a-c). Velocity, namely, axial, radial and tangential profiles decreases with an increasing values of Mn and tends to zero as the distance increases from the boundary. This is because an existence of magnetic field creates Lorenz forces, which act as resistive drag forces opposite to the flow direction, which results in a decrease in velocity. Consequently the thickness of the momentum boundary layer reduces with an increase in Mn. A similar effect is observed in the case of increasing values of S.

Numerical results for different values of the sundry parameters on the local skin friction coefficients $f''(0)$ & $g'(0)$ and Nusselt number $\theta'(0)$ is presented in Table.5.4. It is recorded that an increase in θ_r, Mn and variations of mass suction/ injection parameter such as $f_w < 0, f_w = 0, f_w > 0$ results in the decrease of $f''(0)$ and $g'(0)$ and an increase in $\theta'(0)$. This is because $\theta_r \propto 1/\Delta T$, as θ_r rises temperature difference becomes small which leads to the increment in the temperature gradient, and also, in the case of Mn the result is due to the existence of magnetic field which creates a Lorenz's force, which opposes the fluid flow. This type of resisting force slows down the velocity of the fluid. Further, it is noticed that for larger values of unsteady parameter S, the reduction in the skin friction as well as temperature gradient is recorded. Further, $f''(0)$ and $g'(0)$ are the increasing function of α, this is because an increase in the stretching parameter creates more pressure on fluid flow, which leads to an enhancement in the values of $f''(0)$ and $g'(0)$. Concerning Pr we can conclude that the larger values of this parameter results in the reduction of the thermal boundary layer thickness and hence reduced values of $\theta'(0)$ is recorded. In the case of Bi, Ec and ε_1 the results are opposite to that of Pr and is due to thermal conductivity $K(T) = K_\infty\left(1 + (\varepsilon_1/\Delta T)(T - T_\infty)\right)$ which boosts the temperature gradient.

5.6. Conclusions

In the present article, unsteady MHD flow over an erratic rotating disk with variable fluid properties, mass suction/ injection parameter, viscous dissipation parameter and convective boundary condition is investigated. Some of the important conclusions are made as follows,

- Unsteady parameter lessens the local skin friction and Nusselt number.
- Fluid viscosity and Hartmann number reduces the fluid flow and strengthened the temperature and exactly opposite characteristics are seen in the case of stretching parameter.
- $f''(0)$ and $g'(0)$ are inversely related with respect to the suction and injection parameter.
- The temperature of the fluid increases with raising the values of variable thermal conductivity, Biot number and viscous dissipation parameter whereas inverse impact is seen with Prandtl number.
- For various values of unsteady parameter, fluid viscosity and Hartmann number reduces the skin friction and inverse trend is recorded in the case of stretching parameter.
- Impact of viscous dissipation parameter and Prandtl number on temperature gradient is quite opposite.

Table 5.1: Individual average residual errors as a function of the number of iterations when parameters are fixed at $\alpha = Mn = S = 1, Bi = Ec = 0.5, Pr = 0.72, f_w = \varepsilon_1 = 0.1, \theta_r = -10$.

p	E_p^f	E_p^g	E_p^θ	CPU time (s)
2	$5.29x10^{-4}$	$6.78x10^{-3}$	$2.48x10^{-4}$	11.6205
4	$8.34x10^{-6}$	$1.42x10^{-4}$	$3.67x10^{-5}$	54.5011
6	$1.91x10^{-6}$	$6.26x10^{-6}$	$7.47x10^{-6}$	263.945
8	$3.44x10^{-7}$	$3.51x10^{-7}$	$8.53x10^{-7}$	790.305
10	$5.37x10^{-8}$	$1.86x10^{-8}$	$1.53x10^{-7}$	2169.01
12	$7.67x10^{-9}$	$5.81x10^{-10}$	$4.27x10^{-8}$	4040.75
14	$1.07x10^{-9}$	$3.53x10^{-11}$	$1.98x10^{-8}$	8944.68

Table 5.2: Total squared residual errors and convergence control parameters for different approximation p.

p	$-\hbar_f$	$-\hbar_g$	$-\hbar_\theta$	E_p^t	CPU time (s)
2	0.8991	0.9676	1.086	2.06×10^{-2}	11.6205
4	0.9237	0.9480	1.050	1.39×10^{-4}	54.5011
6	0.9606	0.9544	1.019	1.11×10^{-6}	263.945
8	0.9770	0.9605	1.033	1.29×10^{-7}	790.305
10	0.9839	0.9645	1.043	1.99×10^{-8}	2169.01
12	0.9814	0.9417	1.032	9.15×10^{-9}	4040.75
14	0.9842	0.9875	1.049	2.81×10^{-9}	8944.68

Table 5.3: Comparison of present and previous work for various results of $f''(0)$ *and* $g'(0)$ when $Pr=0.72, Ec=Bi=\varepsilon_1=0.5, Mn=f_w=0, \theta_r \to \infty$.

		$f''(0)$			$-g'(0)$		
	$-S$	**Fang & Tao (2012)**	**Rashidi et al., (2013)**	**Present**	**Fang & Tao (2012)**	**Rashidi et al., (2013)**	**Present**
$\alpha = 0$	0.1	0.530	0.530	0.530	0.578	0.578	0.578
	0.2	0.551	0.551	0.551	0.541	0.541	0.541
	0.5	0.614	0.614	0.614	0.428	0.428	0.428
	1	0.719	0.719	0.719	0.236	0.236	0.236
$\alpha = 2$	0.1	3.111	3.117	3.117	2.053	2.052	2.052
	0.2	3.078	3.078	3.078	2.037	2.037	2.037
	0.5	2.960	2.961	2.960	1.990	1.990	1.990
	1	2.762	2.762	2.762	1.911	1.910	1.910

Table 5.4: Values of local Skin friction, Nusselt number, convergence control parameter and average squared residual error for different physical parameters.

Ec	Bi	θ_r	Pr	ε_1	Mn	f_w	S	α	$-f''(0)$	$-\hbar_f$	E_{10}^f	$-g'(0)$	$-\hbar_g$	E_{10}^g	$-\theta'(0)$	$-\hbar_\theta$	E_{10}^θ	CPU Time(S)
0.5	0.5	-10	0.72	0.1	1	**0.1**	1	**0.5**	4.50838	0.64106	2.26×10^{-4}	2.65815	0.68663	2.84×10^{-4}	0.08706	0.68253	8.26×10^{-5}	1789.5
								1	1.74409	0.93319	1.31×10^{-6}	2.12695	1.01168	2.97×10^{-7}	0.20151	1.03017	3.48×10^{-6}	2527.4
								2	0.64828	1.12736	8.29×10^{-8}	1.83289	1.10466	7.82×10^{-8}	0.24348	1.23999	7.32×10^{-8}	1759.8
0.5	0.5	-10	0.72	0.1	1	**0.1**	**1**	1	1.74409	0.93319	1.31×10^{-6}	2.12695	1.01168	2.97×10^{-7}	0.20151	1.03017	3.48×10^{-6}	2527.4
							2		1.95743	0.80011	8.22×10^{-7}	2.30457	0.82876	8.41×10^{-7}	0.22997	0.87681	1.62×10^{-6}	2013.5
							3		2.15436	0.69615	2.83×10^{-6}	2.47280	0.74192	3.82×10^{-6}	0.24832	0.79265	4.61×10^{-6}	1849.5
0.5	0.5	-10	0.72	0.1	1	**-0.1**	1	1	1.52732	1.03228	3.59×10^{-7}	1.92456	1.00826	2.02×10^{-7}	0.20239	1.09012	2.94×10^{-6}	1846.5
						0			1.63241	0.99685	3.42×10^{-7}	2.02299	0.98864	4.56×10^{-6}	0.20195	1.07423	1.98×10^{-6}	1861.5
						0.1			1.74409	0.93319	1.31×10^{-7}	2.12695	1.01168	2.97×10^{-7}	0.20151	1.03017	3.48×10^{-6}	2527.4
0.5	0.5	-10	0.72	0.1	**1**	0.1	1	1	1.74409	0.93319	1.31×10^{-6}	2.12695	1.01168	2.97×10^{-7}	0.20152	1.03017	3.48×10^{-6}	2527.3
					1.5				1.92585	0.82858	1.75×10^{-6}	2.25486	0.96582	1.58×10^{-6}	0.19025	0.98952	2.74×10^{-6}	2805.2
					2				2.04252	0.75454	2.72×10^{-6}	2.37708	0.81302	8.41×10^{-6}	0.17197	0.85752	4.98×10^{-6}	3092.5
0.5	0.5	-10	0.72	**0.1**	1	0.1	0.5	0.5	0.57351	1.2574	1.11×10^{-7}	1.72308	1.22691	3.64×10^{-7}	0.21911	1.36116	7.28×10^{-6}	1902.5
				0.3					0.57363	1.25936	1.06×10^{-7}	1.72352	1.22691	4.05×10^{-7}	0.21564	1.33647	8.63×10^{-6}	1864.5
				0.5					0.57376	1.26102	1.03×10^{-7}	1.72394	1.22734	4.45×10^{-7}	0.21236	1.31163	8.37×10^{-6}	1953.9
0.5	0.5	-10	**1.09**	0.1	1	0.1	1	1	0.56571	1.23216	1.81×10^{-7}	1.70159	1.22864	3.41×10^{-8}	0.34455	1.27251	1.55×10^{-9}	1965.4
			2						0.56348	1.18879	2.25×10^{-7}	1.69524	1.23198	2.37×10^{-8}	0.38148	1.16059	3.81×10^{-8}	1799.5
			5.09						0.55985	0.87477	8.21×10^{-7}	1.68525	0.83882	8.09×10^{-6}	0.42447	0.68886	1.51×10^{-7}	1810.5
0.5	0.5	**-10**	0.72	0.1	1	0.1	1	1	0.64167	1.12470	9.71×10^{-8}	1.81567	1.10578	9.73×10^{-9}	0.33501	1.26005	2.12×10^{-8}	1889.7
		-5							0.65541	1.13888	8.21×10^{-8}	1.85126	1.10591	1.89×10^{-8}	0.33485	1.26843	2.23×10^{-8}	1881.5
		-2							0.69337	1.17916	5.13×10^{-8}	1.94967	1.13559	8.51×10^{-8}	0.33442	1.29273	2.48×10^{-8}	1839.2
0.5	**0.5**	**-10**	0.72	0.1	1	0.1	1	1	0.56571	1.23216	1.81×10^{-7}	1.70159	1.22864	3.41×10^{-8}	0.34455	1.27251	1.55×10^{-9}	1965.4
	1								0.57207	1.23858	1.81×10^{-7}	1.71876	1.23556	3.11×10^{-8}	0.31453	1.29395	5.74×10^{-9}	1946.4
	2								0.58027	1.23948	1.75×10^{-7}	1.72576	1.24256	2.98×10^{-8}	0.24845	1.31395	3.74×10^{-9}	1956.2
0.5	0.5	-10	0.72	0.1	1	0.1	1	1	0.57351	1.25740	1.11×10^{-7}	1.72308	1.22691	3.64×10^{-7}	0.21911	1.36116	7.28×10^{-6}	1902.5
1									0.57959	1.28798	6.71×10^{-8}	1.73982	1.23648	7.88×10^{-7}	0.12141	1.346422	2.12×10^{-5}	1909.1
1.5									0.58259	1.27858	7.15×10^{-8}	1.74325	1.24245	1.21×10^{-7}	0.82548	1.31254	1.26×10^{-5}	1925.5

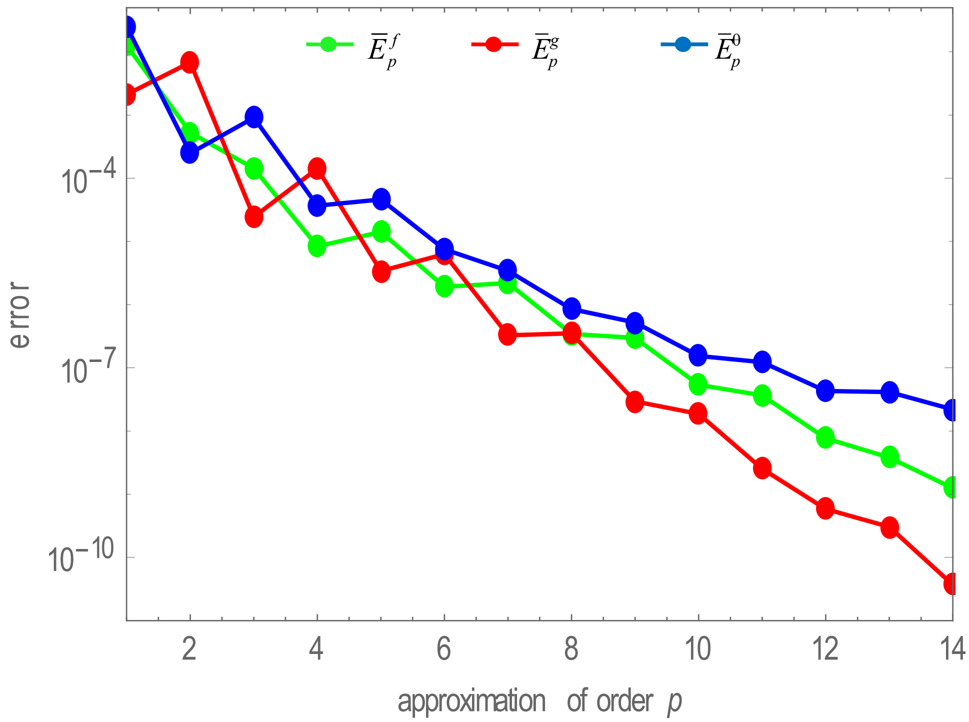

Fig. 5.3.1(a): Residual error vs. order of approximation

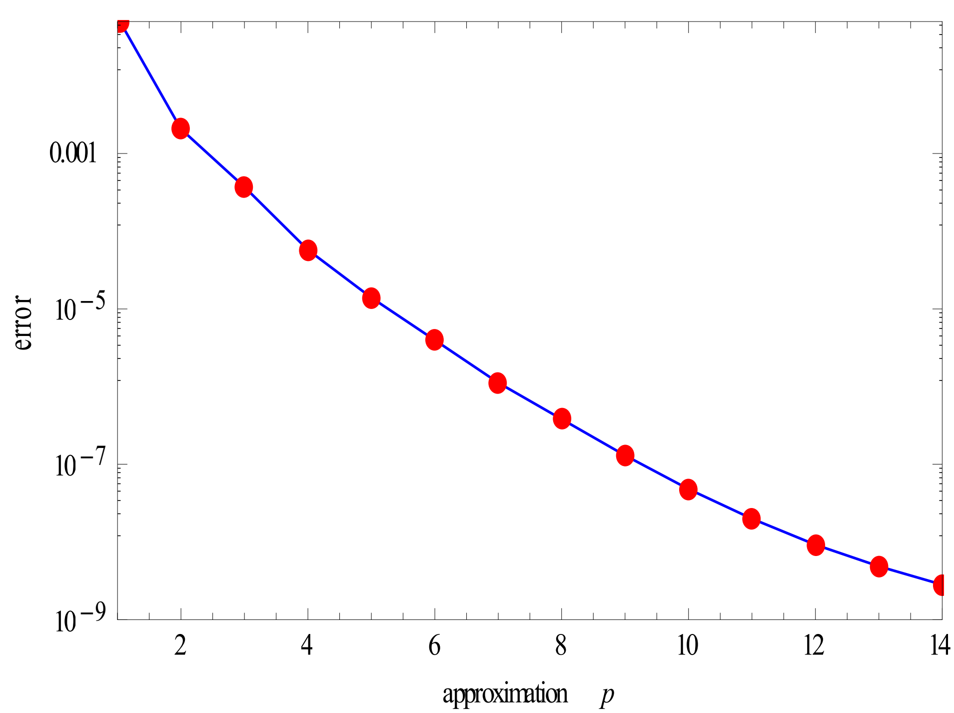

Fig.5.3.1 (b): Total residual error versus order of approximation p

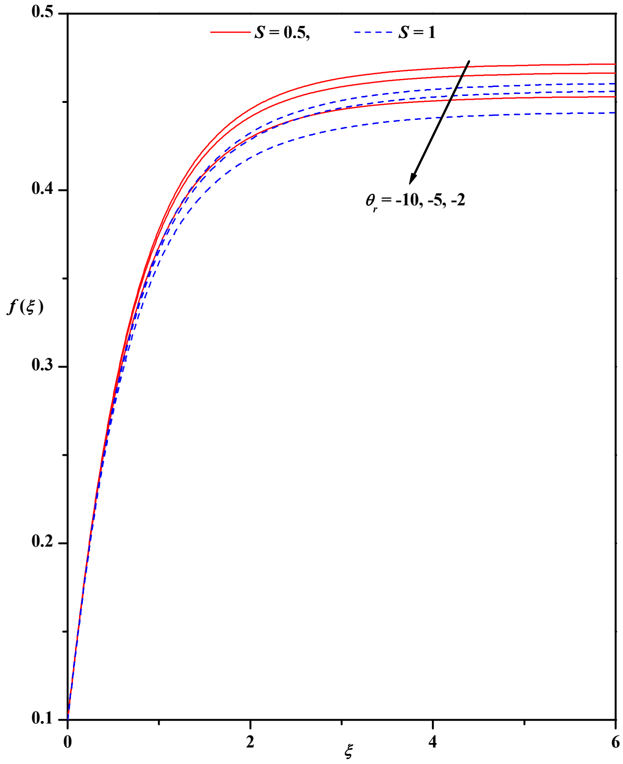

Fig. 5.5.1 (a): Axial velocity profiles for different values of θ_r and S with $\alpha = 0.5$, $Mn = 1$, $\varepsilon_1 = 0.1$, $Bi = 0.5$, $Ec = 0.01$, $Pr = 0.72$, $f_w = 0.1$.

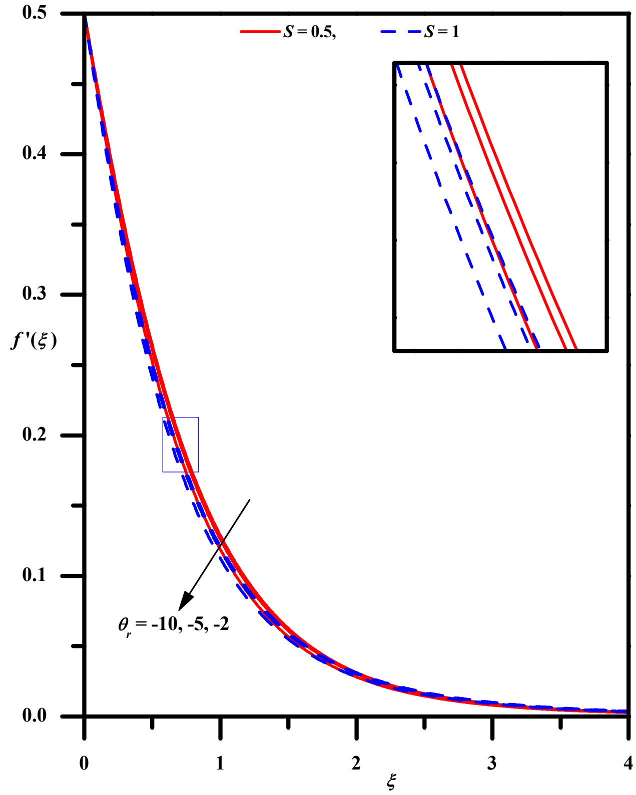

Fig. 5.5.1 (b): Radial velocity profiles for different values of θ_r and S with $\alpha = 0.5$, $Mn = 1$, $\varepsilon_1 = 0.1$, $Bi = 0.5$, $f_w = 0.1$, $Ec = 0.01$, $Pr = 0.72$.

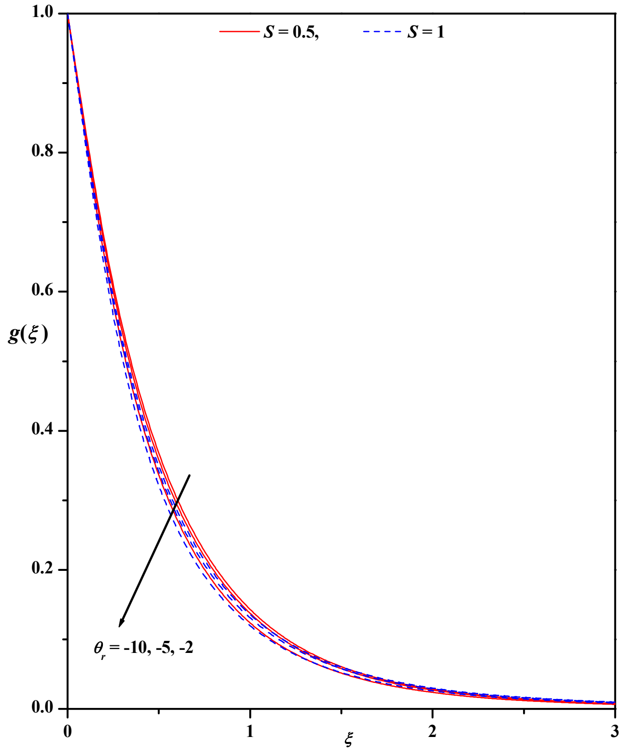

Fig. 5.5.1 (c): Tangential velocity profiles for different values of θ_r and S with $\alpha = 0.5$, $Mn = 1$, $\varepsilon_1 = 0.1$, $Bi = 0.5$, $Ec = 0.01$, $Pr = 0.72$, $f_w = 0.1$.

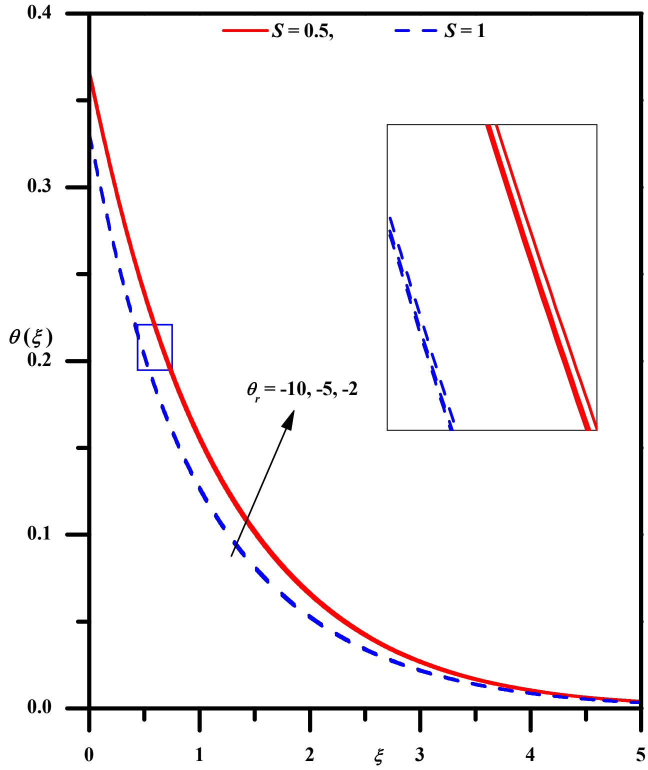

Fig. 5.5.1 (d): Temperature profiles for different values of θ_r and S with $\alpha = 0.5$, $Mn = 1$, $\varepsilon_1 = 0.1$, $Bi = 0.5$, $Ec = 0.01$, $Pr = 0.72$, $f_w = 0.1$.

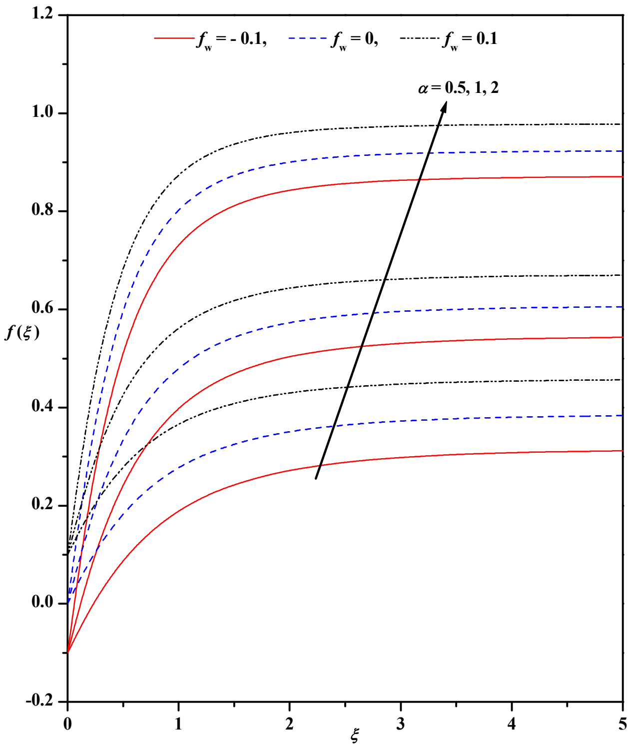

Fig. 5.5.2. (a): Axial velocity profiles for different values of α and f_w with S =1, Mn = 1, ε_1 = 0.1, Bi = 0.5, Ec = 0.5, Pr = 0.72, θ_r = -10.

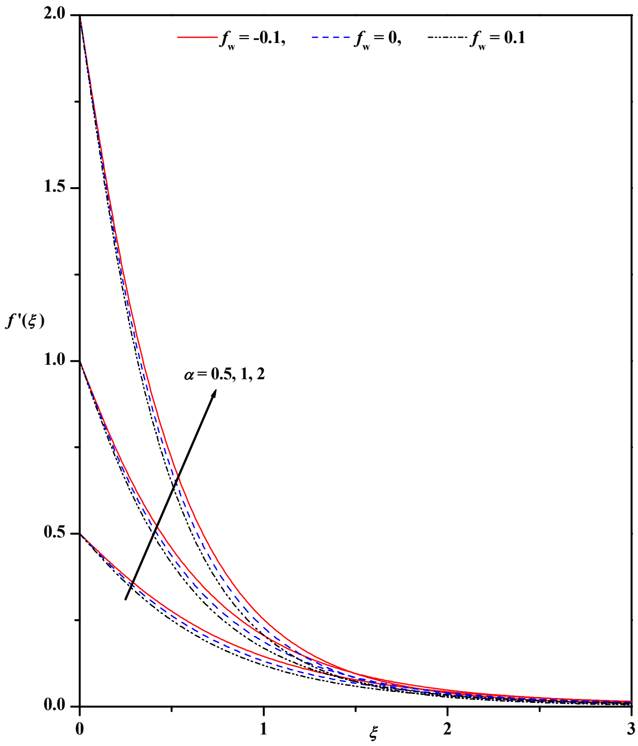

Fig. 5.5.2 (b): Radial velocity profiles for different values of α and f_w with S =1, Mn = 1, ε_1 = 0.1, Bi = 0.5, Ec = 0.5, Pr = 0.72, θ_r = -10.

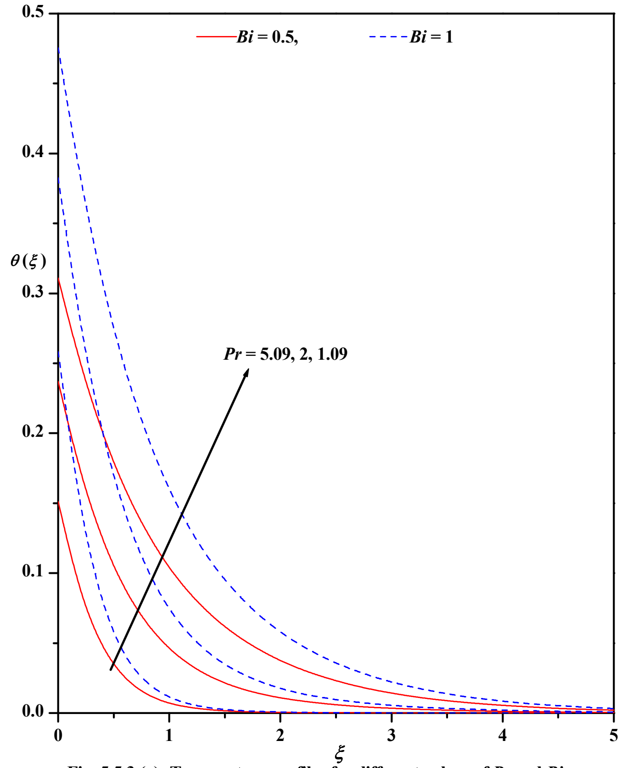

Fig. 5.5.3 (a): Temperature profiles for different values of Pr and Bi with α = 0.5, Mn = 1, ε_1 = 0.1, θ_r = -10, Ec = 0.01, S = 0.5, f_w = 0.1.

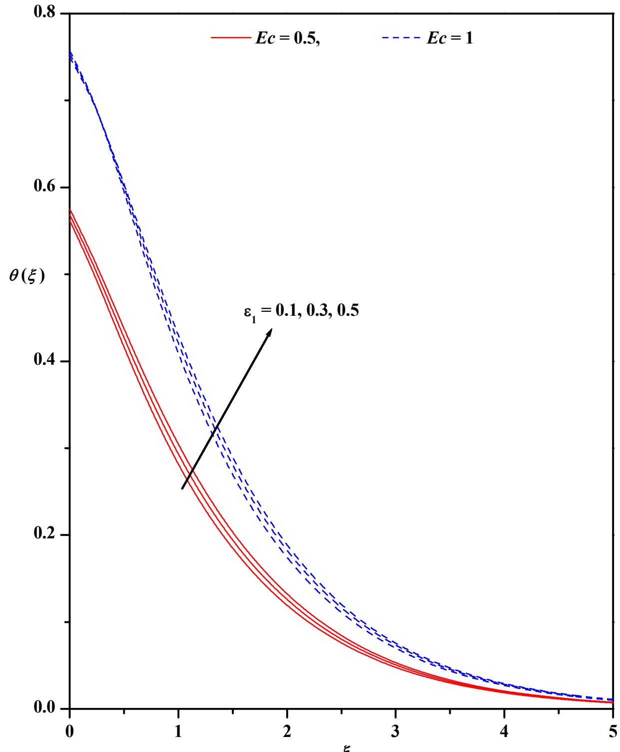

Fig. 5.5.3 (b): Temperature profiles for different values of ε_1 and Ec with α = 0.5, Mn = 1, Pr = 0.72, θ_r = -10, Bi= 0.5, S = 0.5, f_w = 0.1.

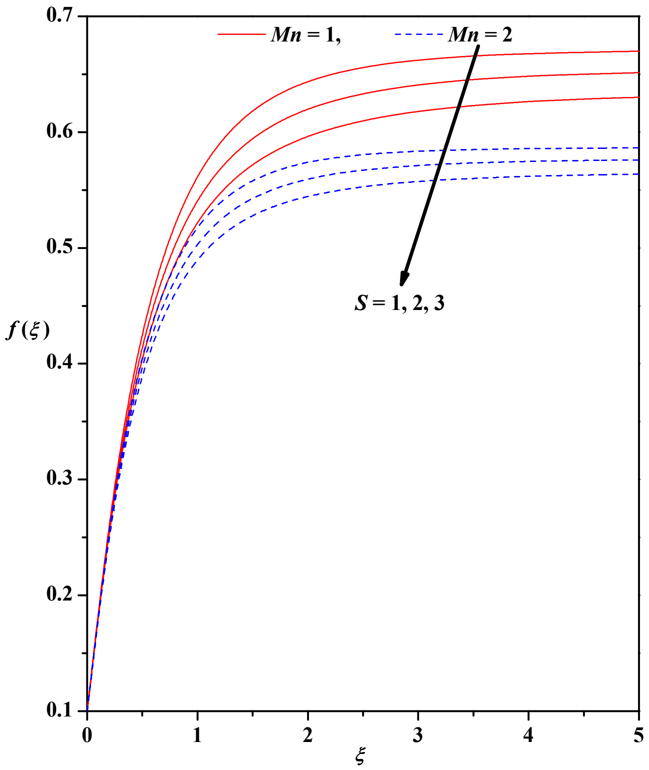

Fig. 5.5.4 (a): Axial velocity profiles for different values of S and Mn with α =1, ε_1 = 0.1, Bi = 0.5, Ec = 0.5, Pr = 0.72, f_w = 0.1, θ_r = -10.

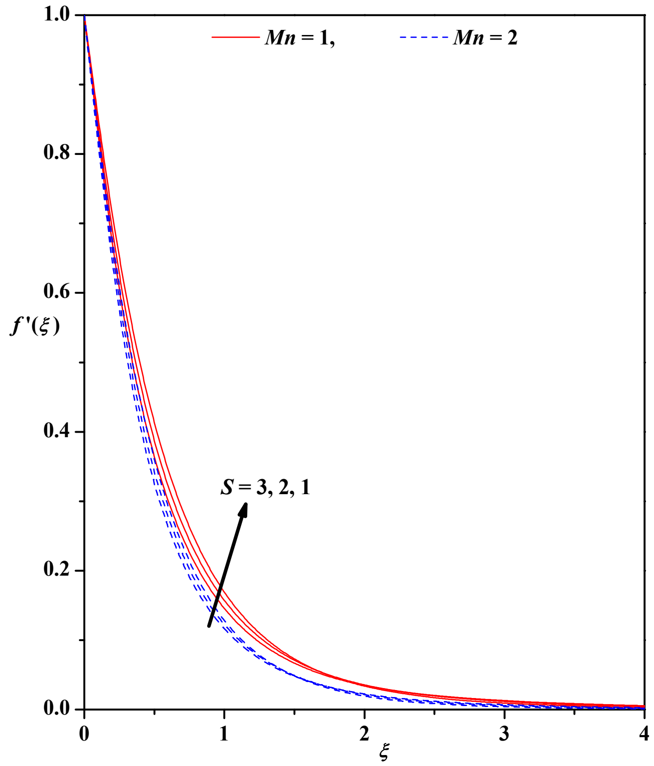

Fig. 5.5.4 (b): Radial velocity profiles for different values of S and Mn with α =1, ε_1 = 0.1, Bi = 0.5, Ec = 0.5, Pr = 0.72, f_w = 0.1, θ_r = -10.

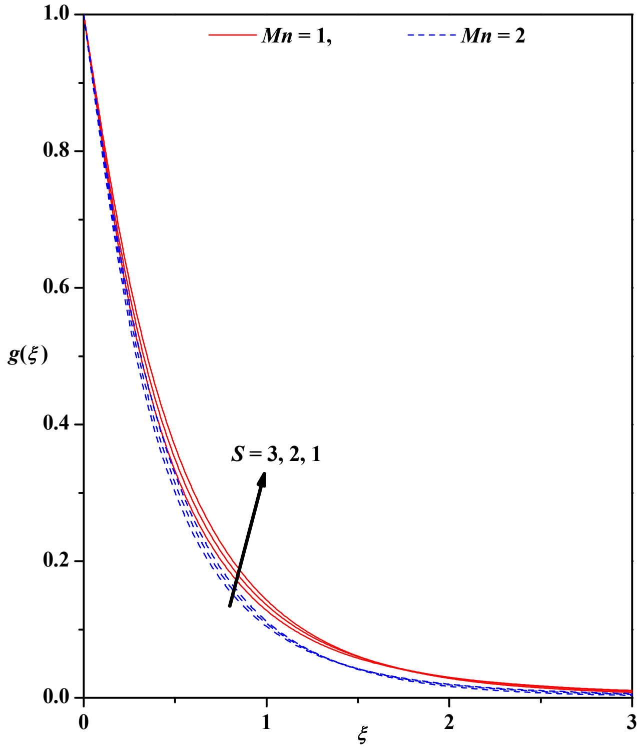

Fig. 5.5.4 (c): Tangential velocity profiles for different values of S and Mn with α =1, ε_1 = 0.1, Bi = 0.5, Ec = 0.5, Pr = 0.72, f_w = 0.1, θ_r = -10.

REFERENCES

Ahmad, S., Arifin, N.M., Nazar, R., and Pop, I., (2008): Mixed convection boundary layer flow along vertical moving thin needles with variable heat flux, *Int. J. Heat Mass Transf.,* **Vol.44,** 473–479.

Abd El-Aziz, M., and Afify, A.A., (2019): Effect of Hall current on MHD flow of Casson nanofluid over a stretching sheet with zero nanoparticle mass flux, *Thermophoresis and Aeromechanics,* **Vol.3,** 429 - 443.

Abdul, M, K., and Abdul, S, M., (2005): The effects of variable properties and hall current on steady MHD laminar convective fluid flow due to a porous rotating disk, *Int. J. Heat Mass Transf.,* **Vol. 48**, 4963 - 4972.

Ahmad, A., Asghar, S., and Afzal, S., (2016): Flow of nanofluid past a Riga plate, *J. Magn. Magn. Mater.,* **Vol. 402,** 44-48.

Ajayi, T.M., Aninasaun, I.L., and Omowaye, A.J., (2017): Effects of viscous dissipation and double stratification on MHD Casson fluid flow over a surface with variable thickness: Boundary layer analysis, *Int. J. Eng. Research in Africa.,***Vol.28,** 73-89.

Akyildiz, F.T., Siginer, D.A., Vajravelu, K., Cannon, J.R., and Van Gorder, R.A.,(2010): Similarity solutions of the boundary layer equations for a nonlinearly stretching sheet, *Math. Meth. Appl. Sci.,* **Vol.33,** 601-606.

Ali, M.E., (1995): On thermal boundary layer on a power law stretched surface with suction or injection, *Int. J. Heat Fluid Flow.,* **Vol. 16**, 280-290.

Anjali Devi, S.P., and Thiyagarajan, M., (2006): Steady nonlinear hydromagnetic flow and heat transfer over a stretching surface of variable temperature, *Heat Mass Transf.,* **Vol.42,** 671-673.

Anjali Devi, S.P., and Prakash, M., (2016): Slip flow effects over a hydromagnetic forced convective flow over a slender stretching sheet, *J. Appl. Fluid. Mech.,* **Vol. 9,** 683-692.

Anjum, A., Farooq, M., Hayat.T., and Alsaedi, A., (2016): Melting heat transfer in the flow over a variable thicked Riga plate with homogeneous- heterogeneous reactions, *J. Mol. Liq.,* **Vol.224,** 1341-1347.

Ayub, M., Abbas, T., and Bhatti, M.M., (2016): Inspiration of slip effects on electromagnetohydrodynamics (EMHD) nanofluid flow through horizontal Riga plate, *Eur. Phys. J .Plus.,* **Vol. 131,** 193.

Aziz, Z.A., Daniel, Y.S., Zuhai La Ismil., and Salah, F., (2018): Thermal stratification effects on MHD radiative flow of nanofluid over nonlinear stretching sheet with variable thickness, *J. Comput. Design Eng.,* **Vol. 5,** 232 – 242.

Bachok, N., Ishak, A., and Pop, I., (2012): Unsteady boundary-layer flow and heat transfer of a nanofluid over a permeable stretching/shrinking sheet, *Int. J. Heat Mass Transf.,* **Vol. 55***,* 2102-2109.

Bank, W.H.H., (1983): Similarity solutions of the boundary layer equations for a stretching wall, *J. de Mech. Theor. Appl.,* **Vol.2,** 375-392.

Bhatti, M.M., Ayub, M., and Abbas, T., (2016): Inspiration of slip effects on electro magneto hydrodynamic (EMHD) nanofluid flow through a horizontal Riga plate, *Eur. Phys. J. Plus.,* **Vol.131,** 193.

Blasius, H., (1908): Grenzschichten in Flussigkeiten mit Kleiner Reiburg, *Z. Angew. Math. Phys.,* **Vol.56,** 1-37.

Bujurke, N.M., Biradar, S.N., and Hiremath, P.S., (1987): Second order fluid flow past a stretching sheet with heat transfer*, Z. Angew. Math. Phys.,* **Vol.38,** 653-657.

Buongiorno, J., (2006): Convective transport in nanofluids, *J. Heat Transf.,* **Vol. 128,** 240–250.

Cattaneo, C., (1948): Sulla conduzione delcalore, *Atti Semin. Mat. Fis. Univ. Modena Reggio Emilia,* **Vol.3,** 83–101

Chen, C.H., (2003): Heat transfer in a power law fluid film over an unsteady stretching sheet, *Heat Mass Transf.,* **Vol.39,** 791-796.

Chen, C.K., and Char, M. I., (1988): Heat transfer on a continuous stretching surface with suction/blowing*, J. Math. Anal. Appl.,* **Vol.35,** 568-580.

Choi, S., (1995): Enhancing thermal conductivity of fluids with nanoparticle. Development and Applications of Non-Newtonian flows, edited by D.A. Siginer and H.P. Wang*, ASME, MD 231 and FED.,* **Vol.66,** 99-105.

Choi, S.U.S., and Eastman, J.A., (1995): Enhancing thermal conductivities of fluids with nanoparticles, *ASME, Int. Mech. Eng. Congress and Exposition. San Francisco, USA.*

Chon, C.H., and Kihm, K.D., (2005): Thermal conductivity enhancement of nanofluids by Brownian motion, *J. Heat Transf.,* **Vol. 127,** 810.

Christov, C. I., (2009): On frame indifferent formulation of the Maxwell–Cattaneo model of finite-speed heat conduction, *Mech. Res. Comm.,* **Vol.36,** 481–486.

Cochran, W.G., (1931): The Flow Due to a Rotating Disk, *Mathematical Proceedings of the Cambridge Philosophical Society.,* **Vol. 30**, 365-375.

Cortell, R., (2005a): A note on magnetohydrodynamic flow of a power law fluid over a stretching sheet, *Appl. Math. Comput.,* **Vol.168,** 557-566.

Cortell, R., (2005b): Flow and heat transfer of a fluid through a porous medium over a stretching surface with internal heat generation/absorption and suction/blowing, *Fluid Dynamics Research.,* **Vol. 37**, 231-245.

Cortell, R., (2007): Viscous flow and heat transfer over a nonlinearly stretching sheet, *Appl. Math. Comput.,* **Vol.184,** 864-873.

Crane, L.J., (1970): Flow past a stretching plate, *Z. Angew. Math. Phys.,* **Vol. 21,** 645.

Dandapath, B.S., and Gupta, A.S., (1989): Flow and heat transfer in a viscoelastic fluid over a stretching sheet, *Int. J. Non-liner. Mech.,* **Vol.24,** 215-219

Daniel, Y.S., Aziz, A.Z., Ismil, Z., and Salah, F., (2018): Impact of thermal radiation on electrical MHD flow nanofluid over nonlinear stretching sheet with variable thickness, *Alex. Eng. J.,* **Vol.57,** 2187-2197.

Das, S.K., Putra, N., Thiesen, P., and Roetzel, W., (2003): Temperature dependence of thermal conductivity enhancement for nanofluids, *J. Heat Transf.,* **Vol.125,** 567–574.

Das, S., Jana, R.N., and Makinde, O.D., (2015): Magnetohydrodynamic mixed convective slip flow over an inclined porous plate with viscous dissipation and joule heating, *Alex. Eng. J.,* **Vol. 54,** 251-261.

Dawe, D.J., (1966): Vibrations of rectangular plates of variable thickness, *J. Mech. Eng. Sci.,* **Vol. 8,** 1.

Dutta, B.K., Roy, P., and Gupta, A.S., (1985): Temperature field in a flow over a stretching sheet with uniform heat flux, *Int. J. Commu. Heat Mass Transf.,* **Vol.12,** 89-94.

Dutta, B.K., and Gupta, A.S., (1987): Cooling of a stretching sheet in a viscous flow, *Ind. Eng. Chem.,* **Vol. 26.** 333 - 336.

Dutta, B. K., (1988): Heat and Mass transform from a stretching sheet in a viscous flow over a stretching sheet with uniform heat flux, *Z. Angew. Math. Phys.,* **Vol.68.** 231- 236.

Ellahi, R., Rai Sajjad Saif, Hayat, T., Muhammad, T., and Alsaedi, A., (2017): Stagnation point flow of second grade nanofluid towards a nonlinear stretching surface with variable thickness, *Results in Phys.,* **Vol. 7,** 2821-2830.

Erikson, L.E., Fan, L.T., and Fox, V.G., (1966): Heat and mass transfer on a moving continuous flat plate with suction or injection, *Ind. Eng. Chem.,* **Vol. 5**, 19-25.

Fan, T., and You, X., (2013): Optimal homotopy analysis method for nonlinear differential equations in the boundary layer, *Numer. Algor.,* **Vol. 62(2),** 337-354.

Fang, T., Zhang, J., and Zhong, Y., (2012): Boundary layer flow over a stretching sheet with variable thickness, *Appl. Math. Compu.,***Vol.218,** 7241-7252.

Fang, T., and Tao H., (2012): Unsteady viscous flow over a rotating stretchable disk with deceleration, '*Communi. Non linear. Sci. Numer. Simul.,* **Vol. 17**, 5064-5072.

Farooq, M., Hayat, T., Alsaedi, A., and Falleh Al - Solamy., (2015): Impact of Cattanneo – Christov heat flux in the flow over a stretching sheet with variable thickness, *AIP Advances.,* **Vol. 5,** 087159.

Farooq, M., Anjum, A., Hayat, T., and Alsaedi, A., (2016): Melting heat transfer in the flow over a Variable thicked Riga plate with homogeneous – heterogeneous reactions. *J. Mol. Liq.,* **Vol.224,** 1341-1347.

Farooq, S., Ahmad, I., Huma Zafar., and Kiyani, M.Z., (2019): Zero mass flux characteristics in Jeffery nanofluid flow by a nonlinear stretchable surface with variable thickness, *Int. J. Heat Mass Transf.,* **Vol.132,** 1166 - 1175.

Fourier, B. J., (1822): Theorie analytique de la chaleur, *Libraires Pour Les Mathematiques, L, Architetcure Hydralique, Et La Marin, Jacob, No. 24 ,Paris.*

Fox, V.G., Erikson, L.E. and Fan, L.T., (1968): Methods for solving the boundary layer equations for moving continuous flat surface with suction and injection, *A. I. Ch. Eng. J.,* **Vol.14**, 726-736.

Fox, V.G., Erickson, L.E., and Fan, L.T., (1969): The laminar boundary on a moving continuous flat sheet immersed in a non-Newtonian fluid, *A. I. Ch. Eng. J.,* **Vol.15,** 327-333.

Fresteri, F., and Osalusi, E., (2007): On MHD and slip flow over a rotating disk with variable properties, *Int. J. Commun. Heat Mass Transf.*, **Vol. 34**, 495- 501.

Gailitis, A., and Lielausis, O., (1961): On a possibility to reduce the hydrodynamic resistance of a plate in an electrolyte, *Appl. Magnet. Hydro. dyncs. Rep. Phys. Inst. Riga,* **Vol.12,** 143-146.

Grinberg, E., (1961): On determination of properties of some potential fields, *Appl. Magnet. Hydro. dyncs.*, **Vol. 12,** 147–154.

Gupta, P.S., and Gupta, A.S., (1977): Heat and mass transfer on a stretching sheet with suction/blowing, Canadian. *J. Chem. Eng.,* **Vol.55,** 744-746.

Hammouch, Z., Shafiq, A., and Turab, A., (2018): Impact of radiation in a stagnation point flow of Walter B fluid towards a Riga plate, *Them. Sci. Eng. Prog.,* **Vol. 6,** 27-33.

Hayat, T., Zubair, M., Ayub, M., Waqas, M., and Alsaedi, A., (2016a): Stagnation point flow towards nonlinear stretching surface with Cattaneo–Christov heat flux, *Eur. Phys. J. Plus.,***Vol. 131,** 355.

Hayat, T., Farooq, M., Aisha Anjum, and Alsaedi, A., (2016b): Melting heat transfer in the flow over a Variable thicked Riga plate with homogeneous – heterogeneous reactions, *J. Mol .Liq.,* **Vol. 224,** 1341-1347.

Hayat, T., Abbas, T., Ayub, M., Farooq, M., and Alsaedi, A., (2016c): Flow of nanofluid due to convectively heated Riga plate with variable thickness, *J. Mol. Liq.,* **Vol. 222,** 854-862.

Hayat, T., Muhammad, T., Meraj Mustafa, and Alsaedi, A., (2017a): Threedimensional flow of Jeffrey fluid with Cattaneo-Christov heat flux: An application to non-Fourier heat flux theory, *Chinese. J. Phys.,* **Vol. 55,** 1067-1077.

Hayat, T., Khan, M., Imtiaz, M., and Alsaedi, A., (2017b): Squeezing flow past a Riga plate with chemical reaction and convective conditions, *J. Mol. Liq.,* **Vol.225,** 569–576.

Hayat, T., Khan, M., Khan, M.I., Alsaedi, A., and Ayub, M., (2017c): Electromagneto squeezing rotational flow of Carbon (C)-Water (H2O) kerosene oil nanofluid past a Riga plate: A numerical study. *PLoS ONE* , **Vol.12,** e0180976-98.

Hayat, T., Muhammad, T., Shehazad, S.A., and Alsaedi, A., (2017d): An analytical solution for magnetohydrodynamics Oldroyd B-nanofluid flow induced by stretching sheet with heat generation/absorption, *Int. J. Therm. Sci.,* **Vol. 111,** 274-288.

Hayat, T., Kiran, A., Imtiaz, M., and Alsaedi, A., (2018a): Effect of homogeneous – heterogeneous reaction in stagnation point flow of third grade fluid past a variable thickness stretching sheet, *Neural. Comput. Appli.,* **Vol.30,** 3071-3080.

Hayat, T., Rashid, M., Alsaedi. A, and Ahmad, B., (2018b): Flow of nanofluid by nonlinear stretching sheet velocity, *Results in phys.,* **Vol. 8,** 1104-1109.

Hayat, T., Madiha Rashid, M., Ijaz Khan., and Alsaedi, A., (2019): Physical aspects of MHD nonlinear radiation heat flux in flow of thixotropic nanomaterial, *Iranian. J. Sci. Tech.,* **Vol. 43,** 2043-2054.

Hobiny, A., Ahmed, B., Alsaedi, A., Jalil, M., and Asghar, S., (2015): Similarity solution for follow over an unsteady nonlinearly stretching rotating disk, *AIP Advances.,* **Vol. 5**, 047113.

Hussain, Z., Hayat, T., Alsaedi, A., and Ahmad, B., (2017): Numerical study for slip flow of carbon water nanofluids, *Comput. Methods App. Mech. Eng.,* **Vol. 316,** 366-378.

Iqbal, Z., Azhar, E., Mehmood, Z., and Maraj, E.N., (2017): Melting heat transport of nanofluidic problem over a Riga plate with erratic thickness: Use of Keller box scheme, *Results in Phys.,* **Vol.9,** 3648-3658.

Ishak, A., Nazar, R., and Pop, I., (2007): Boundary layer flow over a continuously moving thin needle in a parallel free stream, *Chinese Phys. Let.,* **Vol. 24,** 2895–2897.

Ishak, A., Nazar, R., and Pop, I., (2008): Hydromagnetic flow and heat transfer adjacent to stretching vertical sheet, *J. Heat Mass Transf.,* **Vol. 44,** 921-927.

Javed, M., Anjum, M., Mir, N.A., Farooq, M., Ahmad, S., Malik, M.Y., and Alshomrani, A.S., (2018): Physical aspects of heat generation/absorption in the second grade fluid flow due to Riga plate: Applications of Cattanneo – Christov approach, *Results in Phys.,* **Vol.9,** 955-960.

Jawad, R., Oudina, F.M., and Makinde, O.D., (2018): MHD Slip Flow of Cu-Kerosene Nanofluid in a Channel with Stretching Walls Using 3-Stage Lobatto IIIA Formula, *D.D.F.,* **Vol.387,** 51-62.

Kandasamy, R., Muhaimin, and Azme B- Khamis., (2008): Effects of heat and mass transfer on a nonlinear MHD boundary layer flow over a shrinking sheet in the presence of suction, *Appl. Math. Mech. Eng.,***Vol.29,** 1309-1317.

Khader, M. M., and Megahed, A. M., (2015): Boundary layer flow due to a stretching sheet with a variable thickness and slip velocity, *J. Appl. Mech. Tech. Phys.,* **Vol.56,** 241-247.

Khader, M.M., (2016): Shifted Legendre collocation method for the flow and heat transfer due to a stretching sheet embedded in a porous medium with variable thickness, variable thermal conductivity and thermal radiation, *Mediterranean. J. Math.,* **Vol. 13,** 2319-2338.

Khan, K. A., and Aziz, A., (2011): Natural convection flow of a nanofluid over a vertical plate with uniform surface heat flux, *Int. J. Therm. Sci.,* **Vol. 50,** 1207–1214.

Khan, K.A., Butt, A.R., and Raza, N., (2018): Effects of heat and mass transfer on unsteady boundary layer flow of a chemical reacting Casson fluid, *Results in Phys.,* **Vol. 8**, 610-620.

Khan, M., Hayat, T., Imtiaz, M., and Alsaedi, A., (2017): Squeezing flow past a Riga plate with chemical reaction convective conditions, *J. Mol. Liq.,* **Vol.225,** 569-576.

Kuiken, H. K., (1971): The effect of normal blowing on the flow near a rotating disk of infinite extent, *J. Fluid Mech.,* **Vol. 47**, 789-798.

Kumaran, V., and Ramananaiah, G., (1996): A note on the flow over a stretching sheet, *Acta Mech.,* **Vol.116,** 229-233.

Lee, L.L., (1967): Convective transport in nanofluids, *Phys. Fluids.,* **Vol. 10,** 822-828.

Li, C.H., and Peterson, G.P., (2006): Experimental investigation of temperature and volume fraction variations on the effective thermal conductivity of nanoparticle suspensions (nanofluids), *J. Appl. Phys.,* **Vol. 99,** 084314.

Liao, S., (2003): Beyond perturbation: Introduction to homotopy analysis method, *Chapman & Hall/CRC Press, London.*

Liao, S., (2007): A new branch of solutions of boundary-layer flows over a permeable stretching plate, *Int. J. Non-Linear. Mech.,* **Vol. 42,** 819-830.

Liao, S., (2010): An optimal Homotopy – analysis approach for strongly nonlinear equations, *Commu. Non-Linear. Sci. Num. Simu.,* **Vol. 15,** 2003- 2016.

Lin, L., and Lin, F., (2018): Boundary layer flow of fractional Maxwell fluid over a stretching sheet with variable thickness, *Appl. Math. Letter.,* **Vol. 79,** 92-99.

Liu, L., Zheng, L., Liu, F., and Xinxin Zhang., (2016): Anomalous convection diffusion and wave coupling transport of cells on comb frame with fractional Cattaneo–Christov flux, *Commun. Nonlinear. Sci. Numer. Simul.,* **Vol.38,** 45–58.

Magyari, E., and Keller, B., (2000): Exact solutions for self similar boundary layer flows induced by permeable stretching walls, *Eur. J. Mech. B/Fluids.,* **Vol.19,** 109-122.

Mahapatra, T.R., and Gupta, A.S., (2003): Stagnation point flow of a visco –elastic fluid towards a stretching surface, *Chem. Eng. J.,* **Vol.81,** 258-263.

Makinde, O.D., and Aziz, A., (2011): Boundary layer flow of nanofluid past a stretching sheet with convective boundary conditions, *Int. J. Therm. Sci.,* **Vol. 50,** 1326-1332.

Maleki, H., Safaei, M.R., Abdullah., Alrashid, A.A.A., and Kasaeian, A., (2019a): Flow and heat transfer in non-Newtonian nanofluids over porous surfaces, *J. Therm. Anal. Calorimetry.,* **Vol. 135**, 1655-1666.

Maleki, H., Safaei, M.R., Togun, H., and Daheri, M., (2019b): Heat transfer and fluid flow of pseudo-plastic nanofluid over a moving permeable plate with viscous dissipation and heat absorption/generation, *J. Therm. Anal. Calorimetry.,* **Vol. 135**, 1643-1654.

Manjunatha, G., Rajashekar, C., Vaidya, H., Divya, B.B., and Prasad, K.V., (2018): Peristaltic flow of Casson liquid in an inclined porous tube with convective boundary conditions and variable fluid properties, *Frontiers in Heat and Mass Transfer.,* **Vol. 11,** 35.

Masuda, H., Ebata, A., Teramae, K., and Hishiunma, N., (1993): Alteration of thermal conductivity and viscosity of liquid by dispersed by ultra fine particles (dispersion of Al2O3 SiO2 and TiO2 ultra fine particles), *Netsu Bussei.,* **Vol. 4,** 227–233.

Muhammad, A., Saeed, E.A., Khalid, I.Z., Ashfaq, K.M., and Asif, Z.R., (2018): Hydromagnetic mixed convective flow over a wall with variable thickness and Cattanneo – Christov heat flux model, *Results in Phys.,* **Vol.8,** 621-627.

Murshed, S.M.S., Leong. K.C., and Yang, C., (2008): Investigation of thermal conductivity and viscosity of nanofluids, *Int. J Therm. Sci.,* **Vol. 47,** 560-568.

Nadeem, S., and Muhammad, N., (2016): Impact of stratification and Cattaneo–Christov heat flux in the flow saturated with porous medium, *J. Mol. Liq.,* **Vol.224,** 423-430.

Naveed, A., Fitnat, S., Umar, K., Ilyas, K., Tawfeeq, A. A., Imran, F., Syed, T., and Mohyud-Din., (2019): Spherical Shaped (Ag−Fe3O4/H2O) Hybrid Nanofluid Flow Squeezed between Two Riga Plates with Nonlinear Thermal Radiation and Chemical Reaction Effects, *Energies*., **Vol.12,** 76-98.

Nayak, M.K., Hakeem, A.K.A., and Makinde, O.D., (2018a): Influence of Catteneo-Christov heat flux model on mixed convection flow of third grade nanofluid over an inclined stretched Riga plate, *D.D.F.*, **Vol.387,** 121–134.

Nayak, M.K., Shaw, S., Makinde, O.D., and Chamkha, A.J., (2018b): Effects of homogenous–heterogeneous reactions on radiative NaCl-CNP nanofluid flow past a convectively heated vertical Riga plate, *J. Nanofluids.,* **Vol.7,** 657–667.

Nayak, M.K., Shaw, S., Makinde, O.D., and Chamkha, A.J., 2019: Investigation of partial slip and viscous dissipation effects on the radiative tangent hyperbolic nanofluid flow past a vertical permeable Riga plate with internal heating: Bungiorno model, *J. Nanofluids.*, **Vol. 8,** 51-62.

Oudina, F.M., (2019): Convective heat transfer of titania nanofluid flow of different base fluids in cylindrical annuals discrete heat source, *Heat Transf – Asian. Res.*, **Vol.48,** 135-147.

Pantokratoras, A., and Magayri, E., (2009): EMHD free- convection boundary layer flow from a Riga plat, *J. Eng. Math.*, **Vol. 64,** 303-315.

Pantakrotoras, A., (2011): The Blasius and Sakiadis flow along a Riga-plate, *Progr. Comput. Fluid. Dynomic. An Int. J. (PCFD),* **Vol.11,** 329-333.

Partha, M.K., Murthy, P., and Rajasekhar, G.P., (2005): Effect of viscous dissipation on the mixed convection heat transfer from an exponentially stretching surface, *Heat Mass Transf.,* **Vol.41,** 360-366.

Pop, I., Subhashini, S.V., and Sumthi, R., (2013): Dual solutions in a thermal diffusive flow over a stretching sheet with variable thickness, *Int. J. Commu. Heat Mass Transf.,* **Vol. 48,** 61- 66.

Prasad, K.V., and Vajravelu, K., (2009): Heat transfer in the MHD flow of a power law fluid over a non-isothermal stretching sheet, *Int. J. Heat Mass Transf.,* **52**, 4956-4965.

Prasad, K.V., Vajravelu, K., and Datti, P.S., (2010): Mixed convection heat transfer over a nonlinear stretching surface with variable fluid properties, *Int. J. Non-Linear. Mech.,* **Vol. 45,** 320-330.

Prasad, K. V., Vajravelu, K., Vaidya, H., and Raju, B. T., (2015): Heat Transfer in a non-Newtonian nanofluid film over a stretching surface, *J. Nanofluids.,* **Vol.4,** 536-547.

Prasad, K.V., Vajravelu, K., Shivakumara, I. S., Vaidya, H., and Neelufer, Z, Basha., (2016a): Flow and heat transfer of a Casson nanofluid over a nonlinear stretching sheet, *J. Nanofluids.,* **Vol.5,** 743-752.

Prasad, K.V., Vaidya, H., Vajravelu.K., and Rashidi, M.M., (2016b): Effects of variable fluid properties on MHD flow and heat transfer over a stretching sheet with variable thickness, *J. Mech.,* **Vol.33,** 501-512.

Prasad, K.V., Vajravelu, K., Vaidya, H., and Van Gorder, R.A., (2017a): MHD flow and heat transfer in a nanofluid over a slender elastic sheet with variable thickness, *Results in Phys.,* **Vol.7,** 1462-1474.

Prasad, K.V., Vaidya, H., and Vajravelu, K., (2017b): MHD mixed convection heat transfer over a nonlinear slender elastic sheet with variable fluid properties, *Appl. Math. Non-Linear. Sci.,* **Vol. 2,** 351-366.

Prasad, K.V., Vaidya, H., Vajravelu, K., and Rashidi, M., (2017c): Effects of Variable Fluid Properties on MHD Flow and Heat Transfer over a Stretching Sheet with Variable Thickness, *J. Mech.,* **Vol. 33**, 501-512.

Prasad, K.V., Vaidya, H., Vajravelu, K., Neelufer, Z, Basha., and Umesh, V., (2018a): Thermal and species concentration of MHD Casson fluid at a vertical sheet in the presence of variable fluid properties." *Ain Shams Eng. J.,* **Vol. 9,** 1763-1779.

P**rasad, K.V., Vaidya, H., Vajravelu, K., and Ramanjini,V., (2018b):** Analytical study of Cattanneo-Christov heat flux model for Williamson -nanofluid flow over a slender elastic sheet with variable thickness. *J. Nanofluids.,* **Vol.7,** 583-594.

Prasad, K.V., Vajravelu, K., Vaidya, H., Rashidi, M.M., and Neelufer Z, Basha., (2018c): Flow and heat transfer of a Casson liquid over a vertical stretching surface: optimal solution, *A. J. Heat Mass Transf.,* **Vol. 5**, 1-22.

Prasad, K.V., Vaidya, H., Makinde, O.D., and Srikantha Setty, B., (2019a): MHD mixed convective flow of Casson nanofluid over a slender rotating disk with source/sink and partial slip effects, *D.D.F.,* **Vol. 392,** 92-122.

Prasad, K.V., Vaidya, H., Vajravelu, K., and Vishwanatha,U.B., (2019b): Influence of variable liquid properties on mixed convective MHD flow over a slippery slender elastic sheet with convective boundary condition, *J.A.R.F.M.T.S.*, **Vol. 56,** 100-123.

Qayyum, S., Hayat, T., Alsaedi, A., and Shafiq, A., (2016): Inclined magnetic field and heat source/sink aspects in a flow of nanofluid with nonlinear thermal radiation, *Int. J. Heat Mass Transf.,* **Vol.103,** 99 - 107.

Qayyaum, S., Hayat, T., Bashir, Z., and Alsaedi, A., (2017a): Investigation of double diffusion Cattanneo – Christov model in mixed convection flow by variable thickness surface, *Results in Phys.,* **Vol.7,** 3873-3887.

Qayyum, S., Hayat, T., Alsaedi, A., and Ahamad, B., (2017b): Magnetohydrodynamic nonlinear convective flow of Jeffery nanofluid over a nonlinear stretching surface with variable thickness, *Int. J. Mech. Sci.,* **Vol.134,** 306-314.

Rajagopal, K.R., Na, T.Y., and Gupta, A.S., (1984): Flow of a viscoelastic fluid over a stretching sheet, *Rheol. Acta.,* **Vol.23.,** 213-215.

Ramzan, Z., Bilal, M., and Chung, J.D., (2018): Radiative Williamson nanofluid over a convectively heated Riga plate with chemical reaction: A numerical approach, *Chinese. J. Phys.,* **Vol. 55,** 1663-1673.

Rana, P., and Bhargava. R., (2012): Flow and heat transfer of a nanofluid over a nonlinearly stretching sheet, *Comm. Non-Linear. Sci. Numer. Simu.,* **Vol.17,** 212–226.

Rashidi, M.M., Ali, M., Freidoonimehr, and Nazari, F., (2013): Parametric analysis and optimization of entropy generation in unsteady MHD flow over a stretching rotating disk using artificial neural network and particle swarm optimization algorithm, *Energy.,* **Vol. 55**, 497-510.

Rashidi, M.M., Freidoonimehr, N., Hosseini, A., Anwar Bég, O., and Hung, T.K., (2014a): Homotopy simulation of nanofluid dynamics from a non-linearly stretching isothermal permeable sheet with transpiration of nanofluids over a power law stretching sheet, *Meccanica.,* **Vol.49,** 469–482.

Rashidi, M, M., Kavyani, N., and Abelman., S., (2014b): Investigation of entropy generation in MHD and slip flow over a rotating porous disk with variable properties, *Int. J. Heat Mass Transf.,* **Vol. 70**, 892-917.

Rashidi, M.M., Abbas, T., and Bhatti, M.M., (2016): Effects of thermal radiation and electromagnetohydrodynomics on viscous nanofluid through a Riga plate, *Multi.Model.Struct.,* **Vol. 12,** 605-618.

Rashidi, M.M., Bhatti, M.M., and Abbas, T., (2017): Effects of thermal radiation and electro magneto hydrodynamics on viscous nanofluid through a Riga plate, *Multi, Model. Mater. Struct.,* **Vol.12,** 605-618.

Rollins, D., and Vajravelu, K., (1991): Heat transfer in a fluid over a continuous stretching surface, *Acta. Mech.,* **Vol.89,** 167-178.

Sakiadis, B.C., (1961): Boundary layer behavior on a continuous solid surface: I. Boundary layer equations for two dimensional and axisymmetric flow, *A. I. Ch. Eng. J.,* **Vol.7,** 26-28.

Salahuddin, T., Malik, M.Y., Hussain, A., Bilal, S., and Awais, M., (2016): MHD flow of Cattanneo-Christov heat flux model for Williamson fluid over a stretching sheet with variable thickness: Using numerical approach, *J. Magn. Magn. Mater.,* **Vol. 401,** 991-997.

Salahuddin, T., Mair Khan., Malik, M.Y., and Imad Khan., (2017a): Numerical modeling of Carreau fluid due to variable thicked surface, *Results in Phys.,* **Vol. 7,** 2384-2390.

Salahuddin, T., Malik, M.Y., and Khan, M., (2017b): Study of an MHD flow of the Carreau fluid flow over a stretching sheet with variable thickness by using an implicit finite difference scheme, *J. Appl. Mech. Tech. Phys.,* **Vol. 58,** 1033 – 1039.

Shakiba, A., and Rahmi, A.B., (2019): Nanofluid flow and MHD mixed convection inside a vertical annulus with moving walls and transpiration considering the effect of Brownian motion and shape factor, *J. Therm. Anal. Calorimetry.,* **Vol. 137**, 1-15.

Sheikholeslami, M., Hayat, T., and Alsaedi, A., (2016): MHD free convection of Al_2O_3 water nanofluid considering thermal radiation: A numerical study, *Int. J. Heat Mass Transf.,* **Vol.96,** 513-524.

Sheikholeslami, M., and Rokni, H.B., (2017): Effect of melting heat transfer on nanofluid flow in existence of magnetic field considering Buongiorno Model, *Chinese. J. Phys.,* **Vol. 55,** 1115-1126.

Siddappa, B., and Abel, M.S., (1986): Viscoelastic boundary layer flow past a stretching sheet with suction and heat transfer, *Rheol. Acta.,* **Vol.23.,** 815.

Soewono, E., Vajravelu K., and Mahapatra, R.N., (1992): Existence of solutions of a nonlinear boundary value problem, arising in heat and flow transfer over a stretching sheet, *Nonlinear Aanalysis, Theory, Methods and Applications,* **Vol. 18,** 93.

Sugunamma, V., Bhagya Lakshmi, Ananth Kumar., and Ramana Reddy, J.V., (2019): Influence of nonlinear radiation and cross diffusion on MHD flow of Casson and Walter B nanofluid past a variable thickness sheet, *J. Nanofluids.,* **Vol. 8,** 1-11.

Takhar, H.S., Agarwal, R.S., Bhargava, R., and Soundalgekar, V.M., (1995): Flow of a micropolar fluid past a decelerating porous rotating disk, *Int. J. Nonlinear Mech.,* **Vol. 30**, 295-304.

Tanveer, A., Hina, A., Hayat, T., Mustafa, M., and Ahmad, B., (2016): Effects of the Cattaneo– Christov heat flux model on peristalsis, *Eng. Appl. Compu. Fluid Mech.,* **Vol. 10,** 375– 385.

Tiwari, R. K., and Das, M. K., (2007): Heat transfer augmentation in a two-sided lid-driven differentially heated square cavity utilizing nanofluids, *Int. J. Heat Mass Transf.,* **Vol. 50,** 2002–2018.

Tsinober, A.B., and Shtern, A.B., (1961): Possibility of increasing the flow stability in a boundary layer by means of crossed electric and magnetic fields. *Magnet. Hydro. dyncs.,* **Vol. 3,** 103-105.

Turkyilmazoglu, M., (2018): Fluid flow and heat transfer over a rotating vertically moving disk, *Physics of fluids.,* **30**, 063605.

Ullah, I., Hayat, T., Waqas, M., and Alsaedi, A., (2018): MHD stratified nanofluid by slandering surface, *Physica Script.,* **Vol. 93,** 11.

Vajravelu, K., (1994): Convection heat transfer at a stretching sheet with suction or blowing, *J. Math. Analy. Appl.,* **Vol.188,** 1002-1011.

Vajravelu, K., Prasad, K.V., and Chin-on Ng, (2013): Unsteady convective boundary layer flow of a viscous fluid at a vertical surface with variable fluid properties, *Nonlinear anal. Real world Appl.,* **Vol. 14**, 455-464.

Vajravelu, K., and Prasad, K. V., (2014): Keller-Box Method and Its Application, *Higher Education Press and Walter De Gruyter GmbH, Berlin/Boston.*

Vajravelu, K., Prasad, K.V., Ng, C.O., and Vaidya, H., (2016): MHD squeeze flow and heat transfer of a nanofluid between parallel disks with variable fluid properties and transpiration, *Int. J. Mech. Mater. Eng.,* **Vol. 6,** 2014-2019.

Vajravelu, K., Ronald Li., Dewasurendra, M, and Prasad, K.V., (2017): Mixed convective boundary layer flow MHD flow along a vertical elastic sheet, *Int. J. Comput. Math.,* **Vol. 3,** 2501 – 2518.

Van Gorder, R.A., and Vajravelu, K., (2010): A note on flow geometries and the similarity solutions of the boundary layer equations for a nonlinearly stretching sheet, *Arch. Appl. Mech.,* **Vol.80,** 1329-1332.

Van Gorder, R.A., (2019): Optimal homotopy analysis and control of error for implicitly defined fully nonlinear differential equations, *Numer. Algor.,* **Vol. 81,**181-196.

Venkateshwara Rao, G., and Raju, I, S., (1974): A comparative study of variable and constant thickness high precision triangular plate bending elements in the analysis of variable thickness plates, *Nuclear. Eng. Design.,* **Vol.26,** 299-304.

Von Karman, T.V., (1921): Uber Laminare and Turbulente Reibung, *Z. Angew. Math. Phys.,* **Vol. 1**, 232-252.

Wakif, A., Boulahia, Z., Mishra,S.R., and Rashidi, M.M., (2018a): Influence of a uniform transverse magnetic field on the thermo-hydrodynamic stability in water-based nanofluids with metallic nanoparticles using the generalized Buongiorno's mathematical model, *Eur. Phys. J. Plus.,* **Vol.133,** 181-197.

Wakif, A., Boulahia, Z., Ali,F., Eid, M.R., and Sehaqui, R., (2018b): Numerical analysis of the unsteady natural convection MHD couette nanofluid flow in the presence of thermal radiation using single and Two-Phase nanofluid models for Cu–Water nanofluids, *Int. J. Appl. Compu. Math.,* **Vol. 4,** 81.

Wakif, A., Boulahia, Z., and Sehaqui, R., (2018c): A semi-analytical analysis of electro-thermo-hydrodynamic stability in dielectric nanofluids using Buongiorno's mathematical model together with more realistic boundary conditions, *Results in Phys.,* **Vol.9,** 1438-1454.

Waqas, M., Khan, M.W.A., Ijaz Khan, M., and Alsaedi, A., (2017a): MHD stagnation point flow accounting variable thickness and slip conditions, *Colloid and Polymer Sci.,* **Vol. 295,** 1201-1209.

Waqas, M., Hayat, T., Alsaedi, A., Bashir, G., and Alzahrani, F., (2017b): Magnetohydrodynamic stretched flow of tangent hyperbolic nanoliquid with variable thickness, *J. Mol. Liq.,* **Vol.229,** 178-184.

Watson, L.T., and Wang, C.Y., (1979): Deceleration of a rotating disk, *Physics of fluids.,* **Vol. 22**, 2267-2269.

Watson, L.T., Sankara, K.S., and Luegina, C.M., (1985): Deceleration of a porous rotating disk in a viscous fluid, *Int. J. Eng. Sci.*, **Vol. 23**, 131-137.

Zahmatkesh, I., (2008): On the importance of thermophoresis and Brownian diffusion for the deposition of micro- and nanoparticles, *Int. J. Commu. Heat Mass Transf.,* **Vol. 35,** 369 – 375.

Zubair, M., Waqas, M., Hayat, T., Alsaedi, A., and Ayub, M., (2018): Stagnation point flow third grade liquid due to variable thickness: A useful application to Fourier heat flux approach, *Results in Phys.,* **Vol.8,** 1010 – 1016.

Copyright © 2018 by American Scientific Publishers
All rights reserved.
Printed in the United States of America

Journal of Nanofluids
Vol. 7, pp. 1–12, 2018
(www.aspbs.com/jon)

ARTICLE

Analytical Study of Cattaneo-Christov Heat Flux Model for Williamson-Nanofluid Flow Over a Slender Elastic Sheet with Variable Thickness

K. V. Prasad[1,*], Hanumesh Vaidya[2], K. Vajravelu[3], and V. Ramanjini[1]

[1]Department of Mathematics, VSK University, Vinayaka Nagar, Ballari 583105, Karnataka, India
[2]Department of Mathematics, SSA Government First Grade College (Autonomous), Ballari 583101, Karnataka, India
[3]Department of Mathematics, University of Central Florida, Orlando, FL 32816, USA

An analysis has been carried out to examine the Williamson nanofluid flow over a slender elastic sheet with variable thickness using Cattaneo-Christov theory. To explore the heat transfer characteristics, Cattaneo-Christov heat flux model is used instead of classical Fourier's law. The nonlinear governing equations with suitable boundary conditions are initially cast into dimensionless form by similarity transformations. The optimal homotopy analysis method is proposed for the development of analytical solutions. Special prominence is given to the non-dimensional velocity, temperature, concentration and their graphical behavior for various parameters are analyzed and discussed. The impact of Cattanneo-Christov heat flux model is to reduce the temperature and concentration distribution.

KEYWORDS: Williamson Nanofluid Flow, Cattaneo-Christov Heat Flux Model, Brownian Diffusion, Thermophoresis.

1. INTRODUCTION

The technological industry has embraced several methodologies to improve the efficiency of the heat transfer, namely, utilization of extended surfaces, application of vibration to the heat transfer surfaces, and usage of microchannels. The thermal conductivity of a fluid plays a vital role in the process of improving the efficiency of the heat transfer. Most commonly used heat transfer fluids are water, ethylene glycol, and engine oil which are with relatively low thermal conductivities in comparison with solids. The addition of small quantity of solid particles with high thermal conductivity to the fluid (ethylene glycol + water, water + propylene glycol etc.,) results in an increase in the thermal conductivity of a fluid. The Argonne National Laboratory revisited the concept of enhancement of thermal conductivity of fluid by considering suspensions like nanoscale metallic particle and carbon nanotube suspensions and several things remain intangible about this nanostructured material suspension, which has been coined as "nanofluids" by Choi.[1] However, Masuda et al.[2] have observed the similar kind of results earlier to Choi.[1] The term nanofluid attracted numerous researchers, which is a new kind of heat transfer medium with nanoparticles (1–100 nm) which are uniformly disseminated in the base fluid. Choi and Eastman[3] documented that nanofluids exhibit high thermal conductivities compared to other heat transfer fluids and concluded by establishing a dramatic reduction in the heat exchanger pumping power. Moreover, the temperature is one more impartment aspect in the enhancement of thermal conductivity of nanofluids. Das et al.,[4] Chon and Kihm,[5] Li and Peterson[6] have conducted experimental studies on the determination of the thermal conductivity of nanofluids at room temperature and Murshed et al.[7] has reported an experimental and theoretical study on the thermal conductivity and viscosity of nanofluids and concluded that the thermal conductivity of nanofluids depends strongly on temperature. Literature survey reveals that the behavioral study of nanofluids was mainly done by numerous researchers using two models, that is, the Tiwari-Das model[8] and Buongiorno model.[9] Buongiorno model explains the effects of thermophysical properties of the nanofluid and also focus on the heat transfer enhancement observed in convective situations. Further, Zahmatkesh[10] invoked a hybrid Eulerian-Lagrangian procedure to evaluate the airflow and temperature distribution and analyzed the importance of thermophoresis as well as Brownian diffusion in the process of particle deposition. The model used by Rana and Bhargava[11] for the

*Author to whom correspondence should be addressed.
Email: prasadkv2007@gmail.com
Received: 3 September 2017
Accepted: 17 October 2017

nanofluid incorporates the effects of Brownian motion and thermophoresis. Rashidi et al.[12] examined the model used by Ref. [11] by considering the effects of suction or injection. Many researchers have focused on the behaviour of nanofluid using Buongiorno model with different geometry.[13–17]

Heat transfer mechanism in several significant situations was classically explained by Fourier's law of heat conduction.[18] In spite of being the most successful model for the description of heat transfer mechanism, it has a major limitation such as this law leads to parabolic energy equation for the temperature field which contradicts with the principle of causality. The pioneering work of Cattaneo[19] has managed to provide a successful alternative to the Fourier's law of heat conduction with the vital characteristic of thermal relaxation time to present "thermal inertia," which is popularly known as Maxwell-Cattaneo law. Moreover, Cattaneo-Christov heat flux model is the improved version of Maxwell Cattaneo's model in which Christov[20] replaced the time derivative with the Oldroyd's upper-convected derivative to preserve the material-invariant formulation. Several researchers used Cattaneo-Christov heat flux model on Newtonian/non-Newtonian fluids with different physical constraints.[21–25]

All the above-mentioned researchers restricted their analyses to study the boundary layer flow over a linear or nonlinear stretching sheet in a thermally stratified environment which has several engineering applications. However, not much work has been carried out for a special type of nonlinear stretching (that is, stretching sheets with variable thickness; for details, see Fang et al.[26]). The variable thickness has applications to the vibration of orthotropic plates and is observed in many engineering applications more frequently than a flat surface such as machine design, architecture, nuclear reactor technology, naval structures, and acoustical components. Ishak et al.[27] examined the boundary layer flow over a horizontal thin needle and Ahmed et al.[28] analyzed mixed convection flow over a vertically moving thin needle. Recently, Khader and Megahed,[29] Prasad et al.,[30] Salahuddin et al.,[31] Prasad et al.[32] analyzed the effects of various physical parameters on the flow and heat transfer by considering this special form of stretching sheet. In the present analysis, Optimal Homotopy Analysis Method (OHAM)[33–35] is applied for obtaining the solutions of nonlinear BVPs. We carry out an analytical study to observe the impact of Cattaneo-Christov heat flux model on the flow of Williamson fluid over a slender elastic sheet with variable thickness. The obtained results are analyzed graphically for different sundry variables and analysis reveals that the fluid flow is appreciably influenced by the physical parameters. It is expected that the results presented here will not only complement the existing literature but also provide useful information for industrial applications.

2. MATHEMATICAL FORMULATION OF THE WILLIAMSON-NANOFLUID MODEL

Consider a steady two-dimensional boundary layer flow, heat and mass transfer of a viscous incompressible and electrically conducting non-Newtonian Williamson fluid with nanoparticles, in the presence of a transverse magnetic field $B(x)$, past an impermeable stretching sheet ($v_w = 0$, see Liao[34]) with variable thickness. The origin is located at the slit, through which the sheet is drawn in the fluid (see Fig. 1 for details).

The x-axis is chosen in the direction of the motion and the y-axis is perpendicular to it. The stretching velocity of the surface is $U_w(x) = U_0(x+b)^m$ where U_0 is constant, b is the physical parameter related to stretching sheet, and m is the velocity exponent parameter with constant surface temperature T_w and the constant nanoparticle species diffusion C_w. Cattaneo-Christov heat flux model is used instead of Fourier's law to explore the heat transfer characteristic. We assume that the sheet is not flat but rather is defined as $y = A(x+b)^{(1-m)/2}$. The coefficient A is chosen as a small constant so that the sheet is sufficiently thin to avoid a measurable pressure gradient along the sheet ($\partial p/\partial x = 0$). For different applications, due to the acceleration or deceleration of the sheet, the thickness of the stretched sheet may decrease or increase with distance from the slot, which is dependent on the value of the velocity power index m. The problem is valid for $m \neq 1$, since $m = 1$ refers to the flat sheet case. Viscous and Joule dissipation were neglected. Under such assumptions, and by using the usual boundary layer approximation, the governing equations for basic steady conservation of mass, momentum, thermal energy and nanoparticles equations for the non-Newtonian Williamson fluid with nanoparticles can be written in Cartesian coordinates x and y as (see Refs. [31, 32])

$$\frac{\partial u}{\partial x} + \frac{\partial v}{\partial y} = 0 \tag{1}$$

$$u\frac{\partial u}{\partial x} + v\frac{\partial v}{\partial y} = \nu\left(\frac{\partial^2 u}{\partial y^2} + \sqrt{2}\Gamma\frac{\partial u}{\partial y}\frac{\partial^2 u}{\partial y^2}\right) - \frac{\sigma B_0^2}{\rho}u \tag{2}$$

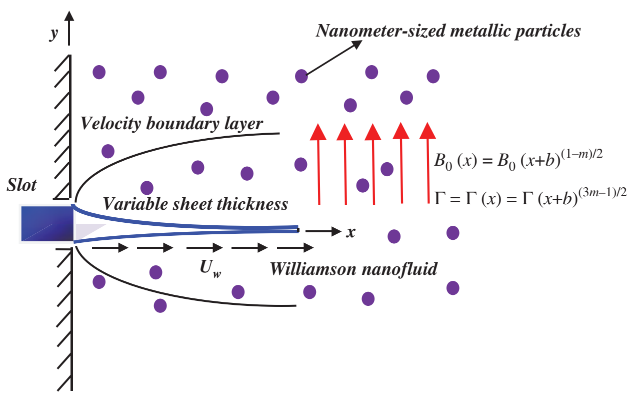

Fig. 1. Schematic diagram of the Casson nanofluid model with a variable stretching sheet.

$$\rho c_p \mathbf{v}\cdot\nabla T = -\nabla\cdot\mathbf{q} \tag{3}$$

$$u\frac{\partial C}{\partial x}+v\frac{\partial C}{\partial y} = D_B\frac{\partial^2 C}{\partial y^2}+\frac{D_T}{T_\infty}\frac{\partial^2 T}{\partial y^2} \tag{4}$$

where u and v are the fluid velocity components measured along the x and y directions, respectively, ρ is the constant fluid density, C_p is the specific heat at constant pressure, ν is kinematic viscosity, D_B is the Brownian diffusion coefficient, D_T is the thermophoresis coefficient, q is normal heat flux vector, T is the temperature, T_∞ is the constant values of the temperature. Also, σ is the electrical conductivity, $\Gamma=\Gamma(x)=\Gamma(x+b)^{(3m-1)/2}$ is the Williamson parameter, and $B_0^2(x)=B_0^2(x+b)^{1-m}$ is the magnetic field, This forms of $B_0^2(x)$ and $\Gamma(x)$ has also been considered by several researchers to study MHD non-Newtonian flow problems and to obtain similarity solution (see Prasad et al.,[30] Salahuddin et al.[31] for details) over a moving or fixed flat plate. $\tau=(\rho c_p)_p/(\rho c_p)_f$ is the ratio between the effective heat capacity of the nanoparticle material and heat capacity of the fluid, ρ_p is the density of the nanoparticle, c_{p_f} is the specific heat of the fluid, and c_{p_p} the specific heat of the nanoparticle (that is, $(\rho c_p)_p$ is the effective heat capacity of the nanoparticle material and $(\rho c_p)_f$ is the heat capacity of the fluid). The boundary conditions for the physical problem under consideration are given by

$$\begin{gathered}u(x,y)=U_w=U_0(x+b)^m,\quad v(x,y)=0,\quad T(x,y)=T_w,\\ C(x,y)=C_w,\quad \text{at } y=A(x+b)^{1-m/2}\\ u(x,y)\to 0,\quad T(x,y)\to T_\infty,\quad C(x,y)\to C_\infty\quad \text{as } y\to\infty\end{gathered} \tag{5}$$

The positive and negative values of m represent two different cases, namely, stretching and shrinking sheets, respectively. The new flux model is known as Cattaneo-Christov heat flux model (see Refs. [19, 20]) which is the generalized form of Fourier's law and is given by

$$\begin{aligned}&q+\beta\left(\frac{\partial q}{\partial t}+\mathbf{V}\cdot\nabla\cdot\mathbf{q}-\mathbf{q}\cdot\nabla\mathbf{V}+(\nabla\cdot\mathbf{V})\mathbf{q}\right)\\&\quad=-k\nabla T+\tau\left[D_B\frac{\partial C}{\partial y}\frac{\partial T}{\partial y}+\frac{D_T}{T_\infty}\left(\frac{\partial T}{\partial y}\right)^2\right]\end{aligned} \tag{6}$$

where $\mathbf{V}$ is the velocity vector, β is the thermal relaxation time, k is the fluid thermal the fluid. It is noted that for $\beta=\tau=0$, Eq. (6) reduces to classical Fourier's law. As it is assumed that fluid is incompressible therefore Eq. (6) takes the form

$$\begin{aligned}&q+\beta\left(\frac{\partial q}{\partial t}+\mathbf{V}\cdot\nabla\mathbf{q}-\mathbf{q}\cdot\nabla\mathbf{V}\right)\\&\quad=-k\nabla T+\tau\left[D_B\frac{\partial C}{\partial y}\frac{\partial T}{\partial y}+\frac{D_T}{T_\infty}\left(\frac{\partial T}{\partial y}\right)^2\right]\end{aligned} \tag{7}$$

eliminating q from Eqs. (3) and (7) we get

$$\begin{aligned}&u\frac{\partial T}{\partial x}+v\frac{\partial T}{\partial y}+\beta\left(u\frac{\partial u}{\partial x}\frac{\partial T}{\partial x}+v\frac{\partial v}{\partial y}\frac{\partial T}{\partial y}+u\frac{\partial v}{\partial x}\frac{\partial T}{\partial y}+v\frac{\partial u}{\partial y}\frac{\partial T}{\partial x}\right.\\&\quad\left.+2uv\frac{\partial^2 T}{\partial x\partial y}+u^2\frac{\partial^2 T}{\partial x^2}+v^2\frac{\partial^2 T}{\partial y^2}\right)\\&\quad=\frac{k}{\rho c_p}\frac{\partial^2 T}{\partial y^2}+\tau\left[D_B\frac{\partial C}{\partial y}\frac{\partial T}{\partial y}+\frac{D_T}{T_\infty}\left(\frac{\partial T}{\partial y}\right)^2\right]\end{aligned} \tag{8}$$

The dimensionless stream function $\psi(x,y)$ is given by $(u,v)=(\partial\psi/\partial y,-\partial\psi/\partial x)$, which satisfies (1) automatically. We transform the system of Eqs. (2), (4) and (8) into a dimensionless form. The suitable similarity transformations for the problem are

$$\begin{gathered}\psi(x,y)=F(\eta)\sqrt{\frac{2}{m+1}U_0\nu}(x+b)^{m+1/2},\\ \Theta(\eta)=\frac{(T-T_\infty)}{(T_w-T_\infty)},\quad \Phi(\eta)=\frac{(C-C_\infty)}{(C_w-C_\infty)},\\ \eta=y\sqrt{\frac{m+1}{2}\frac{U_0}{\nu}}(x+b)^{m-1/2}\end{gathered} \tag{9}$$

With Eq. (9), the velocity components can be written as

$$\begin{aligned}&u=U_wF'(\eta)\quad\text{and}\\ &v=-\sqrt{\nu\frac{m+1}{2}U_0}(x+b)^{m-1/2}\left[F(\eta)+\eta F'(\eta)\left(\frac{m-1}{m+1}\right)\right]\end{aligned} \tag{10}$$

Here prime denotes differentiation with respect to η. In the present work, it is assumed $m>-1$ for the validity of the similarity variable. With the use of (9) and (10), Eqs. (2), (4), (5) and (8) reduces to

$$F'''+FF''-\frac{2m}{(m+1)}(F')^2+\lambda F''F'''-MnF'=0 \tag{11}$$

$$\begin{aligned}&\Theta''+Pr\left(Nb\Theta'\Phi'+Nt(\Theta')^2+F\Theta'\left(1+\frac{\gamma(m-3)}{2}F'\right)\right.\\&\quad\left.-\frac{\gamma(m+1)}{2}F^2\Theta''\right)=0\end{aligned} \tag{12}$$

$$\Phi''+\left(\frac{Nt}{Nb}\right)\Theta''+Le\,F\,\Phi'=0 \tag{13}$$

$$\begin{gathered}F(\alpha)=\frac{\alpha(1-m)}{(1+m)},\quad F'(\alpha)=1,\quad \Theta(\alpha)=1,\quad \Phi(\alpha)=1,\\ F'(\infty)\to 0,\quad \Theta(\infty)\to 0,\quad \Phi(\infty)\to 0\end{gathered} \tag{14}$$

The nondimensional parameters Mn, λ, γ, Pr, Nb, Nt, Le, and α, denoting magnetic parameter, Weissenberg number, thermal relaxation parameter, Prandtl number, Brownian motion parameter, thermophoresis parameter, the Lewis

ARTICLE

ARTICLE

number, and wall thickness parameter, respectively, are given by

$$Mn = \frac{2\sigma B_0^2}{\rho U_0^2(1+m)}, \quad \lambda = \Gamma U_0^3\sqrt{\frac{U_0}{\nu}(m+1)},$$
$$\gamma = \frac{\beta U_0 U_w}{\nu Re}, \quad Pr = \frac{\rho c_p}{k} \quad Nb = \frac{\tau D_B(C_w - C_\infty)}{\nu},$$
$$Nt = \frac{\tau D_T(T_w - T_\infty)}{T_\infty \nu}, \quad Le = \frac{v}{D_B}, \quad \alpha = A\sqrt{\frac{m+1}{2}\frac{U_0}{\nu}} \tag{15}$$

Here $\eta = \alpha$ indicates the plate surface. For the purpose of computation, we define $f(\xi) = F(\eta)$, $\theta(\xi) = \Theta(\eta)$, and $\phi(\xi) = \Phi(\eta)$ where $\xi = \eta - \alpha$. Now the Eqs. (11) to (13) become

$$f''' + ff'' - \frac{2m}{(m+1)}(f')^2 + \lambda f'' f''' - Mnf' = 0 \tag{16}$$

$$\theta'' + Pr\left(Nb\theta'\phi' + Nt(\theta')^2 + f\theta'\left(1+\gamma\frac{(m-3)}{2}f'\right) - \gamma\frac{(m+1)}{2}f^2\theta''\right) = 0 \tag{17}$$

$$\phi'' + \left(\frac{Nt}{Nb}\right)\theta'' + Lef\phi' = 0 \tag{18}$$

and the corresponding boundary conditions (14) for $m \neq -1$ are

$$f(0) = \alpha\frac{1-m}{1+m}, \quad f'(0) = 1, \quad \phi(0) = 1, \quad \theta(0) = 1,$$
$$\lim_{\xi\to\infty} f'(\xi) = \lim_{\xi\to\infty}\theta(\xi) = \lim_{\xi\to\infty}\phi(\xi) = 0 \tag{19}$$

where the prime denotes the differentiation with respect to ξ. With reference to variable transformation, the integration domain will be fixed from 0 to ∞. When we observe the boundary condition $f(0) = \alpha(1-m)/(1+m)$ and for $\alpha = 0$ or $m = 1$, the boundary condition reduces to $f(0) = 0$ which indicates an impermeable surface. The important physical quantities of interest, the skin friction coefficient C_{f_x} the local Nusselt number Nu_x, and the local Sherwood number Sh_x are defined as

$$C_{f_x} = \frac{2\nu(\partial u/\partial y)_{y=A(x+b)^{1-m/2}}}{U_w^2} = \left(\frac{Re_x}{2(m+1)}\right)^{-1/2} f''(0),$$
$$Nu_x = \frac{(x+b)(\partial T/\partial y)_{y=A(x+b)^{1-m/2}}}{(T_w - T_\infty)} = -\left(\frac{(m+1)}{2}Re_x\right)^{1/2}\theta'(0)$$
$$Sh_x = \frac{(x+b)(\partial C/\partial y)_{y=A(x+b)^{1-m/2}}}{(C_w - C_\infty)} = -\left(\frac{(m+1)}{2}Re_x\right)^{1/2}\phi'(0) \tag{20}$$

where $Re_x = U_0(x+b)/\nu$ is the local Reynolds number.

3. EXACT SOLUTIONS FOR SOME SPECIAL CASES

Here we present exact solutions for certain special cases and these solutions serve as a baseline for computing general solutions through numerical schemes. We notice that in the absence of Weissenberg number, thermal relaxation parameter, magnetic field, nanoparticle volume fraction parameter and heat transfer reduces to those of Fang et al.[26] In the limiting case of $\theta_r \to \infty$ and $m = 1$ the boundary layer flow and heat transfer equations degenerate. The solution for the velocity in the presence of magnetic field out to be $f(\xi) = 1 - e^{-\chi\xi}/\chi$ and $f'(\xi) = e^{-\chi\xi}$ where $\chi = \pm\sqrt{1+Mn}$.

3.1. In the Absence of Variable Weissenberg Number, Thermal Relaxation Parameter, Magnetic Field, Nanoparticle Volume Fraction Parameter and Heat Transfer; But in the Presence of Variable Thickness ($\lambda = Mn = \gamma = 0 = Nt = Le = Pr = 0$ $m \neq 1$)

Case (i): When $m = -1/3$, Eq. (16) becomes

$$f''' + ff'' + f'^2 = 0 \tag{21}$$

with the boundary conditions

$$f(0) = 2\alpha, \quad f'(0) = 1, \quad f'(\infty) = 0 \tag{22}$$

On integrating (21) twice yields to

$$f' + \frac{f^2}{2} = (\vartheta + 2\alpha)\eta + (2\alpha^2 + 1) \tag{23}$$

where $\vartheta = f''(0)$. To obtain finite solution it is essential to consider $\vartheta = -2\alpha$.

Thus (23) reduces to

$$f' + \frac{f^2}{2} = (2\alpha^2 + 1) \tag{24}$$

The solution is

$$f(\xi) = \sqrt{2+4\alpha^2}\tanh\left[\frac{\sqrt{2+4\alpha^2}}{2}\xi + \tanh^{-1}\left(\frac{2\alpha}{\sqrt{2+4\alpha^2}}\right)\right] \tag{25}$$

and

$$f'(\xi) = 1 + 2\alpha^2\text{Sech}^2\left[\frac{\sqrt{2+4\alpha^2}}{2}\xi + \tanh^{-1}\left(\frac{2\alpha}{\sqrt{2+4\alpha^2}}\right)\right] \tag{26}$$

Case (ii): When $m = -1/2$, Eq. (16) becomes

$$f''' + ff'' + 2f'^2 = 0 \tag{27}$$

with the boundary conditions

$$f(0) = 3\alpha, \quad f'(0) = 1, \quad f'(\infty) = 0 \tag{28}$$

Equation (27) is equivalent to

$$\frac{1}{f}\frac{d}{d\xi}\left[f^{3/2}\frac{d}{d\xi}\left(f^{-1/2}f' + \frac{2}{3}f^{3/2}\right)\right] = 0 \tag{29}$$

Integrating (29) once reduces to the following form

$$-\frac{1}{2}f'^2+ff''+f^2f'=-\frac{1}{2}+3\alpha\vartheta+9\alpha^2 \tag{30}$$

Applying for free boundary condition we obtain

$$\vartheta=-3\alpha+\frac{1}{6\alpha} \tag{31}$$

An integration of (30) leads to

$$f^{-1/2}f'+\frac{2}{3}f^{3/2}=\frac{2}{3}(3\alpha)^{3/2}+\frac{1}{\sqrt{3\alpha}} \tag{32}$$

The final solution is

$$\xi+D=\frac{1}{2d^2}\ln\left[\frac{f+d\sqrt{f}+d^2}{(d-\sqrt{f})^2}\right]+\frac{\sqrt{3}}{d^2}\tan^{-1}\left(\frac{2\sqrt{f}+d}{d\sqrt{3}}\right) \tag{33}$$

where $d=[(3\alpha)^{3/2}+3/(2\sqrt{3\alpha})]^{1/3}$ and

$$D=\frac{1}{2d^2}\ln\frac{(3\alpha+d\sqrt{3\alpha}+d^2)}{(d-\sqrt{3\alpha})^2}+\frac{\sqrt{3}}{d^2}\tan^{-1}\left(\frac{2\sqrt{3\alpha}+d}{d\sqrt{3}}\right) \tag{34}$$

Since the system of Eqs. (16) to (18) with conditions (19) has no exact analytical solutions, the equations are solved analytically via Optimal Homotopy Analysis Method.

4. SEMI-ANALYTICAL SOLUTION: OPTIMAL HOMOTOPY ANALYSIS METHOD (OHAM)

Optimal homotopy analysis method has been employed to solve the nonlinear, system of Eqs. (16)–(18) with boundary conditions (19). The OHAM scheme breaks down a nonlinear differential equation into infinitely many linear ordinary differential equations whose solutions are found analytically. In the framework of the OHAM, the nonlinear equations are decomposed into their linear and nonlinear parts as follows.

In accordance with the boundary conditions (19), consider the base functions as $\{e^{(-n\xi)}$ for $n\geq 0\}$ then, the dimensionless velocity $f'(\xi)$, temperature $\theta(\xi)$, and concentration $\phi(\xi)$ and can be expressed in the series form as follows

$$f(\xi)=\sum_{n=0}^{\infty}a_n e^{(-n\xi)},\quad \theta(\xi)=\sum_{n=0}^{\infty}b_n e^{(-n\xi)}\quad \text{and}$$

$$\phi(\xi)=\sum_{n=1}^{\infty}c_n e^{(-n\xi)}$$

where a_n, b_n, and c_n are the coefficients. According to the solution expression and boundary conditions (19), we assume the following, we choose the auxiliary linear operators as

$$\mathscr{L}_f=\frac{d^3}{d\xi^3}-\frac{d}{d\xi},\quad \mathscr{L}_\theta=\frac{d^2}{d\xi^2}-f,\quad \text{and}\quad \mathscr{L}_\phi=\frac{d^2}{d\xi^2}-f \tag{35}$$

Initial approximations satisfying the boundary conditions (34) are found to be

$$f_0(\xi)=1+\alpha\left(\frac{1-m}{1+m}\right)-e^{-\xi},\quad \theta_0(\xi)=e^{-\xi},\quad \text{and}$$

$$\phi_0(\xi)=e^{-\xi}$$

Table I. Comparison of results for $-f''(0)$ when $Mn=\lambda=\gamma=Nt=Le=0$ and $Nb\to 0$.

					Present result			
		Fang et al.[26] by shooting method	Khader and Megahed[29] when $\lambda=0$ by Chebyshev spectral method	Prasad et al.[32] when $\varepsilon_1=\varepsilon_2=0, \theta_r\to\infty$ by OHAM	OHAM			
a	m				$-f''(0)$	$\hbar_f$	$\mathscr{E}_{10}^f$	CPU time
0.5	10	1.0603	1.0603	1.0605077120653874	1.0604	1.3249	2.23413×10^{-8}	273.9668
	9	1.0589	1.0588	1.0511040757424492	1.0512	1.3248	1.92781×10^{-8}	269.7467
	7	1.0550	1.0551	1.0552402381500168	1.0551	1.3241	1.18723×10^{-8}	257.20091
	5	1.0486	1.0486	1.048791366557854	1.0487	1.0095	0.97562×10^{-8}	245.996
	3	1.0359	1.0358	1.035877993886442	1.0358	1.0099	3.18554×10^{-9}	245.527
	2	1.0234	1.0234	1.0230051676018523	1.0231	1.0184	2.57682×10^{-9}	267.506
	1	1.0	1.0	1.0	1.0	0	0	98.0504
	0.5	0.9799	0.9798	0.9791336007879321	0.9790	1.0013	6.93683×10^{-8}	264.260
	0	0.9576	0.9577	0.9571649276940054	0.9572	1.5586	0.98174×10^{-7}	230.339
	−1/3	1.0000	1.0000	0.999835549839111	1.0000	1.5691	0.98999×10^{-7}	313.672
	−1/2	1.1667	1.1666	1.1668932098461453	1.1668	1.1992	1.09785×10^{-7}	273.826
0.25	10	1.1433	1.1433	1.1439820336033696	1.1439	1.2573	1.99861×10^{-9}	280.328
	9	1.1404	1.1404	1.1402440847765778	1.1401	1.2586	1.97562×10^{-9}	258.626
	7	1.1323	1.1323	1.1329048196291788	1.1328	1.2635	1.45781×10^{-9}	253.809
	5	1.1186	1.1186	1.1181398433389969	1.1182	1.2724	0.99871×10^{-9}	304.807
	3	1.0905	1.0904	1.090832184327589	1.0907	0.8474	0.96781×10^{-9}	278.567
	1	1.0	1.0	1.0	1.0	0	0	101.036
	0.5	0.9338	0.9337	0.9330216794465643	0.9331	1.40129	1.99959×10^{-8}	252.132
	0	0.7843	0.7843	0.7840615830209784	0.7841	1.13919	0.92790×10^{-7}	238.463
	−1/3	0.5000	0.5000	0.49999454048648743	0.49999	0.7633	0.94699×10^{-6}	241.383
	−1/2	0.0833	0.08322	0.08330568175024846	0.08331	1.2948	4.44657×10^{-6}	265.181

Table II. Values of Skin friction, Nusselt number and Sherwood number for different physical parameters.

Le	Nt	Nb	γ	Pr	m	α	Mn	λ	$-f''(0)$	h_f	E_{10}^f	$-\theta'(0)$	h_θ	E_{10}^θ	$-\phi'(0)$	h_ϕ	E_{10}^ϕ	CPU time
0.2	0.5	0.5	0.2	1	0.5	0.25	1	0	1.37855	−0.873272	8.63×10^{-10}	0.625582	−0.66598	4.08×10^{-6}	0.694768	−1.02251	1.53×10^{-4}	104.641
								0.5	1.76270	−0.462871	2.12×10^{-3}	0.585092	−0.83649	4.23×10^{-5}	0.656452	−1.03779	4.10×10^{-4}	102.29
								0.75	1.86308	−0.236984	9.61×10^{-3}	0.525560	−0.83791	2.60×10^{-4}	0.629833	−0.98909	1.26×10^{-4}	106.89
0.2	0.5	0.5	0.2	1	0.5	0.25	0	0.5	1.19176	−1.979380	7.13×10^{-6}	0.664449	−0.56982	5.38×10^{-5}	0.740098	−0.99473	3.22×10^{-5}	103.62
							1		1.76270	−0.462871	2.12×10^{-3}	0.585092	−0.83649	4.21×10^{-5}	0.656452	−1.07438	4.10×10^{-4}	106.89
							2		1.86308	−0.236932	9.61×10^{-3}	0.525562	−0.83791	2.69×10^{-4}	0.629833	−0.98909	1.26×10^{-3}	102.93
0.2	0.5	0.5	0.2	1	0.6	0.2	0.5	0.5	1.40883	−1.406572	1.28×10^{-6}	0.578156	−1.22059	3.18×10^{-4}	0.674939	−1.15809	2.62×10^{-3}	108.56
						0.4			1.36813	−1.385160	1.02×10^{-6}	0.548096	−1.15795	4.28×10^{-4}	0.641979	−1.22383	3.32×10^{-3}	111.07
						0.6			1.32904	−1.365751	7.79×10^{-7}	0.515830	−1.22647	5.46×10^{-4}	0.610702	−1.58361	4.04×10^{-3}	112.20
0.2	0.5	0.5	0.2	1	−0.3	0.25	0.5	0.5	1.28285	−2.270433	4.69×10^{-4}	1.022861	−1.35472	5.75×10^{-3}	1.123012	−1.28715	2.09×10^{-3}	112.09
					0				1.28606	−2.055212	8.25×10^{-6}	0.837784	−0.43759	1.08×10^{-4}	0.904501	−1.25581	6.17×10^{-5}	109.14
					2				1.36813	−1.385130	1.02×10^{-4}	0.548096	−1.15795	4.28×10^{-4}	0.661497	−1.22383	3.32×10^{-3}	111.59
					5				1.39324	−1.301973	5.64×10^{-7}	0.483733	−1.20376	1.31×10^{-3}	0.577634	−1.22383	4.62×10^{-3}	110.62
					10				1.40469	−1.271321	4.29×10^{-7}	0.244992	−1.18419	4.19×10^{-3}	0.535254	−1.17625	4.95×10^{-3}	111.30
0.22	0.2	0.2	0.5	1	0.3	0.1	0.2	0.1	0.98183	−1.607461	1.77×10^{-6}	0.552611	−0.65837	1.36×10^{-3}	0.296702	−1.14837	9.86×10^{-4}	102.32
				2					0.98183	−1.607461	1.77×10^{-6}	0.652891	−0.35027	1.53×10^{-3}	0.283287	−1.09906	6.31×10^{-3}	111.21
				3					0.98183	−1.607461	1.77×10^{-6}	0.690607	−0.27337	1.99×10^{-3}	0.285916	−1.05317	2.14×10^{-3}	106.23
0.22	0.3	0.3	0.1	1	0.3	0.1	0.5	0.2	1.20094	−1.159821	3.62×10^{-3}	0.417221	−1.03785	5.96×10^{6}	0.07092	−1.03785	2.09×10^{-4}	104.79
			0.5						1.20094	−1.159821	3.62×10^{-3}	0.450824	−0.54876	1.01×10^{-4}	0.127017	−0.73465	2.35×10^{-4}	102.14
			0.9						1.20094	−1.159821	3.62×10^{-3}	0.471138	−0.42114	2.31×10^{-3}	0.152528	−0.69573	1.74×10^{-4}	104.06
0.2	0.5	1.0	0.2	1	−0.3	0.1	0.5	0.1	1.22231	−1.538241	3.73×10^{-6}	0.370061	−0.95174	1.01×10^{-4}	0.534933	−0.90221	4.03×10^{-3}	48.796
		1.5							1.22231	−1.538241	3.73×10^{-6}	0.323654	−0.89234	1.61×10^{-4}	0.584933	−0.83298	2.30×10^{-3}	48.125
		2.0							1.22231	−1.538241	3.73×10^{-6}	0.198278	−1.01025	2.23×10^{-3}	0.676833	−0.93904	2.41×10^{-3}	50.109
0.2	0.5	1	0.2	1	−0.3	0.1	0.5	0.1	1.22231	−1.538241	3.73×10^{-6}	0.334784	−1.06167	1.01×10^{-3}	0.638336	−0.97481	1.59×10^{-3}	48.796
	1.0								1.22231	−1.538241	3.73×10^{-6}	0.291184	−0.95155	1.63×10^{-3}	0.662644	−0.87605	1.80×10^{-3}	48.125
	1.5								1.22231	−1.538241	3.73×10^{-6}	0.200652	−0.87058	3.83×10^{-3}	1.24781	−0.85781	3.41×10^{-3}	52.281
1	0.5	0.5	0.2	1	−0.3	0.1	0.5		1.22231	−1.538241	3.73×10^{-6}	0.334784	−1.06167	1.01×10^{-3}	0.638362	−0.97481	1.59×10^{-4}	101.02
2									1.22231	−1.538241	3.73×10^{-6}	0.295675	−1.06154	1.51×10^{-4}	0.884259	−0.26653	2.87×10^{-5}	104.62
3									1.22231	−1.538241	3.73×10^{-6}	0.257765	−1.05890	2.60×10^{-3}	1.226140	−1.88671	6.07×10^{-3}	112.06

Let us consider the so-called zeroth order deformation equations

$$(1-q)L_f[\hat{f}(\xi;q)-f_0(\xi)] = qH_f(\xi)\hbar_f N_f[\hat{f}(\xi;q)] \tag{36}$$

$$(1-q)L_\theta[\hat{\theta}(\xi;q)-\theta_0(\xi)] = qH_\theta(\xi)\hbar_\theta N_\theta[\hat{\theta}(\xi;q),\hat{f}(\xi;q),\hat{\phi}(\xi;q)] \tag{37}$$

$$(1-q)L_\phi[\hat{\phi}(\xi;q)-\phi_0(\xi)] = qH_\phi(\xi)\hbar_\phi N_\phi[\hat{\phi}(\xi;q),\hat{\theta}(\xi;q),\hat{f}(\xi;q)] \tag{38}$$

Here $q \in [0, 1]$ is an embedding parameter, while $\hbar_f \neq 0$, $\hbar_\theta \neq 0$ and $\hbar_\phi \neq 0$ are the convergence control parameters, and the nonlinear differential operators are defined from Eqs. (30)–(32) as

$$\mathcal{N}_f[\hat{f}] = \frac{\partial^3 \hat{f}}{\partial \xi^3} + \hat{f}\frac{\partial^2 \hat{f}}{\partial \xi^2} - \left(\frac{2m}{m+1}\right)\left(\frac{\partial \hat{f}}{\partial \xi}\right)^2 + \lambda\frac{\partial^2 \hat{f}}{\partial \xi^2}\frac{\partial^3 \hat{f}}{\partial \xi^3} - Mn\frac{\partial \hat{f}}{\partial \xi} \tag{39}$$

$$\mathcal{N}_\theta[\hat{f},\hat{\theta},\hat{\phi}] = \frac{\partial^2 \hat{\theta}}{\partial \xi^2} + Pr\left(Nb\frac{\partial \hat{\theta}}{\partial \xi}\frac{\partial \hat{\phi}}{\partial \xi} + Nt\left(\frac{\partial \hat{\theta}}{\partial \xi}\right)^2 + \hat{f}\frac{\partial \hat{\theta}}{\partial \xi}\right) + Pr\gamma\left(\left(\frac{m-3}{2}\right)\hat{f}\frac{\partial \hat{f}}{\partial \xi}\frac{\partial \hat{\theta}}{\partial \xi} - \left(\frac{m+1}{2}\right)\hat{f}^2\frac{\partial \hat{\theta}''}{\partial \xi}\right) \tag{40}$$

$$\mathcal{N}_\phi[\hat{f},\hat{\theta},\hat{\phi}] = \frac{\partial^2 \hat{\phi}}{\partial \xi^2} + \left(\frac{Nt}{Nb}\right)\frac{\partial^2 \hat{\theta}}{\partial \xi^2} + Le\hat{f}\frac{\partial \hat{\phi}}{\partial \xi} \tag{41}$$

We choose the auxiliary functions as $H_f(\xi) = H_\theta(\xi) = H_\phi(\xi) = e^{-\xi}$. It can be seen from Eqs. (36) to (38) that when $q = 0$, we have $\hat{f}(\xi;0) = f_0(\xi)$, etc., while when $q = 1$, we have $\hat{f}(\xi;1) = f(\xi)$, etc., so we recover the exact solutions when $q = 1$. Expanding in q, we write

$$\hat{f}(\xi;q) = f_0(\xi) + \sum_{n=1}^{\infty} f_n(\xi)q^n,$$

$$\hat{\theta}(\xi;q) = \theta_0(\xi) + \sum_{n=1}^{\infty} \theta_n(\xi)q^n, \quad \text{and}$$

$$\hat{\phi}(\xi;q) = \phi_0(\xi) + \sum_{n=1}^{\infty} \phi_n(\xi)q^n$$

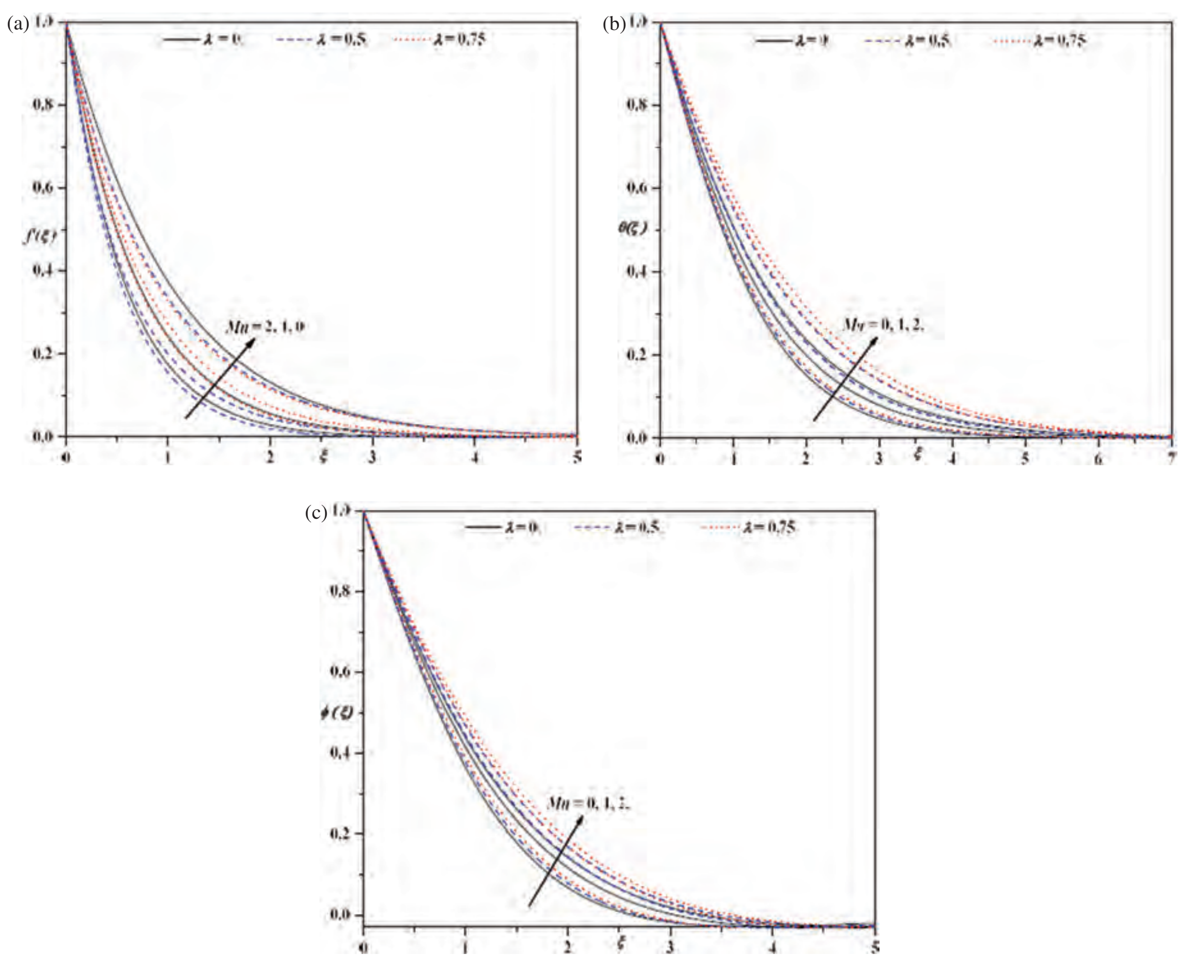

Fig. 2. (a) Horizontal velocity profiles for different values of λ and Mn with $Pr = 1$, $Nb = 0.5$, $Nt = 0.5$, $Le = 0.2$, $m = 0.5$, $\alpha = 0.2$, $\gamma = 0.2$. (b) Temperature profiles for different values of λ and Mn with $Pr = 1$, $Nb = 0.5$, $Nt = 0.5$, $Le = 0.2$, $m = 0.5$, $\alpha = 0.2$, $\gamma = 0.2$. (c) Concentration profiles for different values of λ and Mn with $Pr = 1$, $Nb = 0.5$, $Nt = 0.5$, $Le = 0.2$, $m = 0.5$, $\alpha = 0.2$, $\gamma = 0.2$.

As q varies from 0 to 1, the homotopy solutions vary from the initial approximations to the solutions of interest. It should be noted that the homotopy solutions contain the unknown convergence control parameters, $\hbar_\theta \neq 0$, and $\hbar_\phi \neq 0$, which can be used to adjust and control the convergence region and the rate of convergence of the series solution. To obtain the approximate solutions, we recursively solve the

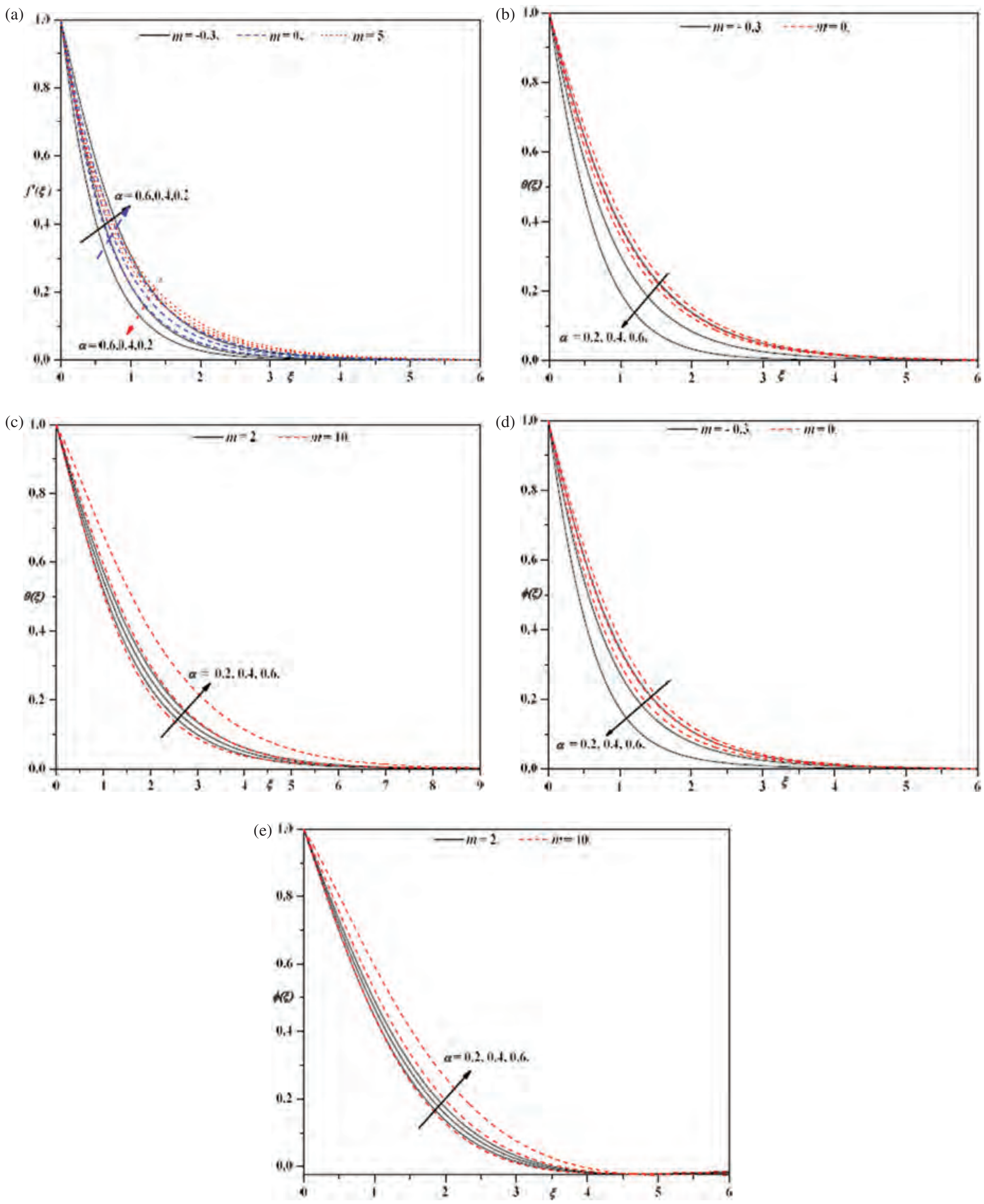

Fig. 3. (a) Horizontal velocity profiles for different values of α and m with $Pr = 1$, $Nb = 0.5$, $Nt = 0.5$, $Le = 0.2$, $Mn = 0.5$, $\lambda = 0.2$, $\gamma = 0.2$. (b) Temperature profiles for different values of α and m with $Pr = 1$, $Nb = 0.5$, $Nt = 0.5$, $Le = 0.2$, $Mn = 0.5$, $\lambda = 0.2$, $\gamma = 0.2$. (c) Temperature profiles for different values of α and m with $Pr = 1$, $Nb = 0.5$, $Nt = 0.5$, $Le = 0.2$, $m = 0.5$, $\alpha = 0.2$, $\gamma = 0.2$. (d) Concentration profiles for different values of α and m with $Pr = 1$, $Nb = 0.5$, $Nt = 0.5$, $Le = 0.2$, $Mn = 0.5$, $\lambda = 0.2$, $\gamma = 0.2$. (e) Concentration profiles for different values of α and m with $Pr = 1$, $Nb = 0.5$, $Nt = 0.5$, $Le = 0.2$, $m = 0.5$, $\alpha = 0.2$, $\gamma = 0.2$.

so-called nth-order deformation equations

$$\mathscr{L}_f[f_n(\xi)-\chi_n f_{n-1}(\xi)] = \hbar_f \mathscr{R}_n^f,$$
$$\mathscr{L}_\theta[\theta_n(\xi)-\chi_n \theta_{n-1}(\xi)] = \hbar_\theta \mathscr{R}_n^\theta,$$
$$\mathscr{L}_\phi[\phi_n(\xi)-\chi_n \phi_{n-1}(\xi)] = \hbar_\phi \mathscr{R}_n^\phi,$$
$$\mathscr{R}_n^f = \frac{1}{(n-1)!}\frac{\partial^{n-1}\mathscr{N}_f[\hat{f}(\xi;q)]}{\partial q^{n-1}}\bigg|_{q=0},$$
$$\mathscr{R}_n^\theta = \frac{1}{(n-1)!}\frac{\partial^{n-1}\mathscr{N}_\theta[\hat{f}(\xi;q),\hat{\theta}(\xi;q),\hat{\phi}(\xi;q)]}{\partial q^{n-1}}\bigg|_{q=0},$$
$$\mathscr{R}_n^\phi = \frac{1}{(n-1)!}\frac{\partial^{n-1}\mathscr{N}_\phi[\hat{f}(\xi;q),\hat{\phi}(\xi;q),\hat{\theta}(\xi;q)]}{\partial q^{n-1}}\bigg|_{q=0},$$
$$\chi_n = \begin{cases} 0, & n\le 1,\\ 1, & n>1\end{cases}$$

In practice, we can only calculate finitely many terms in the homotopy series solution. We, therefore, define the kth order approximate solution can by the partial sums

$$f_{[k]}(\xi) = f_0(\xi)+\sum_{n=1}^{k} f_n(\xi),\quad \theta_{[k]}(\xi) = \theta_0(\xi)+\sum_{n=1}^{k}\theta_n(\xi)$$
$$\text{and}\quad \phi_{[k]}(\xi) = \phi_0(\xi)+\sum_{n=1}^{k}\phi_n(\xi) \tag{42}$$

With these approximations, we may evaluate the residual error and minimize it over the parameters $\hbar_f$, $\hbar_\theta$ and $\hbar_\phi$ in order to obtain the optimal value of $\hbar_f$, $\hbar_\theta$ and $\hbar_\phi$ giving the least possible residual error. To do so, one may use the integral of squared residual errors, however, this is very computationally demanding. To get around this, we use the averaged squared residual errors, defined by

$$\overline{\mathscr{E}_n^f}(\hbar_f) = \frac{1}{M+1}\sum_{k=0}^{M}(\mathscr{N}_f[f_{[M]}(\xi_k)])^2 \tag{43}$$

$$\overline{\mathscr{E}_n^\theta}(\hbar_\theta) = \frac{1}{M+1}\sum_{k=0}^{M}(\mathscr{N}_\theta[f_{[M]}(\xi_k),\theta_{[M]}(\xi_k),\phi_{[M]}(\xi_k)])^2 \tag{44}$$

$$\overline{\mathscr{E}_n^\phi}(\hbar_\phi) = \frac{1}{M+1}\sum_{k=0}^{M}(\mathscr{N}_\phi[f_{[M]}(\xi_k),\theta_{[M]}(\xi_k),\phi_{[M]}(\xi_k)])^2 \tag{45}$$

where $\xi_k = k/M$, $k = 0,1,2,\ldots,M$. Now we minimize the error function $\overline{\mathscr{E}_n^f}(\hbar_f)$, $\overline{\mathscr{E}_n^\theta}(\hbar_\theta)$ and $\overline{\mathscr{E}_n^\phi}(\hbar_\phi)$ in $\hbar_f$, $\hbar_\theta$ and $\hbar_\phi$ and obtain the optimal value of $\hbar_f$, $\hbar_\theta$ and $\hbar_\phi$. For nth order approximation, the optimal value of $\hbar_f$, $\hbar_\theta$ and $\hbar_\phi$ for f,θ and ϕ is given by $d\overline{\mathscr{E}_n^f}(\hbar_f)/dh = 0$, $d\overline{\mathscr{E}_n^\theta}(\hbar_\theta)/dh = 0$ and $d\overline{\mathscr{E}_n^\phi}(\hbar_\phi)/dh = 0$ respectively.

Evidently, corresponds to a convergent series solution. Substituting these optimal values of $\hbar_f$, $\hbar_\theta$ and $\hbar_\phi$ in Eq. (42) we get the approximate solutions of Eqs. (16) to (18) which satisfies the conditions (19). For the assurance of the validity of this method, $-f''(0)$ obtained via OHAM has been compared with Fang et al.,[26] Khader and Megahed[29] and Prasad et al.[32] for various special cases and the results are found to be in excellent agreement (see Table I). In Table II, the optimal values of h_f, h_θ and h_ϕ for the functions $-f''(0)$, $-\theta'(0)$ and $-\phi'(0)$ corresponding to various values of the parameters are given and the corresponding averaged residuals are represented as E_{10}^f, E_{10}^θ and E_{10}^ϕ.

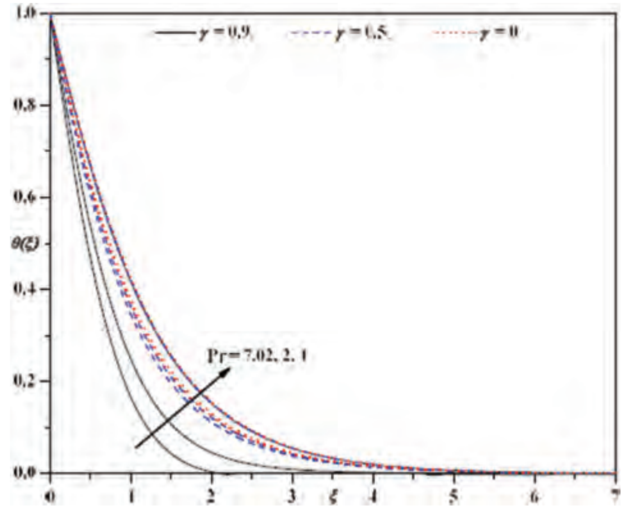

Fig. 4. Temperature profiles for different values of γ and Pr with $Mn = 0.5$, $m = -0.3$, $Nb = 0.5$, $Nt = 0.5$, $Le = 0.2$, $\alpha = 0.2$, $\lambda = 0.2$.

5. RESULTS AND DISCUSSION

The system of Eqs. (16) to (18) subject to the boundary conditions (19) is solved analytically via efficient OHAM. The computations are being carried out using Mathematica 8and obtained the flow, heat,and mass transfer characteristics of Williamson fluid with nanoparticles by considering

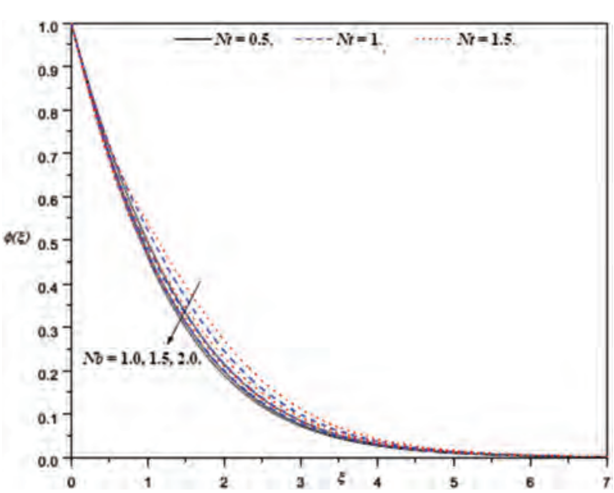

Fig. 5. Concentration profiles for different values of Nt and Nb with $Pr = 1$, $m = 0.5$, $Le = 1$, $Mn = 0.5$, $\lambda = 0.1$, $\gamma = 0.2$, $\alpha = 0.25$.

ARTICLE

Cattaneo-Christov heat flux model for several values of the governing parameters such as Weissenberg number λ, thermal relaxation parameter γ, velocity power index parameter m, the variable thickness parameter α, the Prandtl number Pr, Magnetic parameter Mn, the thermophoresis parameter Nt and the Brownian motion parameter Nb, and the Lewis number Le. Figures 2–5 describes the influence of various physical parameters on the horizontal velocity profile $f'(\xi)$, the temperature profile $\theta(\xi)$, and the concentration profile $\phi(\xi)$ graphically. These profiles $f'(\xi)$, $\theta(\xi)$, and $\phi(\xi)$ are unity at the wall, decreases monotonically and tend to zero asymptotically as the distance increases from the boundary. The computed numerical values for the skin friction $f''(0)$, the Nusselt number $\theta'(0)$ and the wall Sherwood number $\phi'(0)$ are presented in Table II.

Figures 2(a) to (c) illustrates the effect of Mn and λ on $f'(\xi)$, $\theta(\xi)$, and $\phi(\xi)$. It is noticed that $f'(\xi)$ decreases for increasing values of Mn. This is due to the fact that the retarding/drag forces called the Lorentz forces generated by the applied magnetic field act as resistive drag forces opposite to the flow direction which results in a decrease in velocity. Consequently, the thickness of the momentum boundary layer reduces with an increase in Mn. A similar trend is observed in the case of λ, this is because the relaxation time of the fluid enhances for higher values of λ causing a decrease in velocity of the fluid. The exact opposite trend is observed in the case of $\theta(\xi)$ and $\phi(\xi)$ (See Fig. 2(c)). Figures 3(a) through (e) depicts the impact of α and m on $f'(\xi)$, $\theta(\xi)$, and $\phi(\xi)$. An interesting pattern may be observed in the case of positive and negatives of α and m. The behavior of the boundary condition $f(0) = \alpha((1-m)/(1+m))$ depends on the values of α and m. For a given range $\alpha > 0$ and $m < 1$ or $\alpha < 0$ and $m > 1$, it is observed that $f(0) > 0$ which is the case of injection and for the other opposite set of range α and m, we have $f(0) < 0$ which is a suction case.

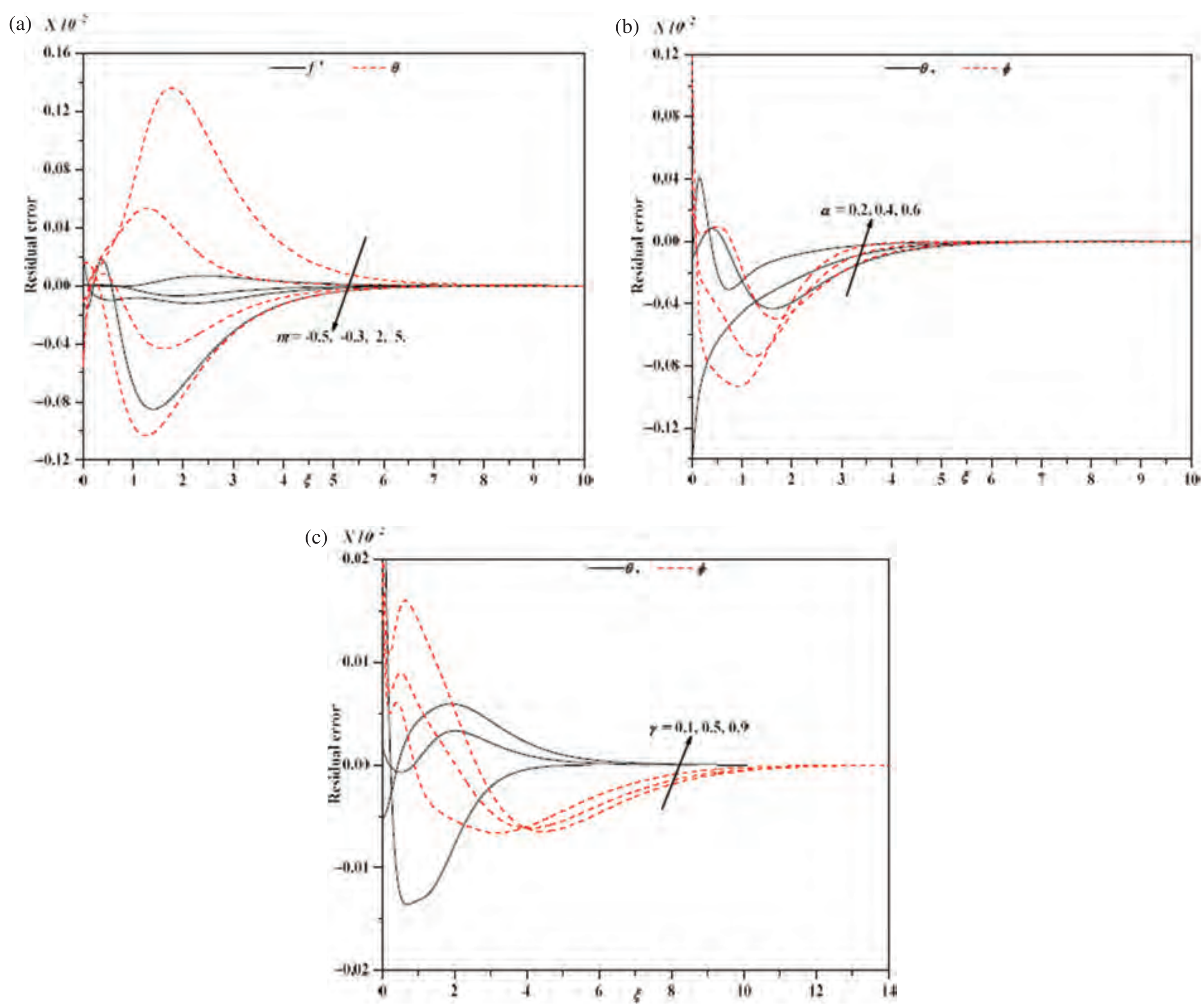

Fig. 6. (a) Residual error profile for horizontal velocity and temperature for different values of m with $\alpha = 0.2$, $\lambda = 0.2$, $\gamma = 0.2$, $Nt = 0.5$, $Nb = 0.5$, $Le = 0.2$, $Pr = 1$, $Mn = 0.5$. (b) Residual error profile for temperature and concentration for different values of α with $m = 0.5$, $\lambda = 0.2$, $\gamma = 0.2$, $Nt = 0.5$, $Nb = 0.5$, $Le = 0.2$, $Pr = 1$, $Mn = 0.5$. (c) Residual error profile for temperature and concentration for different values of γ with $m = 0.5$, $\alpha = 0.2$, $\lambda = 0$, $Nt = 0.5$, $Nb = 0.5$, $Le = 0.2$, $Pr = 1$, $Mn = 0.5$.

From the Figure 3(a), it is clear that as $\alpha > 0$ and $m = -0.3$ the velocity profiles are increasing for the decreasing values of α and the reverse trend is observed in the case of $\alpha > 0$ and $m = 5$. The opposite pattern is noticed in the case of temperature and concentration profiles with $\alpha > 0$ and $m = -0.3, 2, 10$ (See Figs. 3(b to e)). Injection enhances both temperature and nanoparticle concentration. Thermal and concentration boundary layer thickness for the injection case is significantly greater than for the suction case. Effectively suction achieves a strong suppression of nano-particle species diffusion and also regulates the diffusion of thermal energy (heat) in the boundary layer. This response to suction has significant effects on the constitution of engineered nanofluids and shows that suction is an excellent mechanism for achieving flow control, cooling, and nanoparticle distribution in nanofluid fabrication. Figure 4 exhibits the impact of increasing values of γ and Pr on $\theta(\xi)$. Temperature decreases considerably when γ increases and hence thermal boundary layer decreases. In fact, for larger values of γ, the particles of measurable material require more opportunity to hand over heat to its adjacent particles. Thus, larger γ is responsible for the decrease of temperature. Physically, γ appears because of the heat flux relaxation time. The greater values of γ, the liquid particles require more time to exchange heat to their neighboring particles which make a reduction in the temperature. The Cattaneo-Christov heat flux model can be reduced to fundamental Fourier's law of heat conduction in the absence of γ. This observation gives us an insight that, the temperature in Cattaneo-Christov heat flux model is lower than the Fourier's model (In the absence of γ heat transfer instantly throughout the material). Furthermore, the behavior of Pr on the thermal boundary layer with the consideration of γ found to be decreasing the temperature and thereby reduce the thickness of the thermal boundary layer. Figure 5 elucidates the influence of Nt and Nb on $\phi(\xi)$. It is noted that the nanoparticle volume fraction increases with the increase in Nt (increase in thermophoresis force) and thus augments the concentration boundary layer thickness. In this case, the nanoparticles move away from the hot stretching sheet towards the cold ambient fluid under the influence of temperature gradient. But in the case of Nb (smaller nano-particles), the result is the reverse. Moreover, larger values of Nb will stifle the diffusion of nanoparticles away from the surface, which results in a decrease in nanoparticle concentration values in the boundary layer. Finally, in order to obtain the optimal values of $\hbar_f$, $\hbar_\theta$ and $\hbar_\phi$ which is displayed in Eqs. (43)–(45), the residual error for $f'(\xi)$, $\theta(\xi)$ and $\phi(\xi)$ is depicted in Figures 6(a) to (c). It clearly shows the accuracy and convergence of OHAM. These figures show that a tenth-order approximation yields the best accuracy for the present model.

The impact of the physical parameters on $f''(0)$, $\theta'(0)$, and $\phi'(0)$ is presented in Table II. We noticed a decrease in the skin friction as Mn increases, while the opposite pattern is observed for the Nusselt number and the Sherwood number. Increasing Weissenberg number λ enhances the Nusselt number and the Sherwood number whereas thermal relaxation parameter γ decreases the Nusselt number. Sherwood number decreases for increasing values of Le.

6. CONCLUSIONS

In this article, MHD flow, heat and mass transfer of Williamson-Nano fluid over a stretching sheet with variable thickness has been examined. Cattaneo-Christov heat flux model was used to investigate the heat transfer mechanism. Some of the interesting conclusions are as follows:

- The strong variation in the velocity, temperature, and concentration fields is noticed as wall thickness parameter increases accordingly with $m > 1$ or $1 > m > -1$.
- In comparison with Fourier's law, the behavior of temperature profile is of decreasing nature for Cattaneo-Christov heat flux model.
- An increase in the nanoparticle concentration profiles is due to the increase in the thermophoresis parameter and the Brownian motion parameter.
- Due to the effect of Lorentz force, fluid finds a drag force and hence velocity profile decreases while temperature and concentration profiles increases for increasing values of magnetic parameter.
- Weissenberg number is decreasing the function of velocity whereas Lewis number reduces the Sherwood number.

Acknowledgments: The authors appreciate the constructive comments of the reviewers which led to definite improvement in the paper.

References and Notes

1. S. Choi, Enhancing thermal conductivity of fluids with nanoparticle, Developments and Applications of Non-Newtonian Flows, edited by D. A. Siginer and H. P. Wang, ASME, MD 231 and FED **(1995)**, Vol. 66, pp. 99–105.
2. H. Masuda, A. Ebata, K. Teramae, N. Hishi Unma, *Netsu Bussei* 227 **(1993)**.
3. S. U. S. Choi and J. A. Eastman, Enhancing thermal conductivities of fluids with nanoparticles, *ASME, Int. Mech. Engg. Congress and Exposition*, San Francisco, USA **(1995)**.
4. S. K. Das, N. Putra, P. Thiesen, and W. Roetzel, *J. Heat Transfer* 125, 567 **(2003)**.
5. C. H. Chon and K. D. Kihm, *J. Heat Transfer* 127, 810 **(2005)**.
6. C. H. Li and G. P. Peterson, *J. Appl. Phys.* 99, 084314 **(2006)**.
7. S. M. S. Murshed, K. C. Leong, and C. Yang, *Int. J. Therm. Sci.* 47, 560 **(2008)**.
8. R. K. Tiwari and M. K. Das, *Int. J. Heat Mass Transfer* 50, 2002 **(2007)**.
9. J. Buongiorno, *J. Heat Transfer* 128, 240 **(2006)**.
10. I. Zahmatkesh, *International Communications in Heat and Mass Transfer* 35, 369 **(2008)**.
11. P. Rana and R. Bhargava, *Commun. Nonlinear Sci. Numer. Simul.* 17, 212 **(2012)**.

ARTICLE

12. M. M. Rashidi, N. Freidoonimehr, A. Hosseini, O. Anwar Bég, and T. K. Hung, *Meccanica* 49, 469 (**2014**).
13. W. A. Khan and A. Aziz, *International Journal of Thermal Sciences* 50, 1207 (**2011**).
14. O. D. Makinde and A. Aziz, *International Journal of Thermal Sciences* 50, 1326 (**2011**).
15. N. Bachok, A. Ishak, and I. Pop, *Int. J. Heat Mass Transfer* 55, 2102 (**2012**).
16. K. V. Prasad, K. Vajravelu, Vaidya Hanumesh, and B. T. Raju, *J. Nanofluids* 4, 536 (**2015**).
17. K. V. Prasad, K. Vajravelu, I. S. Shivakumara, Vaidya Hanumesh, Basha, Z. Neelufer, *J. Nanofluids* 5, 743 (**2016**).
18. B. J. Fourier, Theorie Analytique De La Chaleur, Paris (**1822**).
19. C. Cattaneo, *AttiSemin. Mat. Fis. Univ. Modena Reggio Emilia* 3, 83 (**1948**).
20. C. I. Christov, *Mech. Res. Commun.* 36, 481 (**2009**).
21. L. Liu, L. Zheng, F. Liu, and X. Zhang, *Commun. Nonlinear Sci. Numer. Simul.* 38, 45 (**2016**).
22. T. Hayat, M. Zubair, M. Ayub, M. Waqas, and A. Alsaedi, *Eur. Phy. J. Plus* 131, 355 (**2016**).
23. A. Tanveer, S. Hina, T. Hayat, M. Mustafa, and B. Ahmad, *Eng. Appl. Comput. Fluid Mech.* 10, 375 (**2016**).
24. S. Nadeem and N. Muhammad, *Mol. Liq.* (**2016**), http://dx.doi.org/10.1016/j.molliq.2016.10.006.
25. Tasawar Hayat, Taseer Muhammad, Meraj Mustafa, and Ahmed Alsaedi, *Chinese Journal of Physics* (**2017**), DOI: 10.1016/j.cjph.2017.03.014.
26. T. Fang, Zhang, and Y. Zhong, *Appl. Math. Comput.* 218, 7241 (**2012**).
27. Ishak, R. Nazar, and I. Pop, *Chinese Phys. Lett.* 24, 2895 (**2007**).
28. S. Ahmad, N. M. Arifin, R. Nazar, and I. Pop, *Heat Mass Transf.* 44, 473 (**2008**).
29. M. M. Khader and A. M. Megahed, *J. Appl. Mech. Tech. Phy.* 6, 241 (**2015**).
30. K. V. Prasad, K. Vajravelu, and Hanumesh Vaidya, *International Journal for Computational Methods in Engineering Science and Mechanics* (**2016**), DOI: 10.1080/15502287.2016.1209795.
31. T. Salahuddin, M. Y. Malik, Arif Hussain, S. Bilal, and M. Awais, *J. Magn. Magn. Mater.* 401, 991 (**2016**).
32. K. V. Prasad, K. Vajravelu, Hanumesh Vaidya, and Robert A. Van Gorder, *Results in Physics* 7, 1462 (**2017**).
33. S. Liao, Beyond Perturbation: Introduction to Homotopy Analysis Method, Chapman and Hall/CRC Press, London (**2003**).
34. T. Fan and X. You, *Numer. Algor.* 62, 337 (**2013**).
35. S. Liao, *Int. J. Non-Line. Mech.* 42, 819 (**2007**).

ARTICLE

Penerbit Akademia Baru

Journal of Advanced Research in Fluid Mechanics and Thermal Sciences

Journal homepage: www.akademiabaru.com/arfmts.html
ISSN: 2289-7879

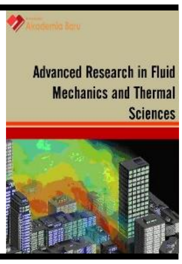

Influence of Variable Transport Properties on Casson Nanofluid Flow over a Slender Riga Plate: Keller Box Scheme

Open Access

Kerehalli Vinayaka Prasad[1], Hanumesh Vaidya[1,*], Gudekote Manjunatha[2], Kuppalapalle Vajravelu[3], Choudhari Rajashekhar[2], V. Ramanjini[1]

[1] Department of Mathematics, VSK University, Vinayaka Nagar, Ballari-583 105, Karnataka, India
[2] Department of Mathematics, Manipal Institute of Technology, Manipal Academy of Higher Education, Manipal, Karnataka, India
[3] Department of Mathematics, University of Central Florida, Orlando, FL 32816, USA

ARTICLE INFO

Article history:
Received 12 July 2019
Received in revised form 25 September 2019
Accepted 26 September 2019
Available online 15 December 2019

Keywords:
Riga plate; Melting heat transfer; variable fluid properties; Keller box method

ABSTRACT

In this article, an analysis has been carried out to study the effects of variable viscosity and variable thermal conductivity on the heat transfer characteristics of a Casson nanofluid over a slender Riga plate with zero mass flux and melting heat transfer boundary conditions. The nonlinear governing equations with the suitable boundary conditions are initially cast into dimensionless form by similarity transformations. The resulting coupled highly nonlinear equations are solved numerically by an efficient second-order finite difference scheme known as Keller Box Method. The effect of various physical parameters on velocity, temperature, and concentration profiles are illustrated through graphs and the numerical values are presented in tables. One of the critical findings of our study is that the effect of variable viscosity on velocity shows reducing nature, but there is an increasing nature in temperature and concentration.

Copyright © 2019 PENERBIT AKADEMIA BARU - All rights reserved

1. Introduction

In recent years, controlling the flow of electrically conducting fluids is one of the primary tasks to the scientists and engineers. The controlled flow of these fluids has enormous applications in industrial and technological processes involving heat and mass transfer phenomenon. However, the polymer industry has adopted a few conventional methods to control the fluid flow such as of suction/blowing and wall motion methods with the assistance of electromagnetic body forces. The flow of the fluids having high electrical conductivity such as liquid metals, plasma, and electrolytes, etc. can be significantly controlled by applying an external magnetic field. This concept can be used for controlling the classical electro magnetohydrodynamic (EMHD) fluid flows. In view of the industrial applications, Gailitis, and Lielausis [1] of the physics institute in Riga, the capital city of the Latvia country designed one of the devices known as Riga plate to generate simultaneous electric

** Corresponding author.*
E-mail address: hanumeshvaidya@gmail.com (Hanumesh Vaidya)

and magnetic fields which can produce Lorentz force parallel to the wall in weakly conducting fluids. This plate consists of a spanwise aligned array of alternating electrodes and permanent magnets mounted on a plane surface. This array generates a surface-parallel Lorentz force with a neglected pressure gradient, which decreases exponentially in the direction normal to the (horizontal) plate. However, in vector product form the volume density of a Lorentz force is written as $\mathbf{F}_1 = \mathbf{J}\times\mathbf{B}$ and in terms of Ohm's law it can be expressed as $\mathbf{J}=\boldsymbol{\sigma}\left(\mathbf{E}+\mathbf{V}\times\mathbf{B}\right)$ where $\boldsymbol{\sigma}$ is an electrical conductivity of the fluid, V is the fluid velocity, and E is the electric field. In the absence of any extrinsic magnetic field, a complete contactless flow can be attained when $\boldsymbol{\sigma}\approx 10^{-6}$ S/m. Where as in the presence of extrinsic magnetic field, an induced high current density $\boldsymbol{\sigma}\left(\mathbf{V}\times\mathbf{B}\right)$ can be obtained and we have $\mathbf{F}_1 = \mathbf{J}\times\mathbf{B} = \boldsymbol{\sigma}\left(\mathbf{V}\times\mathbf{B}\right)\times\mathbf{B} = \boldsymbol{\sigma}\left[\left(\mathbf{V}\times\mathbf{B}\right)\mathbf{B}-\mathbf{B}^2\mathbf{V}\right]$. On the contrary, when $\boldsymbol{\sigma}\approx 10^{6}$ S/m, a low current density $\boldsymbol{\sigma}\left(\mathbf{V}\times\mathbf{B}\right)$ can be seen. To tackle with such cases, an extrinsic magnetic field is used to obtain the EMHD flow. The expression $\mathbf{F}_1 = \mathbf{J}\times\mathbf{B}\approx\boldsymbol{\sigma}\left(\mathbf{E}\times\mathbf{B}\right)$ reveals that the electrical conductivity of a fluid is very small, and it does not rely upon the flow field. According to Grinberg [2], the density force can be written as $\mathbf{F}_1 = \frac{\pi_1 M_0 j_0}{8} e^{-\frac{\pi_1}{a}y}$. Tsinober and Shtern [3] observed the substantial improvement in the strength of the Blasius flow towards a Riga plate, which is due to the more significant influence of wall parallel Lorentz forces. Further, the boundary layer flow of low electrical conductivity of fluids over a Riga plate was scrutinized by Pantokratoras and Magyari [4]. Pantokratoras [5] extended the work of Pantokratoras and Eugen [4] to Blasius and Sakiadis flow.

In addition to controlling the flow of electrically conducting fluids, the technological industry demands the control of heat transfer in a process. This can be achieved with the help of nanofluids technology. Nanofluid is the blend of the nanometer-scale (1nm to100 nm) solid particles and low thermal conductivity base liquids such as water, ethylene glycol (EG), oils, etc. Two different phases are used to simulate nanofluid. In both the methods researchers assumed as the common pure fluid and more precisely in the second method, the mixer or blend is with the variable concentration of nanoparticles. Choi [6] proposed the term nanofluid and verified that the thermal conductivity of fluids could be improved by the inclusion of nanometer-sized metals (Cu, Ag, Au), oxides $(\mathrm{Al_2O_3},\ \mathrm{CuO})$, carbide ceramics (Sic, Tic/carbon nanotubes/fullerene) into the base fluids. Buongiorno [7] established that Brownian diffusion and thermophoresis are important slip mechanisms in nanofluids. Makinde and Aziz [8] examined the impact of Brownian motion and thermophoresis on transport equations numerically. Ahmad *et al.,* [9] and Ayub *et al.,* [10] examined the boundary layer flow of nanofluid due to Riga plate. Further, Hayat *et al.,* [11, 12] analysed squeezing flow of a nanofluid between two parallel Riga plates by considering different external effects. Recently, Naveed *et al.,* [13] continued the work of Ref [12] and studied salient features of $(\mathrm{Ag\text{-}Fe_3O_4/H_2O})$ hybrid nanofluid between two parallel Riga plates. Furthermore, several research articles can be found in the literature that covers the different physical and geometrical aspects of the classical liquids. Few of them can be seen in the references. [14-25].

All the researchers, as mentioned earlier, have concentrated on conventional nonlinear stretching but not on the stretching. Fang *et al.,* [26] have coined the word variable thickness for the specific type of nonlinear stretching and examined the performance of boundary layer flow over a stretching sheet with variable thickness. Khader and Megahed [27] reviewed the work of Fang *et al.,* [26] via Numerical method to explain velocity slip effects. Farooq *et al.,* [28] considered variable thickness geometry with Rega plate to analyze stagnation point flow and Prasad *et al.,* [29-

33] examined the impact of variable fluid properties on the Newtonian/non-Newtonian fluid flow field.

The main objective of the present work is to reduce the skin friction or drag force of the fluids by applying an external electric field in the presence of variable fluid properties over a slender elastic Riga plate under the influence of zero mass flux and heat transfer boundary conditions. Suitable similarity variables are introduced to transform the coupled nonlinear partial differential equations into a set of coupled nonlinear ordinary differential equations. These equations are solved numerically via Keller Box method (See Vajravelu and Prasad [34]). The effects of various governing physical parameters for velocity, temperature, and nanoparticle concentration are discussed through the graphs and tables. The obtained results are compared with the actual results in previous literature and are found to be in excellent agreement. From this, it can be concluded that the present research work provides useful information for Science and industrial sector.

2. Mathematical Analysis of the Problem

Consider an electromagnetic flow of a steady, incompressible non-Newtonian nanofluid over a slender Riga plate with variable fluid properties. Here the non-Newtonian fluid model is the Casson model and the rheological equation of state for an isotropic and incompressible fluid is given by (for details see, Prasad *et al.,* [32]).

$$\tau_{ij} = \begin{cases} 2(\mu_B + P_y / \sqrt{2\pi})e_{ij}, \pi > \pi_c \\ 2(\mu_B + p_y / \sqrt{2\pi_c})e_{ij}, \pi < \pi_c \end{cases} \tag{1}$$

where $\pi = e_{ij}e_{ij}$ and e_{ij} is the $(i,\ j)^{th}$ component of deformation rate, π is the product of the component of deformation rate with itself, π_B is the plastic dynamic viscosity of Casson fluid, P_y is yield stress of the fluid and π_c is a critical value of this product depending on the non-Newtonian model. Further, the Riga plate is considered as an alternating array consisting of electrodes and permanent magnets mounted on a plane surface situated at *y* = 0 having x-axis vertically upwards. The fluid is characterized by a nanoparticle and is analyzed by considering Brownian motion and thermophoresis phenomena. The following assumptions are made

i. Joule heating and viscous dissipation are neglected.
ii. The fluid is isotropic, homogeneous, and has constant electric conductivity.
iii. The velocity of the stretching Riga plate and the free stream velocity are respectively, assumed to be $U_w(x) = U_0(x+b)^m$ and $U_e(x) = U_\infty(x+b)^m$, where U_∞ and U_0 are positive constants, *m* is the velocity power index and *b* is the physical parameter related to slender elastic sheet.
iv. The Riga plate is not flat and is defined as $y = \mathrm{A}\left(x+b\right)^{(1-m)/2}$, $\mathrm{m} \neq 1$, where the coefficient A is chosen as small so that the sheet is sufficiently thin, to avoid pressure gradient along the Riga plate $(\partial p / \partial x = 0)$
v. The temperature and nanoparticle concentration at the melting variable thickness of the Riga plate are T_M and C_M respectively and further T_∞ and C_∞ denote the ambient temperature and nanoparticle concentration of the fluid respectively.
vi. For different applications, the thickness of the stretching Riga plate is assumed to vary with the distance from the slot due to acceleration/deceleration of an extruded plate.

For m =1 thickness of the plate become flat. The physical model of the problem is given below (Figure 1).

Nanofluid

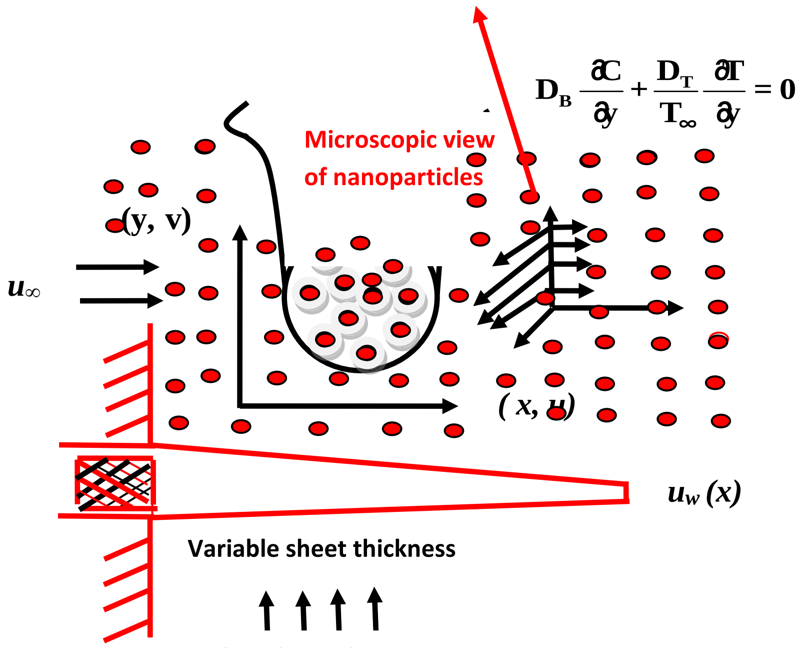

(a)

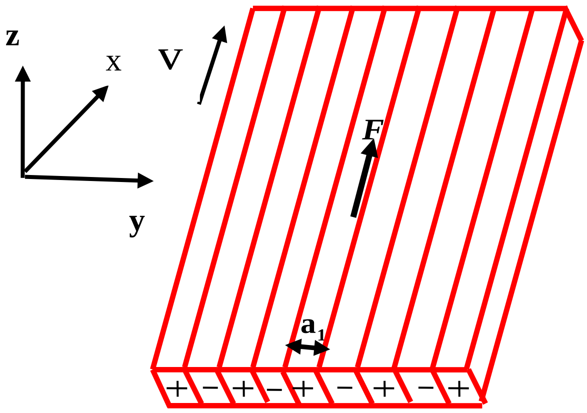

(b)

Fig. 1. Physical model of (a) variable thickness and (b) Riga plate

Based on the above assumptions and the usual boundary layer approximations, the governing equations for continuity, momentum, thermal energy, and concentration for the nanofluid model are expressed as follows

$$\frac{\partial u}{\partial x} + \frac{\partial v}{\partial y} = 0 \quad (2)$$

$$u\frac{\partial u}{\partial x}+\mathrm{v}\frac{\partial u}{\partial y}=\left(1+\frac{1}{\beta}\right)\frac{1}{\rho_\infty}\frac{\partial}{\partial y}\left(\mu(T)\frac{\partial u}{\partial y}\right)+U_e\frac{dU_e}{dx}+\frac{\pi_1 j_0 M_0(x)}{8\rho_\infty}\exp\left(\frac{-\pi_1}{a_1(x)}y\right) \tag{3}$$

$$u\frac{\partial T}{\partial x}+\mathrm{v}\frac{\partial T}{\partial y}=\frac{1}{\rho_\infty c_p}\frac{\partial}{\partial y}\left(K(T)\frac{\partial T}{\partial y}\right)+\frac{Q_0(x)}{\rho_\infty c_p}(T-T_\infty)+\tau\left[D_B(C)\frac{\partial C}{\partial y}\frac{\partial T}{\partial y}+\frac{D_T}{T_\infty}\left(\frac{\partial T}{\partial y}\right)^2\right] \tag{4}$$

$$u\frac{\partial C}{\partial x}+\mathrm{v}\frac{\partial C}{\partial y}=\frac{\partial}{\partial y}\left(D_B(C)\frac{\partial C}{\partial y}\right)+\frac{D_T}{T_\infty}\frac{\partial^2 T}{\partial y^2} \tag{5}$$

where u and v are velocity components along x and y directions respectively. β is the Casson parameter, c_p is the specific heat at constant pressure, and ρ_∞ is the fluid density. The transport properties of the fluid are assumed to be constant, except for the fluid viscosity $\mu(T)$, the fluid thermal conductivity $K(T)$ and Brownian diffusion of the fluid D_B, are assumed to be functions of temperature and nanoparticle concentration, and are expressed as follows

$$\mu(T)=\mu_\infty[1+\delta(T-T_M)]^{-1},\ \text{i.e}\quad \mu(T)=[a_2(T-T_r)]^{-1}, \tag{6}$$

$$K(T)=K_\infty[1+\varepsilon_1((T-T_M)/(T_\infty-T_M))] \tag{7}$$

$$D_B(C)=D_{B_\infty}[1+\varepsilon_2((C-C_M)/(C_\infty-C_M))] \tag{8}$$

here $a_2=\delta/\mu_\infty$ and $T_r=T_\infty-1/\delta$ are constants and their values depend on the reference state and the small parameter δ is known as thermal property of the fluid. Generally, the positive and negative values of a_2 describes two different states, namely, liquids and gases respectively, i.e. for $a_2>0$ represents the liquid state and $a_2<0$ represents gas state. Here μ_∞, K_∞ and D_{B_∞} are ambient fluid viscosity, thermal conductivity and Brownian diffusion coefficient respectively. ε_1 and ε_2 are small parameters known as the variable thermal conductivity parameter and variable species diffusivity parameter respectively. The term $Q_0(x)$ represents the heat generation when $Q_0>0$ and heat absorption when $Q_0<0$, and are used to describe exothermic and endothermic chemical reactions respectively. Further, j_0 is the applied current density in the electrodes, $M_0(x)$ is the magnetization of the permanent magnets mounted on the surface of the Riga plate and $a_1(x)$ is width between the magnets and electrodes. The special forms $Q_0(x)=Q_0(x+b)^{(1-m)/2}$, $M_0(x)=M_0(x+b)^{(1-m)/2}$ and $a_1(x)=a_1(x+b)^{(1-m)/2}$ are chosen to obtain the similarity solutions. τ is defined as the ratio between the effective heat capacity of the nanoparticle material and heat capacity of the fluid, i.e. $\tau=(\rho_\infty c_p)_p/(\rho_\infty c_p)_f$, D_T is the thermophoresis diffusion coefficient and T_0 is solid temperature. The appropriate boundary conditions are

$$\left.\begin{aligned} &u = U_w(x) = U_0(x+b)^m, \\ &K\left(\partial T/\partial y\right) = \rho\left[\lambda_1 + c_s(T_M - T_0)\right]\mathrm{v(x,y)},\ T = T_M \\ &D_B\frac{\partial C}{\partial y} + \frac{D_T}{T_\infty}\frac{\partial T}{\partial y} = 0 \end{aligned}\right\} \text{at } y = A(x+b)^{1-m/2} \tag{9}$$

$$u \to U_e(x) = U_\infty(x+b)^m,\ \ T \to T_\infty,\ C \to C_\infty \quad \text{as } y \to \infty$$

The second boundary condition defined in Eq. (9) $K\left(\partial T/\partial y\right) = \rho\left[\lambda_1 + c_s(T_M - T_0)\right]\mathrm{v(x,y)}$ represents the melting temperature in which λ_1 is the latent heat of fluid, T_M is the melting temperature, T_0 and C_s are the temperature and heat capacity of the concrete surface respectively. On substituting Eq. (6)-(8) in the basic Eq. (3)-(5), it reduces to

$$u\frac{\partial u}{\partial x} + \mathrm{v}\frac{\partial u}{\partial y} = \left(1+\frac{1}{\beta}\right)\frac{1}{\rho_\infty}\frac{\partial}{\partial y}\left(\frac{\mu_\infty}{1+\delta(T-T_\infty)}\frac{\partial u}{\partial y}\right) + U_e\frac{dU_e}{dx} + \frac{\pi j_0 M_0(x)}{8\rho_\infty}\exp\left(\frac{-\pi}{a_1(x)}y\right) \tag{10}$$

$$\begin{aligned} u\frac{\partial T}{\partial x} + \mathrm{v}\frac{\partial T}{\partial y} &= \frac{\partial}{\partial y}\left(\frac{K_\infty}{\rho_\infty c_p}\left(1+\varepsilon_1\left(\frac{T-T_M}{T_\infty - T_M}\right)\right)\frac{\partial T}{\partial y}\right) + \frac{Q_0(x)}{\rho_\infty c_p}(T-T_\infty) \\ &+\tau\left[D_{B_\infty}\left(1+\varepsilon_2\left(\frac{C-C_M}{C_\infty - C_M}\right)\right)\frac{\partial C}{\partial y}\frac{\partial T}{\partial y} + \frac{D_T}{T_\infty}\left(\frac{\partial T}{\partial y}\right)^2\right] \end{aligned} \tag{11}$$

$$u\frac{\partial C}{\partial x} + \mathrm{v}\frac{\partial C}{\partial y} = \frac{\partial}{\partial y}\left(D_{B_\infty}\left(1+\varepsilon_2\left(\frac{C-C_M}{C_\infty - C_M}\right)\right)\frac{\partial C}{\partial y}\right) + \frac{D_T}{T_\infty}\frac{\partial^2 T}{\partial y^2} \tag{12}$$

Now, we transform the system of Eq. (10)-(12) into dimensionless form. To this end, the dimensionless similarity variable be,

$$\eta = y\sqrt{(m+1/2)\frac{U_0(x+b)^{(m-1)}}{\nu_\infty}} \tag{13}$$

and the dimensionless stream function, the dimensionless temperature and the dimensionless nanoparticle concentration are,

$$\psi = \sqrt{(2/m+1)\nu_\infty U_0(x+b)^{(m+1)}}\,\mathrm{F}(\eta),\ \ \Theta(\eta) = \frac{T-T_M}{T_\infty - T_M},\ \ \Phi(\eta) = \frac{C-C_M}{C_\infty - C_M}, \tag{14}$$

with the use of Eq. (13) and (14), the velocity components are,

$$u = \partial\psi/\partial y = U_0(x+b)^m F'(\eta),\ \ \mathrm{v} = -\partial\psi/\partial x = -\sqrt{\frac{2}{(m+1)}\nu_\infty U_0(x+b)^{(m-1)}}\left[\frac{(m+1)}{2}F(\eta) + \eta\frac{(m-1)}{2}F'(\eta)\right] \tag{15}$$

here prime denotes differentiation with respect to η. In the present work, it is assumed m >-1 for the validity of the similarity variable. With the use of Eq. (13)-(15), then Eq. (10)-(12) and the corresponding boundary conditions reduce to:

$$\left(1+\frac{1}{\beta}\right)\left(\left(1-\frac{\Theta}{\theta_r}\right)^{-1}F''\right)'+FF''-\frac{2m}{(m+1)}(F')^2+\frac{2m}{(m+1)}A^*+\frac{2}{(m+1)}Qe^{-\beta_1\eta}=0 \tag{16}$$

$$\left((1+\varepsilon_1\Theta)\Theta'\right)'+\Pr\Theta'[Nb(1+\varepsilon_2\Phi)\Phi'+Nt\Theta'+F]+\frac{2}{(m+1)}\Pr\lambda\Theta=0 \tag{17}$$

$$\left((1+\varepsilon_2\Phi)\Phi'+\left(\frac{Nt}{Nb}\right)\Theta'\right)'+LeF\Phi'=0 \tag{18}$$

$$\begin{gathered}M\Theta'(\alpha)+\Pr\left[F(\alpha)-\frac{\alpha(1-m)}{(1+m)}\right]=0,\ F'(\alpha)=1,\quad \Theta(\alpha)\to 0,\\ Nb\Phi'(\alpha)+Nt\Theta'(\alpha)=0,\quad F'(\infty)\to A^*,\quad \Theta(\infty)\to 1,\quad \Phi(\infty)\to 1\end{gathered} \tag{19}$$

The non-dimensional parameters $\theta_r,\ A^*,\ Q,\ \beta_1,\Pr,\ \alpha, Nb, Nt,\ \lambda, Le$ and M represent the variable viscosity parameter, stretching rate ratio parameter, modified Hartman number, dimensionless parameter, Prandtl number, wall thickness parameter, Brownian motion parameter, thermophoresis parameter, heat source/sink parameter, Lewis number and the dimensionless melting heat parameter respectively and which are defined as follows

$$\begin{gathered}\theta_r=\frac{-1}{\delta(T_\infty-T_M)},\ A^*=\frac{U_\infty}{U_0},\ Q=\frac{\pi j_0 M_0}{8\rho_\infty U_0^2},\ \beta_1=\frac{\pi}{a_1}\sqrt{\frac{2}{(m+1)}\frac{\nu_\infty}{U_0(x+b)^{(m-1)}}},\ \Pr=\frac{\nu_\infty}{\alpha_\infty},\alpha=A\sqrt{\frac{U_0(m+1)}{2\nu_\infty}},\\ Nb=\frac{\tau_\infty D_{B_\infty}(C_\infty-C_M)}{\nu_\infty}, Nt=\frac{\tau_\infty D_{T_\infty}(T_\infty-T_M)}{T_\infty\nu_\infty},\quad \lambda=\frac{Q_0}{\rho_\infty c_p U_0},\ Le=\frac{\nu_\infty}{D_{B_\infty}}\ \text{ and }\ \mathrm{M}=\frac{c_p(T_\infty-T_M)}{\lambda_1+c_s(T_M-T_0)}\end{gathered} \tag{20}$$

The value of the θ_r is determined by the viscosity of the fluid under consideration, it is worth mentioning here that for $\delta\to 0$ *i.e* $\mu=\mu_\infty$ (constant) then $\theta_r\to\infty$. It is also important to note that θ_r is negative for liquids and positive for gases when $(T_\infty-T_M)$ is positive, this is due to fact that the viscosity of a liquid usually decreases with increasing in temperature. Further, $M=0$ shows that there is no melting phenomenon, also it should be noted that M comprises of the Stefan constants $c_p(T_\infty-T_0)/\lambda_1$ and $c_s(T_M-T_0)$ of liquid and solid phase respectively. Now, we define the following $F(\eta)=f(\eta-\alpha)=f(\xi),\ \Theta(\eta)=\theta(\eta-\alpha)=\theta(\xi),\ \Phi(\eta)=\phi(\eta-\alpha)=\phi(\xi),$ here $\eta=\alpha$ indicates the flat surface. Then Eq. (16) to (19) reduce to

$$\left(1+\frac{1}{\beta}\right)\left(\left(1-\frac{\theta}{\theta_r}\right)^{-1}f''\right)'+ff''-\frac{2m}{(m+1)}(f')^2+\frac{2m}{(m+1)}A^*+\frac{2}{(m+1)}Qe^{-\beta_1(\xi+\alpha)}=0 \tag{21}$$

$$\left((1+\varepsilon_1\theta)\theta'\right)' + \Pr\theta'\left(Nb(1+\varepsilon_2\phi)\phi' + Nt\theta' + f\right) + \frac{2}{(m+1)}\Pr\lambda\theta = 0 \tag{22}$$

$$\left((1+\varepsilon_2\phi)\phi' + \left(\frac{Nt}{Nb}\right)\theta'\right)' + Lef\phi' = 0 \tag{23}$$

$$\begin{gathered} M\theta'(0) + \Pr\left[f(0) - \frac{\alpha(1-m)}{(1+m)}\right] = 0, \quad f'(0) = 1, \quad \theta(0) \to 0, \\ Nb\phi'(0) + Nt\theta'(0) = 0, \quad f'(\infty) \to A^*, \quad \theta(\infty) \to 1, \quad \phi(\infty) \to 1 \end{gathered} \tag{24}$$

2.1 Physical Quantities of Interest

The important physical quantities of interest for the governing flow problem, such as skin friction C_{f_x}, the local Nussult number Nu_x, and Sherwood number Sh_x are defined as follow.

$$C_{f_x} = \frac{\tau_w}{U_w^2}, \quad Nu_x = \frac{(x+b)q_w}{(T_\infty - T_M)}, \qquad Sh_x = \frac{(x+b)j_w}{(C_\infty - C_M)} \tag{25}$$

where $\tau_w = \nu\frac{\partial u}{\partial y}$, $q_w = \frac{\partial T}{\partial y}$ and $j_w = \frac{\partial C}{\partial y}$ at $y = A(x+b)^{\frac{(1-m)}{2}}$, are respectively called the skin friction, the heat flux and the mass flux at the wall. These parameters in dimensionless form can be written as

$$\mathrm{Re}_x^{1/2} C_{f_x} = \left((m+1)/2\right)^{1/2}\left(\frac{\theta_r}{(\theta_r-1)}\right)f''(0), \quad \mathrm{Re}_x^{-1/2} Nu_x = -\left((m+1)/2\right)^{1/2}(1+\varepsilon_1)\theta'(0) \text{ and}$$

$\mathrm{Re}_x^{-1/2} Sh_x = -\left((m+1)/2\right)^{1/2}(1+\varepsilon_2)\phi'(0)$, where $\mathrm{Re}_x = U_w(x+b)/\nu_\infty$ is called local Reynolds number.

3. Exact Analytical Solutions for Some Special Cases

In this section, we study the exact solutions for some special cases. It is important to analyze some theoretical analysis of the certain solutions for some given physical parameters and these solutions serve as the base function for computing general solutions through numerical schemes. In the case of absence of Casson parameter β, variable fluid viscosity parameter θ_r, stretching rate ratio parameter A^*, and modified Hartman number Q the present problem reduces to Fang et al. [26]. The discussions here will be emphasized on other parameters except $m \neq 1$.

Case (i): when $m = -1/3$ then Eq. (21) reduces to the following form,

$$f''' + ff'' + (f')^2 = 0 \tag{26}$$

with the associated boundary conditions (24) becomes,

$$f(0)=2\alpha, \quad f'(0)=1, \quad f'(\infty)=0 \tag{27}$$

On integration Eq. (26) twice yields to

$$f'+\frac{f^2}{2}=(\gamma+2\alpha)\eta+(2\alpha^2+1) \tag{28}$$

where $\gamma=f''(0)$, in order to have a finite solution it is essential to consider $\gamma=-2\alpha$

$$f'+\frac{f^2}{2}=(2\alpha^2+1) \text{ when } \xi\to\infty, \text{ we have } f(\infty)=\sqrt{2+4\alpha^2}. \tag{29}$$

The solution is $f(\xi)=\sqrt{2+4\alpha^2}\tanh\left[\frac{\sqrt{2+4\alpha^2}}{2}\xi+\tanh^{-1}\left(\frac{2\alpha}{\sqrt{2+4\alpha^2}}\right)\right]$ and (30)

$$f'(\xi)=1+2\alpha^2\,\mathrm{Sech}^2\left[\frac{\sqrt{2+4\alpha^2}}{2}\xi+\tanh^{-1}\left(\frac{2\alpha}{\sqrt{2+4\alpha^2}}\right)\right] \tag{31}$$

It should be noted that, for $m=-1/3$, the above solutions reduce to the solutions for a flat stretching surface. This confirms that the present numerical solutions are in good agreement with those of Fang *et al.,* [26] and these can be used for numerical code validation in this work.

Case(ii): For $m=-1/2$, we can obtain another analytical solution, for this case, Eq. (21) reduces to,

$$f'''+ff''+2(f')^2=0 \tag{32}$$

with the respective boundary conditions (24) becomes as,

$$f(0)=3\alpha, \quad f'(0)=1, \quad f'(\infty)=0 \tag{33}$$

Eq. (32) can be written in the form of

$$\frac{1}{f}\frac{d}{d\xi}\left[f^{3/2}\frac{d}{d\xi}\left(f^{-1/2}f'+\frac{2}{3}f^{3/2}\right)\right]=0 \tag{34}$$

Integrating Eq. (34) once reduces to the following form

$$-\frac{1}{2}(f')^2+ff''+f^2f'=-\frac{1}{2}+3\alpha\gamma+9\alpha^2 \tag{35}$$

Applying free boundary condition we get,

$$\gamma=-3\alpha+\frac{1}{6\alpha} \tag{36}$$

On integration Eq. (35) leads to

$$f^{-1/2}f'+\frac{2}{3}f^{3/2}=\frac{2}{3}(3\alpha)^{3/2}+\frac{1}{\sqrt{3\alpha}} \tag{37}$$

The final solution is

$$\xi+D=\frac{1}{2d^2}\ln\left[\frac{f+d\sqrt{f}+d^2}{\left(d-\sqrt{f}\right)^2}\right]+\frac{\sqrt{3}}{d^2}\tan^{-1}\left(\frac{2\sqrt{f}+d}{d\sqrt{3}}\right)=0 \tag{38}$$

where

$$d=[(3\alpha)^{3/2}+3/(2\sqrt{3\alpha})^{1/3}$$

and

$$D=\frac{1}{2d^2}\ln\left[\frac{\left(3\alpha+d\sqrt{3\alpha}+d^2\right)}{\left(d-\sqrt{3\alpha}\right)^2}\right]+\frac{\sqrt{3}}{d^2}\tan^{-1}\left(\frac{2\sqrt{3\alpha}+d}{d\sqrt{3}}\right)=0 \tag{39}$$

Since the system of Eq. (21)-(23) with boundary conditions (24) has no exact analytical solutions, they are solved numerically via a Keller-Box method.

4. Method of Solution

The system of highly nonlinear coupled differential Eq. (21) to (23) along with appropriate boundary conditions in Eq. (24) are solved by finite difference scheme known as Keller Box Method. This system is not conditionally stable and has a second order accuracy with arbitrary spacing. For solving this system first write the differential equations and respective boundary conditions in terms of first order system, which is then, converted into a set of finite difference equations using central difference scheme. Since the equations are highly nonlinear and cannot be solved analytically, therefore these equations are solved numerically using the symbolic software known as Fedora. Further nonlinear equations are linearized by Newton's method and resulting linear system of equations is solved by block tri-diagonal elimination method. For the sake of brevity, the details of the solution process are not presented here. For numerical calculations, a uniform step size is taken which gives satisfactory results and the solutions are obtained with an error tolerance of 10^{-6} in all the cases. To demonstrate the accuracy of the present method, the results for the dimensionless Skin friction, Nussult number and Sherwood number are compared with the previous results.

4.1 Validation of Methodology

The main objective of this section is to check the validation of the present work. The present numerical results are compared with the existing work of Farooq *et al.,* [28] and Prasad *et al.,* [31] in the absence and presence of Riga plate with $\Pr = A^* = \varepsilon_1 = \varepsilon_2 = Nt = \lambda = Le = M = 0,\ Nb \to 0,$ $\beta \to \infty, \theta_r \to \infty$ and the results are in excellent agreement with the previous literature (Table 1).

Table 1
Comparison of Skin friction coefficient $-f''(0)$ for different values of wall thickness parameter α and velocity power index m when the presence and absence of a Riga plate at fixed values of $\Pr = A^* = \varepsilon_1 = \varepsilon_2 = Nt = \lambda = Le = M = 0,\ Nb \to 0, \beta \to \infty, \theta_r \to \infty.$

α	m	Presence of Riga plate Farooq *et al.,* [28] by OHAM when $Q = 0.1, \beta_1 = 0.2$	Absence of Riga plate Prasad *et al.,* [31] by OHAM, when $\lambda = 0, Mn = Q = \beta_1 = 0$	Present results, Keller Box Method: Presence of Riga plate	Present results, Keller Box Method: Absence of Riga plate
0.25	02	0.9990	1.0614	0.9990	1.06140
	03	1.0465	1.0907	1.0456	1.09050
	05	1.0908	1.1182	1.0902	1.11860
	07	1.1120	1.1328	1.1121	1.13230
	09	1.1244	1.1401	1.1247	1.14041
	10	1.1289	1.1439	1.1288	1.14334
0.5	02	0.9673	1.0231	0.9672	1.02341
	03	0.9976	1.0358	0.9975	1.03588
	05	1.0252	1.0487	1.0253	1.04862
	07	1.0382	1.0551	1.0383	1.05506
	09	1.0458	1.0512	1.0458	1.05893
	10	1.0485	1.0604	1.0485	1.06034

5. Results and Discussion

The system of nonlinear ordinary differential Eq. (21) to (23) together with the appropriate boundary conditions (24) are numerically solved by using Keller Box method. The influence of various physical parameters such as Casson parameter β, variable fluid viscosity parameter θ_r, velocity power index m, stretching rate ratio parameter A^*, modified Hartman number Q, dimensionless parameter β_1, variable thermal conductivity parameter ε_1, Brownian motion parameter Nb, thermophoresis parameter Nt, Prandtl number $\Pr$, heat source/sink parameter λ, variable species diffusivity parameter ε_2, Lewis number Le, and wall thickness parameter α on the horizontal velocity profile $f'(\xi)$, the temperature profile $\theta(\xi)$, and the concentration profile $\phi(\xi)$ are exhibited through Figure 2-9. The computed numerical values for the skin friction $f''(0)$, the Nussult number $\theta'(0)$ and the wall Sherwood number $\phi'(0)$ are presented in Table 2.

In Table 2 we present the results for $f''(0)$, $\theta'(0)$ and $\phi'(0)$ corresponding to different values of the physical parameters. The skin friction coefficient is a decreasing function of the parameters $m,\ \alpha,\ \beta,\ \beta_1,\ \theta_r$ and increasing function of $A^*,\ Q$. Nusselt number reduces for $m, \alpha, A^*,\ \varepsilon_1$ and increases for $\beta, \beta_1\, \theta_r\ Nb, Nt, \Pr, \text{and}\ \lambda.$ Further, the Sherwood number decreases for $\beta\, \&\, \beta_1$ and increases for A^*.

The effect of velocity power index m and wall thickness parameter α on velocity, temperature and concentration boundary layers are depicted in Figure 2(a) – 2(c). Figure 2(a) elucidates that, for increasing values of m, $f'(\xi)$ reduce and this is due to the fact that the stretching velocity enhances for larger values of m which causes more deformation in the fluid, consequently velocity profiles decrease. A similar trend may be observed in the case of $\theta(\xi)$ (Figure 2(b)), whereas concentration distribution (Figure 2(c)) shows a dual characteristic, that is for larger values of m concentration profiles reduces near the sheet and opposite behaviour is observed away from the sheet. When $m=1$, the sheet become flat. Similarly, for higher values of wall thickness parameter α, velocity profiles fall, but the temperature distribution upgrade near the sheet and downwards away from the sheet. Whereas, the impact of α is quite opposite in the case of concentration distribution. Figure 3(a) through 3(c) indicates the influence of β and β_1 on $f'(\xi), \theta(\xi)$ and $\phi(\xi)$. For greater values of β velocity profiles are compressed, this is because as β increases the corresponding value of yield stress fall as a result velocity boundary layer thickness decreases. The temperature distribution rises for different estimations of β and concentration distribution exhibits exactly reverse trend. Effect of β_1 on these three profiles is same as that of β . It is noticed from in Figure 4(a) to 4(c) that both θ_r and A^* exhibits opposite trend, increasing variable fluid viscosity reduces the velocity and concentration profiles while the enhancement is observed in the case of temperature profiles. This may be due to the fact that, lesser θ_r implies higher temperature difference between the wall and the ambient nanofluid and the profiles explicitly manifest that θ_r is the indicator of the variation of fluid viscosity with temperature which has a substantial effect on $f'(\xi)$ and hence on $f''(\xi)$, where as in the case of temperature the effect is reversed. Figure 5 illustrates the impact of A^* and Q on $f'(\xi)$. An improvement in A^* corresponds to the enhancement of velocity boundary layer thickness. The enhancement in the velocity profile is observed for amplifying Q. Conventionally the velocity profiles are the decreasing function of Hartman number where as in this case the Lorentz force which is produced due to the magnetic arrays parallel to the surface is responsible for the enhancement of the momentum boundary layer thickness. The influence of Nb and Nt on temperature and concentration distribution are sketched in Figure 6(a) and 6(b). It is seen that the higher values of Nb enhances temperature profiles and its boundary layer thickness, whereas concentration distribution suppressed near the sheet and swells away from the sheet. The larger Nt creates a thermophoresis force which compels the nanoparticles to flow from the hotter region to the colder region which results in raising temperature profiles. In the case of concentration distribution, the duel behavior is noticed which reduces near the sheet and increases away from it (See Figure 6(b)). The characteristic of Prandtl number $\Pr$ and variable thermal conductivity parameter ε_1 on temperature distribution is demonstrated in Figure 7. Usually temperature distribution reduces for higher values of $\Pr$ and enhances for larger values of ε_1, but in this work quite opposite behaviour can be seen, this is due to the presence of melting heat transfer parameter M and stretching rate ratio parameter A^*. Figure 8 records the effect of heat source/sink parameter λ on $\theta(\xi)$, an increase in λ means rise in the temperature difference $(T_\infty - T_M)$, which leads to an increment in temperature distribution. Figure 9 is plotted for different values of Le and ε_2 on $\phi(\xi)$. Lower the Brownian diffusion coefficient $D_{B\infty}$ the higher Lewis number: This leads to a decrease in the thickness of the nanoparticle concentration boundary layer. It is interesting to note that a distinct rock bottom in the nanoparticle volume fraction profiles occur in the fluid adjacent to the boundary for higher values of Le and lower values of ε_2. This means that the nanoparticle volume fraction near the boundary is lesser than the nanoparticle volume fraction at the boundary; accordingly, nanoparticles are likely to transfer to the boundary.

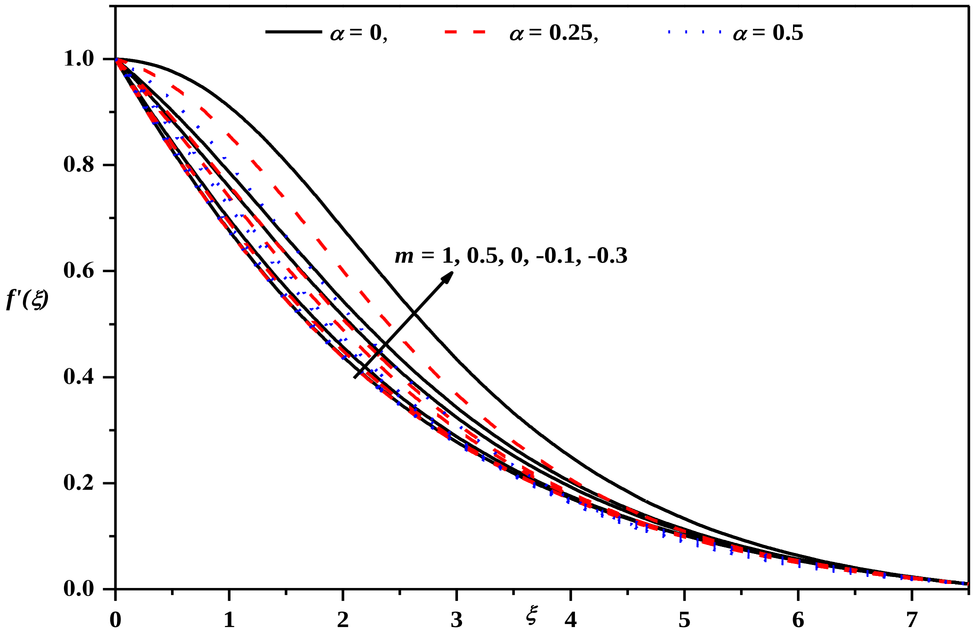

(a)

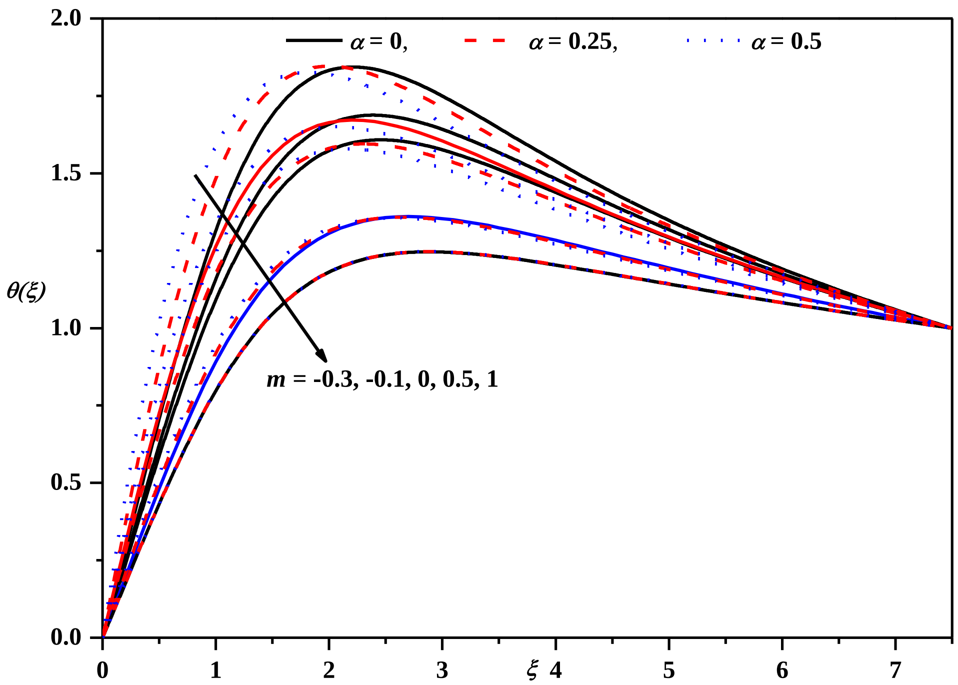

(b)

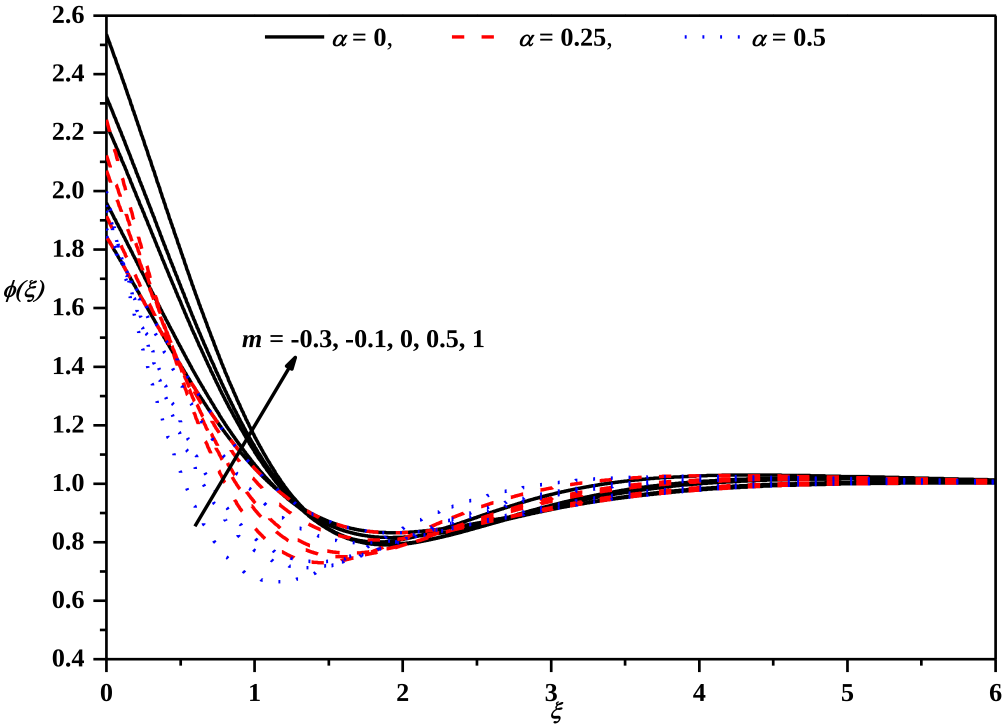

(c)

Fig. 2. The effect of velocity power index m and wall thickness parameter α on (a) horizontal velocity, (b) temperature and (c) concentration boundary layers profiles for different values of Pr = 1, Nb = 0.5, Nt = 0.5, Le = 0.96, M = 0.2, λ = 0.1, ε_1 = 0.1, ε_2 = 0.1, θ_τ = -5, Q= 0.2, β_1 = 0.3, β = 0.2, A^* = 0.01.

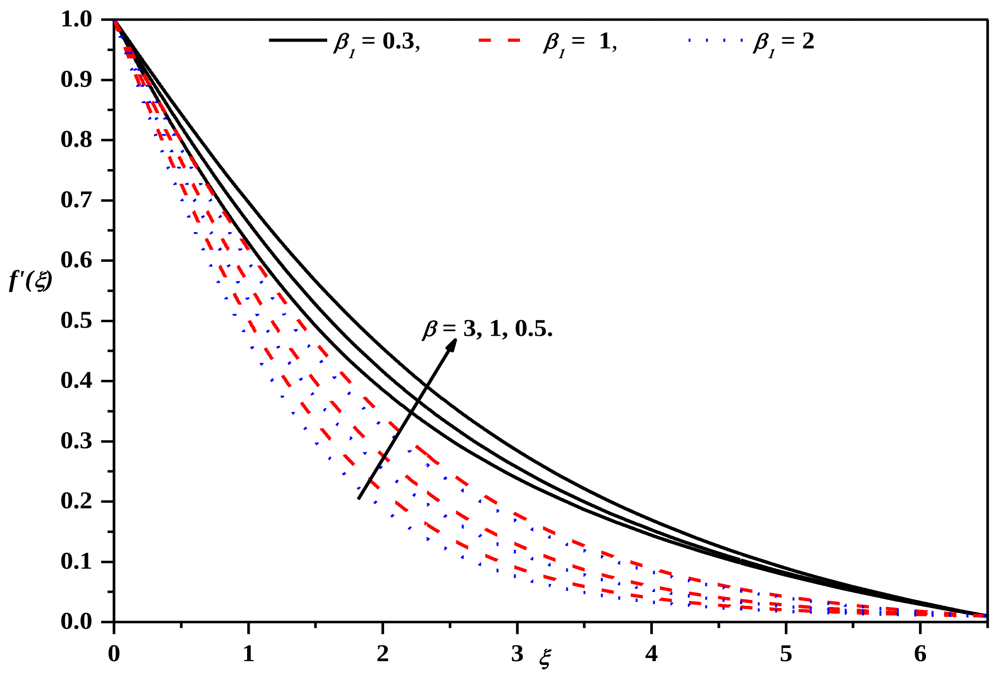

(a)

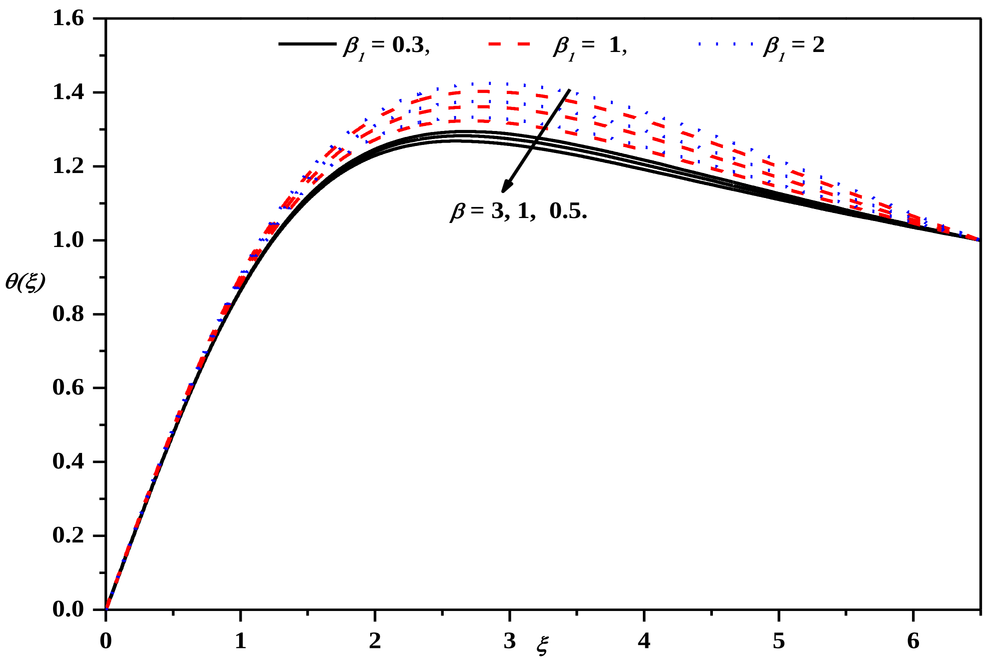

(b)

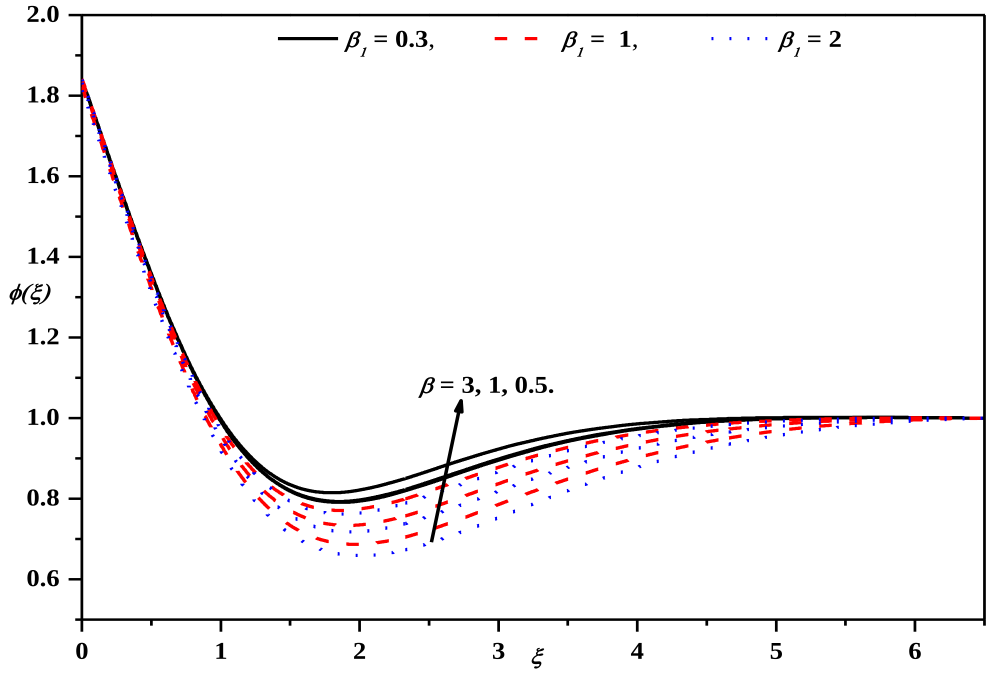

(c)

Fig. 3. The influence of β and β_1 on (a) horizontal velocity, (b) temperature and (c) concentration profiles for different values of *Pr* = 1, *Nb* = 0.5, *Nt* = 0.5, Le = 0.96, *M* = 0.2, λ = 0.1, ε_1 = 0.1, ε_2 = 0.1, θ_τ = -5, *Q*= 0.1, α = 0.25, A^* = 0.01

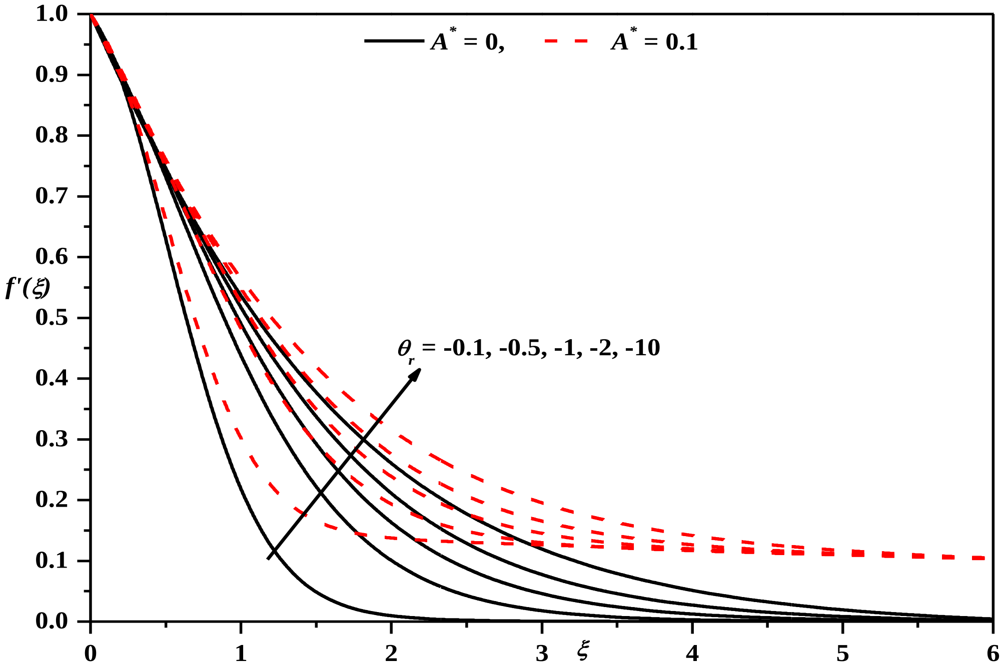
1.0
0.9
0.8
0.7
0.6
0.5
0.4
0.3
0.2
0.1
0.0
f'(ξ)
A* = 0,
A* = 0.1
θr = -0.1, -0.5, -1, -2, -10
0
1
2
3
ξ
4
5
6

(a)

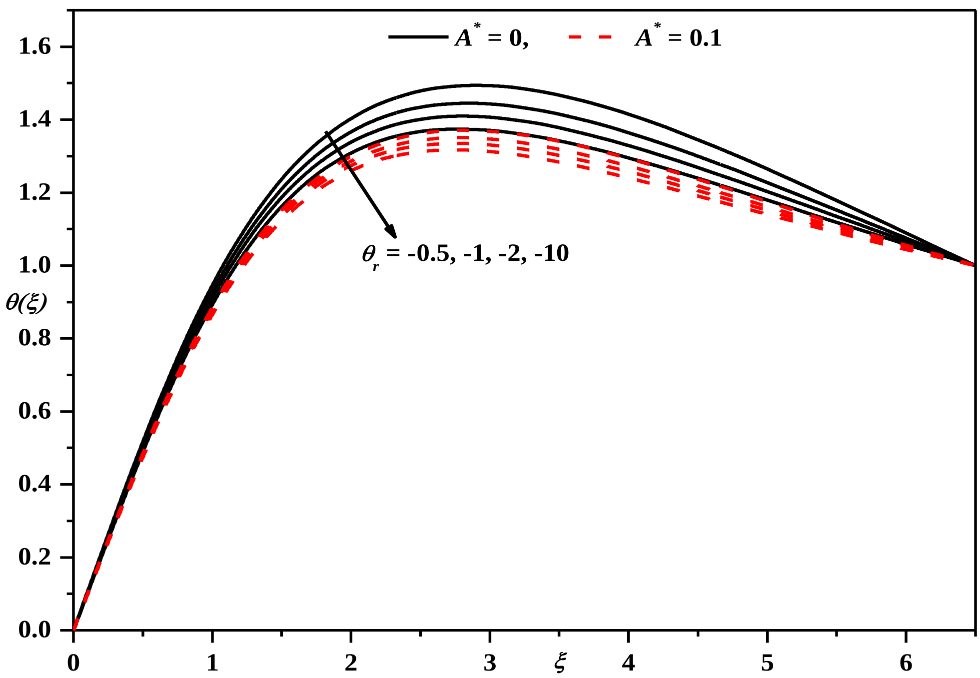
1.6
1.4
1.2
1.0
0.8
0.6
0.4
0.2
0.0
θ(ξ)
A* = 0,
A* = 0.1
θr = -0.5, -1, -2, -10
0
1
2
3
ξ
4
5
6

(b)

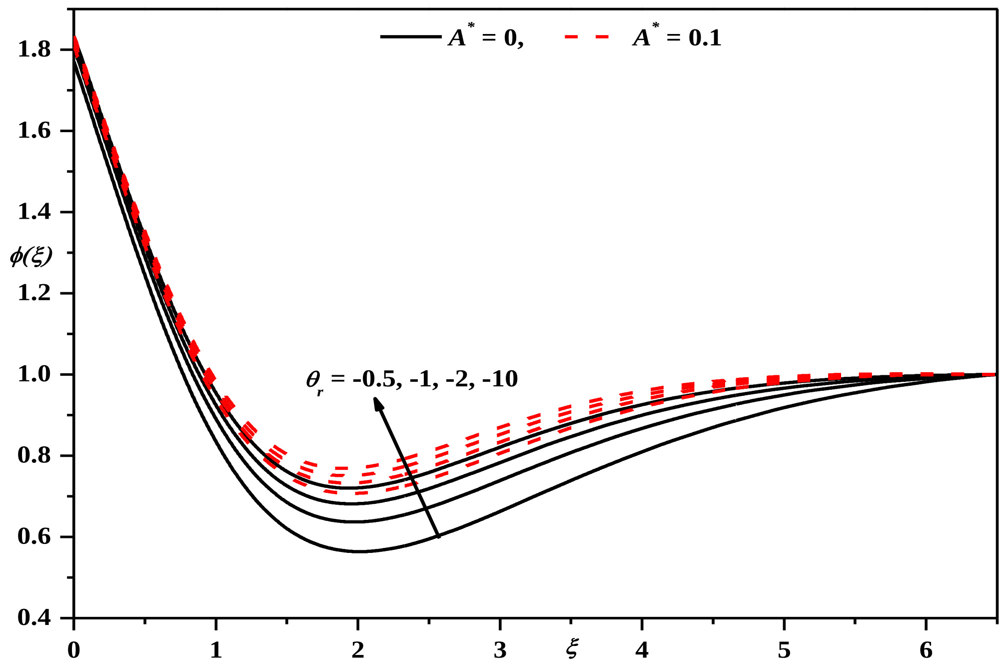

(c)

Fig. 4. The (a) horizontal velocity, (b) temperature and (c) concentration profiles for different values of θ_τ and A^* with Pr = 1, Nb = 0.5, Nt = 0.5, Le = 0.96, M = 0.2, λ = 0.1, ε_1 = 0.1, ε_2 = 0.1, Q= 1, α = 0.25, m = 0.5

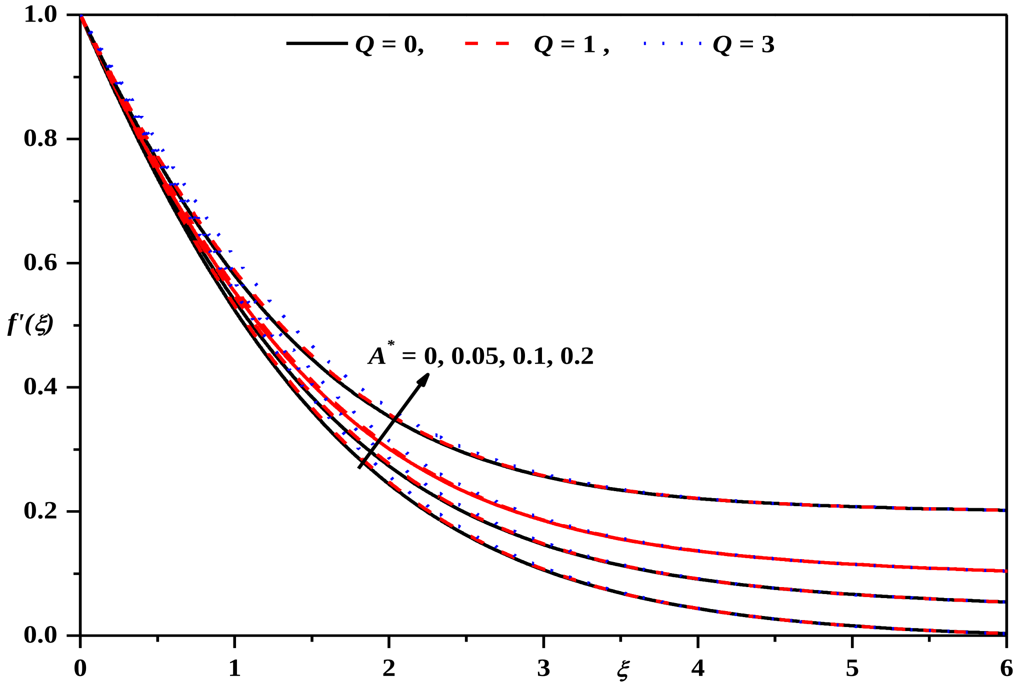

Fig. 5. The horizontal velocity profiles for different values of A^* and Q with Pr = 1, Nb = 0.5, Nt = 0.5, Le = 0.96, M = 0.2, λ = 0.1, ε_1 = 0.1, ε_2 = 0.1, α = 0.25, θ_τ = -5, m = 0.5, β_1 = 0.3 and β = 1

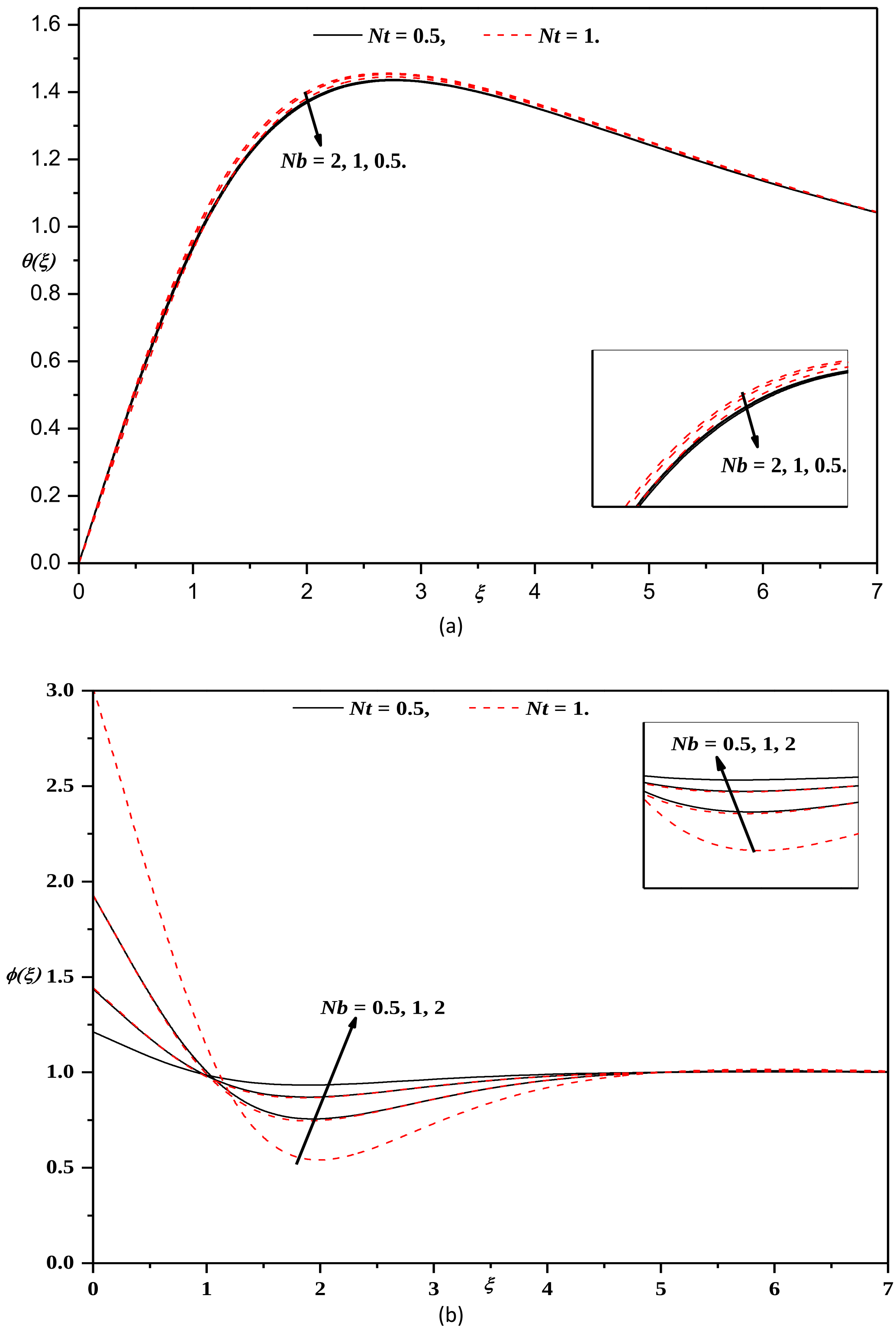

Fig. 6. The influence of Nb and Nt on the (a) temperature and (c) concentration profiles with Pr = 1, Le = 0.96, M = 0.2, λ = 0.1, ε_1 = 0.1, ε_2 = 0.1, α = 0.25, Q = 1, β_1 = 2, β = 1, θ_τ = -0.5 and A^* = 0.01

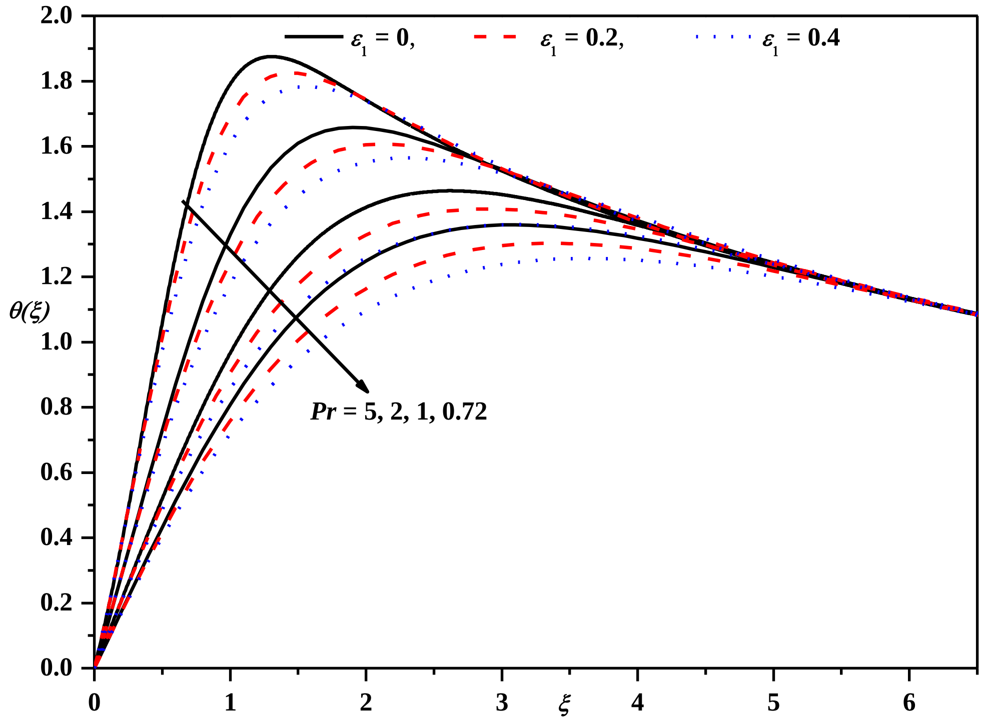

Fig. 7. The temperature profiles for different values of ε_1 and *Pr* with *m* = 0.5, *Nb* = 0.5, *Nt* = 0.5, *Le* = 0.96, *M* = 0.2, λ = 0.1, ε_2 = 0.1, α = 0.25, θ_τ = -5, *Q* = 1, β_1 = 0.3, β = 1, and A^* = 0.01

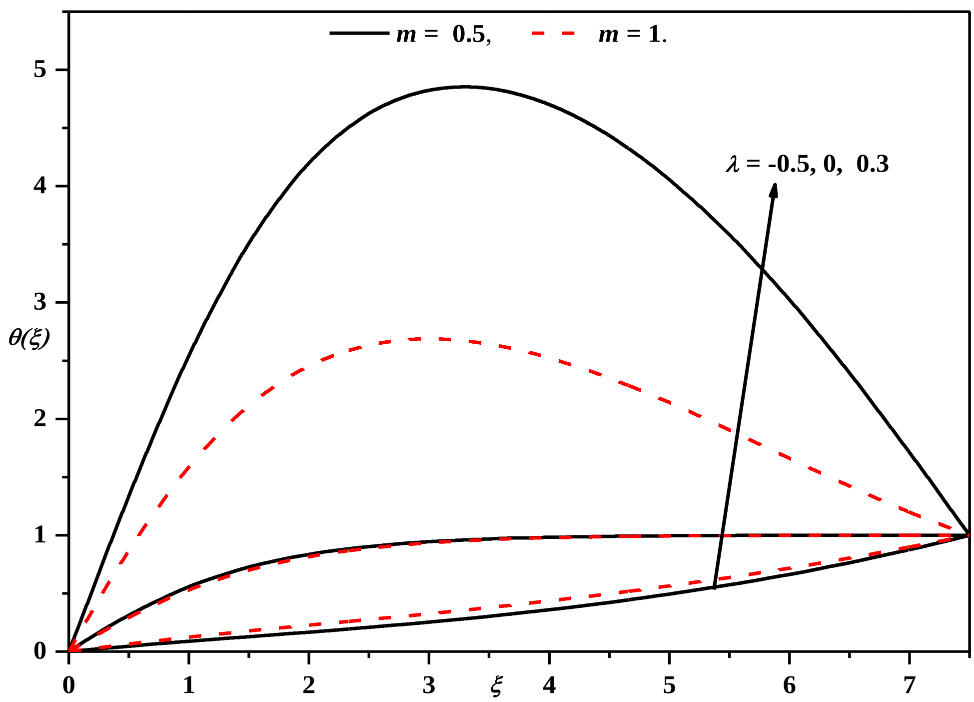

Fig. 8. The temperature profiles for different values of λ *and m with Le* = 0.96, *Nb* = 0.5, *Nt* = 0.5, *M* = 0.2, λ = 0.1, ε_2 = 0.1, α = 0.25, θ_τ = -5, *Q* = 1, β_1 = 0.3, β = 1, and A^* = 0.01

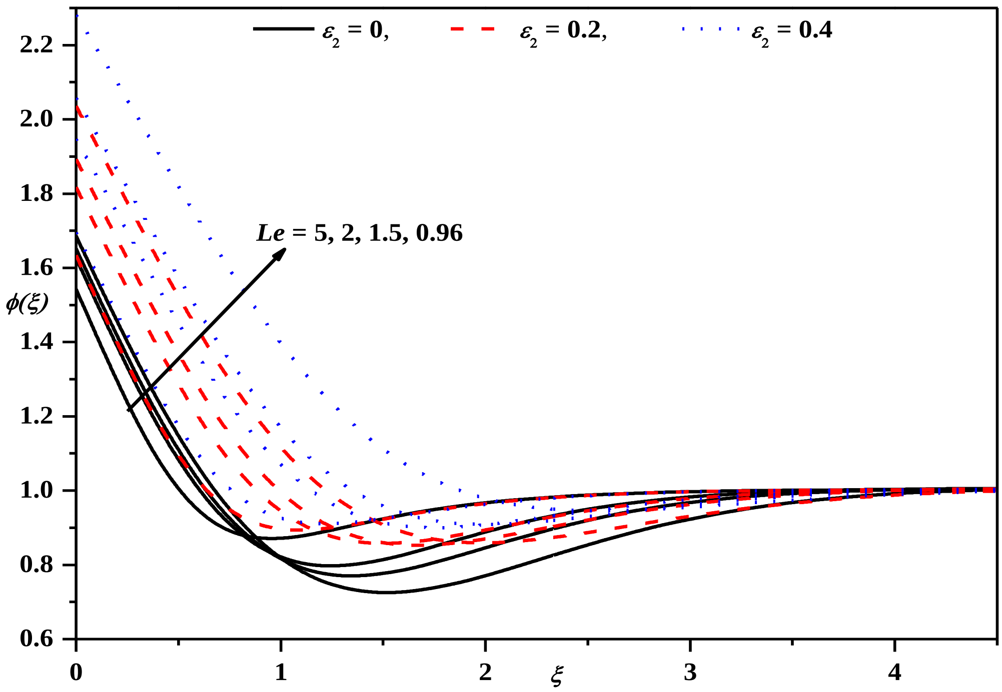

Fig. 9. The concentration profiles for different values of ε_2 and *Le* with *m* = 0.5, *Nb* = 0.5, *Nt* = 0.5, *M* = 0.2, λ = 0.1, α = 0.25, θ_τ = -5, *Q* = 1, β_1 = 0.3, β = 1, and A^* = 0.01

Table 2
Values of Skin friction, Nusselt number and Sherwood number for different physical parameters

Pr	Le	Nb	Nt	ε_1	ε_2	λ	A^*	M	β_1	β	Q	θ_r	m	$\alpha = 0.25$			$\alpha = 0.5$		
														$f''(0)$	$\theta'(0)$	$\phi'(0)$	$f''(0)$	$\theta'(0)$	$\phi'(0)$
													-0.3	-0.0573	1.883	-1.8833	-0.1095	2.4189	-2.4189
1	0.96	0.5	0.5	0.1	0.1	0.1	0.01	0.2	2	1	0.1	-5	-0.1	-0.1990	1.520	-.15201	-0.2243	1.8289	-1.8289
													0.0	-0.2369	1.390	-1.3905	-0.2561	1.6311	-1.6311
													0.5	-0.3297	1.025	-1.0256	-0.3356	1.0937	-1.0937
													1.0	-0.3697	08643	-0.8643	-0.3685	0.8643	-0.8643
Pr	Le	Nb	Nt	ε_1	ε_2	λ	A^*	M	m	θ_r	Q	β	α		$\beta_1 = 1.0$			$\beta_1 = 2.0$	
												0.5		-0.4136	0.987	-0.9876	-0.4489	0.9879	-0.9879
1	0.96	0.5	0.5	0.1	0.1	0.1	0.01	0.2	0.5	-5	0.1	1.0	0.25	-0.4925	0.996	-0.9962	-0.5414	0.9969	-0.9969
												2.0		-0.5851	1.003	-1.0036	-0.6519	1.0044	-1.0044
												5.0		-0.6114	1.004	-1.0045	-0.6839	1.0056	-1.0056
Pr	Le	Nb	Nt	ε_1	ε_2	λ	A^*	M	β_1	Q	θ_r	β	α		$m = 0.5$			$m = 1.0$	
											-10			-0.5288	0.968	-0.9682	-0.5628	0.8093	-0.8093
											-5.0			-0.5165	0.971	-0.9710	-0.5516	0.8105	-0.8105
1	0.96	0.5	0.5	0.1	0.1	0.1	0.1	0.2	2	1	-2.0	1	0.25	-0.4863	0.977	-0.9776	-0.5234	0.8128	-0.8128
											-1.0			-0.4494	0.984	-0.9842	-0.4878	0.8143	-0.8143
											-0.5			-0.4009	0.989	-0.9890	-0.4395	0.8152	-0.8152
θ_r	Le	Nb	Nt	A^*	ε_2	λ	m	M	β_1	Pr	Q	β	α		$\varepsilon_1 = 0.2$			$\varepsilon_1 = 0.4$	
										0.72				-0.5275	0.873	-0.8735	-0.5283	0.8758	-0.8758
-5	0.96	0.5	0.5	0.01	0.1	0.1	0.5	0.2	2	1.0	0.1	1	0.25	-0.5113	1.042	-1.0429	-0.5118	1.0531	-1.0531
										2.0				-0.4932	1.394	-1.3949	-0.4934	1.4314	-1.4314
										5.0				-0.4844	1.681	-1.6814	-0.4850	1.7462	-1.7462
Pr	Le	m	λ	A^*	ε_2	β_1	ε_1	M	Nb	θ_r	Q	β	α		$Nt = 0.5$			$Nt = 1$	
									0.5					-0.5111	1.036	-1.0366	-0.5149	0.9594	-1.9188
1.0	0.96	0.5	0.1	0.01	0.1	0.3	0.1	0.2	1.0	-5	0.1	1	0.25	-0.5101	1.054	-1.5272	-0.5113	1.0229	-1.0229
									2.0					-0.3415	4.900	-3.6755	-0.5096	1.0544	-0.5272
β_1	M	Nb	Nt	A^*	ε_1	m	λ	Le	Pr	θ_r	Q	β	α		$\varepsilon_2 = 0.2$			$\varepsilon_2 = 0.2$	
								1.5						-0.3365	1.0526	-1.0526	-0.3394	0.9289	-0.9289
0.3	0.2	0.5	0.5	0.01	0.1	0.5	0.1	2.0	1	-5	0.1	1	0.25	-0.3358	1.0755	-1.0755	-0.3385	0.9599	-0.9599
								5.0						-0.3339	1.1495	-1.1495	-0.3359	1.0579	-1.0579

6. Conclusions

The present article examines the effects of variable fluid properties on the heat transfer characteristics of a Casson nanofluid over a slender Riga plate with zero mass flux and melting heat transfer boundary conditions. Here, the thickness of the sheet is erratic. The critical points of the present study are summarized as follows:

i. The effect of velocity power index *m* on velocity and temperature field is similar, that is, in both the cases the profiles increases as *m* reduces, whereas in the case of concentration distribution dual nature is observed.
ii. Velocity and concentration distributions reduces for increasing values of Casson parameter, but the temperature distributions show exactly opposite behavior for larger values of Casson parameter.
iii. Enhanced variable fluid viscosity parameter influences the velocity and temperature field in opposite manner.
iv. The modified Hartmann number enhances the velocity distribution and reduces the temperature distribution.
v. The squeezed thermal boundary layer is observed for the increasing values of variable thermal conductivity parameter.
vi. The concentration distribution improves for higher values of variable species diffusivity parameter. The duel nature of the concentration profiles is recorded for the Brownian motion parameter and thermophoresis parameter.

Acknowledgement
This research was funded by a grant from Government of India, Ministry of Tribal Affairs (Scholarship Division), New Delhi for supporting financially under Scheme of National Fellowship and Scholarship for Higher Education. (Grant No. 2017-18-NFST-KAR-00764).

References

[1] Gailitis, A. and Lielausis, O. "On a possibility to reduce the hydrodynamic resistance of a plate in an electrolyte." *Appl. Magnetohydrodynamics Rep.Inst. Phys. Inst. Riga* 13, (1961): 143-146.
[2] Grinberg, E. "On determination of properties of some potential fields." *Applied Magnetohydrodynamics* 12, (1961): 147–154.
[3] Tsinober, A. B., and A. G. Shtern. "Possibility of increasing the flow stability in a boundary layer by means of crossed electric and magnetic fields." *Magnetohydrodynamics* 3, no. 2 (1967): 152-154.
[4] Pantokratoras, Asterios, and Eugen Magyari. "EMHD free-convection boundary-layer flow from a Riga-plate." *Journal of Engineering Mathematics* 64, no. 3 (2009): 303-315.
[5] Pantokratoras, Asterios. "The Blasius and Sakiadis flow along a Riga-plate." *Progress in Computational Fluid Dynamics, An International Journal* 11, no. 5 (2011): 329-333.
[6] Choi, Stephen US, and Jeffrey A. Eastman. *Enhancing thermal conductivity of fluids with nanoparticles*. No. ANL/MSD/CP-84938; CONF-951135-29. Argonne National Lab., IL (United States), 1995.
[7] Buongiorno, Jacopo. "Convective transport in nanofluids." *Journal of Heat Transfer* 128, no. 3 (2006): 240-250.
[8] Makinde, Oluwole D., and A. Aziz. "Boundary layer flow of a nanofluid past a stretching sheet with a convective boundary condition." *International Journal of Thermal Sciences* 50, no. 7 (2011): 1326-1332.
[9] Ahmad, Adeel, Saleem Asghar, and Sumaira Afzal. "Flow of nanofluid past a Riga plate." *Journal of Magnetism and Magnetic materials* 402 (2016): 44-48.
[10] Ayub, M., T. Abbas, and M. M. Bhatti. "Inspiration of slip effects on electromagnetohydrodynamics (EMHD) nanofluid flow through a horizontal Riga plate." *The European Physical Journal Plus* 131, no. 6 (2016): 193.
[11] Hayat, T., Mumtaz Khan, M. Imtiaz, and A. Alsaedi. "Squeezing flow past a Riga plate with chemical reaction and convective conditions." *Journal of Molecular Liquids* 225 (2017): 569-576.

[12] Hayat, Tasawar, Mumtaz Khan, Muhammad Ijaz Khan, Ahmed Alsaedi, and Muhammad Ayub. "Electromagneto squeezing rotational flow of Carbon (C)-Water (H2O) kerosene oil nanofluid past a Riga plate: A numerical study." *PloS one* 12, no. 8 (2017): e0180976.

[13] Naveed, A., Fitnat, S., Umar, K., Ilyas, K., Tawfeeq, A. A., Imran, F. and Syed, T. Mohyud-Din. "Spherical shaped (Ag−Fe3O4/H2O) hybrid nanofluid flow squeezed between two Riga plates with nonlinear thermal radiation and chemical reaction effects." *Energies* 12, no. 1 (2019): 76.

[14] Sheikholeslami, Mohsen, and Houman B. Rokni. "Effect of melting heat transfer on nanofluid flow in existence of magnetic field considering Buongiorno Model." *Chinese Journal of Physics* 55, no. 4 (2017): 1115-1126.

[15] Wakif, Abderrahim, Zoubair Boulahia, Farhad Ali, Mohamed R. Eid, and Rachid Sehaqui. "Numerical analysis of the unsteady natural convection MHD couette nanofluid flow in the presence of thermal radiation using single and two-phase nanofluid models for Cu–Water nanofluids." *International Journal of Applied and Computational Mathematics* 4, no. 3 (2018): 81.

[16] Wakif, Abderrahim, Zoubair Boulahia, and Rachid Sehaqui. "A semi-analytical analysis of electro-thermo-hydrodynamic stability in dielectric nanofluids using Buongiorno's mathematical model together with more realistic boundary conditions." *Results in Physics* 9 (2018): 1438-1454.

[17] Wakif, Abderrahim, Zoubair Boulahia, S. R. Mishra, Mohammad Mehdi Rashidi, and Rachid Sehaqui. "Influence of a uniform transverse magnetic field on the thermo-hydrodynamic stability in water-based nanofluids with metallic nanoparticles using the generalized Buongiorno's mathematical model." *The European Physical Journal Plus* 133, no. 5 (2018): 181.

[18] Reza, Jawad, Fateh Mebarek-Oudina, and Oluwole Daniel Makinde. "MHD slip flow of Cu-Kerosene nanofluid in a channel with stretching walls using 3-stage Lobatto IIIA formula." In *Defect and Diffusion Forum*, vol. 387, pp. 51-62. Trans Tech Publications, 2018.

[19] Prasad, K. V., Hanumesh Vaidya, Oluwole Daniel Makinde, and B. Srikantha Setty. "MHD mixed convective flow of Casson nanofluid over a slender rotating disk with source/sink and partial slip effects." In *Defect and Diffusion Forum*, vol. 392, pp. 92-122. Trans Tech Publications, 2019.

[20] Mebarek-Oudina, Fateh. "Convective heat transfer of Titania nanofluids of different base fluids in cylindrical annulus with discrete heat source." *Heat Transfer—Asian Research* 48, no. 1 (2019): 135-147.

[21] Hayat, Tasawar, Taseer Muhammad, Sabir Ali Shehzad, and Ahmed Alsaedi. "An analytical solution for magnetohydrodynamic Oldroyd-B nanofluid flow induced by a stretching sheet with heat generation/absorption." *International Journal of Thermal Sciences* 111 (2017): 274-288.

[22] Daniel, Yahaya Shagaiya, Zainal Abdul Aziz, Zuhaila Ismail, and Faisal Salah. "Impact of thermal radiation on electrical MHD flow of nanofluid over nonlinear stretching sheet with variable thickness." *Alexandria Engineering Journal* 57, no. 3 (2018): 2187-2197.

[23] Hayat, Tasawar, Madiha Rashid, Ahmed Alsaedi, and Bashir Ahmad. "Flow of nanofluid by nonlinear stretching velocity." *Results in Physics* 8 (2018): 1104-1109.

[24] El-Aziz, M. Abd, and A. A. Afify. "Effect of Hall current on MHD slip flow of Casson nanofluid over a stretching sheet with zero nanoparticle mass flux." *Thermophysics and Aeromechanics* 26, no. 3 (2019): 429-443.

[25] Rajashekhar, C., G. Manjunatha, Hanumesh Vaidya, B. Divya, and K. Prasad. "Peristaltic flow of Casson liquid in an inclined porous tube with convective boundary conditions and variable liquid properties." *Frontiers in Heat and Mass Transfer (FHMT)* 11 (2018).

[26] Fang, T., Zhang, J. and Zhong. Y. "Boundary layer flow over a stretching sheet with variable thickness." *Applied Mathematics and Computations* 218, (2012): 7241-7252.

[27] Khader, M. M. and Megahed, A, M. "Boundary layer flow due to a stretching sheet with a variable thickness and slip velocity." *Journal of Applied Mechanics and Technical Physics* 56, (2015): 241-247.

[28] Farooq, M., Anjum, A., Hayat, T. and Alsaedi, A. "Melting heat transfer in the flow over a variable thicked Riga plate with homogeneous-heterogeneous reactions." *Journal of Molecular liquids* 224, (2016): 1341-1347.

[29] Prasad, K. V., Hanumesh, V., Vajravelu. K. and Rashidi, M. M. "Effects of variable fluid properties on MHD flow and heat transfer over a stretching sheet with variable thickness." *Journal of Mechanics* 33, (2016): 501-512.

[30] Prasad, K. V., Vajravelu, K., Hanumesh, V. and Robert A.Van Gorder. "MHD flow and heat transfer in a nanofluid over a slender elastic sheet with variable thickness." *Results in Physics* 7, (2017): 1462-1474.

[31] Prasad, K. V., Hanumesh, V., Vajravelu, K. and Ramanjini, V. "Analytical study of Cattanneo-Christov heat flux model for Williamson -Nanofluid flow over a slender elastic sheet with variable thickness. " *Journal of Nanofluids* 7, (2018): 583-594.

[32] Prasad, K.V., Hanumesh V., Vajravelu, K., Neelufer. Z. Basha and Umesh, V. "Thermal and species concentration of MHD Casson fluid at a vertical sheet in the presence of variable fluid properties." *Ain Shams Engineering Journal* 9, no. 4 (2018): 1763-1779.

[33] Prasad, K., Hanumesh Vaidya, K. Vajravelu, and U. Vishwanatha. "Influence of Variable Liquid Properties on Mixed Convective MHD Flow over a Slippery Slender Elastic Sheet with Convective Boundary Condition." *Journal of Advanced Research in Fluid Mechanics and Thermal Sciences* 56, no. 1 (2019): 100-123.

[34] Vajravelu, Kuppalapalle, and Kerehalli V. Prasad. *Keller-box method and its application*. Vol. 8. Walter de Gruyter GmbH & Co KG, 2014.

ವಿಜಯನಗರ ಶ್ರೀ ಕೃಷ್ಣದೇವರಾಯ ವಿಶ್ವವಿದ್ಯಾಲಯ
"ಜ್ಞಾನ ಸಾಗರ" ಆವರಣ, ವಿನಾಯಕ ನಗರ, ಕಂಟೋನ್ಮೆಂಟ್, ಬಳ್ಳಾರಿ - 583 105
VIJAYANAGARA SRI KRISHNADEVARAYA UNIVERSITY
"Jnana Sagara" Campus, Vinayaka Nagara, Cantonment, BALLARI - 583 105

REGISTRAR
08392-242703
08392-242097

No. VSKU/ACA/PH.D/2017-18/692 DATE:10.08.2017

Ph.D REGISTRATION NOTIFICATION

This is to notify that the application of Sri/Smt. **RAMANJINI V** for registration for Ph.D Programme has been accepted after processing his/her application along with the required certificates and documents as per the Ph.D regulations of the University. The details regarding the Ph.D. Programme of the above candidate are appended below:

1. Name and Address of the Guide	:**Dr. K.V.Prasad** Dept.of Studies and Research in Mathematics Vijayanagar Sri Krishnadevaraya University, Ballari.
2. Name and Address of the Co-Guide	:————
3. Department of Studies	: Mathematics
4. Area of Research Work	: Applied Mathematics
5. Topic of Proposed Research	: An Analytical Approach to Study the Flow and Heat Transfer of a Newtonian/Non-Newtonian fluids over a Slender elastic sheet
6. a) Date of Registration	: 20.04.2016
b) Registration No.	: PHD16MA08
c) Mode	: Full Time
7. Place of Work	: Vijayanagar Sri Krishnadevaraya University, Ballari.
8. Last date of course work duration	: 19.10.2016

CONDITIONS:

1. Half-yearly progress reports from the date of registration shall be submitted regularly through the guide and head of the Departments to the Special Officer (Academic Section). The Report should be certified by the guide.
2. Every such Half-Yearly report shall be submitted within fifteen days of the completion of the period.
3. If a Candidate fails to submit two consecutive half- yearly progress reports in time his/her registration shall stand cancelled.
4. The Candidate has to remit the prescribed annual tuition fee regularly. (The annual tuition fee should be paid along with I, III, V, VII, IX, progress reports and laboratory fees along with first Progress Report).
5. Please quote your Registration Number (as in Sl. No. 6 (b) for all future correspondence.

Registrar
Vijayanagara Sri Krishnadevaraya University
Ballari

Copy to:

01. Concerned Department Chairman and Guide.
02. Office Copy.

Scanned by CamScanner

URKUND

Urkund Analysis Result

Analysed Document: V Ramanjini, Dept of Mathematics. VSKUB.pdf (D63347289)
Submitted: 2/3/2020 6:51:00 AM
Submitted By: kumbargoudar@gmail.com
Significance: 9 %

Sources included in the report:

https://www.frontiersin.org/articles/10.3389/fphy.2019.00186/full
https://link.springer.com/article/10.1007/s00231-004-0565-x
https://www.sciencedirect.com/science/article/pii/S2451904918306115
https://link.springer.com/content/pdf/10.1007%252Fs00009-015-0594-3.pdf
https://www.scientific.net/JERA.28.73
https://www.ncbi.nlm.nih.gov/pmc/articles/PMC4273992/
https://www.researchgate.net/figure/Effects-of-L-and-i-ion-velocity-profile_fig3_307667869
https://www.nature.com/articles/srep04404
https://www.mdpi.com/2624-8174/1/1/12/htm
https://www.scirp.org/html/8-7402926_61465.htm
https://www.researchgate.net/publication/231144234_Boundary_Layer_Flow_and_Heat_Transfer_over_an_Exponentially_Shrinking_Sheet
https://www.researchgate.net/publication/281494439_Boundary_layer_flow_due_to_a_stretching_sheet_with_a_variable_thickness_and_slip_velocity
https://www.researchgate.net/publication/307583205_Two-phase_Boundary_Layer_Flow_Heat_and_Mass_Transfer_of_a_Dusty_Liquid_past_a_Stretching_Sheet_with_Thermal_Radiation
https://file.scirp.org/Html/5-1720665_70899.htm
https://www.nature.com/articles/srep17848
https://ctp.itp.ac.cn/EN/10.1088/0253-6102/71/12/1405
https://www.mdpi.com/2076-3417/9/10/2124/htm
https://www.researchgate.net/publication/324547399_Melting_heat_transfer_analysis_of_non-Newtonian_Casson_fluid_due_to_moving_plate
https://www.ijirset.com/upload/2017/ncrtamst/3_Melting.pdf
https://www.ias.ac.in/article/fulltext/pram/092/02/0021
https://link.springer.com/article/10.1186/1687-2770-2013-196
https://link.springer.com/article/10.1186/2228-5326-2-24
https://www.researchgate.net/publication/311510221_Effects_of_Viscous_Dissipation_and_Double_Stratification_on_MHD_Cas

Scanned by CamScanner

.KUND

,ctps://www.ajol.info/index.php/ijest/article/download/147126/136634
https://link.springer.com/article/10.1007/s40819-015-0080-4
https://www.nature.com/articles/s41598-018-35462-9
https://link.springer.com/article/10.1186/s13661-017-0827-4
https://www.researchgate.net/publication/260725799_Numerical_solution_for_boundary_layer_flow_due_to_a_nonlinearly_stretching_sheet_with_variable_thickness_and_slip_velocity
https://www.researchgate.net/publication/220557964_Boundary_layer_flow_over_a_stretching_sheet_with_variable_thickness
https://www.researchgate.net/publication/273911573_Flow_of_Casson_nanofluid_with_viscous_dissipation_and_convective_conditions_A_mathematical_model
https://www.researchgate.net/publication/301658677_Impact_of_Cattaneo-Christov_heat_flux_model_in_flow_of_variable_thermal_conductivity_fluid_over_a_variable_thicked_surface
https://www.researchgate.net/publication/259434359_Unsteady_Boundary_Layer_Flow_of_Nanofluid_Past_an_Impulsively_Stretching_Sheet
https://www.researchgate.net/publication/316338372_Buoyancy_effects_on_nanofluid_flow_past_a_convectively_heated_vertical_Riga-plate_A_numerical_study
https://www.researchgate.net/publication/318184133_Unsteady_Convective_Boundary_Layer_Flow_for_MHD_Williamson_Fluid_Over_an_Inclined_Porous_Stretching_Sheet_with_Non-Linear_Radiation_and_Heat_Source
https://www.researchgate.net/publication/258308020_Casson_fluid_flow_and_heat_transfer_over_a_nonlinearly_stretching_surface
https://content.sciendo.com/downloadpdf/journals/ijame/23/1/article-p137.xml
https://www.researchgate.net/publication/288827520_Heat_and_mass_transfer_in_MHD_non-Newtonian_bio-convection_flow_over_a_rotating_coneplate_with_cross_diffusion

Instances where selected sources appear:

313

31/1/20

LIBRARIAN
Vijayanagara Sri Krishnadevaraya University
Vinayak Nagar, Hospet Road, Cantonment,
BELLARY - 583104. (Karnataka)

Scanned by CamScanner

/

No.19012/03/2018-Sch.
Government of India
Ministry of Tribal Affairs
(Scholarship Division)

412-B, Shastri Bhawan,
New Delhi, dated, 7th June, 2018

No: 201718-NFST-KAR-00764

To

Mr. RAMANJINI V
S/o VENKATESHA
R/o RESEARCH SCHOLAR, DEPT OF MATHEMATICS,VSK UNIVERSITY, VINAYAKANAGAR BALLARI 583105, KARNATAKA,BALLARI,KARNATAKA,583105

Subject: **Fellowship under the scheme "National Fellowship and Scholarship for Higher Education of ST Students" to pursue M.Phil./Ph.D. Degree.**

Sir/Madam,

Congratulations!! With reference to your application for the National Fellowship for ST candidates, I am happy to inform you that based on the recommendation of the Selection Committee, the Ministry of Tribal Affairs has selected you for the National Fellowship for ST Candidates for the year 2017-18. The tenure of the fellowship is as per guidelines and it commences from 2017-18 onwards. The summary of the financial assistance offered under the scheme is as follows:

Course	Fellowship	Contingency	HRA	Escorts/ Reader Assistance
M.Phil	@ Rs. 25000/- per month	i.) Rs.10000/- per year for Humanities & Social Sciences ii.) Rs.12000/-per year for Science, Engineering Technology	As per rules of the University/ Institutions/ Colleges	Rs.2000/-p.m in case of physically handicapped and blind candidates for all the subjects
Ph.D	@ Rs.28000/- per month	i) Rs.20500/- per year for Humanities & Social Sciences ii.) Rs.25000/- per year for Science, Engineering Technology		

2. It may be noted that the selection is subject to the condition that the awardee has already secured admission and registered for regular and full time M.Phil./Ph.D. course in a university / Institution recognized by the UGC, while applying for the fellowship.

3.1 The awardee is required to submit the following documents, along with check list duly verified by the University, to the Ministry:-

(i) Caste Certificate
(ii) BPL card (if applicable)
(iii) Post-Graduation passing marksheet (equivalent % of CGPA, if applicable)
(iv) Disability certificate (if applicable)
(v) Certificate from Head of the Department/Institution stating that student has secured admission under the Ph.D/M.Phil and registered with the University/Institution for doing research w.e.f (*date to be mentioned*)
(vi) Details about the project (Topic & Methodology etc.)
(vii) Bond on Non-Judicial paper (Rs. 20/-) (original to be produced at the time joining)

3.2 The above documents may be sent, by Speed Post before 30.6.2018, to Section Officer(Scholarships), Ministry of Tribal Affairs, Government of India, 412, B-Wing, Shastri Bhawan, New Delhi-110001)

Scanned by CamScanner

TUMKUR UNIVERSITY

B.H. Road, TUMAKURU - 572103, Karnataka

DEPARTMENT OF STUDIES AND RESEARCH IN MATHEMATICS

Certificate

This is to certify that Prof./Dr./Mr./Mrs. RAMANJINI. Y.

of V.S.K. UNIVERSITY BALLARI

has participated as Delegate / Resource Person / Chaired a Session / Presented a Paper titled Analytical study of cattaneo-christ ov-heat flux model for Williamson-Nanofluid flow Over a slender Elastic sheet With variable thickness. in the National Conference on "Recent Advances in Mathematical Sciences and Applications" organized by the Department of Studies and Research in Mathematics, Tumkur University, Tumakuru, Karnataka during 1st and 2nd December, 2017.

Prof. Patil Mallikarjun B.	**Prof. B.S. Gunjal**	**Prof. Jayasheela**
Organising Secretary	Registrar	Vice Chancellor

Scanned by CamScanner

M117A

International Conference on Advances in Pure & Applied Mathematics 2018

Sep 06 - 08, 2018

Organized by

School of Mathematics, Madurai Kamaraj University, Madurai, India
International Multidisciplinary Research Foundation, India

CHOOSE TO BE HUGE

Govt., of India Approved Conference : MHA Vide F.No 42180123/CC-195, MEA Vide F.No AA/162/01/2018-903

Participation & Presentation Certificate

This is to certify that

MR. V. RAMANJINI

has participated and presented in the

International Conference on Advances in Pure & Applied Mathematics 2018

with a paper titled

MHD HEAT TRANSFER OF A CASSON NANOFLUID OVER A SLENDER RIGA PLATE

at School of Mathematics, Madurai Kamaraj University, Madurai, TN, India.

Dr.M Lellis Thivagar
Member Syndicate
Chairperson, School of Mathematics
Madurai Kamaraj University, Madurai

Dr. Ratnakar D Bala
Conference Chairman
Director (Academics), International
Multidisciplinary Research Foundation

www.imrfedu.org | Proceedings ISBN 978-93-86435-53-8

Scanned by CamScanner

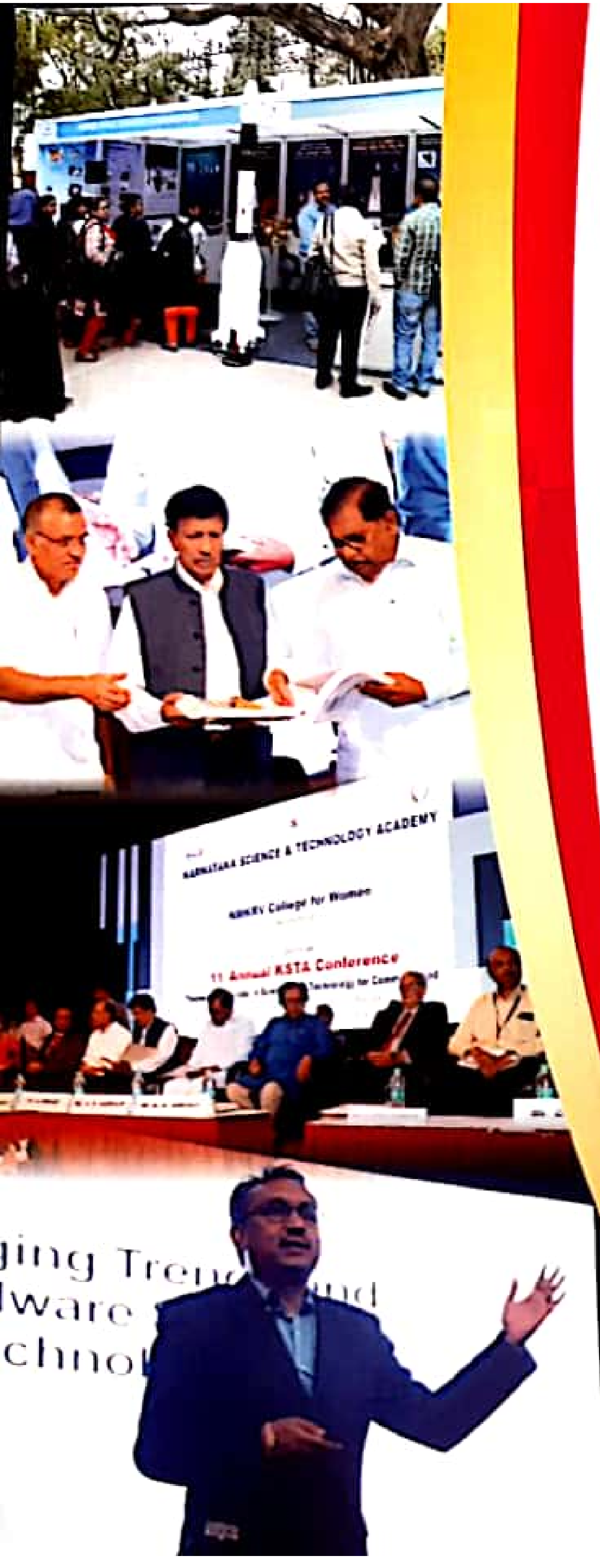

Department of IT & BT,
Government of Karnataka

KARNATAKA SCIENCE AND TECHNOLOGY ACADEMY

Department of Science and Technology, Govt. of Karnataka
"Prof. U.R. Rao, Vijnan Bhavan", Major Sandeep Unnikrishnan Road, GKVK Campus,
Dottabettahalli Layout, Vidyaranyapura Post, Bengaluru- 560 097

&

NMKRV College for Women

(AUTONOMOUS)
#45/1, 22nd Cross, Jayanagar III Block, Bengaluru – 560 011

Jointly Organize

11th Annual KSTA Conference

February 01-02, 2019 (Friday & Saturday)

THEME : NEW VISTAS IN SCIENCE AND TECHNOLOGY FOR COMMON GOOD

Certificate

This is to certify that Ms./Mr./Prof./Dr. **V. RAMANJINI**

of **VSKU BELLARY**

has participated as a Delegate / Presented Poster in the Poster Presentation held during February 01-02, 2019, at NMKRV College for Women, Bengaluru.

Dr. H. Honne Gowda	Dr. S.K. Shiva Kumar	Dr. Snehalata G Nadiger
(Special Director, (Technical) DST Member Secretary, KSTA	Chairman, KSTA / Former Director, URSO,ISRO	Principal NMKRV College

Scanned by CamScanner

ACHARYA

ACHARYA INSTITUTE OF GRADUATE STUDIES

NAAC Re-accredited 'A' Grade & Affiliated to Bengaluru Central University

Acharya Dr. Sarvepalli Radhakrishnan Road, Acharya PO, Soladevanahalli, Bengaluru-560 107, India

2nd INTERNATIONAL CONFERENCE

Global Advancement Of Mathematics-2019

Certificate

of Appreciation

Awarded to

RAMANJINI.V, Vijayanagara Sri Krishnadevaraya University

for Presenting/Participating

the paper entitled

Effect of Mixed Convective Nanofluid Flow Over a Stretchable Riga plate in the presence of Viscous dissipation and Chemical Reaction

in the 2nd International conference

on Global Advancement of Mathematics (GAM-2019)

held on 25th & 26th June 2019.

Lokesha.V
Prof. Lokesha
Convener

Vaidya
Prof. Gurunath Rao Vaidya
Conference Chair

Scanned by CamScanner

CURRICULUM VITAE

V. RAMANJINI

Permanent Address:

S/o Venkatesha. V, Valmiki street, Somappa Camp, SreeRamarangapura (Suggenahalli Kottal), S. R. R. PURA Post-583129, Kampli (Tq), Ballari (Dist).

Email Address: ramanjinibly@gmail.com

Mobile No: 7204364277

Educational Qualification:

Examination Passed	Examining Body/ University	Year of Passing	%Marks
S.S.L.C	Karnataka Secondary School Education Board, Bangalore	2007	75.36%
B.Sc.	Gulbarga University, Gulbarga.	2012	82.51%
M.Sc.	Gulbarga University, Gulbarga.	2014	83.20%

Other achievements

- Awarded with National Fellowship for Higher Education, **(Award Letter No: 201718-NFST-KAR-00764),** Govt. of India (RGNF) in 2017 for tenure of 5 years for pursuing Ph.D.

Papers Presentation in National/ International Conferences

- Presented a paper entitled **" Analytical study of Cattanneo – Christov heat flux model for Williamson nanofluid flow over a slender elastic sheet with variable thickness",** in the **national conference on recent advances in Mathematical sciences and applications,** organized by the Department of Mathematics, Tumkur Univrsity, Tumkur, Karnataka, during 1st and 2nd December 2017.

- Presented a paper entitled **"MHD heat transfer of Casson nanofluid over a slender Riga plate", in the international conference on advances in pure and applied Mathematics 2018,** organized by School of Mathematics, Madurai Kamaraj University in association with International Multidisciplinary Research Foundation (IMRF), Madurai, Tamilnadu, 6th - 8th September, 2018.

- Presented a paper entitled **"Influence of variable transport properties on Casson nanofluid over a slender Riga plate: Keller box scheme", in the national conference named as New Vistas in Science and Technology in Common Good,** organized by NMKRV College for women in association with KSTA Bangalore, 1st and 2nd February 2019.

- Presented a paper entitled **"Effect of mixed convective nanofluid flow over a stretchable Riga plate in the presence of viscous dissipation and chemical reaction", in the 2nd international conference on global advancement of Mathematics (GAM-2019),** organized by Acharya institute of graduate studies, Bangalore – 560107, India, held on 25th and 26th June 2019.

LIST OF PUBLICATIONS

- K.V. Prasad, Hanumesh Vaidya, K. Vajravelu, and **V. Ramanjini**, **"Analytical Study of Cattanneo-Christov Heat Flux Model for Williamson -Nanofluid Flow Over a Slender Elastic Sheet with Variable Thicknesss",** Published in the ***Journal of Nanofluids,*** **Vol. 7,** 583-594, 2018.

- K.V. Prasad, Hanumesh Vaidya, K. Vajravelu, **V. Ramanjini**, G. Manjunatha and C. Rajashekhar, **"Influence of variable transport properties on Casson nanofluid over a slender Riga plate: Keller box scheme",** Published in the ***Journal of Advanced Research in Fluid Mechanics and Thermal Science,*** **Vol.64(1),** 19-42, 2019.

- K.V. Prasad, Hanumesh Vaidya, O.D. Makinde, K. Vajravelu, **V. Ramanjini**, **"Mixed convective nanofluid flow over a coagulated Riga plate in the presence of viscous dissipation and chemical reaction,"** communicated to the ***Journal of Applied and Computational Mechanics,*** 2020.

K.V. Prasad, Hanumesh Vaidya, K. Vajravelu, O.D. Makinde and **V. Ramanjini,** **"Influence of suction/injection and heat transfer on unsteady MHD Flow over a stretchable rotating disk,"** accepted for publishing in the ***International Journal of Latin American Applied Research,*** 2019.